CHEMICAL REVIEWS

pubs.acs.org/CR

Review

Alternative Micro/Nanofabrication Approaches for Wearable Electronics

Jianxin Zhang and Minqiang Wang*

Cite This: https://doi.org/10.1021/acs.chemrev.5c00801

Read Online

ACCESS | Metrics & More | Article Recommendations

ABSTRACT: The rapid advancement of wearable electronics over the recent decadal span has positioned it as a cornerstone of scientific innovation and everyday life, bridging applications from fitness tracking to advanced medical diagnostics. These technologies enable real-time physiological monitoring, personalized healthcare, and precision medicine, yet their progress is hindered by the limitations of conventional fabrication methods, which struggle to accommodate unconventional nanomaterials and the escalating complexity of wearable devices. This review addresses this gap by spotlighting cutting-edge micro/nanofabrication techniques and novel nanomaterials poised to redefine wearable electronics. We systematically examine breakthroughs in sensing nanomaterials across dimensional architectures, while highlighting innovative printing methodologies that enable scalable, cost-effective, and geometrically tailored fabrication of flexible, high-performance devices. By analyzing these advances, we explore their transformative applications in wearable biochemical, biophysical, electrophysiological, and multimodal electronics, underscoring their potential to elevate device performance and user experience universally. Finally, we critically evaluate the advantages, persistent challenges, and prospects of these micro/nanofabrication strategies, offering insights to guide next-generation wearable electronics. This review aims to catalyze interdisciplinary innovation, fostering the integration of these techniques into diverse applications and accelerating the evolution of wearable electronics.

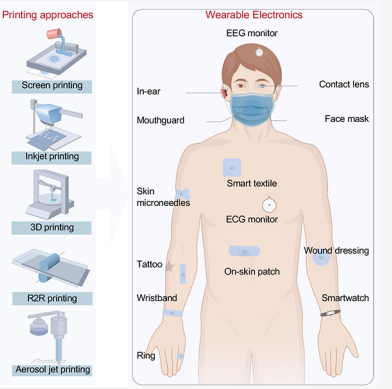

CONTENTS

Received: September 18, 2025
Revised: December 23, 2025
Accepted: December 30, 2025

https://doi.org/10.1021/acs.chemrev.5c00801
Chem. Rev. XXXX, XXX, XXX−XXX

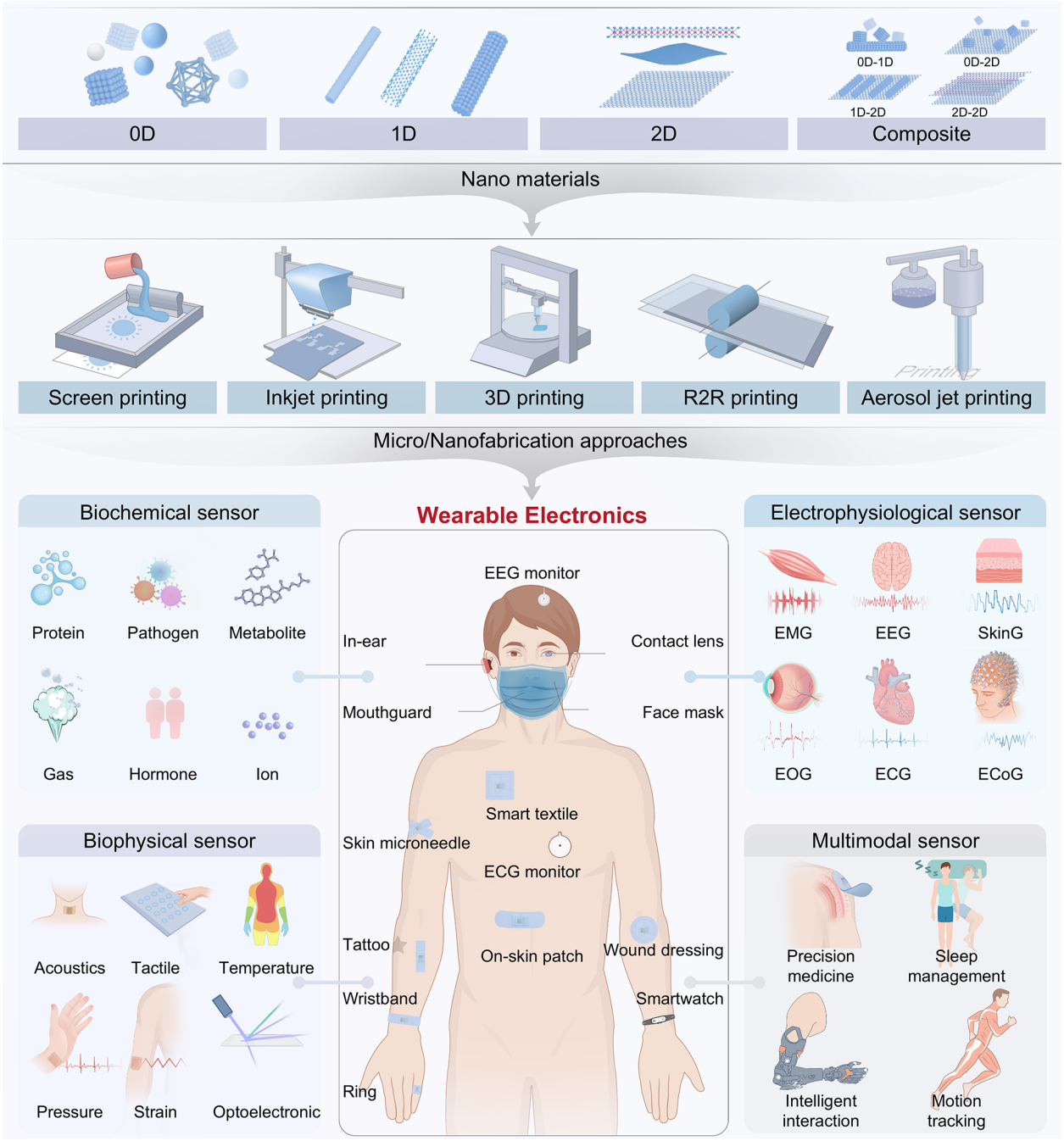

Figure 1. Overview of alternative micro/nanofabrication approaches for wearable electronics. Abbreviations: 0D, zero-dimensional; 1D, one-dimensional; 2D, two-dimensional; 3D, three-dimensional; R2R, roll-to-roll; EMG, electromyography; EEG, electroencephalography; SkinG, skin conductance; EOG, electrooculography; ECG, electrocardiography; ECoG, electrocorticography.

1. INTRODUCTION

The wearable electronics domain has experienced radical paradigm shifts across the recent decadal span,[1−3] emerging as a crucial domain within science and technology as well as a significant aspect of daily life. Ranging from fitness trackers[4] to sophisticated medical devices,[5] wearable electronics are redefining human technological interactions.[6] Wearable electronics enable diverse critical applications encompassing personalized healthcare monitoring,[7] athletic performance assessment,[8] aging populations surveillance,[9] occupational safety monitoring,[10] physiological sensing of biological systems,[11] environmental quality detection,[12] human−machine interfacing,[13] brain−computer communication,[14] and implementation of embodied intelligence[15] and digital twin technologies.[16] While existing reviews have extensively examined flexible and wearable devices and their functional materials,[17−21] there remains a notable gap in comprehensive discussions on the specialized fabrication techniques essential

https://doi.org/10.1021/acs.chemrev.5c00801
Chem. Rev. XXXX, XXX, XXX−XXX

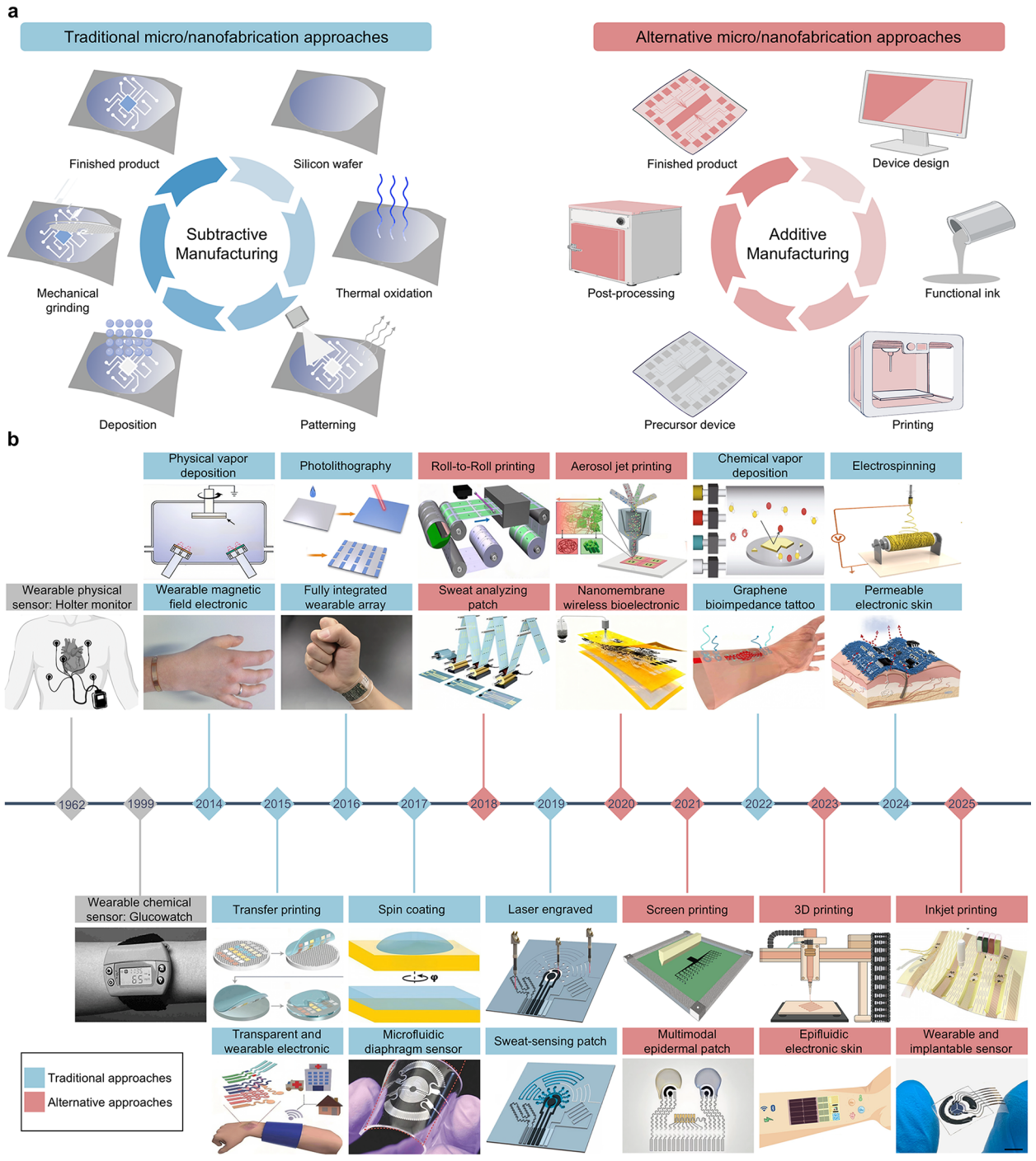

Figure 2. Wearable electronics enabled by micro/nanofabrication approaches. (a) Schematic comparison of traditional subtractive manufacturing versus additive printed electronics fabrication processes. (b) The representative examples like the Holter monitor (a physical sensor) and the Glucowatch (a chemical sensor). Traditional approaches such as photolithography, laser engraving, electrospinning, chemical vapor deposition, sputter deposition, transfer printing, and spin coating. Alternative micro/nanofabrication approaches such as screen printing, roll-to-roll printing, 3D printing, inkjet printing, and aerosol jet printing. Reproduced with permission from refs 3, 6, 30, 55, 97, 98 100−116. Copyright 2001 Elsevier BV, 2014 John Wiley and Sons, 2024 John Wiley and Sons, 2015 John Wiley and Sons, 2022 Springer Nature, 2016 Springer Nature, 2024 Springer Nature, 2017 John Wiley and Sons, 2019 American Association for the Advancement of Science, 2018 American Chemical Society, 2019 American Association for the Advancement of Science, 2019 Springer Nature, 2020 Springer Nature, 2025 John Wiley and Sons, 2021 Springer Nature, 2020 Springer Nature, 2022 Springer Nature, 2015 Springer Nature, 2023 American Association for the Advancement of Science, 2024 Springer Nature, 2025 Springer Nature, 2025 Springer Nature, 2022 American Association for the Advancement of Science.

for their development. Notably, the integration of innovative nanomaterials presents significant opportunities to enhance performance and drive further progress in this rapidly evolving field.[22]

Although traditional fabrication techniques such as coating technology,[23] electrochemical deposition[24] remain effective for conventional applications, they often fall short in meeting the intricate demands of modern wearable electronics, particularly

https://doi.org/10.1021/acs.chemrev.5c00801
Chem. Rev. XXXX, XXX, XXX−XXX

Table 1. Comparative Analysis of Micro/nanofabrication Approaches for Wearable Electronics

fabrication technique	resolution	cost	throughput capacity	technical complexity	material solution	applicable materials type	advantages	limitations	ref
photolithography	<100 nm	significant	high	cleanroom environment	photoresist solution	silicon-based materials, etc.	superior precision and resolution	capital-intensive, stringent environmental controls, process complexity	32−35
laser processing	<1 μm	substantial	low	laser control systems		metals and alloys, etc.	high precision, maskless patterning	slow processing speed, limited material range	36−39
electrospinning	<500 nm fiber diameter	moderate	moderate	electrospinning apparatus	sol−gel precursor solution	polymer nanofibers, etc.	high surface area, comfortable mechanical property	orientation control difficulty, limited productivity	40−44
chemical vapor deposition	nanoscale coating	significant	moderate	reaction chambers		metal films, carbon-based materials, etc.	superior film quality	high temperature requirement, hazardous gas handling, significant energy consumption	45−48
physical vapor deposition	nanoscale thickness control	substantial	moderate	vacuum technology		metals and alloys, metal oxides, etc.	uniform deposition	high equipment cost, vacuum requirement	49−52
transfer printing	micro-nano scale	moderate	moderate	parameter control	functional ink or paste	conductive materials, etc.	substrate versatility	low transfer yield	53−56
spin coating		moderate	low	spin coater	aquatic or organic solution	elastomers, etc.	macroscopic uniformity, cost-friendly	patternization difficulty	57−59
screen printing	>50 μm	moderate	high	straightforward equipment	high viscosity functional ink or paste	conductive materials, semiconductor materials, etc.	operational simplicity	resolution limitation, multilayer registration challenge	60−63
roll-to-roll printing	micro-nano scale	moderate	high	precision web handling	low to medium viscosity functional ink or paste	conductive materials, etc.	industrial-scale efficiency	complex postprocessing requirement	64−67
3D printing	∼30 μm	moderate	moderate	model preparation complexity	photosensitive resin, functional ink or paste	conductive materials, photosensitive resins, etc.	geometric design freedom	precision constraint, material property restriction	68−71
inkjet printing	∼30 μm	moderate	moderate	precision nozzle systems	low to medium viscosity functional ink or paste	conductive materials, composite functional materials, etc.	pattern design freedom	nozzle fouling issue, stringent rheological requirement	72−75
aerosol jet printing	∼10−30 μm	moderate	moderate	precise control of aerosol generation	functional ink or paste	conductive materials, composite functional materials, etc.	pattern design freedom	poor adaptability to certain high-viscosity materials, slow printing speed	76−79

when integrating novel and unconventional nanomaterials. This limitation has spurred growing interest in advanced micro/nanofabrication methodologies, which hold the potential to transform the design paradigms and functional capabilities of next-generation wearable electronics. Such innovative approaches enable the development of adaptable and high-performance wearable technologies, keeping pace with the rapidly evolving technological landscape.[25] The progress in this field is driven by a diverse array of micro/nanofabrication techniques, each offering unique advantages tailored to specific applications, underscoring the dynamic and multifaceted nature of wearable electronics research.

With the shifting demands of the wearable electronics industry, various innovative micro/nanofabrication approaches are being developed, providing new solutions for the creation of flexible, high-performance devices. Approaches such as printing are being increasingly adopted in the fabrication of wearable electronics.[26] Printing is compatible and versatile, offering precise control to fabricate multiple sensors and integrated systems on flexible wearable substrates. It is an effective method for achieving cost-effective and high-throughput production. Each printing technique has been designed to overcome the limitations of traditional processes, facilitating the wearable electronics creation of intricate micro/nanostructures with improved functionality and scalability. By embracing these alternative printing approaches, the industry is equipped to produce highly integrated, multifunctional wearable electronics that meet modern demands. Printing methods represent pioneering manufacturing technology for wearable electronics, wherein suspensions of functional sensing materials are precisely deposited onto a flexible substrate via compatible printing devices.[27] This technique is increasingly prevalent in flexible and wearable electronics. Using printing methods, wearable electronics can be produced at a high throughput, with controlled patterns, precise thicknesses, carefully designed high-performance sensing material ink, and predesignated boundaries. These methods are notably suited for large-area flexible materials and provide a low-cost, streamlined process for high-throughput production.

While significant progress has been made in printing technologies for wearable electronics, previous research efforts have predominantly concentrated on printer development,

https://doi.org/10.1021/acs.chemrev.5c00801
Chem. Rev. XXXX, XXX, XXX−XXX

with comparatively less emphasis on advancing material compatibility. Moreover, there remains a notable absence of comprehensive reviews addressing recent innovations in printing methodologies for wearable electronics. The strategic selection of printing materials and techniques plays a pivotal role in enabling functional device integration and system-level implementation, particularly for wearable applications. This review systematically examines traditional approaches for wearable electronics, active sensing materials and their synthesis method, material properties, human interface signal transduced mechanisms, fundamental system-level components for wearable electronics and micro/nanofabrication approaches used in the development of wearable electronics (Figure 1). Our analysis provides an in-depth evaluation of emerging micro/nanofabrication approaches specifically designed for wearable electronics. Furthermore, we investigate the diverse applications of these techniques across various wearable sensor modalities, including biochemical, biophysical, electrophysiological, and multimodal sensing platforms. By elucidating the unique capabilities of these innovative fabrication methods, we demonstrate their potential to significantly enhance device performance while optimizing user experience. This comprehensive assessment not only maps the current technological landscape but also underscores the transformative impact these advanced manufacturing approaches may have on the future of wearable electronics. Through this work, we aim to bridge critical knowledge gaps and provide valuable insights for researchers working at the forefront of wearable technology development.

2. TRADITIONAL FABRICATION APPROACHES

With the rise of concepts such as flexible electronics[1] and the Internet of Things (IoT),[28] there is an increasingly urgent need to integrate sensors into wearable electronics like clothing[29] and skin patches.[7,30] To this end, the initial approach was to leverage established semiconductor micro/nanoprocessing techniques (such as conventional silicon-based photolithography) by adapting these precision processes, originally designed for rigid chips (Figure 2a, panel 1), for application on flexible substrates. Most of these conventional manufacturing methods are essentially subtractive techniques. Although they laid the foundation for the early development of wearable electronics, they fundamentally conflict with the requirements of flexible applications. Most of these traditional technologies suffer from their inherent limitations such as incompatibility with flexible materials (e.g., high temperatures), complex process flows, and high manufacturing costs. These traditional manufacturing techniques have set significant obstacles for the development of the next generation of wearable electronic devices that combine high flexibility and dense integration. The manufacturing paradigm for wearable electronics is undergoing a significant shift, with additive manufacturing technologies progressively supplanting conventional fabrication techniques. This transition is driven by the distinct advantages of additive printing approaches, which are emerging as a dominant methodology in this field. Key attributes include their intrinsic compatibility with flexible substrates, enablement of digital rapid prototyping, lower capital investment, and simplified processing workflows (Figure 2a, panel 2). To provide a comprehensive perspective on this technological evolution, this section commences with a thorough analysis of the traditional micro/nanofabrication techniques tailored for wearable electronics. This establishes a foundational context for the subsequent discussion of the emergent additive printing approaches that are reshaping the field.

The landscape of wearable electronics and concomitant micro/nanofabrication strategies has undergone a radical transformation over the past decade (Figure 2b, Table 1). The conceptual genesis of wearable electronics can be traced back to the introduction of the Holter monitor in 1962, a seminal development that established the paradigm for ambulatory, long-term physiological data acquisition.[31] This evolutionary trajectory has culminated in the development of advanced architectures, including multimodal epidermal systems, electronic skin (E-skin), and fully integrated bioelectronics, thereby endowing wearable platforms with unprecedented capabilities. At present, the synergistic advancement of novel device functionalities alongside the high-precision fabrication techniques necessary for their implementation constitutes the defining frontier of the discipline, highlighting a critical need for methodological convergence to realize next-generation applications.

2.1. Photolithography

The transcription of intricate geometric patterns from a mask onto a substrate is achieved in photolithography by exploiting photoresponsive resists via spatially modulated light exposure,[80] demonstrating superior fidelity in pattern reproduction and the capability to resolve complex micro/nanoscale features.[81] Such precision is critical for realizing the high-density interconnects and active areas essential for advanced wearable sensor architectures.[82] Nevertheless, the operational implementation of photolithography imposes substantial technoeconomic barriers. The process necessitates significant capital expenditure on specialized infrastructure, including precise alignment systems, exposure units, and development stations. Furthermore, the stringent requirement for controlled cleanroom environments to mitigate particulate contamination drastically escalates both process complexity and operational expenditures. Consequently, the dichotomy between the superior lithographic resolution and the associated infrastructural burdens remains a pivotal consideration when evaluating the scalability of wearable electronics manufacturing.[83]

2.2. Laser Processing

Through photothermal or photochemical mechanisms, laser processing utilizes precisely focused, high-energy photonic beams to induce surface modifications or volumetric ablation.[84] This maskless, direct-write paradigm facilitates the digital fabrication of three-dimensional (3D) microarchitectures on diverse flexible matrices,[85] thereby circumventing the need for physical masks.[86] A prominent application within wearable electronics involves the synthesis of laser-induced graphene (LIG) electrodes. Here, the judicious optimization of laser fluence and scanning speed permits the fine-tuning of electrical conductivity and porous morphology across various precursor materials,[85] enabling electrode performance tailored to specific transduction mechanisms. The digital nature of this technique offers distinct advantages for rapid prototyping and design iteration. However, despite the flexibility of modern laser systems (e.g., CO_2 lasers[87]), their adoption is tempered by the high cost of sophisticated optical trains and control electronics. Moreover, the serial nature of laser writing inherently constrains throughput compared to parallel processing techniques. When applied to ultrathick precursors or large-area substrates, issues regarding power dissipation and

https://doi.org/10.1021/acs.chemrev.5c00801
Chem. Rev. XXXX, XXX, XXX−XXX

beam uniformity arise, necessitating a careful balance between the versatility of maskless operation and the limitations of production speed.

2.3. Electrospinning

Continuous fibers with diameters typically in the micro-nanometer scale are produced through electrospinning by utilizing electrohydrodynamic forces to draw polymer solutions.[88] The resultant nonwoven nanofibrous mats exhibit exceptionally high specific surface areas and hierarchical 3D porosity, attributes that are instrumental in maximizing analyte interaction sites to enhance sensor sensitivity and dynamic response. Additionally, the intrinsic mechanical compliance of these fibrous networks permits seamless integration with textile substrates, yielding breathable, moisture-permeable interfaces that preserve user comfort during extended monitoring.[89] Despite these merits, the stochastic nature of fiber deposition makes precise control over fiber alignment and individual morphology technically challenging. This lack of deterministic structural control can compromise device-to-device reproducibility in industrial-scale manufacturing. Consequently, current research trajectories are directed toward process optimization strategies aimed at enhancing deposition uniformity while retaining the functional advantages inherent to nanofibrous sensor scaffolds.

2.4. Chemical Vapor Deposition (CVD)

To generate conformal thin films on solid interfaces, chemical vapor deposition (CVD) employs a class of processes governed by heterogeneous gas-phase reactions and mass transport phenomena.[90] This methodology affords the thickness of electrode layers, ranging from subnanometer scales to several hundred nanometers. The deposited films are characterized by superior structural integrity, including uniform topographical coverage, high crystallinity, and minimal lattice defect densities.[91] However, the widespread utilization of CVD is impeded by high infrastructural costs associated with tubular or hot-wall reactors, ultrahigh vacuum systems, and cleanroom facilities. Furthermore, the elevated thermal budgets typically required for precursor decomposition present severe compatibility issues with thermally labile flexible substrates, such as polyethylene terephthalate (PET) and polydimethylsiloxane (PDMS). These thermal constraints, coupled with the energetic demands and the necessity for rigorous waste gas abatement, underscore the need for low-temperature CVD variants or alternative transfer protocols.

2.5. Physical Vapor Deposition (PVD)

The atomistic generation of vapor species from condensed sources and their subsequent transport through a vacuum or low-pressure environment to condense upon a substrate characterizes physical vapor deposition (PVD).[92] Sputter deposition, a prevalent PVD modality, utilizes plasma-induced ion bombardment to eject target atoms, which then traverse a ballistic trajectory to form dense, nanoscale functional coatings on flexible supports.[93] Conversely, simpler thermal evaporation techniques are frequently employed for depositing delicate materials in devices such as ultraflexible perovskite solar cells.[94] PVD methodologies enable the sequential deposition of distinct material classes in a single process run, thereby facilitating the monolithic fabrication of multifunctional sensor stacks.[95] While PVD offers unparalleled film density and multilayer capabilities, the complexity and vacuum-dependence of the equipment pose significant hurdles to high-throughput manufacturing of wearable electronics.

2.6. Transfer Printing

The deterministic assembly of functional thin films from rigid donor substrates onto flexible or stretchable receiving surfaces can be achieved via transfer printing.[96] The fidelity and economic viability of this approach are intrinsically linked to the quality of the donor substrate processing. This technique distinguishes itself by offering exceptional compatibility with diverse soft materials, enabling high-level heterogeneous integration. Furthermore, it facilitates the simultaneous transfer of multilayer stacks while mitigating interfacial thermal and mechanical stress, operating effectively within temperature windows compatible with delicate polymer matrices.[96] However, the yield of the transfer process is critically dependent on the viscoelastic properties of the stamp (aging effects) and the kinetic control of interfacial adhesion. Furthermore, scaling to large-area transfers introduces susceptibility to wrinkling and registration misalignment, necessitating the implementation of sophisticated tension control mechanisms to ensure structural fidelity.

2.7. Spin Coating

As a foundational solution-processing technique, spin coating employs centrifugally driven flow to deposit thin films with high macroscopic uniformity.[59] By dispensing a liquid precursor onto a rotating substrate, this method achieves a homogeneous material distribution, establishing itself as a cornerstone in the fabrication of wearable electronics,[97] thin-film transistors,[98] and advanced semiconductor devices.[99] It is particularly vital for defining the active layers in flexible optoelectronic systems,[57,58] as well as for establishing planarization and encapsulation layers. The ubiquity of spin coating derives from its ability to produce exceptionally planar films utilizing cost-effective equipment operable at ambient pressures. Despite these logistical advantages, the process suffers from intrinsic inefficiencies in material utilization, as the majority of the precursor solution is ejected from the substrate periphery. Moreover, spin coating acts strictly as a global deposition technique, yielding blanket films without lateral resolution. Consequently, the realization of functional circuit patterns necessitates subsequent subtractive steps, thereby increasing process complexity.

Conventional manufacturing paradigms, epitomized by subtractive microfabrication, are characterized by stringent processing requirements and high capital intensity. These approaches have achieved unparalleled levels of device integration and performance on rigid, planar substrates, serving as the cornerstone of modern information technology. However, an intrinsic dependence on inflexible substrates, demanding high-temperature and high-vacuum processing environments, and intricate, multistep photolithography and etching cycles, present fundamental, inherent limitations for translation to the burgeoning fields of flexible and wearable electronics. Therefore, developing additive manufacturing technologies suitable for flexible substrates and compatible with low-temperature and normal-pressure conditions, such as printed electronics, has become an inevitable choice for promoting the development of the next generation of wearable electronic products.

https://doi.org/10.1021/acs.chemrev.5c00801
Chem. Rev. XXXX, XXX, XXX−XXX

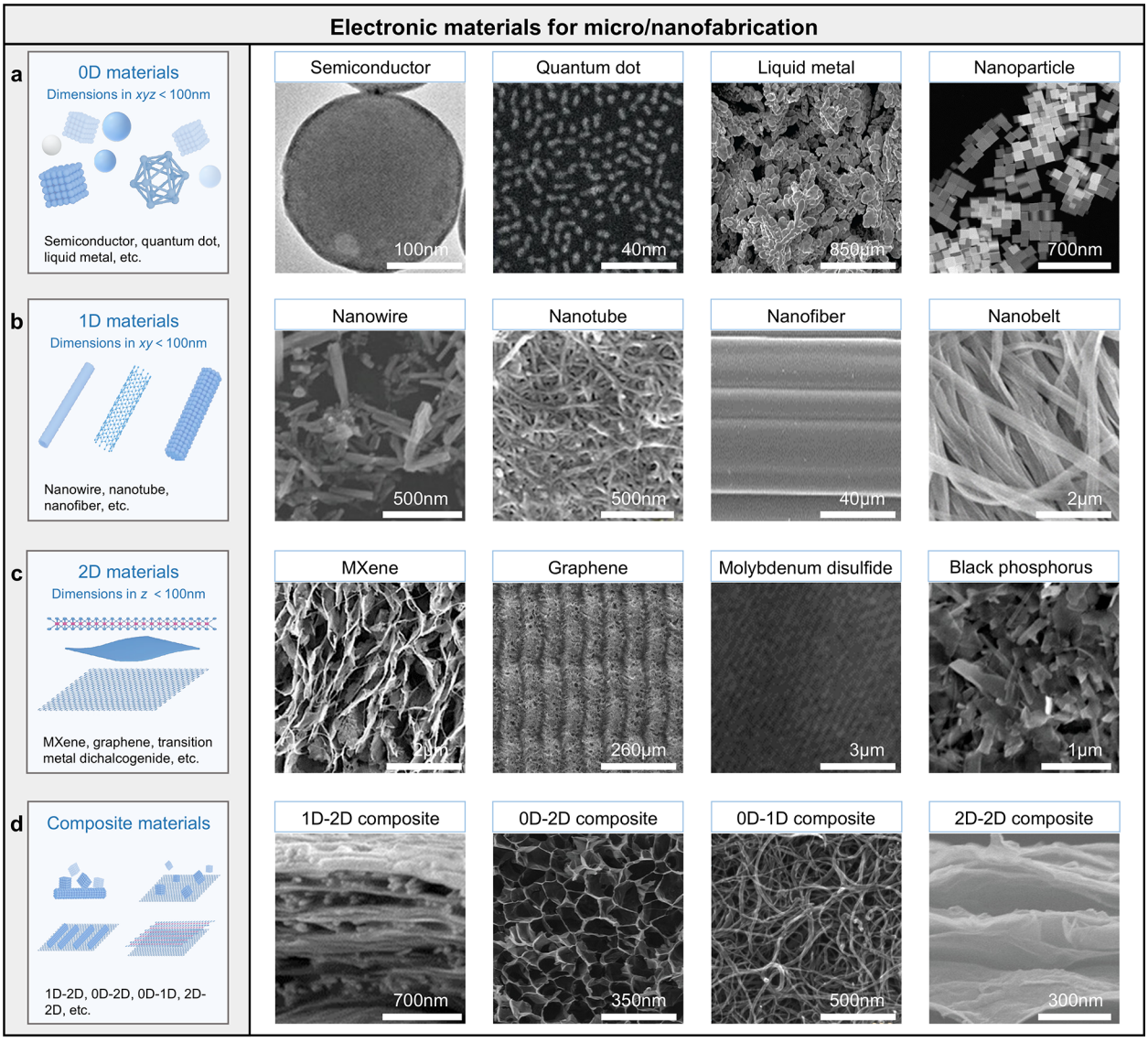

Figure 3. Electronic materials for micro/nanofabrication. (a) 0D materials: semiconductor, quantum dot, liquid metal, nanoparticle. Reproduced with permission from refs 107,160−162. Copyright 2025 John Wiley and Sons, 2021 Springer Nature, 2022 American Association for the Advancement of Science. (b), 1D materials: nanowire, nanotube, nanofiber, nanobelt. Reproduced with permission from refs 163−166. Copyright 2023, 2021 John Wiley and Sons, 2024 Springer Nature. (c) 2D materials: MXene, graphene, MoS_2, black phosphorus. Reproduced with permission from refs 6,167−169. Copyright 2018, 2019 Springer Nature, 2021 Elsevier BV, 2024 John Wiley and Sons. (d) Composite material: 1D−2D composite, 0D−2D composite, 0D−1D composite, 2D−2D composite. Reproduced with permission from refs 170−173. Copyright 2024 Springer Nature, 2024 John Wiley and Sons, 2025 Springer Nature, 2024 American Association for the Advancement of Science.

3. ELECTRONIC MATERIALS AND INTRINSIC PROPERTIES

3.1. Electronic Materials for Micro/Nanofabrication

Although micro/nanofabrication strategies for wearable electronics have matured significantly, the realization of fully integrated, functional systems relies critically on synergistic material properties and structural heterogeneity. A persistent challenge, however, is the paucity of sensing active materials amenable to these advanced processing protocols, which currently restricts device versatility. To overcome this bottleneck, the rational design and selection of materials possessing tunable electrochemical activity and mechanical compliance are paramount. The material toolkit currently utilized spans a dimensional continuum, progressing from zero-dimensional (0D) architectures[117] to one-dimensional (1D)[118] and two-dimensional (2D) nanomaterials,[119] alongside hierarchical composite assemblies (Figure 3). The incorporation of such nanostructured elements fundamentally enhances signal transduction via high specific surface-to-volume ratios, while concurrently resolving the mechanical mismatch between active components and deformable substrates through inherent flexibility and stretchability.

3.1.1. 0D Materials. Constrained to the nanoscale in all three spatial dimensions (Figure 3a), 0D materials exhibit intrinsic physicochemical properties that render them integral to the advancement of wearable electronics.[117] These nanostructures are delineated by composition and functional utility into four primary classes: (i) metal and semiconductor nanoparticles, exemplified by gold (AuNPs)[120] and silver (AgNPs),[121] which are characterized by superior charge transport and catalytic efficacy; (ii) quantum dots, including CdSe[122] and ZnS[123] variants, distinguished by exceptional optoelectronic attributes, specifically tunable fluorescence emission;[124] (iii) 0D liquid metal (LM), which represent a pivotal research trajectory due to their combination of electrical conductivity, mechanical compliance, and biocompatibility; and (iv) morphologically complex architectures like mesoporous nanoparticles[125] and nanoclusters,[126] which maximize specific surface area and con-

https://doi.org/10.1021/acs.chemrev.5c00801
Chem. Rev. XXXX, XXX, XXX−XXX

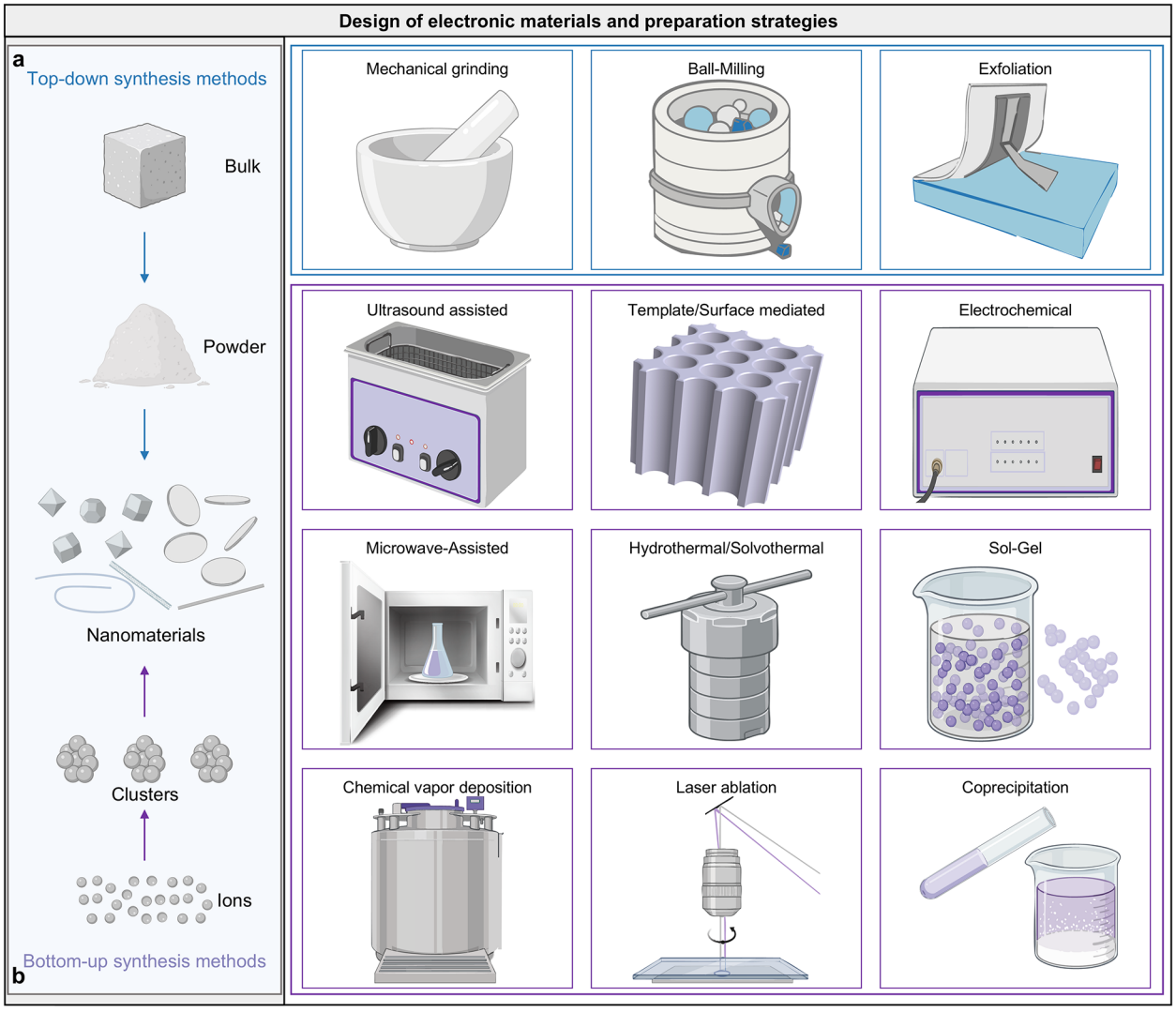

Figure 4. Design of electronic materials and preparation strategies. (a) Top-down synthesis methods: mechanical grinding, ball-milling, exfoliation. (b) Bottom-up synthesis methods: ultrasound assisted, template/surface mediated, electrochemical, microwave-assisted, hydrothermal/solvothermal, sol−gel, chemical vapor deposition, laser ablation, coprecipitation.

ductivity. Fundamentally, quantum confinement within 0D systems induces discrete electronic energy levels, generating distinctive optical and electrical phenomena essential for device miniaturization.[117] Furthermore, the high surface-to-volume ratio inherent to 0D materials affords a high density of active sites for analyte interaction, substantially augmenting sensor transduction performance.[127] Consequently, these characteristics establish 0D materials as fundamental enablers for next-generation wearable sensing platforms, addressing critical requirements for high sensitivity, selectivity, and component densification.

3.1.2. 1D Materials. Nanostructure units with dimensions exceeding the nanometer scale in one direction while maintaining nanoscale dimensions in the other two directions are defined as 1D materials (Figure 3b).[128] Prominent examples of 1D materials include: nanowires,[129] nanotubes,[130] nanofibers,[131] nanobelts,[132] and nanorods.[133] These materials exhibit a unique linear structure that confers a high aspect ratio and substantial specific surface area.[134] Furthermore, the inherent flexibility and mechanical strength of 1D materials, attributed to their 1D linear morphology, enable them to accommodate the bending and stretching associated with human motion in wearable electronics.[135] Additionally, 1D materials can be integrated with other functional materials, such as metal nanoparticles,[136] to create composite structures that exhibit synergistic effects, thereby further enhancing sensor performance.[137] As a result, 1D materials demonstrate exceptional capabilities in the realm of wearable electronics.

3.1.3. 2D Materials. Materials that are defined by a characteristic thickness of one or a few atomic layers extending in two dimensions, with a thickness on the order of nanometers in the third dimension (Figure 3c), are known as 2D materials.[138] Their unique physicochemical properties have catalyzed extensive investigation into their utility for next-generation wearable electronics.[139,140] Paradigmatic examples of this material family include: (1) MXenes, exemplified by titanium carbide ($Ti_3C_2T_x$), which afford metallic conductivity, hydrophilicity, and tunable surface termination chemistries;[141] (2) graphene, a monolayer honeycomb lattice of carbon[142] distinguished by exceptional electrical transport, mechanical robustness, and intrinsic flexibility; (3) transition metal dichalcogenides (TMDs), typified by molybdenum disulfide (MoS_2)[143] and tungsten disulfide (WS_2),[144] which exhibit semiconducting behavior coupled with photoresponsivity; and (4) black phosphorus, where the layer-dependent tunability of the band gap critically modulates electrochemical properties and adsorption capabilities, thereby facilitating the selective detection of diverse analytes. The applicability of these materials in wearable systems derives primarily from their atomic thinness, which enables conformal integration onto flexible substrates such as PET[143] and PDMS.[145] Furthermore, the exceptionally large specific surface area and high density of surface active sites position

https://doi.org/10.1021/acs.chemrev.5c00801
Chem. Rev. XXXX, XXX, XXX−XXX

Table 2. Design and Preparation Technology Route for Electronic Materials-Oriented Approaches

preparation strategy	target materials	typical morphologies	process temperature	advantages	limitations	ref
mechanical grinding	metals, ceramics, etc.	irregular particles, flakes	room temperature	low equipment requirement, absence of chemical reagents	uneven particle size distribution, difficulty in morphology control	179−182
ball-milling	metal alloys, carbon materials, etc.	spherical, regular particles	room to low temperature	alloying capability, high process control ability	risk of local overheating, adverse effect on material structure	183−187
exfoliation	2D materials, lamellar compounds, etc.	sheets, films	room temperature	low equipment requirement, monolayer preparation capability	low yield, scalability issue	188−190
ultrasound assisted	composite materials, MOFs, etc.	spherical, nanoparticles, porous structures	room to medium temperature	fast reaction rate, good product dispersion	high sensitivity to ultrasonic parameter	191−193
template/surface mediated	ordered porous materials, etc.	ordered array, porous structures	room to medium temperature	high morphology control ability	requirement of template removal	194−197
electrochemical	metal oxides, conductive polymers, etc.	sheets, wires	room temperature	mild reaction condition, high process control ability	dependence on conductive substrate, electrolyte waste generation	85,198−200
microwave-assisted	carbon materials, metal oxides, MOFs, etc.	spherical, rod-shaped	high temperature	fast reaction rate	requirement for microwave-responsive reactant	201−203
hydrothermal/solvothermal	metal oxides, sulfides, prussian blue analogues, etc.	spherical, rod-shaped, flower-like, sheets	medium to high temperature	high product crystallinity, good morphology control	requirement for high-pressure equipment, risk of solvent pollution	204−207
sol−gel	metal oxides, aerogels, etc.	particles, films	room to high temperature	uniform composition, high purity	product agglomeration, cracking and shrinking during drying	208−211
chemical vapor deposition	carbon materials, semiconductors, etc.	films, tubulars	high temperature	controllable thickness and composition, process maturity	high equipment cost, strict precursor requirement	45,212−215
laser ablation	carbon materials, porous materials, etc.	nanoparticles, tubulars	instantaneous high temperature	high product purity, clean process	high equipment cost, laser safety risk	36,216−218
coprecipitation	metal oxides, prussian blue analogues, etc.	spherical, nanoparticles	room to medium temperature	process simplicity, low cost	poor morphological and size uniformity, risk of impurity introduction	219,107,220,221

2D materials as effective scaffolding for functionalization or hybridization with zero-, one-, and two-dimensional heterostructures, a strategy essential for achieving superior sensing performance.[146]

3.1.4. Composite Structural Materials. The rapid evolution of flexible electronics and wearable electronics imposes increasingly stringent requirements on sensor materials; conventional monolithic materials frequently fail to meet these multifactorial demands (Figure 3d).[147] Consequently, composite materials have emerged as critical enablers in wearable electronics design by leveraging synergistic interactions among disparate components.[148] Common composite architectures include polymer-based composites,[149] carbon-based composites,[150] metal-based composites,[151] and gel-based composites.[152] Through the integration of diverse constituent material phases, as well as the possible synergy and conjugation among materials, multifunctional capabilities such as augmented electrical conductivity,[153] mechanical pliability,[154] self-healing,[155] and antimicrobial[156] activity can be simultaneously realized. Furthermore, performance metrics may be finely tuned via manipulation of component ratios[157] and structural configurations, such as porous networks[158] or layered constructs.[159] By overcoming the intrinsic limitations of monolithic materials systems, composite materials provide a pathway toward highly sensitive and durable wearable electronics.

In addition to the previously discussed nanomaterials, bulk materials (e.g., metal blocks) are also explored for the development of electronics, although several challenges persist. While conventional bulk materials are characterized by desirable properties, such as high electrical conductivity, their inherent rigidity and difficulty in shaping restrict their applicability in flexible device architectures. To address these constraints, considerable efforts have been devoted to integrating bulk materials with nanomaterials, with the aim of achieving an optimal balance between superior functional performance and the necessary manufacturing flexibility.

While advances in materials science and micro/nanofabrication are unlocking new possibilities for composite-based wearable electronics, a pivotal challenge lies in navigating the inherent trade-offs between material functionality and manufacturing scalability. Printing is a key enabler for cost-effective, large-scale production, yet it imposes stringent constraints on the materials themselves.[174] For example, 3D printing of functional composites offers excellent mechanical robustness but often compromises on device size and complexity.[175] In contrast, inkjet printing of additive-free inks can achieve superior functional performance, but at the cost of strict ink formulation requirements (e.g., material particle size, viscosity) and a general limitation to planar device architectures.[176] Consequently, the forefront of research is focused on co-optimizing novel material systems with advanced fabrication strategies to resolve these compromises and realize the full potential of next-generation wearable electronics.

3.2. Design of Electronic Materials and Preparation Strategies

To meet the stringent requirements of wearable electronics for high sensitivity, excellent flexibility and stability, it is crucial to develop controllable and efficient electronic nanomaterial preparation technologies. From the perspective of implementation approaches, the existing preparation methodologies mainly follow two basic paradigms: the first is the top-down method of microscopically reducing macroscopic bulk materials, the second is the bottom-up method of constructing from basic units such as atoms and molecules (Figure 4, Table 2).[177,178]

3.2.1. Top-Down Synthesis Methods. Macroscopic material is progressively broken down via physical or mechanical methods (e.g., grinding, ball milling, exfoliating) in the top-down approach, yielding nanoscale entities (Figure 4a).[222] A paramount merit of this paradigm lies in its mature, straightforward processing, rendering it eminently suitable for large-scale industrial implementation and high-volume manufacturing. However, precise control over final particle dimensions, geometry, and surface states remains elusive, frequently resulting in broad size polydispersity and morphological hetero-

https://doi.org/10.1021/acs.chemrev.5c00801
Chem. Rev. XXXX, XXX, XXX−XXX

geneity. Furthermore, the rigorous high-energy processing involved may introduce crystallographic defects or surface contaminants, which can deleteriously affect the material's intrinsic properties and functional performance.

3.2.1.1. Mechanical Grinding. A straightforward mechanical approach for converting bulk-like materials into nanomaterials is grinding, which features minimal equipment complexity and ease of operation, eliminating the need for elaborate chemical reagents or rigorous reaction conditions.[179] This approach generally reduces reliance on organic solvents and chemical additives, mitigating environmental impact and suppressing the generation of undesirable byproducts.[180] Moreover, the relatively modest capital and operational expenditures offer distinct advantages for mass production. Nevertheless, the inherently manual nature of many grinding protocols can compromise particle distribution uniformity, leading to significant challenges in reproducibility and the consistent regulation of nanomaterial properties.

3.2.1.2. Ball-Milling. Another effective method for comminuting bulk materials into nanoscale powders is ball-milling, wherein spherical grinding media impart impact and shear forces within a confined milling chamber. The process exploits mechanical energy derived from impact and friction to induce grain refinement and particle size reduction.[187] Beyond dimensional modulation, ball-milling facilitates the intimate homogenization of heterogeneous components, rendering it particularly efficacious for nanocomposite synthesis.[223] High-energy ball-milling further enables material activation, enhancing reactivity and promoting phenomena such as mechanical alloying and solid-state phase transformations.[224] However, the kinetic energy dissipated as heat during collisions, between media, vessel walls, and the precursor, can induce thermal excursions that inadvertently modify the physicochemical attributes of the resulting nanomaterials.

3.2.1.3. Exfoliation. 2D nanomaterials, such as graphene and MXenes,[188,225] are predominantly isolated via mechanical exfoliation, a technique valued for its direct and minimally destructive nature. This method involves the physical delamination of bulk layered crystals into constituent nanosheets via applied mechanical forces.[226] The operational simplicity of mechanical exfoliation, distinguished by the absence of sophisticated instrumentation or chemical reagents, facilitates straightforward implementation in laboratory environments. Conversely, inherent limitations include low throughput and restricted scalability, which impede industrial application. Additionally, stochastic variability in nanosheet thickness and lateral dimensions presents challenges to uniformity and reproducibility, limiting the precise control over nanomaterial properties essential for consistent device performance.

By virtue of their structural integrity and macroscopic dimensions, bulk materials serve as a stable and uniform starting matrix for processing. The essence of the top-down paradigm lies in the mechanical or chemical deconstruction or exfoliation of these bulk precursors into nanoscale products with specific dimensions and functionalities. Consequently, the intrinsic properties, crystal structure, and mechanical characteristics of the bulk material fundamentally dictate the efficiency of the top-down preparation process and the performance of the resulting nanomaterials.

3.2.2. Bottom-Up Synthesis Methods. In contrast to top-down approaches, bottom-up strategies utilize atoms or molecules as the fundamental building blocks. In these methods, chemical processes drive the assembly of these units into defined nanostructures within controlled environments, governed by the thermodynamics and kinetics of nucleation and growth (Figure 4b).[227] The distinct advantage of this paradigm is its high degree of controllability, enabling the precise tailoring of parameters that are critical for advanced functional applications. Nevertheless, significant challenges remain regarding the complexity of reaction pathways, where the assembly process exhibits high sensitivity to experimental variables such as temperature, pressure, and precursor concentration.

3.2.2.1. Ultrasound Assisted. This technique exploits the acoustic cavitation effect generated by ultrasonic waves to drive chemical transformations of molecules and atoms in solution, facilitating efficient nanomaterial synthesis.[228] The rapid reaction kinetics associated with sonochemistry promote the nucleation and uniform dispersion of nanoparticles. However, the methodology is constrained by operational limitations, including acoustic noise generation, and the inherent difficulty in strictly regulating particle morphology and size distribution.

3.2.2.2. Template/Surface Mediated. To fabricate nanomaterials with strict regulation of dimensionality and spatial arrangement, template- or surface-mediated synthesis is a widely adopted approach.[229] This method employs hard or soft templates as scaffolds to construct desired nanostructures, thereby enabling the engineering of specific physicochemical properties.[229] However, the interaction between the template and the precursor can significantly influence the performance of the final material.[230] Furthermore, the multistep nature of this process, particularly the potentially costly and chemically intensive template removal phase, introduces technical complexities and economic constraints.

3.2.2.3. Electrochemical. Electrochemical deposition facilitates the fabrication of nanostructures with tunable composition and morphology through the precise modulation of applied potential and reaction duration.[231] While the mild, controllable reaction conditions allow for the facile fabrication of films and nanostructures, large-scale implementation is impeded by the requirement for conductive substrates and the environmental burden associated with waste generation, specifically from spent electrolytic solutions.[232]

3.2.2.4. Microwave-Assisted. Another rapid and efficient approach to accelerating chemical reactions via microwave radiation facilitates the fast fabrication of nanostructured materials.[233] This method leverages uniform internal heating to significantly enhance reaction rates and reduce synthesis times. Despite these kinetic advantages, the technique is restricted to microwave-susceptible reaction systems. Additionally, scalability is often compromised by nonuniform field distribution and the challenges associated with precise internal temperature monitoring.

3.2.2.5. Hydrothermal/Solvothermal. Precise control over particle size and morphology is achievable by modifying reaction conditions in hydrothermal/solvothermal synthesis.[234] These facile, cost-effective techniques are characterized by their broad applicability in synthesizing diverse material compositions and structures.[235] However, limitations include the substantial consumption of chemical reagents and the potential for environmental pollution if not managed correctly. Furthermore, the requirement for high-temperature and high-pressure conditions over extended periods introduces inherent safety risks.[236]

3.2.2.6. Sol–Gel. The sol–gel process relies on hydrolysis and polycondensation reactions to transition a precursor solution into a solid gel network, with final products obtained through subsequent drying and sintering.[211] Conducted under mild, low-temperature conditions, this approach facilitates the incorporation of various dopants, yielding high-purity nanomaterials.[208] A critical bottleneck, however, is the drying phase, where capillary forces can induce uncontrollable aggregation or structural collapse, thereby complicating product reproducibility and consistency.

3.2.2.7. CVD. For the controlled growth of films and nanostructures from gaseous precursors, one widely utilized technique is CVD.[237] It offers robust controllability, allowing for the precise manipulation of film thickness, morphology, and stoichiometry via the adjustment of parameters such as temperature, pressure, and precursor flow rate.[212] Conversely, the requirement for sophisticated vacuum systems, high processing temperatures, and the management of toxic byproducts renders the method capital-intensive and operationally complex.[215]

3.2.2.8. Laser Ablation. Laser ablation represents a sophisticated synthetic methodology wherein laser irradiation induces extreme physicochemical conditions on a target surface to facilitate the formation of specialized nanoarchitectures.[238] Despite its ability to produce unique structures, the method entails significant operational complexity and high instrumentation costs. Additionally, the ablation process may induce material vaporization or thermal decomposition, generating aerosols that necessitate rigorous extraction and filtration

https://doi.org/10.1021/acs.chemrev.5c00801
Chem. Rev. XXXX, XXX, XXX−XXX

Table 3. Essential Material Properties for Wearable Electronics

material category	conductivity	biocompatibility	stability	cost	ref
carbon-based materials (graphene, CNTs, rGO, etc.)	significant	moderate	significant	moderate	241−245
metal-based materials (Au, Ag, Pt, etc.)	significant	significant	significant	significant	246−249
metal oxides (ZnO, TiO_2, etc.)	moderate	significant	significant	reduced	250−253
semiconductors (MoS_2, WSe_2)	reduced	moderate	moderate	reduced	168,254−257
conductive polymers (PANI, PEDOT: PSS, PPy, etc.)	significant	significant	moderate	moderate	258−261
MXene materials ($Ti_3C_2T_x$, V_2CT_x, etc.)	significant	moderate	moderate	significant	262−266
MOF materials (ZIF-8, UiO-66, etc.)	reduced	significant	significant	moderate	267−271
natural materials (lignin, etc.)	reduced	significant	significant	reduced	272−277
hydrogels (alginate, gelatin, PVA, etc.)	moderate	significant	moderate	moderate	278−281

systems. The use of high-power lasers also imposes strict safety protocols to mitigate potential ocular and dermal hazards.

3.2.2.9. Coprecipitation. Coprecipitation involves the nucleation of compounds from solution and is widely utilized for its scalability and stoichiometric homogeneity.[239] While advantageous for its simplicity and cost-effectiveness, the method suffers from difficulties in controlling particle size and morphology due to agglomeration tendencies and high sensitivity to pH fluctuations. The purity and reproducibility of the product are heavily dependent on precipitation conditions,[240] and high-temperature annealing is often required to enhance crystallinity and remove lattice water.

Collectively, bottom-up synthesis methods represent a constructive strategy for nanomaterial fabrication, orchestrating atomic, molecular, or nanocluster precursors into well-defined architectures through chemical synthesis and controlled deposition. A distinct attribute of this methodology is the capacity for atomic-level precision. Judicious regulation of reaction parameters (temperature, precursor concentration, and pH) facilitates the synthesis of nanomaterials characterized by narrow size distributions, programmable morphologies, and consequently, tailored functional properties. In stark contrast to top-down approaches, this process provides a thermodynamically driven pathway for engineering nanomaterials with bespoke functionalities, where performance is intrinsically governed by structural precision.

3.3. Essential Material Properties

The interface between abiotic electronic systems and the biotic human periphery introduces complex engineering constraints that transcend conventional circuit design. Unlike rigid, planar industrial components, epidermal electronics must maintain conformal contact with the viscoelastic skin surface while accommodating dynamic physiological deformations. This rigorous operational environment demands that sensing matrices sustain functionality under persistent mechanical excursions, including tensile strain, flexion, and interfacial shear. As the critical transduction and sensing layer, the material composition dictates the ultimate stability and fidelity of the device. Consequently, successful candidates must synergistically combine high electrical conductivity with biocompatibility, environmental resilience, and cost-effective scalability. A failure to reconcile these often-conflicting properties creates a significant bottleneck in signal integrity and user safety. Thus, establishing a robust equilibrium among these interdependent metrics is essential for advancing the translational potential and commercial viability of skin-interfaced platforms (Table 3).

3.3.1. Conductivity. Electrical conductivity constitutes a pivotal figure of merit for sensing active layer materials in wearable electronics, directly governing the fidelity of signal acquisition across diverse physiological modalities and the response kinetics of the device.[282] Efficient charge transport within these sensing architectures must satisfy two distinct criteria: First, electron mobility must be sufficiently high[283] to mitigate signal attenuation, a factor that critically determines detection accuracy and temporal resolution. Second, the material must sustain consistently low electrical resistance[284] to preserve signal integrity and preclude information loss arising from ohmic dissipation.

Among emerging candidates, MXenes exhibit exceptional potential. The metallic character of the transition metal layers provides a high density of free electrons, while the planar 2D topology facilitates efficient carrier migration by minimizing scattering sites. Consequently, MXenes synergize the intrinsic metallic conductivity of the constituent elements with the anisotropy of 2D layered structures to achieve superior electrical performance. Parallel to these developments, conductive polymers (including polypyrrole (PPy)[285] and polyaniline (PANI)[286]) and conductive hydrogels[287] have been established as viable synthetic analogs. The former facilitates charge transport through π-conjugated structures, while the latter establishes conductive pathways via incorporated conductive fillers (such as silver nanowires (AgNWs) or carbon nanotubes (CNTs)) or through dynamically interlocked polymer chains. The conductivity of semiconductor materials, conversely, is intrinsically linked to layer thickness and material composition. For instance, MoS_2 undergoes a band structure transition from an indirect bandgap semiconductor in its bulk form (bandgap ~1.2 eV)[288] to a direct bandgap semiconductor in its monolayer limit (bandgap ~1.8 eV).[289] Furthermore, phase engineering offers a route to modulate electronic properties by inducing transitions between the semiconducting 2H phase, the metallic 1T phase, and other metastable phases,[290] thereby yielding tunable electrical conductivity. These materials not only accommodate mechanical deformation but also sustain robust electrical performance under complex environmental perturbations.

3.3.2. Biocompatibility. Biocompatibility encompasses the biological response to sensing active materials, addressing the safety profile of material-tissue interactions.[291] As the integumentary system functions as the primary barrier between the internal physiology and the external environment, it possesses heightened sensitivity to exogenous agents. Wearable electronic systems frequently necessitate prolonged intimate contact with the epidermis, mucosal membranes, or compromised tissue surfaces.[292] Consequently, materials lacking adequate biocompatibility may precipitate adverse host responses. To ensure biological safety, materials are subjected to comprehensive toxicological profiling: Cytotoxicity assays evaluate the impact of material extracts on dermal fibroblasts.[293] Analytical techniques identify potentially toxic chemical residues from synthesis processes.[294] Skin sensitization studies assess allergic responses following dermal contact.[295] Finally, longitudinal wear trials evaluate comfort and irritation through standardized participant questionnaires.[220,296]

Natural polymeric materials, such as cellulose-based textiles[297] and chitosan membranes,[298] offer distinct advantages in this domain, as their structural homology to endogenous tissues minimizes immunological rejection. In contrast to heavy metal nanomaterials, the constituent elements of transition metal dichalcogenides (such as Mo, W, and S) exhibit lower intrinsic toxicity within therapeutic concentration windows. Furthermore, their versatile surface chemistry facilitates biofunctionalization; for example, the covalent or noncovalent grafting of biocompatible polymers can significantly enhance their cytocompatibility.[299] Biological hydrogels utilizing water as a dispersion medium, including alginate[300] and gelatin-based[301] formulations, provide not only mechanical compliance but also, in specific configurations, antimicrobial efficacy (e.g., silver ion-loaded hydrogels[302]), thereby enabling simultaneous physiological monitoring and therapeutic intervention.

3.3.3. Stability. The transition of wearable electronics from transient prototypes to reliable, long-term monitoring platforms is

https://doi.org/10.1021/acs.chemrev.5c00801
Chem. Rev. XXXX, XXX, XXX−XXX

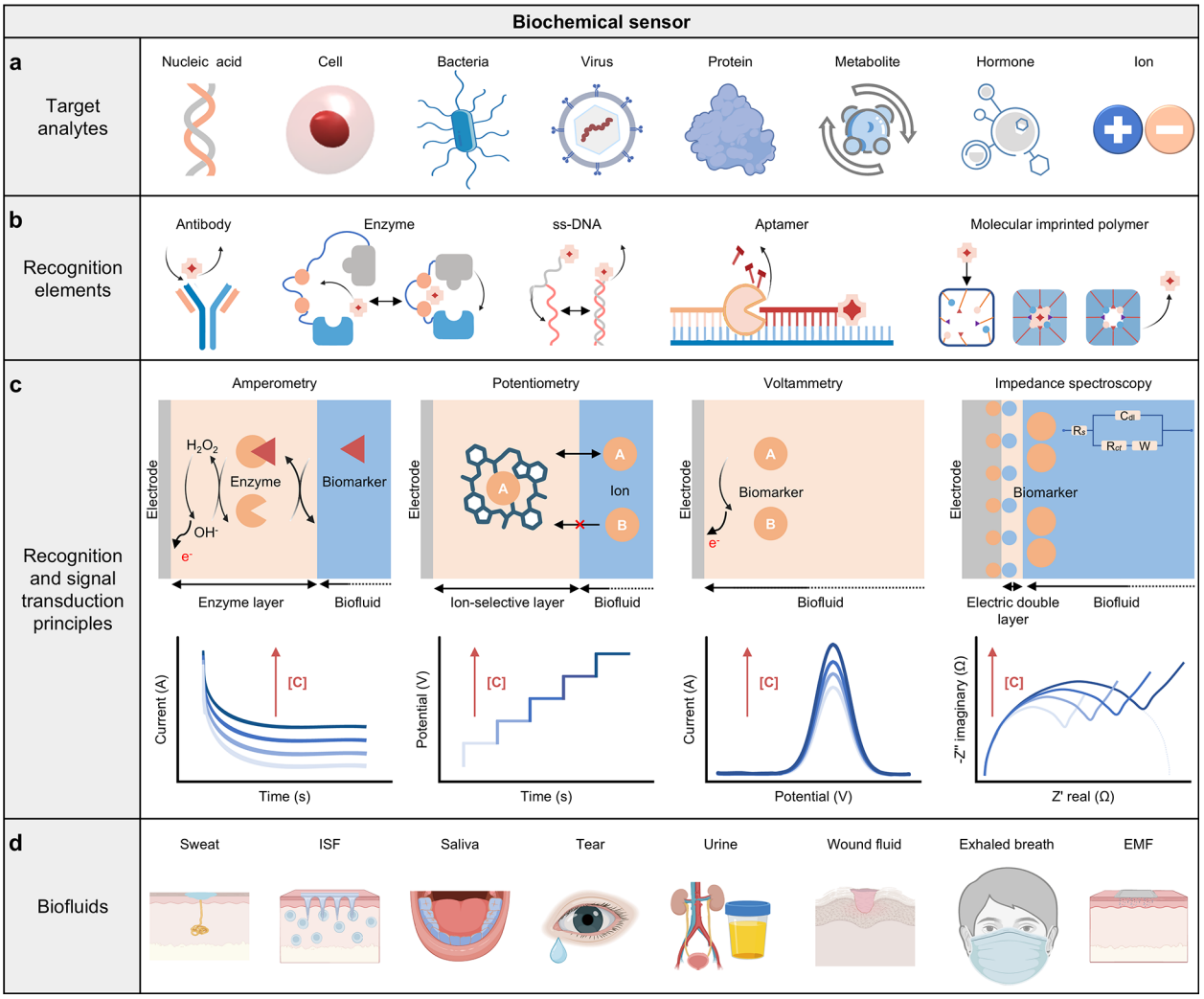

Figure 5. The primary biorecognition and signal transduction strategies in wearable biochemical sensors. (a) Schematic representation of various biochemical analytes. (b) Target recognition mechanisms involving bioaffinity receptors and biochemical sensing molecular switches. (c) Recognition and signal transduction principles for wearable electrochemical biosensors. (d) Wearable biochemical sensors for sweat, ISF, saliva, tear, urine, wound fluid, exhaled breath, and EMF analysis. Abbreviations: R_{ct}, charge transfer resistance; W, Warburg impedance; C_{dl}, double-layer capacitance; R_s, solution resistance; C, concentration; ISF, interstitial fluid; EMF, epidermal molecular flux.

predicated on stability. Specifically, the capacity to withstand simultaneous physicochemical and environmental stressors. Chemically, physiological fluids such as sweat present a corrosive electrolyte environment detrimental to metallic interconnects, while oral fluids introduce enzymatic challenges and microbial activity; similarly, the acidic gastric milieu poses a threat to structural integrity. Physically, routine locomotion imposes cyclic mechanical loading, articular movement necessitates high deformability, and interactions with textiles generate tribological wear, while recumbency introduces sustained compressive stress. These challenges are compounded by environmental variables, including seasonal thermal fluctuations that induce expansion/contraction cycles. The failure to maintain material stability under these multifactorial pressures results in impedance drift and structural degradation, ultimately precipitating functional failure and truncated device operational lifespans.

A pertinent example is observed in MXenes, where surface functional groups are susceptible to oxidative degradation under ambient conditions, a process that disrupts the conductive percolation network and leads to irreversible performance decay.[303] To mitigate this, strategies involving surface modification[304] (including molecular passivation) or composite engineering[305] (constructing interpenetrating networks with hydrolytically stable matrices) have been developed, extending the functional lifetime of specific MXene composites to several weeks. Inorganic nanomaterials, such as CNTs, graphene, and AuNPs, are favored for their intrinsic chemical inertness,[306] while metal nanoparticles may be stabilized against corrosion via surface passivation.[307] Furthermore, fiber architectures effectively dissipate applied stress,[308] granting resilience against repetitive mechanical fatigue. Advanced composite designs thus aim to establish synergistic chemical stability and mechanical durability, thereby ensuring prolonged operational viability in complex service environments.[309]

3.3.4. Cost. The translation of wearable electronics from laboratory scale to commercial viability is critically constrained by economic feasibility. As sensing materials constitute a substantial fraction of the total bill of materials, their cost directly dictates market competitiveness. Reliance on noble metals (e.g., gold or platinum) or synthetic protocols requiring high energy input significantly elevates the cost-per-unit area, impeding widespread adoption. Conversely, natural materials offer an economically advantageous alternative: abundant fibers, including cotton and cellulose derivatives, are inexpensive and amenable to straightforward processing into sensing substrates. The integration of these cost-effective precursors facilitates scalable manufacturing, thereby accelerating the democratization of personalized health monitoring technologies.

https://doi.org/10.1021/acs.chemrev.5c00801
Chem. Rev. XXXX, XXX, XXX−XXX

Beyond these fundamental economic metrics, specific application scenarios impose stringent functional prerequisites: motion tracking systems necessitate robust dermal adhesion to preclude motion artifacts during physical exertion[310] and resistance to biofouling (e.g., repellence of sweat-borne lipids and particulates[311]); flexible display interfaces demand exceptional ductility and optical transparency;[55,310] while medical-grade implants require selective permeabilit.[312] Furthermore, the ergonomic and aesthetic aspects of device design are essential for user compliance, such as minimizing weight and utilizing transparent encapsulation materials. The systematic and synergistic optimization of these interdependent parameters represents the critical pathway toward the functional advancement and practical ubiquity of wearable electronic technologies.

4. SENSING SIGNAL TRANSDUCTION AND CLASSIFICATION

Wearable electronics require *in situ*, real-time data streams to facilitate ongoing monitoring, which constrains the selection of applicable sensing methodologies. Current wearable electronics are primarily categorized into biochemical,[313] biophysical,[314] and electrophysiological[10] types based on their capacity to quantify human physiological signals. These signal transduction mechanisms enable continuous, real-time, *in situ* monitoring in flexible or wearable formats, providing direct access to the signals under investigation. Furthermore, integration of multiple transduction modes facilitates multimodal analysis,[315] expanding functional capabilities for human disease assessment.

4.1. Biochemical Sensor

The transition from static, single-point measurements to the dynamic, continuous monitoring of in vivo biochemical markers represents a paradigm shift in biomedical research and clinical diagnostics. Conventional blood assays, while foundational to clinical chemistry, provide valuable yet temporally discrete data points, offering only a snapshot of an individual's physiological state.[316] In contrast, wearable biochemical platforms that continuously interrogate biofluids can generate high-resolution temporal profiles of target analytes.[107] The operational principle of these sensors typically hinges on the biofunctionalization of a working electrode (WE) surface with high-affinity recognition elements,[317] such as enzymes or antibodies. The specific binding or catalytic conversion of a target analyte by these immobilized moieties transduces the biochemical recognition event into a quantifiable electrochemical signal.[316] Notwithstanding their demonstrated analytical prowess, ensuring long-term operational stability and analytical fidelity on the epidermal environment remains a critical barrier to the widespread clinical adoption and full realization of continuous biochemical monitoring technologies.

4.1.1. Analytes. The operational efficacy of wearable biochemical sensors hinges critically on the interfacial architecture of the WE. This surface is predominantly functionalized with selective biorecognition motifs designed to sequester target analytes or mediate interfacial redox kinetics.[318] Upon exposure to biofluids, the specific interaction between the immobilized receptors and unknown analytes (Figure 5a) modulates the physicochemical properties of the electrode interface. This transduction mechanism effectively translates biomolecular recognition events into distinct electrical signatures, thereby establishing a direct correlation that enables the precise detection and quantification of the target species.

4.1.1.1. Nucleic Acid. The fundamental operational principle of nucleic acid biosensors involves the immobilization of a single-stranded DNA (ss-DNA) probe at the WE interface to hybridize with the complementary target DNA or ribonucleic acid (RNA).[319] This surface modification is typically realized through the chemisorption of thiolated DNA probes onto gold-deposited electrode surfaces.[320] The sensitivity of nucleic acid biorecognition has been further augmented by the integration of redox electrochemical signal beacons, which transduce specific hybridization events into quantifiable electrochemical signals.[321]

4.1.1.2. Cell. Cellular parameters, including population density, morphology, and barrier integrity, function as critical biomarkers yielding insights into organismal physiology.[322] A single pathological cell often exhibits distinct phenotypic traits distinguishing it from healthy counterparts, underscoring the necessity for accurate early stage identification, particularly in oncology.[323] Compared to metabolomic and proteomic profiling, whole-cell detection presents inherent complexity. Variations in electrical signals resulting from cellular heterogeneity primarily manifest as impedance changes, the magnitude of which is convoluted by these multifactorial influences.[324]

4.1.1.3. Bacteria. In the context of cutaneous wounds or specific microbiomes (e.g., oral and intestinal environments), microbial colonization can precipitate chronic infections and persistent inflammatory responses.[325] Consequently, real-time, rapid detection of bacterial pathogens is pivotal for effective wound management and accelerated healing.[292,326] Electrochemical detection strategies often exploit specific probe-surface interactions, analogous to protein biomarker assays.[327] Furthermore, as various bacteria secrete exotoxins during proliferation, the bacterial load can be indirectly assessed by quantifying toxin levels.[328]

4.1.1.4. Virus. Prevalent viral pathogens in clinical practice include influenza viruses, noroviruses, and coronaviruses.[28] While initial infection assessments may rely on hematological markers such as leukocyte counts, C-reactive protein (CRP), and platelet metrics,[329] definitive identification mandates sophisticated techniques like genomic sequencing or immunoassays.[330] Contemporary wearable sensing platforms predominantly leverage specific antigen−antibody recognition[331] to generate electrochemical signals, thereby facilitating high-sensitivity, specific viral detection.

4.1.1.5. Protein. Proteins ubiquitous in biological matrices exhibit dynamic expression profiles in response to physiological or pathological stimuli.[332] Specific proteins exclusively expressed in neoplastic cells serve as high-fidelity markers for early cancer diagnosis.[333] Consequently, proteomic biomarkers are instrumental across clinical domains, including prognostication and therapeutic monitoring.[334] The enzyme-linked immunosorbent assay (ELISA) remains a cornerstone strategy for direct protein detection.[335] Beyond antibodies, aptamers have emerged as robust alternatives for capturing protein analytes.[336] These motifs bind targets with high affinity via specific noncovalent interactions, driven by their distinct three-dimensional conformations.

4.1.1.6. Metabolite. Metabolite monitoring enables the tracking of metabolic fluxes associated with disease states or therapeutic interventions.[337] These low-molecular-weight compounds are typically detected via direct redox reactions, enzymatic catalysis, or synthetic receptors. Electroactive species, such as ascorbic acid (AA) and uric acid (UA),

https://doi.org/10.1021/acs.chemrev.5c00801
Chem. Rev. XXXX, XXX, XXX−XXX

Table 4. Comparative Analysis of Biorecognition Elements for Analytical Applications

biorecognition element	target analytes	detection mechanism	chemical functionalization capability	continuous detection feasibility	advantages	limitations	ref
antibody	metabolite, pathogen, small molecule, protein, peptide, nucleic acid, lipid	direct binding affinity	limited	limited	exceptional sensitivity and selectivity	extended incubation requirement	7,346−349
enzyme	metabolite, small molecule	catalytic conversion	limited	excellent	highly specific catalytic activity	environmental instability	350−353
single-stranded DNA	metabolite, pathogen, hormone, small molecule, protein, peptide, nucleic acid, lipid	hybridization/binding	excellent	excellent	programmable sequence design	potential degradation	354−356
aptamer	metabolite, pathogen, hormone, small molecule, protein, peptide, nucleic acid, lipid	direct binding affinity	excellent	excellent	versatile functionalization strategy	potential degradation	357−359
molecularly imprinted polymer	metabolite, small molecule, protein, peptide, lipid	direct binding affinity	excellent	excellent	cost-effective synthesis, superior stability	challenging for macromolecular	107,360−362

undergo direct oxidation at WEs modified with conductive materials.[338] However, this direct electrocatalytic approach is susceptible to interference from coexisting species in complex matrices. Selectivity can be enhanced by engineering permselective organic films on the electrode surface. Conversely, nonelectroactive metabolites, such as glucose[339] and lactate,[340] necessitate oxidase-mediated catalysis. Beyond enzymatic strategies, detection methodologies also employ molecularly imprinted polymer (MIP) as synthetic antibody mimics.[341] MIP technology is applicable in analytical chemistry[107] and drug delivery,[342] ensuring high selectivity while maintaining electrode conductivity.

4.1.1.7. Hormone and Neurotransmitter. Hormone biomarkers and neurotransmitters function as essential chemical messengers mediating intercellular communication. These essential signaling molecules mediate intercellular communication,[343] with detection principles paralleling those of metabolite analysis. Electroactive analytes, such as epinephrine and norepinephrine, are detectable via direct oxidation,[344] whereas nonelectroactive targets utilize aptamer-based recognition, immunoassays, or molecular imprinting.[343]

4.1.1.8. Ion. Inorganic ions (e.g., Na^+, K^+, Ca^{2+}) act as vital physiological indicators, particularly regarding hydration status and osmotic balance. Wearable ion sensing predominantly relies on ion-selective electrode (ISE) technology.[345] These platforms typically comprise conductive substrates, transduction layers, and ion-selective membrane (ISM). Upon applying a potential across the ISM, target ions selectively permeate the barrier, generating a potential difference across the electrical double layer at the membrane−solution interface. This potential correlates with ionic concentration, enabling accurate, time-resolved monitoring of physiological status.

Despite progress, the expansion of detectable analytes in wearable electronics encounters significant hurdles, including insufficient sensitivity and selectivity in complex biofluids and a restricted repertoire of targetable molecules, particularly high-molecular-weight proteins and hormones. Addressing these limitations requires a paradigm shift toward the synergistic integration of multidisciplinary technologies to broaden the panel of disease-relevant analytes and pioneer novel sensing modalities.

4.1.2. Biorecognition Element. The analytical fidelity of biosensing architectures, encompassing both qualitative identification and quantitative profiling, is intrinsically governed by the transduction mechanisms employed. Critical to this detection capability is the robust immobilization of specific recognition receptors onto the WE surface (Figure 5b, Table 4). These biorecognition elements constitute the vital transducer interface, converting specific molecular binding events into electrochemical signals that correlate directly with biomarker concentration. Because suboptimal integration at this interface inevitably precipitates signal degradation and reduced selectivity, optimizing the physicochemical compatibility of these components with the sensor's operational envelope remains a fundamental prerequisite and a key avenue for advancing diagnostic precision.

4.1.2.1. Antibody. Antibodies[7] serve as affinity proteins capable of binding target biomarkers. These recognition elements exhibit exceptional intrinsic sensitivity and specificity, parameters that can be further refined through rational design or directed evolution strategies.[349] While antibodies offer high affinity, their integration into contemporary bioaffinity sensors is frequently constrained to single-use formats. The requirement for multiple incubation and washing steps for receptor regeneration introduces significant complexities for *in situ* continuous biosensing applications.[346]

4.1.2.2. Enzyme. Enzymes[351] represent a foundational class of biorecognition elements in wearable electronics. The majority of enzyme-based sensors couple redox events generated during catalysis with direct or mediator-facilitated electron transfer to the electrode.[363] To accommodate complex metabolic pathways, multiple enzymes can be integrated into reaction cascades, establishing defined input-substrate and output-product trajectories. A distinct advantage of enzyme-based wearable electronics is their suitability for continuous monitoring via catalytic turnover, provided product inhibition is adequately mitigated. Although enzyme-based platforms possess excellent selectivity derived from biological specificity, they remain susceptible to environmental perturbations. To enhance operational stability, enzymes may be encapsulated within MOF, such as zeolitic-imidazolate framework-8 (ZIF-8), thereby facilitating cascade reactions that preserve catalytic activity under physiologically challenging conditions and augment sensor performance.[364]

4.1.2.3. ss-DNA. Electrochemical ss-DNA[356] switches have recently demonstrated efficacy for the reagent-free monitoring of proteins in diverse biological matrices, leveraging the dynamics of molecular pendulums.[354] Mechanistically, the application of a positive potential to the electrode surface induces electrostatic attraction of DNA molecules labeled with redox reporters, thereby reducing the probe−electrode distance. Subsequent target molecule binding modulates the

https://doi.org/10.1021/acs.chemrev.5c00801
Chem. Rev. XXXX, XXX, XXX−XXX

Table 5. Principles and Applications of Electrochemical Analysis Technology

electrochemical analysis type	applied signal	measured signal	core principle	typical application	ref
amperometry	constant potential	current	Faraday's law	enzyme-based glucose monitoring	221,366−369
potentiometry	zero current	voltage	Nernst equation	ion-selective monitoring	3,7,85,370,371
voltammetry	sweeping potential	current	voltammetry map	electroactive molecule monitoring	60,147,372,373
impedance spectroscopy	sinusoidal voltage	impedance/conductance	electrical properties of the interface	cell viability and monitoring	324,374−376

effective mass of the pendulum structure, generating a signal response proportional to the analyte concentration.

4.1.2.4. Aptamer. Aptamers[358] comprise affinity ligands composed of RNA, ss-DNA, or non-natural nucleic acid scaffolds. Utilizing established in vitro selection and enrichment methodologies, these molecules achieve binding affinities and specificities comparable to antibodies. Furthermore, the capacity for chemical synthesis facilitates precise modifications that enhance integration into electronic sensor platforms.[359] Generally, aptamers exhibit superior physicochemical stability relative to antibodies, capable of refolding following exposure to denaturing solvents or elevated temperatures, which supports continuous wearable monitoring via various regeneration strategies.[365] Signal transduction typically relies on target-induced conformational changes that modulate the electron transfer distance between the electrode and a redox reporter (e.g., methylene blue[343] and ferrocene[319]).

4.1.2.5. MIP. MIP[107] offer significant advantages over traditional biological ligands, including enhanced thermal stability, cost-effectiveness, and rapid scalability.[361] The molecular imprinting process entails the formation of a prepolymerized complex in solution via covalent or noncovalent interactions between a template molecule and a functional monomer. This complex is subsequently polymerized with a cross-linking agent to establish a rigid polymer matrix. Upon extraction of the template molecules, imprinted cavities are generated that are complementary to the target in size, shape, and chemical functionality. Consequently, the resultant polymer selectively recognizes and binds the analyte in a manner analogous to antibody−antigen interactions. While the efficacy of imprinting small molecules is well-established, the intrinsic characteristics of proteins (specifically macromolecular size and complex conformational flexibility) continue to present substantial challenges for the development of robust protein-MIPs.

A paramount challenge for biorecognition elements lies in sustaining the continuous operation required for longitudinal monitoring. This necessitates the integration of effective regeneration protocols into wearable electronics to restore the sensor to its baseline state, with the specific regeneration chemistry dependent on the sensor architecture. Furthermore, biological fouling and surface passivation can induce false-positive or false-negative signals, diminishing sensitivity over time. As noninvasive wearable electronics evolve toward long-term continuous monitoring, addressing these interfacial phenomena is imperative to ensure sensors maintain fidelity while exposed to highly heterogeneous biofluids.

4.1.3. Sensing Module and Electrochemical Analysis. Bioelectrochemical systems transduce biological recognition events into measurable electrical signals through the use of electrode-based platforms. In its simplest configuration, a two-electrode setup comprises a WE, at which the electrochemical reaction of interest occurs, and the electrode that provides a known and stable potential and further produces sensing current (I_{sn}) is called the reference electrode (RE). A certain stimulus voltage (V_{st}) is supplied between WE and RE. Ideally, the potential at the electrode−electrolyte interface would be identical to V_{st}. However, beyond the inherent impedance of the electrode−electrolyte interface, the inevitable solution resistance (R_s) along the ionic path to the RE leads to a voltage drop, termed the IR drop. As this value fluctuates with reaction kinetics and environmental conditions, it is widely regarded as a significant experimental error. To mitigate this effect, a three-electrode configuration is ubiquitously employed in modern electroanalysis to eliminate the negative effects of IR drop. This architecture introduces a counter electrode (CE) that serves as the source for the I_{sn}, there will be no current flows through the RE, thereby electrically isolating the RE, and the reaction potential will be accurately controlled. Due to the advantage of eliminating the IR drop effect, the three-electrode system is widely used in electrochemical biosensors. The superior potential control afforded by the three-electrode system makes it the standard for most electroanalytical techniques used in biosensing, which typically employ direct current or low-frequency alternating current waveforms as the electrical stimulus. Consequently, powerful methods such as amperometry, potentiometry, voltammetry, and electrochemical impedance spectroscopy (EIS) are routinely utilized to characterize the bioelectrochemical sensor interfacial phenomena and will be reviewed in this section (Figure 5c, Table 5).

4.1.3.1. Amperometry. In amperometric sensors, the applied potential facilitates the redox reaction of biomolecules, with the electron transfer between these molecules and the electrode quantified as a current signal.[377] Enzymes are commonly incorporated in wearable amperometric sensors due to the remarkable selectivity and reversibility provided by biocatalytic reactions, enabling continuous analysis of target molecules. Biomarkers from biofluids undergo oxidation into byproducts under the catalytic action of the oxidases. Detection of target molecules is accomplished through amperometric techniques, wherein the resulting current response is proportional to the concentration of the target biomarker.

4.1.3.2. Potentiometry. Potentiometric sensors operate based on the potential difference between a RE and a WE without requiring an applied current or potential. ISEs are commonly utilized in wearable biosensors to monitor levels of electrolytes or ions such as Na^+, K^+, and Ca^{2+} in biofluids.[345,378] The WE, commonly referred to as ISE, is typically modified with an ion-selective recognition membrane composed of ion-carrier molecules. The polymer membrane-based ISE allows only corresponding ions with specific charges and sizes to interact. This selective recognition process generates an electrochemical phase boundary potential, which is then converted into a voltage signal by the sensor. According to the Nernst equation, the potential signal measured between the ISE and a RE, such as Ag/AgCl,

https://doi.org/10.1021/acs.chemrev.5c00801
Chem. Rev. XXXX, XXX, XXX−XXX

exhibits a logarithmic linear relationship with the target ion concentration.[379]

4.1.3.3. Voltammetry. Voltammetry involves controlled variation of applied potential with defined steps and rates while monitoring the resulting current signals. Various scanning methods exist for potential variation, including cyclic voltammetry (CV), differential pulse voltammetry (DPV), and square wave voltammetry (SWV). Voltammetry is typically employed to monitor electroactive molecules, such as UA and AA, by detecting their direct redox reactions at specific redox potentials on the electrode surface under an applied potential waveform. Compared to CV, DPV and SWV minimize background charging currents, thus achieving highly sensitive electrochemical measurements. Similarly, anodic stripping voltammetry encompassing a preconcentration step of the analyte followed by a voltammetric scan can detect extremely low concentrations of heavy metals (Cu^{2+}, Zn^{2+}) in biofluids.[380] However, in the absence of specific biological receptors such as enzymes or MIP, the selectivity of voltammetry for detecting electroactive molecules is limited, as different substances may exhibit similar redox potentials and similar indistinct potentials are indicated in the voltammetry curves.

4.1.3.4. EIS. EIS characterizes interfacial phenomena at the electrode−electrolyte boundary. In the context of impedimetric biosensing, the sensor is interrogated by a small-amplitude sinusoidal voltage perturbation, and the resulting phase-shifted and attenuated current response is recorded. For practical sensing applications, this response is often monitored at a single, optimized frequency or a limited subset of discrete frequencies that exhibit maximum sensitivity to the analyte binding event, thereby ensuring a reliable analytical signal. The behavior of the biosensor interface is conceptually modeled by an equivalent electrical circuit (EEC), whose components (e.g., charge-transfer resistance, double-layer capacitance) are altered by the biological process. The real and imaginary components of the impedance are then algebraically derived from this phase-amplitude response to extract the quantitative sensing signal. This principle underpins applications such as the label-free monitoring of changes in cell quantity, size, and shape.[324]

Collectively, sensing modules and electrochemical analysis methods constitute a powerful toolkit for transducing chemical phenomena into electrical signals via faradaic or nonfaradaic processes. These techniques rely on the precise measurement of perturbations in current, potential, or impedance arising from interfacial electron transfer or surface modifications. However, reliance on a single transduction modality can render analytical results vulnerable to matrix-induced interferences and systematic errors. To address this deficiency, the strategic integration of complementary electroanalytical techniques is recommended. By simultaneously monitoring distinct electrochemical parameters, it is possible to cross-validate findings and deconvolute analyte signals from environmental noise, thereby substantially augmenting the robustness and fidelity of bioelectrochemical analysis.

4.1.4. Biofluids. Biofluids within the human body, including sweat, urine, tears, saliva, and interstitial fluid (ISF), constitute rich repositories of clinically relevant biomarkers encompassing metabolites, ionic species, and proteins. The concentrations of these analytes exhibit correlative relationships with their corresponding blood levels,[381] rendering these alternative biofluids valuable for noninvasive diagnostic applications. Contemporary developments in wearable electrochemical monitoring have expanded to encompass additional biofluid targets, including wound fluid,[326,382] exhaled breath,[383] and epidermal molecular flux (EMF) monitoring.[384] Furthermore, certain wearable sensing modalities achieve biofluid analysis through implantable or ingestible configurations, enabling access to cerebrospinal fluid[313] and gastric fluid compartments.[370,385] Nevertheless, the analytical characterization of these biofluids presents significant challenges attributable to their complex microenvironments (exemplified by the bacterial flora and food debris present in the oral cavity), anatomically constrained accessibility (such as the ocular irritation associated with tear stimulation and the subcutaneous localization of ISF), and inherent matrix complexity (Figure 5d, Table 6).

4.1.4.1. Sweat. Sweat constitutes a preeminent biofluid matrix for noninvasive, wearable health monitoring applications.[410] Sweat glands facilitate continuous secretion and transport to the epidermal interface via dermal ductal networks,[411] enabling real-time acquisition. This dynamic physiological monitoring offers superior temporal resolution compared to the discrete blood sampling methodologies.[412] Contemporary acquisition strategies are bifurcated into iontophoresis (IP) and capillary-driven accumulation. IP utilizes low-intensity current to facilitate the transdermal delivery of agonists (e.g., pilocarpine[107]), actively inducing local secretion. However, the translational utility of IP is constrained by stringent safety and analytical requirements: current density and duration must be precisely modulated to prevent thermal or electrochemical tissue damage,[413] and exogenous stimulation may perturb local homeostasis, altering analyte stoichiometry. Furthermore, intersubject variability in skin impedance and secretory responsiveness introduces significant uncertainty in quantitative reproducibility. Conversely, capillary wicking relies on interfacial tension within microfluidic channels or porous matrices to transport sweat.[414] The fidelity of this passive approach depends on the biocompatibility and inertness of the substrate to minimize nonspecific adsorption. While intimate epidermal contact is requisite for fluid capture,[415] excessive compression poses a risk of ductal occlusion. Additionally, advanced encapsulation is often necessary to mitigate evaporative concentration artifacts in microliter-scale samples.

A fundamental impediment to wearable biosensing fidelity is the inherent variability and instability of sweat composition and secretion rates.[416] A primary source of error is the dilution effect,[417] given the aqueous dominance of the matrix, fluctuating secretory flux induces concentration shifts that obscure true physiological baselines. Moreover, perspiration involves complex active secretion and ductal reabsorption mechanisms rather than simple passive filtration,[418] meaning rate variations directly modulate analyte partitioning kinetics. To remediate hydrodynamic artifacts, contemporary strategies integrate real-time rate correction via flow sensors, normalizing raw data through established rate-concentration transfer functions.[417] Complementary advances in microfluidic management[85,413] and algorithmic filtering of rate-induced transients further enhance signal fidelity. Beyond hydrodynamics, environmental parameters (temperature, humidity) and physiological states can induce fluctuations in secretion volume and composition. The dermal barrier further restricts biomarker transport, resulting in low abundance relative to blood[388] and limiting detection primarily to small molecular species.[419] Furthermore, achieving efficient collection in

https://doi.org/10.1021/acs.chemrev.5c00801
Chem. Rev. XXXX, XXX, XXX−XXX

Table 6. Comparative Analysis of Biofluid Sources for Wearable Biosensing Applications

biofluid	target biomarkers	sampling methods	wearable formats	advantages	limitations	ref
sweat	metabolite, electrolyte, metal, protein, hormone, neurotransmitter, peptide, fatty acid	iontophoresis, capillary wicking, passive collection	epidermal patch, temporary tattoo sensor, textile-integrated device	non-invasive sampling, rich biochemical composition	evaporative loss, contamination, limited permeation of high-molecular-weight biomarker	362,386−388
interstitial fluid	metabolite, electrolyte, metal, protein, peptide, amino acid, fatty acid, coenzyme, hormone, neurotransmitter, circulating RNA	microneedle-based extraction, reverse iontophoresis	microneedle array, transdermal patch	rich biochemical composition, minimally invasive compared to venipuncture	user discomfort, limited sampling rate	389−392
saliva	metabolite, electrolyte, protein, hormone, pathogenic	direct contact, immersion	intraoral device, mouth guard	noninvasive and continuous sampling	high viscosity, contamination, complex microbial environment	317,393,394
tear	metabolite, electrolyte, protein, cytokine, antibiotic	direct contact, immersion	smart contact lenses	non-invasive sampling	low secretion rate, potential for ocular irritation	354,395−397
urine	metabolite, electrolyte, toxin, protein, peptide, amino acid, hormone	direct immersion	smart diaper, wearable collection device	non-invasive sampling, relatively large sample volume	restricted to a discrete urination event	398−401
wound fluid	metabolite, electrolyte, nutrient, gas, protein, inflammatory mediator, proteolytic enzyme, pathogenic bacteria, growth factor, cellular component	direct contact	smart wound dressing	rich in clinically relevant biochemical analytes for wound healing assessment	complex and variable composition	292,326,402,403
exhaled breath	volatile organic compounds, aerosolized metabolites, pathogenic bacteria and viruses, and respiratory gas	gas capture, condensation collection	smart face mask, breath analyzer	noninvasive and continuous sampling	limited biomarker diversity, user discomfort	404−407
epidermal molecular flux	volatile epidermal gas, metabolite, electrolyte, metal, protein, hormone, neurotransmitter, peptide, fatty acid	hydrogel-based, closed-cavity	epidermal patch with a collection chamber	noncontact sampling, diverse biochemical information	poor analyte dispersion characteristic, limited permeation of high-molecular-weight biomarker	408,409

populations with diminished perspiration remains a challenge; this often necessitates stimulation methods that may compromise user comfort or analytical integrity,[420] while skin surface contaminants introduce significant interference.[421]

4.1.4.2. ISF. The dermis, characterized by high ISF content, represents the optimal interface for ISF access.[389] Current methodologies predominantly utilize microneedle arrays (comprising hollow, porous, or hydrogel architectures[392]) to facilitate direct monitoring or extraction. This approach significantly reduces invasiveness relative to venipuncture.[422] Micrometer-scale precision in insertion depth is paramount to restrict penetration to the epidermal or superficial dermal layers, thereby isolating probes from deep-tissue vasculature and nerve endings to mitigate hemorrhage and nociception.[423] Despite the minimal invasiveness, patient compliance remains influenced by psychological apprehension regarding puncture. A formidable challenge to long-term functionality is the nonspecific adsorption of proteins at the device-tissue interface.[424] Consequently, advanced surface engineering strategies are critical to inhibit macromolecular accumulation. Alternative strategies, such as reverse iontophoretic extraction, are restricted to small molecules and require precise current modulation to prevent cutaneous irritation.[425] Furthermore, extraction efficiency is highly susceptible to physiological variations in skin impedance and hydration, causing fluctuations in yield.[426] ISF exhibits superior compositional stability and a rich profile of soluble analytes closely correlated with blood.[427] However, long-term sampling stability is suboptimal compared to sweat. Prolonged microneedle arrays deployment may elicit cutaneous hypersensitivity, edema, or inflammation, which can skew analyte concentrations, compromising the representativeness of the sampled fluid.[389]

4.1.4.3. Saliva. Saliva secreted through oral glandular activity offers a rich source of biomarkers, including hormonal mediators and proteins.[428] Monitoring is achieved via intraoral patches[429] or mouthguard-integrated platforms.[430] *In situ* methodologies deploy orthodontic-like architectures for real-time interfacial contact,[431] while indirect protocols utilize absorbent matrices for ex situ analysis.[432] While saliva sampling obviates invasive puncture and provides substantial volumes for extended monitoring, it is rheologically complex and highly susceptible to extrinsic variables.[433] Postprandial alterations, hydration status, and oral hygiene introduce significant analytical deviations. Furthermore, the complex oral microbiome environment can adversely affect sensor sensitivity and precision.[433]

4.1.4.4. Tear. Tears provide a noninvasive medium containing numerous biomarkers, accessible via contact lens-integrated sensors or collection patches.[395] While these modality enhances user acceptance by avoiding tissue trauma, they face challenges related to minimal sample volumes and temporal variability. Tear secretory volumes are limited and highly sensitive to environmental (humidity, airflow) and physiological (stress, blinking) dynamics, resulting in unstable availability that compromises reproducibility. Furthermore, contact lens-based systems pose risks of ocular irritation and potential tissue damage from sensor components. Device engineering must strictly satisfy biocompatibility requirements and miniaturization constraints to accommodate anatomical limitations.[397,433]

4.1.4.5. Urine. Urine offers comprehensive insights into metabolic status and organ function, containing abundant metabolites and electrolytes.[400] Collection is noninvasive and

https://doi.org/10.1021/acs.chemrev.5c00801
Chem. Rev. XXXX, XXX, XXX−XXX

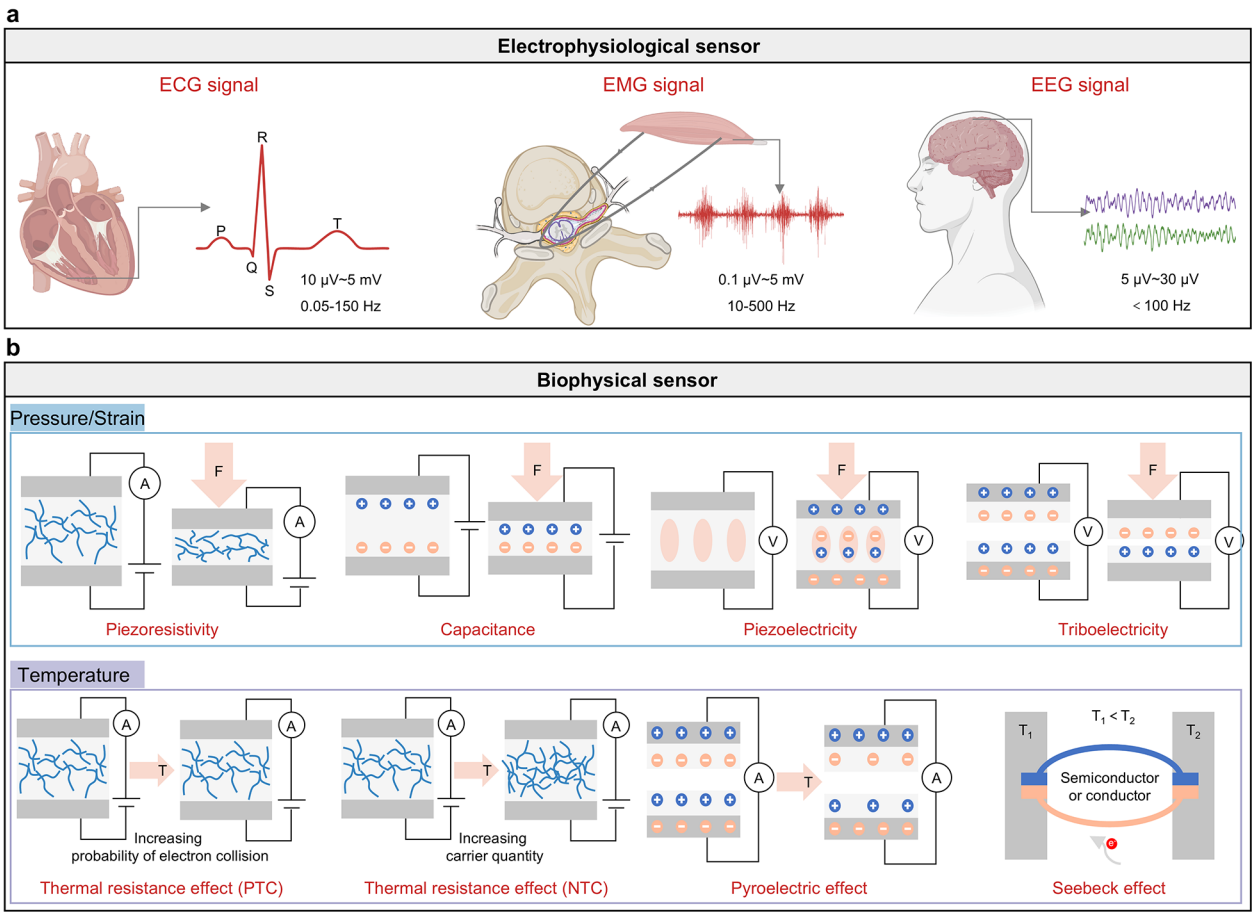

Figure 6. The primary signal generation and transduction mechanisms of wearable electrophysiological and biophysical sensors. (a) Origins and characteristics of electrophysiological signals. (b) Operational principles of biophysical pressure/strain sensors and temperature sensor (schematic deformations are not to scale). Panel 1: Working principles of pressure/strain sensors. (1) Piezoresistive sensor: Utilizes the conductive bridging effect in composite materials, where resistance changes with applied strain. (2) Capacitive sensor: Applied pressure alters the distance between electrodes, thereby changing the capacitance. (3) Piezoelectric sensor: External pressure induces a proportional change in electric dipole alignment and surface charge density. (4) Triboelectric sensor: Generates a signal via contact electrification between two dissimilar surfaces. Panel 2: Working principles of biophysical temperature sensors. (1) Positive temperature coefficient thermistor: Based on composite materials, its resistance increases as temperature rises. (2) Negative temperature coefficient thermistor: Based on composite materials, its resistance decreases as temperature rises. (3) Pyroelectric sensor: Utilizes the change in spontaneous polarization in anisotropic materials in response to a time-varying temperature (dT/dt). (4) Seebeck effect sensor: A temperature gradient across the junction of two dissimilar materials generates a proportional voltage. Abbreviations: ECG, electrocardiography; EMG, electromyography; EEG, electroencephalography; F, force; T, temperature.

high-volume, typically utilizing direct immersion or absorbent materials.[434] Sensors must be disposable or easily sterilized to prevent contamination and resist the corrosive matrix. A primary limitation is the restriction to discrete measurements during micturition, precluding continuous monitoring. Applicability is often limited to specific demographics (e.g., infants, elderly) within wearable contexts. Additionally, analyte concentrations are heavily modulated by hydration status and dietary intake, with excessive fluid consumption leading to dilution effects.[398,433]

4.1.4.6. Wound Fluid. Wound exudate, produced during healing to maintain moisture and deliver nutrients, serves as a critical biomarker source, particularly in chronic nonhealing wounds.[171,325,403] Intelligent dressings integrate sensors for direct contact analysis[382,435] or utilize adhesive patche.[292,382,403] Sterility and nonadherence to tissue are imperative. However, this modality is inapplicable to low-exuding wounds and is constrained by the compositional heterogeneity of exudate. Anatomical inconsistencies and the risk of infection further complicate the standardization of biomarker concentration analysis.

4.1.4.7. Exhaled Breath. Exhaled breath offers a noninvasive avenue for high-frequency monitoring of respiratory and gastrointestinal conditions[406] via volatile organic compounds (VOCs) and exhaled breath condensate (EBC).[407,436] Wearable devices enable real-time capture of gaseous samples.[437] However, mask-based systems may impede user comfort. A significant technical challenge is the high-humidity environment, which necessitates robust waterproofing or sealing layers to prevent sensor degradation.[404] Furthermore, breath composition is susceptible to environmental pollutants and recent behavioral factors (diet, smoking), potentially introducing analytical deviations.

4.1.4.8. EMF. The cutaneous interface governs transdermal chemical transport, influencing health outcomes.[408] EMF encompasses water vapor, metabolites, and VOCs.[384,409] The principal advantage of EMF is its noncontact sampling capability.[438] Monitoring is facilitated by sealed chambers for gaseous analytes[384] or hydrogels for solid epidermal

https://doi.org/10.1021/acs.chemrev.5c00801
Chem. Rev. XXXX, XXX, XXX−XXX

markers.[420] However, poor dispersion of solid markers may compromise epidermal flux efficiency, and sealed chambers may affect comfort. Similar to sweat, the permeation of high-molecular-weight biomarkers is restricted, limiting the scope of detectable analytes.

Wearable biofluid-based sensors still need to be validated through gold-standard diagnostic methods and blood sample test results. Future research needs to further evaluate the impact of measurement environments on device reliability, including: biological factors (such as biofouling or cross-contamination from other biochemical substances in the biofluids matrix), chemical factors (such as pH value changes), physical factors (such as differences in sweat produced during vigorous exercise versus resting states), cross-contamination between biofluids (such as interactions between sweat, saliva, and breath samples), collection methods (such as differences between sweat samples obtained through IP versus exercise-induced sweat), and variations in biofluids secretion sites (such as the uneven distribution of different types of sweat glands along the skin surface, which secrete sweat with specific biochemical components). Additionally, the degradation of the soft−hard interface between the skin and device over time poses risks of fluid leakage, channel blockage, and mechanical failure, warranting advanced research.

4.2. Electrophysiological Sensors

Electrophysiological sensors constitute a critical component in wearable technology, facilitating the monitoring of bioelectric potentials, including ECG,[439] EMG,[440] and electroencephalography (EEG)[10] (Figure 6a). These sensors also find application in neurodegenerative diseases, sleep disorders, sports injury prevention, etc. A significant challenge in the implementation of these sensors lies in establishing a stable, electrically robust, and conformal interface between the skin and the device, while simultaneously shielding against the surrounding electromagnetic wave interference. This typically necessitates the utilization of conductive gels to minimize electrical impedance at the interface.

4.2.1. ECG. An ECG assesses variations in the electrical activity of the heart through surface electrodes (Figure 6a, panel 1). Excitation of cardiomyocytes generates action potentials, resulting in potential differences observable on the body surface. ECG electrodes record these potential differences, providing insights into cardiac rhythm and conduction dynamics. These signals are characterized by distinct waveforms, including P waves, Q-, R- and S-wave (QRS) complexes, and T waves.[441]

4.2.2. EMG. EMG is a technique used to record the electrical activity of skeletal muscle fibers (Figure 6a, panel 2). During muscle contraction, action potentials are initiated at the neuromuscular junctions of muscle fibers.[442] Surface or intramuscular electrodes detect these voltage changes, which reflect muscle activation and fatigue states.[440,443] The EMG signal originates from the action potentials generated by skeletal muscle fibers, typically exhibiting amplitudes ranging from tens of microvolts to several millivolts.

4.2.3. EEG. The EEG records the electrical activity of neuronal populations in the brain via scalp-mounted electrodes (Figure 6a, panel 3).[444] Neuronal activation generates weak electrical signals that propagate through the scalp and are subsequently detected by the EEG electrodes.[445] Notable waveforms include delta (δ), theta (θ), alpha (α), beta (β), and gamma (γ) waves.[10,446] The EEG signal originates from synchronously generated electrical activity in the cerebral cortex, typically characterized by low voltage (microvolt level) with a diverse frequency spectrum.

Wearable electrophysiological sensing technology has achieved real-time monitoring of key physiological indicators such as electrooculography (EOG), skin conductance (skinG). Nevertheless, the clinical translation and large-scale adoption of this technology still face formidable challenges. On a technical level, core bottlenecks constraining signal reliability include precise device calibration, the effective filtering of motion artifacts, and individual variations in sensor placement. To overcome these hurdles, future research must focus on developing robust calibration models and signal processing algorithms by investigating electrophysiological waveforms in-depth, innovating sensor technology to enhance signal-to-noise ratio (SNR) and biocompatibility. The challenges in clinical integration are equally prominent. To ensure acceptance by the healthcare system, it is imperative to conduct rigorous clinical validation of accuracy and reliability across large-scale, diverse population cohorts and to establish standardized benchmarks against clinical gold-standard, thereby guaranteeing the sustained precision and clinical significance of device calibrations and real-time physiological metrics.

4.3. Biophysical Sensors

The operational paradigm of biophysical sensors relies on the transduction of mechanical deformations,[170,447] thermal fluctuations,[448] or kinetic movements[449] into readable electrical signals via the modulation of capacitance or resistance within the sensing architecture (Figure 6b). A pivotal advancement in this domain involves the integration of acoustic[450] and ultrasonic[451] modalities, which significantly expands the scope of physiological monitoring. These sophisticated biophysical sensing systems facilitate the comprehensive analysis of gait kinetics, locomotor activity, respiratory mechanics, and vocalization patterns. Wearable pressure sensors, in particular, exploit a spectrum of electromechanical transduction mechanisms to convert physiological pressure gradients into quantifiable electrical outputs. Contemporary research in pressure sensing emphasizes the optimization of sensitivity and mechanical compliance through the synergy of novel material integration and structural engineering, with a specific focus on micropatterned architectures.[452] Concurrently, high-fidelity wearable temperature sensors enable the real-time quantification of cutaneous thermal variations, providing critical data streams for prophylactic healthcare, exertion management, and personalized therapeutic interventions.

4.3.1. Pressure/Strain Sensor. Mechanically compliant sensors capable of resolving strain and pressure constitute a rapidly evolving frontier at the intersection of materials science and biomedical engineering. The utility of these devices spans the real-time monitoring of subtle endogenous physiological pressures, such as intraocular pressure[293] and arterial blood pressure (BP),[453] to gross exogenous biomechanical stimuli, including flexion[454] and tensile deformation.[455] The fundamental transduction mechanism hinges on the strategic implementation of mechanoresponsive materials,[456] which actuate the conversion of mechanical energy into discernible electrical signals. This transduction is generally governed by one of four established physical principles: piezoresistivity, capacitance, piezoelectricity, or triboelectricity (Figure 6b, panel 1).

https://doi.org/10.1021/acs.chemrev.5c00801
Chem. Rev. XXXX, XXX, XXX−XXX

4.3.1.1. Piezoresistivity. Wearable piezoresistive sensors[457] transduce surface pressure into resistance modulations via the piezoresistive effect, facilitating quantitative pressure metering and continuous surveillance. Resistance-based mechanisms satisfy diverse application requirements by employing scalable material systems, facile fabrication protocols, and conventional readout instrumentation. Under compressive strain, the diminution of interparticle separation promotes quantum tunneling effects and the percolation of conductive networks. Despite the high gauge factors exhibited by composite-based sensors, they frequently suffer from hysteresis, signal drift, sluggish response kinetics, and batch-to-batch variability. These limitations arise primarily from the stochastic nature of contact junction formation and the instability of tunneling interfaces. Furthermore, the susceptibility of material resistance to environmental variables, such as thermal fluctuations and humidity, compromises longitudinal signal fidelity. Consequently, future research must prioritize the decoupling of pressure-induced resistance changes from these confounding environmental factors to ensure clinical-grade accuracy.

4.3.1.2. Capacitance. Capacitive sensors[458] generally utilize a parallel-plate architecture wherein a dielectric material is sandwiched between two electrodes. These devices exhibit capacitance modulation under normal pressure due to the mechanical deformation of the dielectric layer. The capacitance variation is intrinsically governed by the interplay between the spatial dielectric constant, the relative permittivity of the dielectric medium, the effective electrode overlap area, and the separation distance. In contrast to piezoresistive mechanisms, capacitive sensors demonstrate a reduced dependence on the intrinsic charge transport properties of specific functional materials, operating effectively within a fundamental conductor−insulator-conductor configuration. Nevertheless, the selection of constituent materials and their geometric dimensions critically dictates baseline capacitance and pressure sensitivity. Specifically, dielectric materials with lower elastic moduli undergo greater deformation under a given stress, thereby enhancing sensitivity. While the straightforward design and fabrication of capacitive sensors are advantageous, inherent limitations such as modest capacitance modulation ranges and diminishing SNR at reduced dimensional scales necessitate the development of advanced dielectric microstructures to amplify sensitivity.

4.3.1.3. Piezoelectricity. Distinct from piezoresistive and capacitive modalities that necessitate external power supplies, piezoelectric materials function as energy-autonomous systems, generating surface potential differences in response to mechanical deformation.[454] These materials facilitate the sensing of dynamic pressure through direct mechanical-to-electrical energy transduction. In crystalline inorganic materials, the piezoelectric effect originates from ionic displacement within noncentrosymmetric crystal lattices, whereas in organic piezoelectric polymers, it derives from the conformational reorientation of polar polymer chains. This mechanism enables the measurement of potential differences without voltage bias, supporting the development of self-powered sensing platforms.[459] Fundamentally, the process relies on pressure-induced lattice deformation in materials with noncentrosymmetric point group symmetry, where external force shifts the geometric centers of positive and negative charges. This polarization subsequently induces charge redistribution in proximal conductive materials, requiring readout circuits optimized for high-impedance sources to prevent charge leakage.

4.3.1.4. Triboelectricity. Analogous to piezoelectric sensors, triboelectric devices[460] convert mechanical pressure variations into electrical outputs without external power input. The mechanism relies on contact electrification, where charge separation is driven by disparities in electronegativity, surface morphology, and physicochemical properties between contacting interfaces. Upon intimate contact between two dissimilar materials, electron transfer occurs across the interface to equilibrate chemical potentials. The transduction process proceeds through distinct contact and separation phases. During contact, opposing charges neutralize; during separation, the establishment of a dipole layer creates an electron potential gradient, driving current flow through an external load. Recent advances integrating nanostructured materials have substantially augmented the effective surface area, thereby enhancing charge density and triboelectric performance.[461] However, addressing the mechanical wear associated with friction and ensuring long-term stability remains a critical direction for the maturation of this technology.

4.3.2. Temperature Sensor. Physiological temperature serves as a critical biomarker intimately linked to homeostatic regulation and pathological states. While conventional mercury thermometers and rigid electronic circuitry provide accuracy, they lack the mechanical compliance necessary for continuous, noninvasive monitoring. In contrast, wearable sensing platforms offer conformal adhesion to cutaneous surfaces and enhanced biocompatibility, enabling real-time tracking of thermal dynamics.[462] These flexible systems facilitate deployment across varied operational settings, proving particularly valuable for detecting pyretic deviations. Despite the relatively narrow thermal window of the human body, precise detection is achieved through three predominant transduction mechanisms: the thermal resistance effect, the pyroelectric effect, and the Seebeck effect (Figure 6b, panel 2).

4.3.2.1. Thermal Resistance Effect. Thermoresistive transduction represents the most prevalent mechanism in flexible temperature sensing, manifesting as a modulation of electrical resistance in response to thermal perturbations. This behavior bifurcates into positive temperature coefficient (PTC)[463] and negative temperature coefficient (NTC)[464] responses. The PTC characteristic typically arises from enhanced scattering probabilities of high-energy charge carriers as thermal energy increases, yielding elevated resistance. Conversely, NTC behavior is governed by the thermal activation of charge carriers, thermal energy promotes the excitation of valence electrons to conduction states, thereby augmenting carrier density and reducing overall resistance.

4.3.2.2. Pyroelectric Effect. The pyroelectric effect exploits the spontaneous polarization of anisotropic, noncentrosymmetric dielectric materials in response to transient thermal stimuli (dT/dt).[465] Under time-dependent temperature fluctuations, the internal dipole moments of these polar materials reorient, inducing uncompensated bound charges at the material surfaces and generating a measurable current.[466] This dynamic response mechanism is integral to the fabrication of nanogenerators, facilitating dual functionality in energy harvesting and self-powered temperature sensing.[467]

4.3.2.3. Seebeck Effect. The Seebeck effect represents a thermoelectric conversion phenomenon that exploits temperature gradients across heterogeneous material junctions to drive charge carrier migration and establish electrical current

https://doi.org/10.1021/acs.chemrev.5c00801
Chem. Rev. XXXX, XXX, XXX−XXX

Component category	Core component	Primary function	Materials/Technologies	Critical design parameters
Substrate	Flexible polymer/elastomer	Mechanical support	PET, PI, PDMS, PU, SEBS	Mechanical flexibility, biocompatibility
	Textile-based substrate	Mechanical support	Cotton, polyester, conductive textile	Laundering durability, elastic recovery
	Paper-based substrate	Mechanical support	Cellulose-based material	Mechanical flexibility, degradation, extensibility
Electronic processing unit	Microcontroller unit	Computational operation, logic control	—	Power consumption, miniaturization
	Analog-to-digital /digital-to-analog conversion	Sensor signal conversion	—	Conversion precision, sampling frequency
	Memory module	Data storage	—	Storage capacity, data transfer rate
Wireless communication unit	Bluetooth low energy	Short-range data transmission	—	Communication range, power consumption
	Wireless local area network	Short-range data transmission	—	Communication range, power consumption
	Fifth-generation mobile communication	Long-range data transmission	—	Communication range, power consumption
	Near field communication	Proximity data transmission	—	Communication range, security protocol
Power subsystem	Energy harvesting module	Ambient energy harvesting	Photovoltaic cell	Energy conversion efficiency, output stability
	Energy storage module	Electrical power supply	Flexible aqueous battery	Mechanical flexibility, energy density, safety
	Power management	Safe battery operation	—	—
Encapsulation	Hydrophobic barrier structure	Moisture ingress prevention	Waterproof adhesive resin	Ingress protection rating, vapor permeability
	Biocompatible encapsulation	Skin irritation prevention	Medical-grade PET	Chemical stability, biocompatibility
	Electromagnetic interference shielding	Signal interference shielding	Conductive epoxy resin	Mechanical flexibility, electromagnetic isolation

Figure 7. Fundamental system-level components for wearable electronics. Abbreviations: PET, polyethylene terephthalate; PI, polyimide; PDMS, polydimethylsiloxane; PU, polyurethane; SEBS, styrene−ethylene−butylene−styrene.

flow.[468] The Seebeck coefficient is defined as the ratio of induced electric field intensity to the applied temperature gradient: Seebeck coefficient = dV/dT, where dV and dT denote the potential difference and temperature differential between the cold junction (T_1) and hot junction (T_2), respectively.[469] Compared to alternative temperature measurement mechanisms, the Seebeck effect demonstrates immunity to mechanical strain influences, thereby circumventing temperature-strain signal coupling phenomena commonly encountered in flexible and stretchable temperature sensing devices.[470] However, Seebeck effect manifestation requires the establishment of temperature differentials across the sensing element.[471] Because the human body temperature is relatively constant, and as the heat is transferred to the device, the signal generated by the Seebeck effect becomes lower.

5. FUNDAMENTAL SYSTEM-LEVEL COMPONENTS

Upon synthesis and deposition on flexible supports via micro/nanofabrication protocols, wearable sensor electrodes are integrated with electronic circuitry and power subsystems to constitute comprehensive wearable systems. These circuits execute critical operations: harvesting and regulating energy from flexible power units, acquiring electrical signals indicative of physiological parameters from sensing electrodes, and subsequently conditioning, amplifying, and wirelessly transmitting the resultant data. The architectural design of such systems necessitates the rigorous definition of boundary conditions, including data fidelity requirements, user comfort, energy consumption constraints, and wireless telemetry range specifications (Figure 7).

5.1. Substrate

The substrate serves as the foundational chassis, providing mechanical support and a stable platform for the functional components of wearable electronics.[472] To satisfy the rigorous demands of practical deployment, an ideal substrate must exhibit a multifaceted performance profile. Mechanical compliance is paramount; the device must conform intimately to the curvilinear topography of the human body and accommodate dynamic strain associated with natural kinematic movement.[472] Furthermore, the substrate requires sufficient mechanical toughness to withstand external physical pressure during routine operation, thereby maintaining the structural integrity of the electronic assembly.[473] Biocompatibility is a non-negotiable criterion; materials at the biointerface must demonstrate negligible cytotoxicity and allergenic potential to ensure safety during prolonged epidermal contact.[474] Substrate

https://doi.org/10.1021/acs.chemrev.5c00801
Chem. Rev. XXXX, XXX, XXX−XXX

permeability also constitutes a critical parameter, facilitating moisture management to enhance user comfort during extended wear.[475]

Prevalent substrate materials include a spectrum of flexible polymers and elastomers, notably polyethylene terephthalate (PET), polyimide (PI), polydimethylsiloxane (PDMS), polyurethane (PU), and styrene-ethylene-butylene-styrene (SEBS) block copolymers.[296] Contemporary requirements for enhanced biocompatibility, breathability, and seamless integration have catalyzed interest in textile- and paper-based substrates, utilizing cotton, conductive fabrics, and cellulosic materials.[476] Concurrently, advances in materials science have enabled the engineering of novel composite substrates. These composites synergistically merge the advantageous mechanical and physicochemical properties of constituent materials, mitigating the mechanical impedance mismatch between rigid electronics and soft tissue, thus optimizing overall system performance and broadening the design space for next-generation electronics.

5.2. Electronic Processing Unit

The electronic processing unit functions as the computational core of the wearable system, orchestrating signal amplification, filtration, analog-to-digital conversion (ADC), and advanced data processing to derive diagnostic insights from raw sensor inputs. Biosignals acquired in wearable configurations typically possess low amplitudes and are highly susceptible to motion artifacts and environmental noise, necessitating robust signal conditioning strategies. The architectural design of these units demands a critical optimization between computational throughput and power efficiency. Given that wearable devices operate under stringent energy budgets, the processing architecture must maximize algorithmic capability while minimizing quiescent and active power consumption to extend battery life.

State-of-the-art implementations frequently utilize low-power microcontroller units (MCU) as central control elements, complemented by optimized algorithms for efficient signal analysis.[6] The signal chain generally incorporates digital-to-analog conversion (DAC) and ADC stages to digitize physiological signals.[477] Following digitization, data are buffered in read-only memory (ROM) or random-access memory (RAM) modules for transient or persistent storage.[478] Commensurate with the expanding functional density of wearable technologies, modern processing units increasingly integrate on-node computational capabilities, such as artificial intelligence (AI) and machine learning (ML) algorithms.[479] These edge-computing enhancements facilitate the real-time fusion and analysis of multimodal data, providing end-users with comprehensive, high-fidelity monitoring of health status and biophysical activity.

5.3. Wireless Communication Unit

Wireless telemetry is indispensable for the functionality of modern wearable electronics, governing data offloading and system interconnectivity.[480] Among these, wireless local area network (WLAN), fifth-generation mobile communication technology (5G), Bluetooth low energy (BLE), and near field communication (NFC) are selected based on their specific power consumption profiles and integration feasibility. Under standard operating conditions, WLAN performance is dictated by router specifications and spectral allocation.[481] BLE protocols, operating at 2.4 GHz, offer an effective transmission range of approximately 100 m using compact antenna designs, though they necessitate an autonomous, continuous power reserve.[482] Conversely, NFC technology operates over significantly shorter ranges of approximately 10 cm but offers a distinct advantage in energy management.[483]

5.4. Power Subsystem

The functionality and utility of wearable electronics are fundamentally governed by the efficacy of their power subsystems, which face the dichotomy of delivering high conversion efficiency and extended operational autonomy within increasingly miniaturized, conformable form factors. A resilient power architecture for such biointegrated devices is predicated on the synergistic engineering of three functionally distinct yet deeply coupled domains. First, energy harvesting confers device autonomy,[484] thereby establishing a persistent power supply. Second, energy storage serves as the requisite buffer, utilizing high energy-density and power-density electrochemical systems.[485] This component must reliably accumulate intermittent energy from harvesting modules or external charging interfaces while dynamically addressing the stochastic load profiles of the system. Finally, power management functions as the regulatory core. It executes critical operations including voltage conversion, implementation of sophisticated charging protocols,[486] and multitiered protection against electrical or thermal anomalies, thus optimizing energy throughput and ensuring systemic safety. The holistic codesign and functional integration of these three domains are paramount, collectively dictating the energy efficiency, operational endurance, and clinical or commercial viability of advanced wearable systems.

5.4.1. Energy Harvesting Modules. Ubiquitous energy sources present in the physiological and ambient environment, including ranging from biochemical energy in perspiration and body heat, to biomechanical kinetic energy, can also be harvested to sustain wearable devices. For on-skin sensing applications, the critical challenge lies in developing flexible harvesting modules that maintain conformal skin contact, efficiently transduce environmental stimuli, and seamlessly integrate with storage elements to buffer power disparities.

5.4.1.1. Biofuel Cells-Based Sweat Power Generation. Biofuel cells (BFCs) exploit enzymatic catalysis to harvest bioelectricity from redox-active metabolites present in perspiration.[487] In the context of wearable electronics, BFCs represent a chemically intrinsic power solution, with lactate serving as a primary fuel source due to its high physiological concentration during physical exertion. Lactate BFC architectures typically comprise an anode functionalized with lactate oxidase (LOx) and redox mediators to facilitate lactate oxidation, coupled with a cathode engineered with high-surface-area catalysts to accelerate the oxygen reduction reaction.[488] While lactate remains the predominant fuel, BFCs utilizing glucose, ethanol, and other biomarkers have also been demonstrated,[489] expanding the scope of metabolic energy harvesting.

5.4.1.2. Kinetic Generator. Biomechanical motion offers a substantial reservoir of kinetic energy, harvestable via triboelectric nanogenerators (TENGs)[490] and piezoelectric nanogenerators (PENGs).[491] Since their seminal introduction in 2012,[492] TENGs have been rigorously optimized for wearable applications. These devices operate on the principles of contact electrification and electrostatic induction between materials with distinct electron affinities. Wearable TENG and PENG architectures effectively scavenge energy from heel strikes

https://doi.org/10.1021/acs.chemrev.5c00801
Chem. Rev. XXXX, XXX, XXX−XXX

during ambulation or joint flexion during muscle contraction, delivering power densities sufficient to drive functional wearable electronics.[493,494]

5.4.1.3. Thermoelectric Generator. Thermoelectric generators transduce the thermal gradient between the human epidermis and the ambient environment into electrical energy via the Seebeck effect.[495] However, the performance of conventional thermoelectric generators is intrinsically limited by fluctuations in ambient temperature, which dictates the magnitude of the thermal gradient. Contemporary research emphasizes the material engineering of semiconductors with enhanced Seebeck coefficients and suppressed thermal conductivity.[496] Furthermore, recent advances address the thermodynamic equilibrium caused by device heat accumulation; strategies include the integration of heat sinks on flexible substrates to sustain the necessary temperature differential between the body and the environment.[497]

5.4.1.4. Photovoltaic Cells. Ambient illumination represents a high-density power source applicable to diverse operational scenarios. While commercial photovoltaics rely heavily on rigid inorganic silicon due to superior quantum efficiency,[498] their mechanical rigidity and spectral mismatch with indoor lighting constrain their utility in conformal wearables. The emergence of organic−inorganic perovskite photovoltaics in 2009 initiated a paradigm shift, offering exceptional photoelectric performance and tunable bandgaps.[499] These next-generation cells are capable of high power density in both outdoor and low-light indoor environments.[500] Crucially, organic and perovskite materials offer distinct advantages over inorganic counterparts for wearables, including solution-processability, and inherent mechanical flexibility suitable for skin-interfacing devices.

5.4.1.5. Wireless Energy Harvesting. Battery-free architectures can utilize radio frequency identification (RFID) protocols, harvesting electromagnetic energy via near-field inductive coupling between conductive coils and NFC-enabled readers.[501] However, the geometric footprint required for inductive coils poses challenges for miniaturization, particularly in deep-tissue implants such as cardiac pacemakers.[502] In this context, magnetoelectric (ME) wireless power transfer has emerged as a transformative alternative, enabling scalable, untethered bioelectronic networks.[503] The defining advantage of ME transduction is its field-mediated operation, which obviates the need for precise focal alignment. Nevertheless, the utility of wireless harvesting is bounded by transduction inefficiencies. The multistage electrical-magnetic conversion is susceptible to attenuation, a deficiency that becomes critical in long-term in vivo applications where energy dissipation manifests as parasitic heat.[504] This uncoupled energy presents nontrivial risks of thermal cytotoxicity or histological damage to surrounding tissues, necessitating rigorous thermal management.

5.4.1.6. Hybrid Energy Harvesting. Given that individual harvesting modalities possess intrinsic limitations, hybrid architectures combining multiple transduction mechanisms allow for enhanced reliability and expanded application scenarios. Complementary harvesting[505] (e.g., simultaneous photovoltaic and thermoelectric, or biochemical and biomechanical) ensures continuous power output even when a single source is intermittent. Furthermore, synergistic integration can extract energy from a single complex source, such as sunlight (providing both photons and heat) or sweat (coinciding with motion), thereby maximizing the total power conversion efficiency of the system.

In summary, energy harvesting modules provide critical supplementary power, extending the operational duty cycle of wearable devices. When coupled with efficient storage, these systems can mitigate reliance on bulky lithium-ion batteries (LIBs), reducing recharging frequency and enhancing user compliance.

5.4.2. Energy Storage Modules. Energy storage constitutes the most materials-intensive challenge within the wearable power subsystem. These components must deliver reliable electrochemical performance within safe thermal limits while emulating the mechanical properties of textiles, including softness and washability.[506] Contemporary flexible storage technologies predominantly follow two morphological trajectories: rechargeable flexible batteries and supercapacitors. Structurally, these devices have evolved into thin-film[507] and fiber-based[508] configurations, utilizing modified electrolytes to achieve the flexibility and stretchability mandated by practical wearable applications.[509]

5.4.2.1. Flexible Battery. Commercial wearable devices largely rely on rechargeable LIBs due to their high specific energy. However, conventional LIBs pose inherent safety risks, including thermal runaway and electrolyte leakage.[510] Development trajectories for wearable batteries focus on structural innovations, such as fiber-woven or interlocking architectures, to impart stretchability.[508] Alternative chemistries aim to circumvent the safety and rigidity limitations of LIBs by employing aqueous electrolytes and polyvalent metal ions.[511] Notable examples include aqueous cobalt−zinc,[512] flexible zinc-ion,[513] and ammonium-ion batteries,[514] which offer environmentally benign and biocompatible power sources suitable for intimate skin contact.

5.4.2.2. Wearable Supercapacitor. Supercapacitors offer a distinct power profile characterized by rapid charge/discharge rates and high power density.[515] Charge storage is achieved through two principal mechanisms: electric double-layer capacitance at the electrode/electrolyte interface and pseudocapacitance arising from reversible surface redox reactions.[516] Current research prioritizes the maximization of areal capacitance concurrent with miniaturization. Strategies to enhance EDLC involve heteroatom doping of carbonaceous materials to increase specific surface area, while transition metal oxides and conductive polymers are employed to augment pseudocapacitive contributions. Morphological engineering parallels that of batteries, focusing on conformable films[516] and fiber-like[517] architectures compatible with textile integration.

A paradigm shift is required to transition from rigid, sealed energy storage to wearable systems. Unlike traditional designs that prioritize energy density within fixed volumes, wearable power sources must exhibit dynamic mechanical adaptability. Flexibility and stretchability are fundamental prerequisites; devices must withstand repetitive bending, twisting, and strain without structural delamination or performance degradation. Furthermore, given the proximity to the skin, safety is nonnegotiable. Risks such as toxic electrolyte leakage and overheating must be eliminated through the use of thermally stable, flame-retardant electrolytes and biocompatible encapsulation. Ultimately, stability in this domain is bifurcated: mechanical stability ensures physical integrity under deformation, while electrochemical stability guarantees that performance metrics (capacity, voltage plateau) remain invariant under mechanical stress, ensuring reliable long-term service.

https://doi.org/10.1021/acs.chemrev.5c00801
Chem. Rev. XXXX, XXX, XXX−XXX

5.4.3. Power Management Unit. For long-term, epidermal electronic applications, safety and operational endurance are paramount. The power management unit typically integrates a power management integrated circuit with peripheral protection networks to regulate charge/discharge cycles. The power management integrated circuit orchestrates power distribution based on the real-time state of device subcomponents, prioritizing critical sensing or transmission functions to ensure operation within safe thermal, current, and voltage envelopes.[518] In energy harvesting scenarios, boost converters are essential to up-convert low-voltage outputs from harvesters to levels sufficient for storage charging.[486] These circuits facilitate the rectification and regulation of sporadic energy inputs into batteries or supercapacitors. Additionally, precision threshold control and overvoltage/overcurrent protection mechanisms are critical to preventing degradation of the storage medium, thereby securing the operational integrity of the wearable system.

5.5. Encapsulation

Encapsulation represents a pivotal stage in the fabrication of wearable electronics, facilitating component integration while simultaneously shielding internal mechanisms and augmenting overall device efficacy. Robust encapsulation architectures are essential for mitigating component degradation induced by environmental stressors, thereby ensuring operational reliability across rigorous conditions.[519] For instance, hydrophobic barrier structures enable functionality in aqueous media by precluding fluid permeation and subsequent failure of electronic circuits.[520] Concurrently, electromagnetic shielding strategies suppress internal signal crosstalk and attenuate external electromagnetic interference.[521] The design of encapsulation protocols requires meticulous engineering to minimize impedance to electronic performance. Optimal architectures must achieve a balance between protective utility and signal transmission efficiency, while also addressing ergonomic factors such as device aesthetics and mechanical compliance. The utilization of low-density materials and compact structural designs significantly alleviates the physical burden during prolonged epidermal contact. Furthermore, the selection of highly biocompatible encapsulation interfaces is imperative to sequester potentially cytotoxic internal elements, preventing the leaching of hazardous substances into biological tissues.[522]

The constituents of fundamental system-level components function synergistically to establish comprehensive sensing platforms. Rather than a mere aggregation of discrete parts, the architecture of a wearable system operates as a cohesive, interdependent continuum where the sensing interface, substrate, processing logic, wireless communication modules, power subsystems, and encapsulation strategies are inextricably coupled. The operational parameters of these fundamental units are intrinsically linked and reciprocally constraining. For example, enhanced sensor fidelity mandates increased data throughput, which necessitates superior computational capacity from the processing unit. This escalation in processing load directly correlates with increased energy consumption, imposing stringent constraints on the energy density and form factor of the power source. Therefore, the advancement of wearable technology requires not merely the isolated enhancement of individual metrics, but a holistic, system-level optimization to establish a synergistic equilibrium among conflicting performance vectors.

6. CORE PERFORMANCE CHARACTERIZATION

Rigorous quantification of performance metrics constitutes a fundamental prerequisite for evaluating the technological maturity and translational viability of wearable electronic systems. These figures of merit are not merely decisive in establishing a device's capacity to resolve subtle physiological signals with high fidelity, but they are also inextricably linked to functional reliability in uncontrolled environments and, consequently, user adoption. A systematic and critical interrogation of these indicators is therefore indispensable. Accordingly, this section provides a comprehensive assessment of these core performance characteristics (Table 7). To advance the field, future endeavors must prioritize the establishment of consensus testing standards and robust validation frameworks that effectively bridge the gap between idealized laboratory characterization and *in situ* performance under realistic operational conditions.

6.1. Sensitivity

The capacity of a sensing platform to transduce minute variations in an input stimulus into a quantifiable output signal is defined as sensitivity.[298,541] Within the linear dynamic range of a calibration curve, this metric is mathematically defined by the slope, where sensitivity = Δoutput/Δinput. To decouple performance from geometric disparities and facilitate rigorous cross-comparison among diverse architectures, sensitivity is frequently normalized to the electrode area.[107,542] The magnitude of sensitivity is governed by the convolution of several physicochemical determinants, including the electrochemically active surface area,[220] the intrinsic electronic transport properties of the sensing material, and the micro/nanoscopic topology of the sensing interface.[543] Consequently, state-of-the-art strategies for augmenting sensitivity predominantly emphasize materials design and surface engineering. Prevalent approaches include the integration of functional nanostructures[107,120,136] to leverage quantum confinement effects and elevated surface-area-to-volume ratios; the modulation of electronic transport via doping and advanced synthesis methodologies;[544] and the rational architecting of the sensing interface to maximize the density, accessibility, and utilization of active sites. A critical limitation in contemporary literature is the tendency to optimize sensitivity in isolation, neglecting trade-offs with other pivotal metrics. An exclusive focus on hyper-sensitivity through aggressive surface modification or extreme nanostructuring frequently precipitates increased baseline noise and compromised reproducibility, ultimately undermining the device's practical utility. Rectifying this deficiency necessitates a holistic optimization framework that harmonizes sensitivity with device durability and operational reliability.

6.2. Limit of Detection (LOD)

The limit of detection (LOD) serves as a fundamental figure of merit for wearable sensors, delineating the minimum analyte concentration or physiological signal intensity distinguishable from background noise with statistical confidence. Quantitatively, the LOD is conventionally expressed as LOD = $3\sigma/s$,[361,545] where σ represents the standard deviation of the blank measurement and s denotes the analytical sensitivity. The achievable LOD is dictated by the interplay of baseline noise, temporal signal drift, and the inherent responsivity of the transduction element. Minimizing the LOD typically demands a coordinated, multilevel engineering strategy. Hardware-level interventions focus on the design of low-noise electronic front-

https://doi.org/10.1021/acs.chemrev.5c00801
Chem. Rev. XXXX, XXX, XXX−XXX

Table 7. Evaluation of Core Performance Characterization for Wearable Electronics

performance parameter	definition	calculation method	influencing factors	improvement strategies	ref
sensitivity	rate of response change relative to input stimulus	slope of linear fitting curve (Δoutput/Δinput)	effective electrode area, material property, surface morphology	nanomaterial utilization, structured surface design	158,159,523,524,525,526
limit of detection (LOD)	minimum detectable stimulus magnitude	calculation via the LOD = $3\sigma/s$ formula	baseline noise, signal drift, material limitation	noise reduction circuit implementation, material optimization	353,371,527
response time	duration to reach 90% of the steady-state response	step response test measurement	mass transfer rate, reaction kinetics, geometric structure	electrode geometry optimization, diffusion condition control	49,164,528,529
linear range	concentration span exhibiting linear response	linear regression analysis ($R^2 \geq$ 0.99)	surface saturation, nonlinear dynamic effect	piecewise linear calibration, nonlinear algorithm compensation	159,396,457,530−532
selectivity	target analyte recognition capability	response comparison against the interferent	cross-reactivity, matrix effects, competitive adsorption	anti-fouling design, selective recognition membrane integration	107,172,345,533−535
stability	performance consistency over time	temporal RSD% calculation	material aging, surface contamination/passivation, temperature fluctuation	device encapsulation, periodic regeneration, temperature compensation	40,303,306,316,536,537
reproducibility	response consistency across batch/operator	inter-batch RSD% calculation	fabrication process variation, environmental condition, operational standardization	fabrication standardization, environmental condition control	107,220,538
signal-to-noise ratio (SNR)	ratio of effective signal strength to background noise	calculation via the SNR = S/N formula	electromagnetic interference, thermal noise, circuit noise	electromagnetic shielding, filter circuit integration	314,539,540

ends, impedance matching optimization, and the deployment of effective electromagnetic shielding. From a signal processing perspective, LOD enhancement is achieved through advanced noise-suppression algorithms, signal averaging, and optimized transconductance for intrinsic amplification.[546] Concurrently, materials science contributes by chemically modifying or structurally engineering the transducer to amplify specificity and gain toward the target analyte.[547] A prevalent deficiency in reported systems is the insufficient accounting for real-world stochastic factors, such as motion artifacts, biofouling, and long-term drift, when determining LOD values. LOD established under idealized laboratory conditions frequently overestimate performance in wearable or in situ applications. To mitigate this discrepancy, future investigations should emphasize standardized LOD determination under application-relevant conditions.

6.3. Response Time

The response time is defined as the interval required for the sensor output to reach 90% or 95% of its steady-state value, respectively, following a step perturbation in analyte concentration or input signal.[548] The overall temporal behavior is governed by mass transport kinetics to the transducer surface, the thermodynamics of the dynamic interface, and device geometry, specifically the thickness, porosity, and tortuosity of diffusion-limiting layers. Engineering strategies to accelerate response and recovery kinetics, therefore, focus on mitigating transport and interfacial resistance. Representative approaches include the fabrication of micro- and nanostructured electrodes to truncate diffusion path lengths. Alternative methods involve optimizing membrane architectures by minimizing thickness and tuning porosity, introducing aligned transport channels, and enhancing analyte delivery efficiency via microfluidic integration, convective flow, or active pumping mechanisms. However, efforts to minimize response time frequently overlook the critical interdependence between kinetics, sensitivity, and stability. Excessive reduction of membrane thickness or aggressive porosity enhancement can compromise mechanical integrity, exacerbate signal noise, and heighten vulnerability to environmental perturbations. Addressing these limitations requires systematic kinetic modeling that incorporates realistic transport phenomena, alongside the design of adaptive architectures that sustain rapid response while preserving structural robustness and signal fidelity.

6.4. Linear Range

The linear range is defined as the concentration interval or stimulus magnitude over which the measured signal maintains a robust linear relationship with the input. Within this regime, the sensor output is directly proportional to the analyte level, enabling reliable quantification via linear regression.[549] The quality of this fit is commonly evaluated using the coefficient of determination (R^2), with values approaching 1.0 indicating high linearity. Deviations typically emerge at concentrations exceeding the upper limit, where phenomena such as active-site saturation, mass-transport limitations, or the onset of complex nonlinear reaction kinetics become dominant. At the lower limit, the linear range is constrained by the LOD, below which signals are indistinguishable from noise. A broad linear range is advantageous as it permits direct analysis across a wide spectrum of concentrations, thereby obviating the need for sample pretreatment steps such as dilution or gain adjustment. Strategies to extend the effective analytical range include the

https://doi.org/10.1021/acs.chemrev.5c00801
Chem. Rev. XXXX, XXX, XXX−XXX

employment of piecewise linear calibration models,[220,535] the application of advanced nonlinear regression, and the leveraging of ML algorithms for signal linearization and adaptive calibration.[550] A recurrent deficiency in current practice is the inadequate characterization of the linear range under conditions reflecting the complexity of real-world samples, including matrix effects. Additionally, reliance solely on global R^2 values can obscure local deviations from linearity that are critical for specific concentration regions of clinical relevance. To overcome these limitations, future investigations should adopt rigorous statistical assessments of linearity (e.g., residual analysis, lack-of-fit tests) and explicitly report local calibration performance within subranges of specific interest.

6.5. Selectivity

Sensor selectivity denotes the ability of a device to generate a distinct, quantifiable response to a specific target analyte or biophysical stimulus within a complex biological or environmental matrix, while exhibiting negligible response to coexisting nontarget species. The fidelity of selective detection is often compromised by physicochemical processes, including cross-reactivity with structurally similar interferents, nonspecific adsorption, matrix effects, and competitive binding at the recognition interface. Accordingly, enhancing selectivity necessitates the rational design of antifouling interfaces[551] to suppress nonspecific adsorption and the development of molecular recognition elements with high intrinsic binding affinity and specificity.[6,85,107] For devices transducing biophysical phenomena rather than chemical interactions, selectivity is augmented by judicious material selection to ensure preferential responsivity, sophisticated packaging to attenuate extraneous inputs, and the utilization of advanced signal processing for feature extraction. To address this, future efforts should emphasize systematic interferent screening under physiologically relevant conditions, quantitative reporting of selectivity metrics, and the integration of multimodal sensing or data-fusion strategies that leverage orthogonal signals to deconvolute analyte-specific responses from background interference.

6.6. Stability

The stability of a sensor, defined as its capacity to maintain consistent performance indices over extended operation or storage, is a decisive determinant of functional lifetime and commercial feasibility. Stability is commonly bifurcated into short-term stability (repeatability) and long-term stability. Short-term stability characterizes signal drift or fluctuation during discrete measurement cycles, directly impacting precision. Long-term stability refers to the gradual degradation or attenuation of response under specific environmental or in situ conditions. Quantitative assessment typically involves longitudinal monitoring of a standard reference, deriving figures of merit such as signal retention, relative standard deviation (RSD), and drift rates. High stability mitigates the need for frequent recalibration and is critical for continuous monitoring where maintenance is constrained. Degradation arises from intrinsic mechanisms, such as chemical aging and decomposition of sensing materials, and extrinsic influences, including biofouling, passivation, and environmental fluctuations (temperature, humidity, mechanical stress). Improving stability requires a multifaceted strategy: physical approaches such as robust encapsulation to shield active components; procedural interventions including optimized storage and periodic regeneration; and computational strategies utilizing drift-correction algorithms and reference channels. Future work need to prioritize standardized, long-term stability protocols, including accelerated aging studies and comprehensive reporting of failure modes and recalibration intervals.

6.7. Reproducibility

Reproducibility quantifies the consistency of sensor outputs across distinct fabrication batches and among different operators or setups. It is commonly evaluated using the RSD of key performance parameters measured across multiple devices under nominally identical conditions.[107,382] The primary sources of variability include stochastic fluctuations in materials synthesis and micro/nanofabrication, heterogeneity in film morphology, variations in device assembly, and deviations in ambient testing conditions. These factors contribute to performance dispersion, complicating cross-study comparisons and hindering large-scale manufacturing. Enhancing reproducibility requires a concerted focus on process control and methodological standardization. Core strategies encompass the stringent automation of synthesis and fabrication workflows, rigorous regulation of the testing environment, and strict adherence to standard operating procedures covering device preparation, calibration, and data analysis.

6.8. Signal-to-Noise Ratio (SNR)

The SNR is a fundamental descriptor characterizing the quality and reliability of an analytical signal, defined as the ratio of signal power to noise power (SNR = S/N) and conventionally expressed in decibels. A high SNR is imperative for discriminating the desired signal from the noise floor.[552] Dominant noise sources include extrinsic contributions, such as electromagnetic interference and mechanical perturbations, and intrinsic noise generated within the sensor and readout electronics.[451] These sources broaden signal distributions and impose limits on the minimum detectable stimulus. Strategies to enhance SNR involve hardware-level optimization and postacquisition signal processing. The latter employs digital/analog filtering, baseline correction, and advanced algorithms like wavelet denoising to selectively suppress noise components outside the signal's feature space.

Performance characterization of wearable electronics hinges on a suite of well-defined analytical metrics indispensable for benchmarking technological efficacy. However, a holistic evaluation must extend beyond fundamental sensing capabilities to encompass application-specific attributes, including biocompatibility,[261] mechanical resilience,[456] user ergonomics, and environmental robustness. To bolster scientific rigor, standardized and meticulous reporting of experimental validation protocols is imperative. This includes complete documentation of electrode geometry, electrochemical cell configuration, ambient conditions, and interferent concentrations. Critically, the validation of novel wearable devices requires benchmarking against recognized gold-standard methodologies, such as mass spectrometry for elemental analysis or certified medical-grade monitors. The accuracy and reliability of data must be rigorously established through robust statistical techniques, including deviation analysis, spike-and-recovery assays, or Bland–Altman analysis, to affirm the device's analytical concordance and practical viability.

7. SCREEN PRINTING

Screen printing constitutes a paradigmatic additive manufacturing strategy for wearable electronics, employing a squeegee-

https://doi.org/10.1021/acs.chemrev.5c00801
Chem. Rev. XXXX, XXX, XXX−XXX

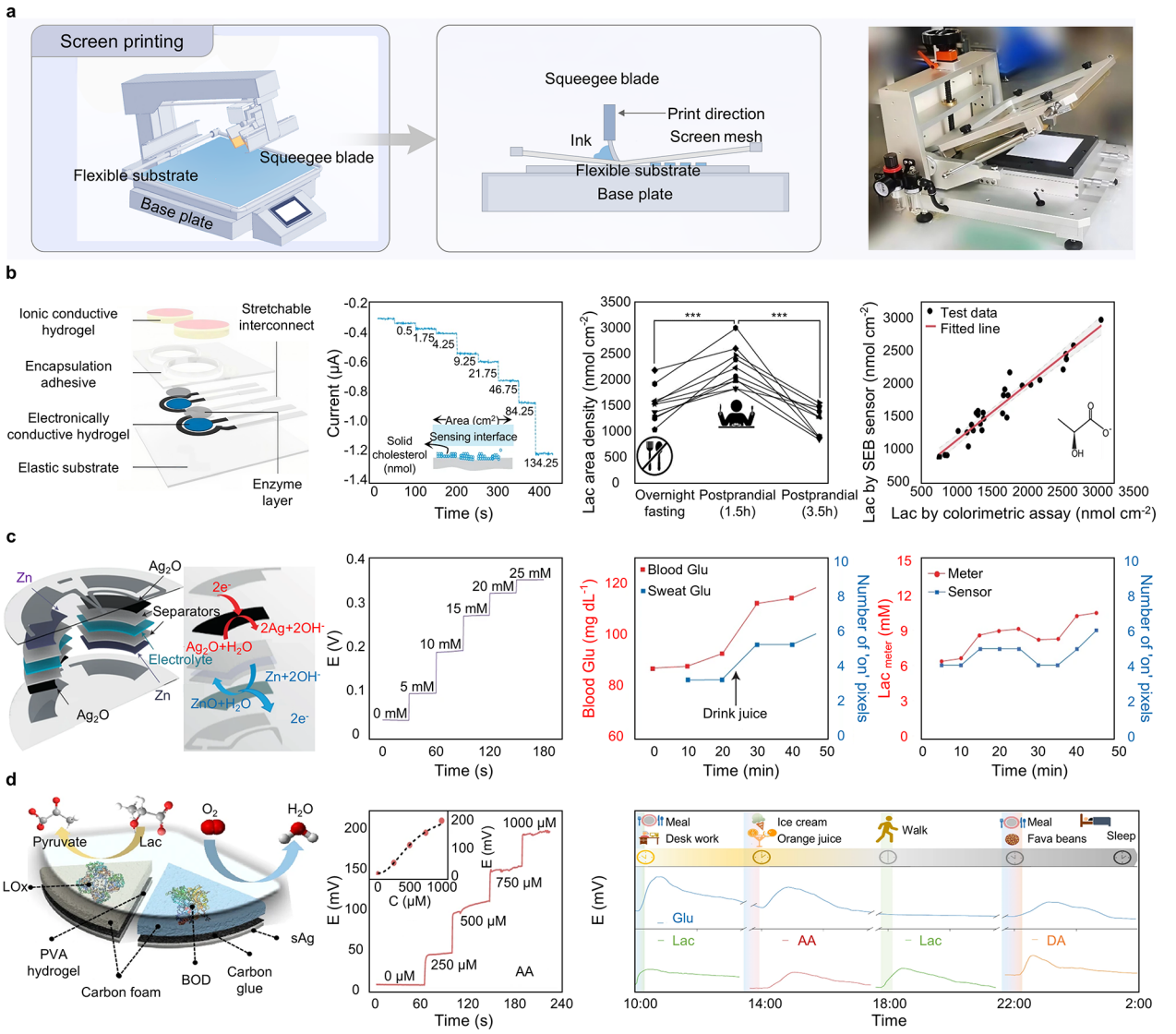

Figure 8. Preparation of wearable electronics via screen printed and wearable biochemical sensors. (a) Schematic illustration depicting the fabrication process of screen printed wearable electronics. Photographs of printing equipment. (b) Cross-sectional schematics of the device architecture. Chronoamperometric response recorded from cholesterol-oxidase-based sensors. Comparative analysis of epidermal lactate concentrations measured in the solid state at baseline, 1.5 h postprandially, and 3.5 h postprandially. Correlation between lactate levels quantified by the SEBS-based sensor and those obtained via tape-stripping combined with a commercial colorimetric assay kit, assessed at three distinct time points per subject. Reproduced with permission from ref 352. Copyright 2024 Springer Nature. (c) Layer-by-layer schematics of the Ag_2O−Zn battery, accompanied by the electrochemical reaction mechanisms occurring at the anode and cathode. Potentiometric signals were recorded with incremental increases in lactate concentration from 0 mM to 25 mM. Simultaneous measurement of sweat glucose using the wearable patch alongside corresponding blood glucose levels. Sweat lactate quantification was performed using both a commercial meter and the wearable patch sensor. Reproduced with permission from ref 570. Copyright 2022 Springer Nature. (d) Structural schematics illustrating the individual layers constituting enzymatic BFCs. In vitro sensor performance curves, including an inset calibration curve specific to AA detection. Continuous full-day biomarker monitoring achieved with the wearable fingertip microgrid device under varying physical activity conditions. Reproduced with permission from ref 542. Copyright 2024 Springer Nature. Abbreviations: Lac, lactate; SEB, solid epidermal biomarkers; Glu, glucose; LOx, lactate oxidase; PVA, poly(vinyl alcohol); BOD, bilirubin oxidase; sAg, stretchable silver inks; AA, ascorbic acid; DA, dopamine; C, concentration.

mediated hydraulic mechanism to extrude functional inks through stenciled meshes into electrode arrays.[22] Distinguished by operational simplicity, high-throughput capabilities, and economic scalability, this technique is uniquely advantageous for industrial-scale fabrication.[553] Although the spatial resolution is generally inferior to photolithographic standards, the trade-off is favorably balanced by cost efficiency and manufacturing velocity. The versatility of the method enables direct patterning onto a broad spectrum of substrates, encompassing not only planar flexible films but also non-conformal, topologically complex surfaces such as spherical, deformable, or ultrathin geometries.[554] Furthermore, the capacity to modulate film thickness affords critical adaptability in optimizing device impedance and sensitivity for diverse applications.[555]

7.1. Core Process and Workflow

Fundamentally, the technique relies on the hydrodynamic transport of a functional fluid through specific apertures in a mesh screen to replicate a geometric design on a receiver substrate (Figure 8a).[555] The standard apparatus comprises the

https://doi.org/10.1021/acs.chemrev.5c00801
Chem. Rev. XXXX, XXX, XXX−XXX

mesh stencil, the squeegee, the viscoelastic ink, the printing platform, and the flexible substrate.[556]

7.1.1. Material and Ink Design. The fidelity of screen-printed devices is governed intrinsically by the rheological profile of the functional ink.[557] An ideal formulation must demonstrate non-Newtonian behavior, specifically pronounced pseudoplasticity (shear-thinning) and thixotropy.[558] This profile necessitates a high zero-shear viscosity to maintain suspension stability at rest, transitioning to a low-viscosity state under the shear stress of the squeegee to facilitate mesh percolation. Subsequent rapid structural recovery upon stress cessation is imperative to preserve pattern acuity and mitigate defects such as slump or capillary bleeding. Furthermore, thermodynamic homogeneity within the dispersion is essential to prevent mesh occlusion and ensure layer uniformity.

Ink formulations are generally complex multicomponent systems, categorized by their continuous phase into organic, aqueous, or emulsion-based vehicles.[559] The physicochemical properties (conductivity, rheology, and environmental stability) emerge from the synergistic interaction of constituents: a functional phase, a polymeric binder, a solvent vehicle, and specific additives. The functional phase, dictating electronic utility, may consist of noble metal nanoparticles (e.g., gold),[560] conductive polymers, or carbon allotropes.[558] These are dispersed within a binder matrix, such as epoxy resin,[561] which provides cohesive integrity and substrate adhesion. The solvent vehicle, utilizing agents like dimethylformamide (DMF),[555] tetrahydrofuran (THF),[562] or deionized water,[563] is selected based on solubility parameters, evaporation kinetics, and rheological targets. Finally, additives including surfactants and rheology modifiers are introduced to fine-tune the printing dynamics.

7.1.2. Stencil Fabrication. The definition of the electrode geometry begins with the fabrication of the stencil, typically a woven mesh[553,555,563,564] coated with a photosensitive emulsion. Patterns generated via computer-aided design (CAD)[221] are transferred through photolithography. This process selectively cross-links the emulsion in exposed regions, while unexposed areas remain soluble and are washed away, thereby creating the negative space through which ink is deposited.

7.1.3. Printing Operation. The deposition phase involves the translation of a squeegee across the stencil at controlled velocity and pressure, generating the hydraulic force necessary to drive the ink through the mesh apertures onto the substrate.[557] A critical mechanism in this process is the snap-off, which is the immediate separation of the screen from the substrate driven by the elastic recoil of the tensioned mesh behind the moving squeegee. This rapid detachment is pivotal for shearing the ink column, defining sharp feature edges, and preventing lateral spreading. Consequently, the control of snap-off distance is a determining factor in minimizing feature size and maximizing resolution.

7.1.4. Post-Processing. Postdeposition, the fluidic film must undergo microstructural consolidation to evolve into a functional solid. This is predominantly achieved via thermal annealing, with protocols determined by the ink's thermal chemistry and the substrate's glass transition temperature.[296,555] This stage drives solvent volatilization, binder polymerization, and the sintering of conductive fillers to establish electrical percolation pathways. The thermal budget constitutes a critical processing window; insufficient curing leaves residual solvents that disrupt percolation and degrade stability,[565] while excessive thermal load can compromise substrate integrity or embrittle the electrode. For silver-based systems, the sintering temperature directly modulates neck formation and grain growth, which are fundamental to conductivity.[566] Thus, precise thermal management is essential for optimizing the electromechanical and environmental robustness of the device.

7.1.5. Multilayer Registration and Integration. The realization of sophisticated architectures, such as electrochemical sensors requiring orthogonal working, reference, and counter electrodes alongside dielectric barriers, necessitates sequential multilayer deposition.[221,567] High-fidelity registration is achieved through optical alignment systems tracking fiducial markers, ensuring precise overlay between layers. Each deposition typically requires an intermediate curing step. Finally, an encapsulation layer is applied to define the active sensing area and hermetically seal the conductive traces against short-circuiting or environmental corrosion.[147,296]

While the workflow appears sequential, the final device performance is not merely cumulative but emergent, resulting from the complex coupling of material rheology and process dynamics. Achieving reproducible functionality demands a holistic optimization strategy rather than the isolation of discrete steps.

7.2. Critical Process Parameters and Physicochemical Significance

The operational stability and signal fidelity of screen-printed wearable sensors are dictated by a high-dimensional space of interdependent physicochemical and engineering variables. Mastery of these parameters is a prerequisite for transitioning from benchtop prototyping to scalable manufacturing.

7.2.1. Stencil Architecture and Geometric Constraints. The stencil mesh count, wire diameter, and emulsion thickness determine the hydrodynamic volume and geometric limits of the print. These factors present a fundamental trade-off: high-density meshes enhance spatial resolution and edge definition but restrict ink flux, potentially leading to insufficient film thickness. Conversely, low-density meshes increase deposition volume but degrade feature acuity. Therefore, stencil design requires a calculated balance to maximize conductivity while preserving pattern fidelity.

7.2.2. Squeegee Mechanics. Ink transfer dynamics are modulated by the squeegee's tribological and kinematic properties, including durometer (hardness), attack angle, pressure, and speed. A compliant (low-durometer) squeegee conforms to substrate topography but may compromise ink clearance.[568] High pressure aids mesh penetration but risks substrate distortion. Furthermore, traverse velocity dictates the shear rate applied to the ink; excessive speeds may exceed the ink's relaxation time, leading to incomplete filling, while insufficient speeds allow for solvent evaporation or capillary bleeding.

7.2.3. Substrate Properties and Interfacial Science. Interfacial thermodynamics at the ink−substrate boundary governs wetting behavior and film morphology. Low surface energy substrates often necessitate plasma treatment or chemical modification to promote adhesion and uniform spreading.[569] Surface topography, including roughness and porosity, significantly influences ink consumption and film homogeneity.[569] Additionally, the thermal stability of the substrate imposes an upper bound on processing temperatures,

https://doi.org/10.1021/acs.chemrev.5c00801
Chem. Rev. XXXX, XXX, XXX−XXX

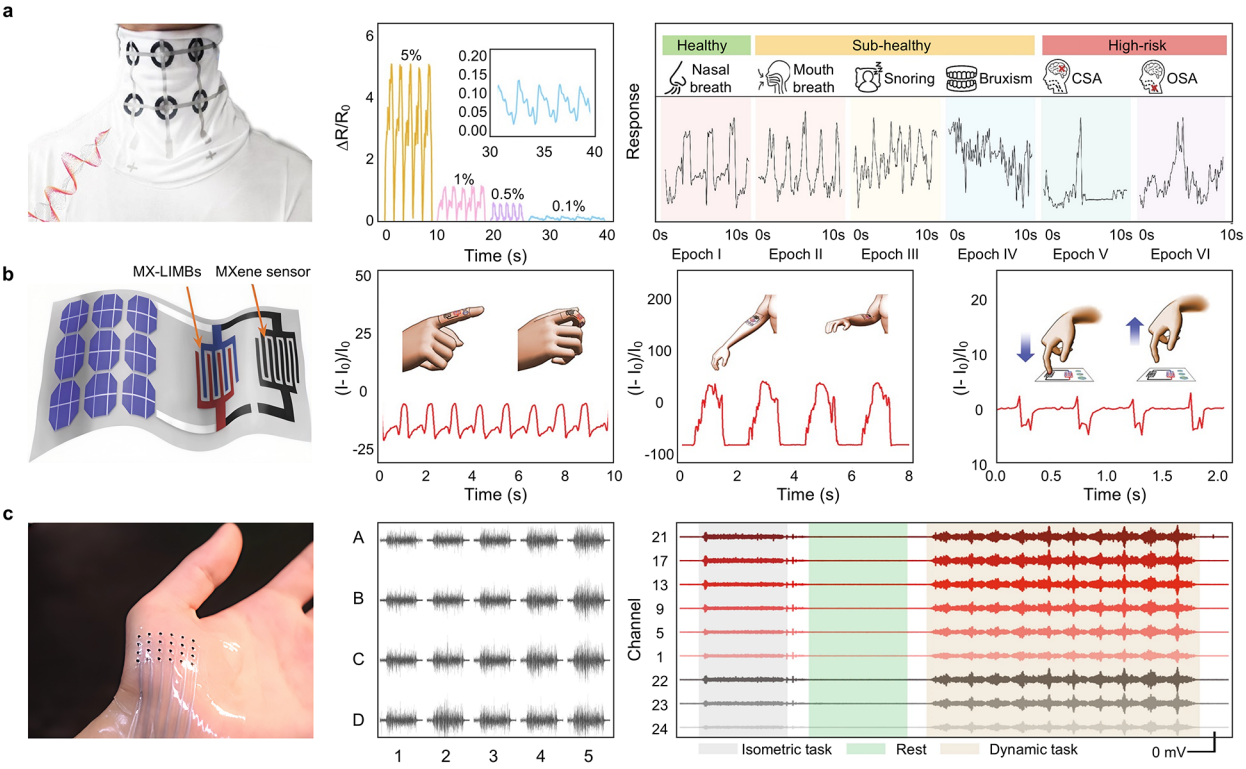

Figure 9. Screen printed wearable biophysical and electrophysiological sensors. (a) A six-channel strain sensor array was fabricated and printed onto the collar region of a garment to detect the subtle vibrations of the extrinsic laryngeal muscle and monitor sleep behavior. Resistance response to cyclic tensile strains of 5%, 1%, 0.5%, and 0.1% is presented. The inset provides a magnified view of the resistance response at 0.1% strain. Visualization of signal profiles corresponding to six distinct sleep patterns is shown, with emphasis on the channel exhibiting the highest power spectral density. Reproduced with permission from ref 571. Copyright 2025 National Academy of Sciences. (b) Schematic fabrication of MX-LIMBs from stepwise screen printing. Current change of the MXene hydrogel sensor powered by the integrated MX-LIMBs in response to the bending of a finger, an elbow, and pressing vertically. Reproduced with permission from ref 572. Copyright 2021 John Wiley and Sons. (c) Configuration of the metal−polymer electrode array patch positioned on the abductor pollicis brevis muscle. sEMG signals recorded from each channel of the array patch placed on the BB muscle are presented. sEMG signals of the BB under a 5 kg load session. Reproduced with permission from ref 440. Copyright 2023 Springer Nature. Abbreviations: CSA, central sleep apnea; OSA, obstructive sleep apnea; MX-LIMBs, MXene-microsupercapacitors and lithium-ion microbatteries.

thereby constraining the degree of sintering and the ultimate conductivity achievable.

7.2.4. Environmental Conditions. Ambient thermodynamic conditions exert a profound influence on process consistency. Variations in temperature and relative humidity alter solvent evaporation rates and ink viscosity, potentially leading to screen mesh clogging or pattern bleeding. Rigorous environmental control is therefore mandatory for reproducibility.

The intricate coupling of these variables highlights a critical deficiency in traditional "Edisonian" (trial-and-error) optimization approaches, which fail to account for parameter interactions. To advance the field, there is an imperative shift toward multivariate optimization strategies, utilizing design of experiments (DoE) and ML algorithms to systematically map the processing landscape and identify robust operational windows.

7.3. Fabrication and Application of Screen Printed Wearable Electronics

7.3.1. Screen Printed Biochemical Sensors. Recent advancements in screen printed wearable electronics have introduced sensors capable of the *in situ* detection of solid epidermal biomarkers (SEB).[352] A representative device, fabricated on a SEBS elastomer substrate, integrates a stretchable silver-based interconnect with an electrochemical hydrogel (ECH) precursor layer (Figure 8b). A pivotal innovation in this design is the bilayer ion-electron hydrogel architecture, which mediates the dissolution, diffusion, and electrochemical oxidation/reduction of solid analytes. Validation in human subjects confirmed a linear correlation between the sensor response and epidermal lactate area density, accurately tracking physiological fluctuations in the postprandial state. While these results corroborate the utility of SEB sensors for monitoring metabolic responses, clinical translation is currently hindered by substantial interfacial and analytical challenges. Primarily, long-term operational stability remains compromised by continuous mechanical deformations and the complex biological matrix of sweat, where interference can degrade signal integrity. Beyond transduction mechanics, the reliance on external power and data processing modules restricts the widespread deployment of these devices. To address the demand for autonomy, subsequent research has engineered fully integrated sensing platforms. One such system synergizes a screen printed electrochemical sensor with a cofabricated Ag_2O−Zn stretchable battery and a low-power electrochromic display.[570] A vertical stacking configuration was adopted to minimize the device footprint and reduce internal resistance by truncating the ion diffusion length between the battery and electrodes (Figure 8c). The efficacy of this

https://doi.org/10.1021/acs.chemrev.5c00801
Chem. Rev. XXXX, XXX, XXX−XXX

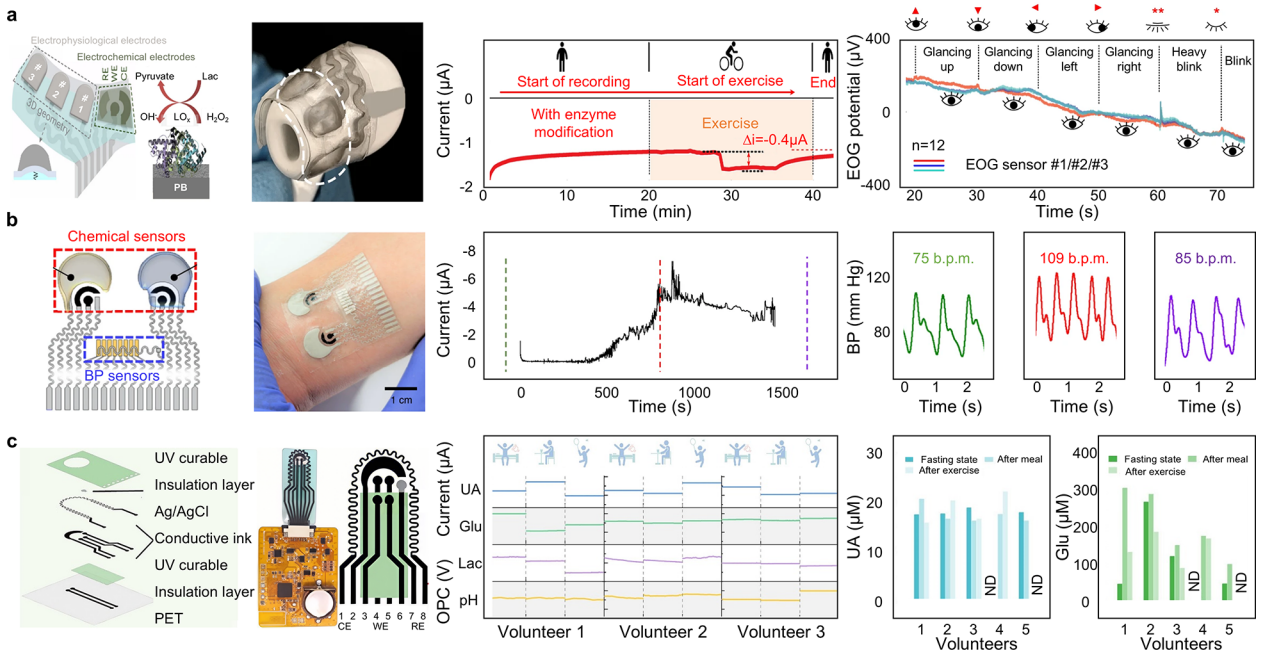

Figure 10. Screen printed wearable multimodal sensors. (a) Schematic layout of the in-ear integrated sensor system. Assembled configuration of the in-ear integrated electrophysiological and electrochemical sensing electrodes. Representative chronoamperometric recording of on-body lactate sensing utilizing enzyme-functionalized electrochemical electrodes under controlled conditions. EOG characterization, demonstrating transient electrophysiological responses to distinct eye movement modalities recorded within a single ear using ipsilateral referencing. Reproduced with permission from ref 296. Copyright 2023 Springer Nature. (b) Schematic illustration of the sensor architecture highlighting the integration of BP and electrochemical sensing modules. Evaluation of skin conformability and mechanical robustness of the device subjected to deformations. Continuously monitor the concentration of lactate in the sweat of physically active subjects during active exercise, with dashed lines marking the time corresponding to the plotted BP data (before, during and after exercise). Time-resolved recordings of BP and HR signals were captured before, during, and following stationary cycling exercise. Reproduced with permission from ref 30. Copyright 2021 Springer Nature. (c) Layered screen printing fabrication schematic of the device. Photograph of the assembled device connected to the FPCB. Scale bar: 10 mm. Quantitative measurements of UA, glucose, lactate, and pH levels in three volunteers were assessed under fasting conditions, 1 h postprandially, and 1 h postexercise. Statistical comparison of UA, glucose, lactate, and pH concentrations across the three physiological states in the volunteer cohort. Reproduced with permission from ref 573. Copyright 2025 Elsevier BV. Abbreviations: RE, reference electrode; WE, working electrode; CE, counter electrode; Lac, lactate; PB, Prussian blue; LOx, lactate oxidase; EOG, electrooculography; BP, blood pressure; PET, polyethylene terephthalate; FPCB, flexible printed circuit board; UA, uric acid; Glu, glucose; ND, not detected.

autonomous platform was validated via noninvasive sweat analysis, where it successfully tracked exercise-induced variations in lactate and glucose concentrations consistent with established metabolic profiles. Expanding on the paradigm of on-body energy harvesting, an autonomous, fingertip-mounted health monitoring system was developed to integrate multiplexed biosensing with energy generation and storage.[542] This platform harvests energy from passively collected sweat utilizing lactate-based BFCs, utilizing a porous carbon foam architecture to maximize enzyme and mediator loading, thereby enhancing energy density (Figure 8d). The harvested bioenergy is regulated by a microgrid incorporating a stretchable silver chloride-zinc (AgCl-Zn) battery, ensuring the uninterrupted operation of the MCU and sensors during periods of minimal perspiration. Continuous analyte sampling is maintained by an osmosis-driven microfluidic interface. This self-powered architecture enables the simultaneous, longitudinal monitoring of multiple metabolites (e.g., glucose, AA, lactate, and Levodopa), marking a significant progression toward autonomous personalized health tracking. However, the modest power density of BFCs and the temporal degradation of enzymatic activity remain critical bottlenecks for high-power, long-duration applications, necessitating further optimization in catalytic materials and system efficiency.

7.3.2. Screen Printed Biophysical and Electrophysiological Sensors. Screen printing technologies have established a versatile foundation for fabricating wearable systems dedicated to biophysical and electrophysiological monitoring. In the domain of sleep medicine, conventional polysomnography is often limited by high skin-electrode impedance and ergonomic constraints, which degrade the fidelity of nocturnal data. To mitigate these issues, a skin-conformable smart textile system was engineered for high-fidelity sleep monitoring[571] (Figure 9a). A deep learning architecture, SleepNet, was utilized to deconvolve complex, multichannel data streams, classifying six distinct physiological states and sleep patterns. Visualization of the model's output confirmed its capability for comprehensive pattern recognition while rejecting artifacts. This artifact-resistant electronic textile represents a substantial technological progression, offering robust diagnostic capabilities. However, analogous to biochemical sensors, maintaining signal stability against environmental variables such as perspiration and humidity is critical. Furthermore, a fundamental requisite for practical adoption is the provision of a stable power supply capable of sustaining overnight operation. Addressing the energy challenge, recent innovations in ink formulations have enabled the direct screen printing of MXene-based microsupercapacitors (MSCs) and lithium-ion microbatteries (LIMBs), facilitating the monolithic integration

https://doi.org/10.1021/acs.chemrev.5c00801
Chem. Rev. XXXX, XXX, XXX−XXX

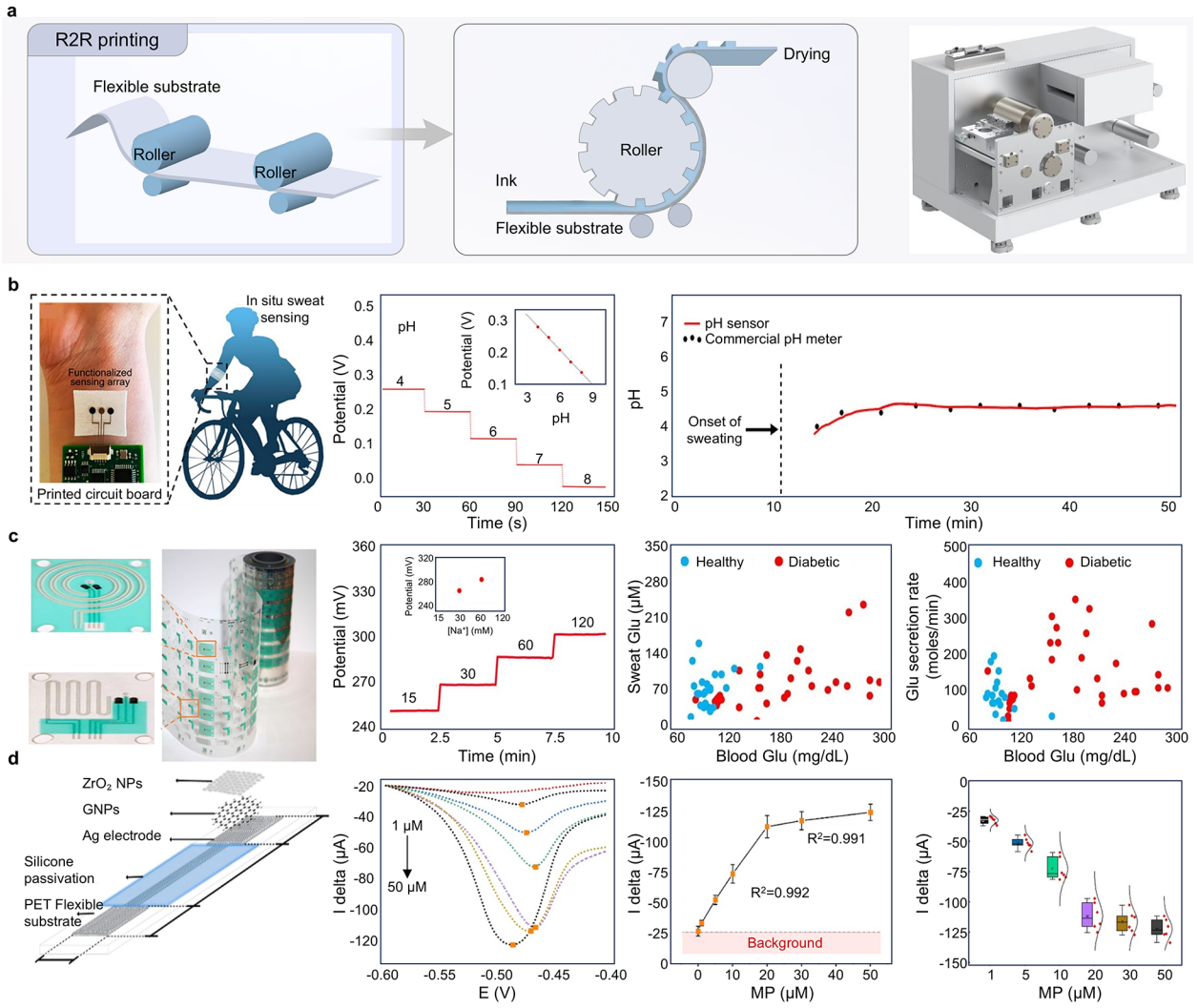

Figure 11. Preparation of wearable electronics via R2R printed and wearable biochemical sensors. (a) Schematic illustration depicting the fabrication process of R2R printed wearable electronics. Photographs of printing equipment. (b) R2R printing electrode subsequently functionalized for application as *in situ* sensing platforms. Functionalization of R2R gravure printed electrodes into pH sensors, calibration curves are presented in the insets. Comparative analysis of real-time sweat pH measurements obtained via the wearable sensor against *ex situ* measurements of collected sweat samples using a commercial pH meter. Reproduced with permission from ref 103. Copyright 2018 American Chemical Society. (c) Optical depicting the patterned sensing electrodes fabricated through the R2R printing process. Performance characterization of Na^+ sensors functionalized on printed electrodes. Correlation between fasting sweat glucose levels and blood glucose concentrations measured in both healthy and diabetic cohorts. Relationship between average sweat glucose secretion rates and corresponding blood glucose levels across healthy and diabetic populations. Reproduced with permission from ref 111. Copyright 2019 American Association for the Advancement of Science. (d) Schematic illustration of the silver/graphene nanoplatelets/zirconium dioxide (Ag/GNPs/ZrO_2) composite electrode deposited on PET substrate. Detection outcomes of MP utilizing the sensor. Calibration curve depicting the concentration-dependent response of MP. Box plots representing the distribution of data points obtained from the calibration curve measurements. Reproduced with permission from ref 584. Copyright 2021 American Chemical Society. Abbreviations: Glu, glucose; ZrO_2 NPs, zirconia nanoparticles; GNPs, graphene nanoplatelets; MP, methyl parathion.

of self-powered sensing platforms. An exemplary all-flexible system integrates a tandem solar cell, LIMBs for energy storage, and an MXene hydrogel-based pressure sensor on a single substrate.[572] This architecture demonstrated exceptional sensitivity to biomechanical stimuli (Figure 9b), with the MSC and LIMBs components providing stable voltage to power electromechanical transduction. These results underscore the potential of all-MXene systems as autonomous functional units for next-generation pressure sensing. Nonetheless, the susceptibility of MXene nanosheets to oxidation compromises long-term stability. Future research must prioritize the passivation of MXene structures to prevent degradation without attenuating electrochemical or sensing performance. Ultimately, the performance of both sleep monitoring systems and self-powered platforms is contingent upon the electrode-skin interface. For applications such as surface electromyography (sEMG), electrodes must exhibit high signal fidelity, mechanical compliance, and durable adhesion. A materials-centric solution was presented through the formulation of an adhesive dry electrode composed of tannic acid, poly(vinyl alcohol) (PVA), and poly(3,4-ethylenedioxythiophene): polystyrenesulfonate (PEDOT: PSS) (TPP).[440] These composite leverages synergistic bioadhesion, conductivity, and elasticity to ensure stable epidermal contact (Figure 9c). A

https://doi.org/10.1021/acs.chemrev.5c00801
Chem. Rev. XXXX, XXX, XXX−XXX

fully stretchable metal−polymer electrode array patch (MEAP) fabricated via scalable screen printing enabled real-time, multiplexed sEMG monitoring of the abductor pollicis brevis and biceps brachii (BB). Despite these advances, the performance of bioadhesive conductors under conditions of profuse sweating and prolonged mechanical stress requires further characterization.

7.3.3. Screen Printed Multimodal Sensors. Screen printing has emerged as a pivotal strategy for engineering integrated wearable electronics capable of concurrent biochemical, biophysical, and electrophysiological interrogation. A primary objective is to bridge the diagnostic gap between central nervous system activity and systemic metabolic states. A significant development in this arena is an in-ear sensor array that cointegrates electrochemical and electrophysiological modalities (Figure 10a).[296] Exploiting the functional topography of the ear canal, the sensor segregates electrophysiological electrodes toward the temporal lobe (minimal perspiration) and electrochemical electrodes toward regions of higher sweat flux. When integrated into standard earphones, such platforms provide a dual-domain perspective on neurometabolic status. However, integrating complex sensing, power, and wireless communication modules within the spatial constraints of an earphone without compromising user ergonomics presents a formidable engineering challenge. Expanding multimodal integration to broader epidermal surfaces, researchers have developed flexible patches for the simultaneous monitoring of cardiovascular parameters, specifically heart rate (HR) and BP, and chemical biomarkers. To capture the interplay between hemodynamic and metabolic fluctuations, a skin-conformable patch was fabricated to perform continuous BP and chemical sensing (Figure 10b).[30] Specialized inks and stretchable substrates imparted the necessary mechanical resilience. During constant-intensity cycling, the device successfully monitored BP and sweat lactate dynamics. While effective for capturing acute physiological responses, maintaining signal fidelity and calibration stability under continuous mechanical strain remains difficult. Moreover, the passive reliance on natural sweating limits utility in sedentary individuals, and exercise-induced pH fluctuations can complicate continuous chemical analysis. Overcoming these limitations, particularly the dependence on passive perspiration, necessitates active sweat induction. An integrated screen printed wearable system was engineered for on-demand stimulation, collection, and in situ analysis of sweat, yielding personalized data for noncommunicable disease management.[573] The core of this platform is a multimodal and multichannel flexible sensor array (MMFSA) capable of real-time quantification of key biomarkers (Figure 10c). Interfaced with a flexible printed circuit board (FPCB) for programmable voltage control, wireless communication, and electrical stimulation, the platform successfully resolved metabolically induced biochemical fluctuations against a stable background in human studies. The broader impact of such systems lies in their potential to evolve into autonomous, closed-loop health management platforms.

In conclusion, screen printing is indispensable for the cost-efficient, large-scale production of electrodes and functional components in wearable electronics. However, limited resolution remains a constraint. Future advancements must focus on refining printing plates and functional inks to enhance feature resolution. Additionally, improving the rheological stability and printability of functional inks on flexible substrates is imperative for the robust fabrication of next-generation wearable sensors.

8. ROLL-TO-ROLL (R2R) PRINTING

The translational trajectory of wearable electronics from laboratory-scale prototypes to commercially viable commodities, particularly for applications such as chronic disease monitoring, is principally obstructed by the exigencies of scalable manufacturing. R2R processing has been established as a preeminent strategy to circumvent this scalability bottleneck, providing a high-throughput, cost-efficient platform conducive to the fabrication of devices with superior stability. The R2R printing deposition technique is distinctively advantageous for its capacity to rapidly delineate high-resolution conductive or functional architectures, a capability that transcends the limitations of conventional batch processes like screen printing.[574] This continuous fabrication methodology functions effectively under diverse environmental constraints, ranging from atmospheric to low-vacuum conditions.[575] A predominant deposition strategy employs solvent-based coating, wherein functional constituents (e.g., conductive or sensing agents) and polymeric binders are dissolved or dispersed within a solvent vector, applied as a wet film onto a transiting web, and subsequently solidified via solvent evaporation mechanics. Collectively, these attributes position R2R printing as a pivotal manufacturing paradigm for the mass production of sensor electrodes, thereby ensuring their economic feasibility as disposable or replaceable modules for ubiquitous deployment in medical diagnostics and screening.

8.1. Core Process and Workflow

R2R printing constitutes a continuous manufacturing paradigm predicated on the rigorous transport of a flexible substrate, termed the web, across rollers synchronized at differential velocities to sustain constant tensile stress (Figure 11a).[576] The operational workflow is a sequential, modular progression initiated with substrate introduction. Typically comprised of PET, PI, or cellulosic substrates such as paper, the polymeric film is fed from an unwind station. The web subsequently undergoes surface energy modification, conventionally via corona discharge or plasma treatment, to augment wettability and interfacial adhesion for ensuing stratums.[577] Following surface activation, the substrate traverses a series of deposition modules where functional materials are applied via high-throughput printing or coating methodologies, including gravure,[103,574,578] flexography,[579] or slot-die coating.[580] The sequence concludes with postprocessing units dedicated to curing, consolidation, and lamination, after which the fully integrated device is spooled at a rewind station.

8.1.1. Material and Ink Design. The efficacy of R2R printing is intrinsically linked to the synergistic engineering of functional inks and substrate materials. Functional inks require rheological profiles meticulously tailored for high-velocity deposition regimes. This requirement necessitates formulations exhibiting relatively low viscosity to facilitate efficient fluid transfer dynamics from the printing apparatus to the web, concomitant with high solid loading to maximize material throughput per pass. To guarantee the formation of homogeneous, large-area coatings yielding reproducible device metrics, the colloidal stability of the ink remains a paramount variable. Functional nanoparticles must maintain a refined dispersion state throughout extended operation cycles to mitigate aggregation-induced performance attenuation.[581]

https://doi.org/10.1021/acs.chemrev.5c00801
Chem. Rev. XXXX, XXX, XXX−XXX

8.1.2. Process Control and Multi-Layer Integration. The realization of functional multilayer devices is contingent upon registration, the exact spatial alignment of sequentially deposited layers. High-fidelity registration systems, utilizing sensors to track fiducial markers,[582] are indispensable for ensuring appropriate interlayer overlap, electrical continuity, and structural integrity. However, a critical impediment in R2R manufacturing is the divergence between idealized theoretical models and the stochastic nature of high-yield production. Dynamic perturbations in web tension, subtle fluctuations in ink rheology, and variations in ambient environmental conditions can introduce stochastic defects, including film heterogeneity, pattern distortion, and registration drift. This discrepancy between design specifications and manufacturing realities creates a substantive performance gap between benchtop prototypes and mass-produced units. Consequently, a critical trajectory for the advancement of the field involves the integration of in-line metrology with closed-loop feedback control mechanisms. The implementation of such adaptive process control systems is imperative for enabling real-time parametric adjustments, thereby mitigating process variability, suppressing defect rates, and substantially enhancing the yield and reliability of R2R-printed flexible electronics.

8.2. Critical Process Parameters and Physicochemical Significance

8.2.1. Web Tension Control and Substrate Mechanics. The precise regulation of web tension is fundamental to preserving the structural quality and dimensional fidelity of R2R-printed films.[583] Deviations from the optimal tension envelope precipitate distinct failure modes: insufficient tension leads to web wrinkling, registration errors, and coating nonuniformity, whereas excessive tension induces plastic deformation, dimensional instability, or catastrophic substrate rupture. The mechanical response of the web is governed by its intrinsic viscoelastic properties, primarily the elastic modulus and thickness. In the context of flexible electronics, substrates typically range from 12 to 125 μm in thickness; the diminished flexural rigidity inherent to thinner films necessitates exceptionally rigorous tension control protocols to prevent deformation.

8.2.2. Web Speed and Throughput Optimization. Web velocity serves as the primary determinant of production throughput and, by extension, the economic viability of the R2R platform. The optimization of web speed represents a complex, multiparametric challenge due to its profound coupling with hydrodynamic process variables. In gravure printing, for example, ink transfer efficiency is intricately dependent on web velocity, governed by the interplay of capillary and viscous forces within the engraved cells.[581] Excessive velocity results in incomplete ink evacuation and resultant print defects, while insufficient velocity undermines productivity efficiency.

8.2.3. Post-Processing Protocol. The postdeposition thermal protocol, encompassing drying and sintering phases, dictates the kinetic and thermodynamic evolution of the film structure and is decisive in achieving target material properties. For conductive films formulated with metal nanoparticles, the specific sintering temperature and duration determine the extent of interparticle necking and the elimination of organic stabilizing ligands, mechanisms that collectively define the ultimate electrical conductivity.[103]

8.2.4. Environmental Condition. The R2R processing environment must be tailored to accommodate the chemical stability of the constituent materials. Operations conducted under ambient atmospheric conditions offer distinct advantages regarding cost efficiency and operational simplicity, proving suitable for robust solvent-based systems and functional polymers. Conversely, materials susceptible to oxidative or hydrolytic degradation necessitate processing within controlled, low-humidity, or inert atmospheres. The maintenance of such high-purity environments within large-scale, high-velocity machinery presents a formidable engineering and economic challenge, thereby catalyzing ongoing research into the development of environmentally robust material formulations.

8.3. Fabrication and Application of R2R Printed Wearable Electronics

8.3.1. R2R Printed Biochemical Sensors. The applicability of R2R gravure printing for electrochemical sensing has been corroborated through the fabrication of electrodes exhibiting uniform redox kinetics. This was achieved on 150-m-long flexible substrates utilizing inks and electrode geometries specifically optimized for the intaglio process, yielding platforms amenable to functionalization for diverse electrochemical sensing paradigms.[103] These electrodes have been successfully translated to in-field applications, including the real-time, continuous monitoring of analytes in sweat (Figure 11b). The mechanical durability and practical utility of these sensors were validated via continuous, on-body pH monitoring during stationary exercise. While this concordance confirmed the fidelity of printed sensor arrays for tracking physiological indicators in mechanically demanding in situ environments, a pivotal limitation in rudimentary wearable architectures arises from the confounding influence of variable sweat secretion rates. This variation induces analyte dilution, leading to significant measurement inaccuracies that compromise clinical validity. A sophisticated manufacturing strategy addresses this deficiency by integrating R2R printing with laser-engraved microfluidics to generate mass-producible, integrated patches capable of simultaneous electrochemical sensing and precise sweat flow management (Figure 11c).[111] Manufactured on a 100-m web at a throughput of 60 devices per minute, these systems feature a dual-layer architecture for the concurrent quantification of biomarkers and sweat rate. Clinical studies involving healthy and diabetic cohorts demonstrated the anticipated inverse relationship between sweat glucose concentration and sweat rate. Critically, by compensating for dilution effects, the system established a robust correlation between the calculated sweat glucose secretion rate and systemic blood glucose levels, representing a fundamental advancement toward noninvasive glycemic monitoring. The versatility of these scalable R2R techniques extends beyond biomedical diagnostics to environmental surveillance. To mitigate environmental and health risks associated with nitroaromatic organophosphorus pesticides (NOPPs), an enzymeless sensor was fabricated via R2R printing (Figure 11d). The device design leveraged the electrocatalytic and adsorptive capabilities of zirconia (ZrO_2), combined with highly conductive graphene nanoplatelets (GNPs).[584] Utilizing SWV for the sensitive detection of methyl parathion (MP), the sensor exhibited a linear current response proportional to MP concentration, underscoring the potential of R2R printing for

https://doi.org/10.1021/acs.chemrev.5c00801
Chem. Rev. XXXX, XXX, XXX−XXX

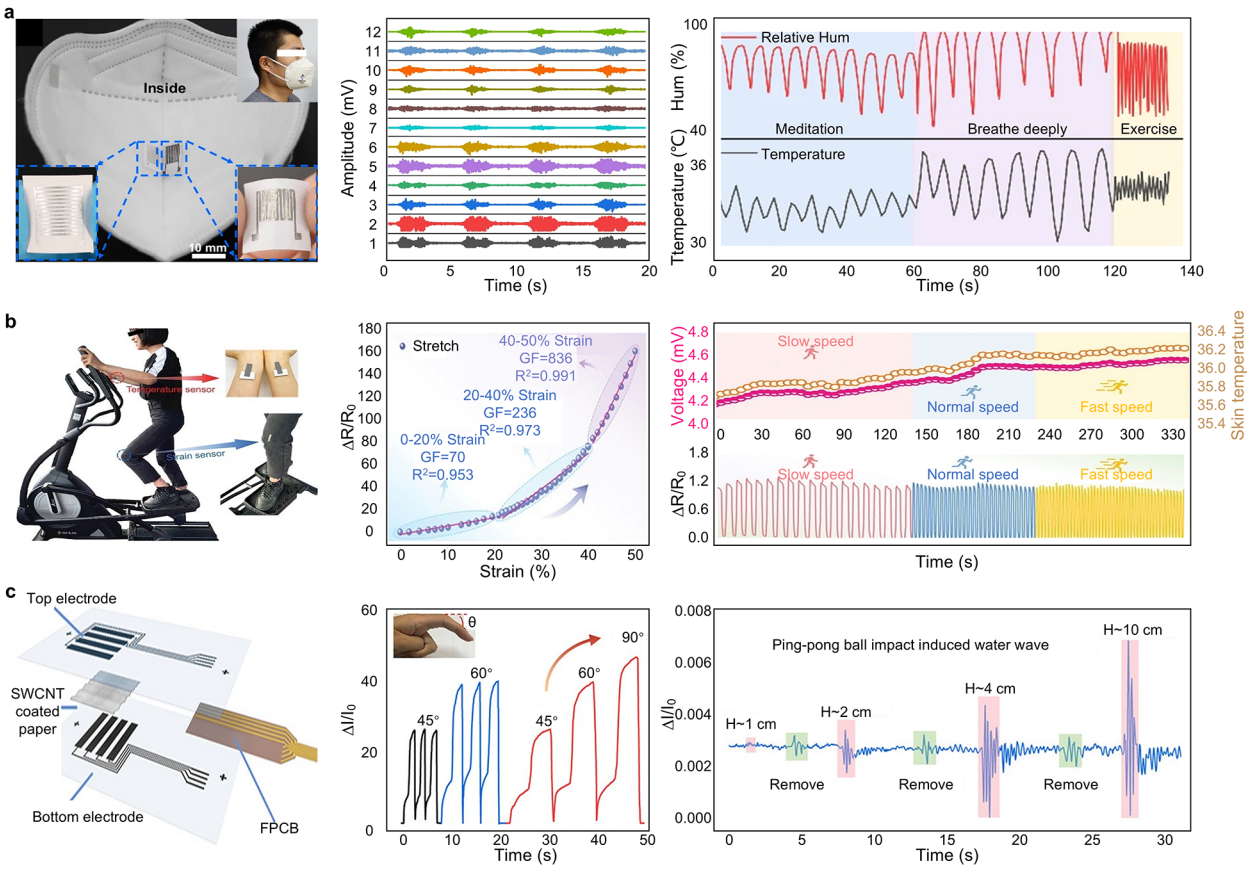

Figure 12. R2R printed biophysical and electrophysiological sensors. (a) Integration of temperature and humidity sensors within the face mask architecture. sEMG signals recorded from various anatomical locations during a snatch movement. Response profiles of temperature and humidity sensors correlated with variations in respiratory intensity. Reproduced with permission from ref 67. Copyright 2024 Springer Nature. (b) Schematic illustration depicting real-time monitoring of temperature and knee joint flexion during human locomotion. Relative resistance variation exhibited by the CAST-PTFE film subjected to tensile strain up to 50%. Continuous monitoring of output voltage alongside relative resistance changes in the CAST-PTFE film under dynamic conditions. Reproduced with permission from ref 64. Copyright 2024 John Wiley and Sons. (c) Exploded view of a paper-based flexible pressure sensor array. Signal of the R2R-based sensor for different angles of finger flex. Response of a sensor for the test of releasing a ping-pong ball from different heights, where H is the distance between the ping-pong ball and the surface of the water. The pink area corresponds to the immediate period following the release of the ping-pong ball, while the green area corresponds to the period when the ping-pong ball is gently removed from the water tank. The change of water wave pressure caused by ping-pong ball falling at different heights. Reproduced with permission from ref 585. Copyright 2023 American Chemical Society. Abbreviations: Hum, humidity; GF, gauge factor; SWCNT, single-walled carbon nanotube; FPCB, flexible printed circuit board.

the high-throughput production of low-cost, disposable sensors dedicated to environmental safety.

8.3.2. R2R Printed Biophysical and Electrophysiological Sensors. The R2R printing of biophysical and electrophysiological sensors for monitoring physiological parameters has garnered significant attention within the materials science community. A primary engineering challenge in this domain involves the activation of printed circuits, particularly those utilizing high-melting-point metals, to achieve optimal conductivity without inducing thermal degradation of mechanically compliant substrates. To circumvent this, a pressure-constrained sonication activation (PCSA) methodology was introduced to sinter a broad spectrum of metallic and nonmetallic inks on flexible substrates, a technique readily scalable for R2R integration.[67] This versatile roll-based approach facilitated the fabrication of multifunctional modules, including face masks embedded with temperature and humidity sensors (Figure 12a). The R2R methodology has been further extended to textile substrates, where electrode arrays monitor sEMG signals from distinct muscle groups during complex motor tasks. Advanced human-machine interfaces and wearable health systems necessitate skin-conformable thermoelectric films possessing dual-sensing capabilities for temperature and strain. However, reconciling high mechanical flexibility with superior thermoelectric and piezoresistive performance remains a materials science bottleneck. An R2R-compatible strategy addressed this dichotomy by fabricating ultraflexible composite films from $Cu_{25}As_{35}Se_6Te_{34}$ (CAST) glass and polytetrafluoroethylene (PTFE), which exhibited robust dual-mode sensing.[64] For thermal monitoring, the interface maintained direct skin contact, while the contralateral surface was thermally isolated by a foam layer to minimize convective heat loss. Concurrently, strain sensing relied on deformation-induced resistance modulation (Figure 12b). While these findings highlight the efficacy of CAST-PTFE composites for monitoring biomechanical dynamics, the inclusion of arsenic and selenium warrants critical scrutiny. Despite PTFE encapsulation, the long-term biocompatibility and potential risk of elemental leaching must be rigorously evaluated, particularly for medical-

https://doi.org/10.1021/acs.chemrev.5c00801
Chem. Rev. XXXX, XXX, XXX−XXX

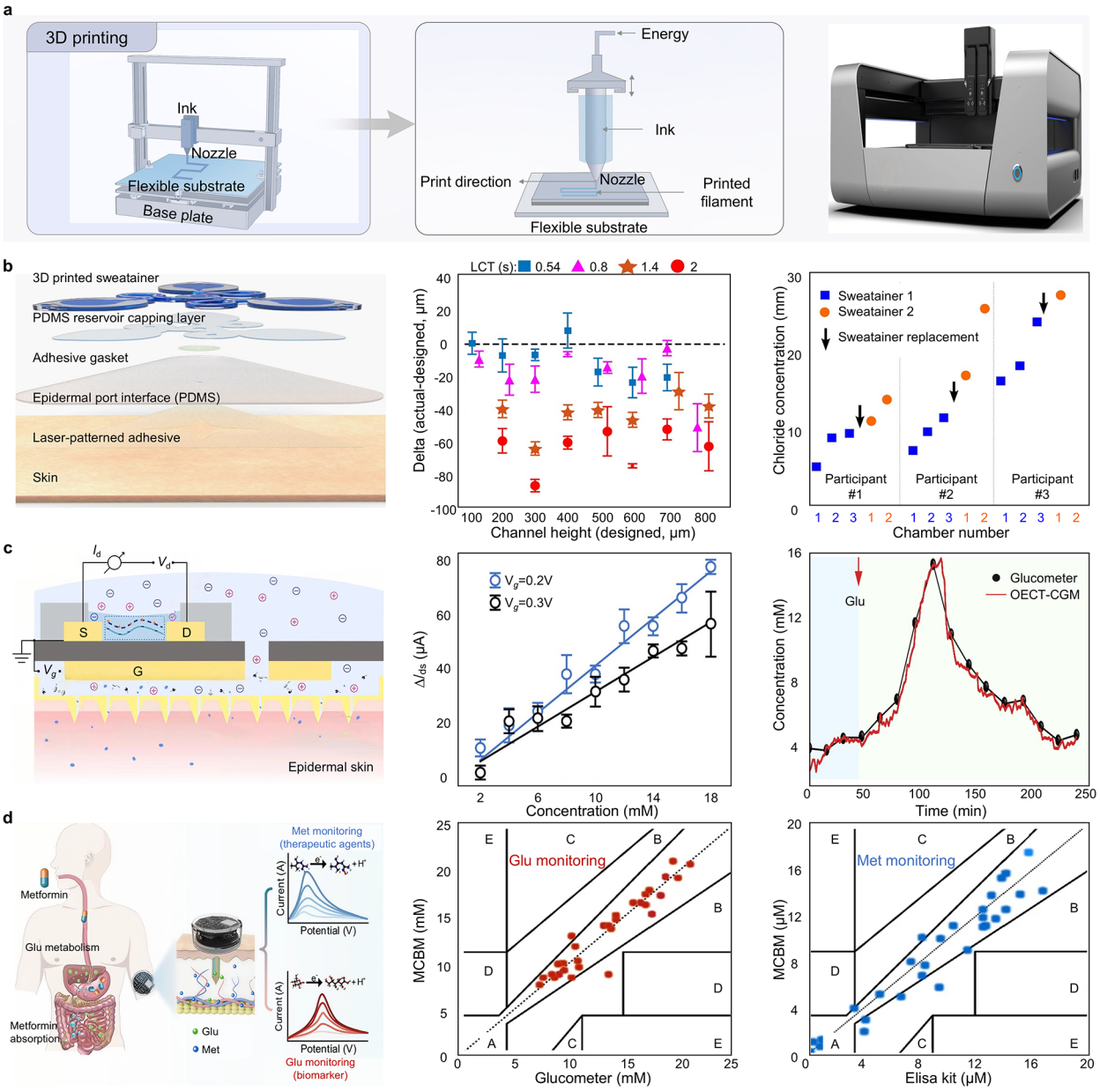

Figure 13. Preparation of wearable electronics via 3D printed and wearable biochemical sensors. (a) Schematic illustration depicting the fabrication process of 3D printed wearable electronics. Photographs of printing equipment. (b) Schematic depiction emphasizing the principal components of the sweatainer system and the epidermal interface. Plot illustrating the deviation of the printed channel height from the designed specifications as a function of LCT. Plot displaying sweat chloride concentrations obtained from two sequentially worn colorimetric sweatainers during a controlled exercise protocol. Scale bars: 5 mm. Reproduced with permission from ref 414. Copyright 2023 American Association for the Advancement of Science. (c) Schematic of the OECT glucose sensor and the sensing mechanism. Linear fitting of the current response of OECT to different glucose levels (2−18 mM), demonstrating a tunable sensitivity by controlling the V_g value. Comparison of real-time recording results between OECT-CGM and glucometer (in vivo) (black, 16 data points of the glucose concentration collected by a glucometer; red, readout of glucose concentrations collected by OECT-CGM). Reproduced with permission from ref 617. Copyright 2024 American Association for the Advancement of Science. (d) Microneedle-based minimally invasive dual-biomarker sensor. Clarke error grid analysis of glucose measured by the MCBM system in comparison with the commercial glucometer. Error grid analysis of Met using MCBM system in comparison with Met ELISA kit. Reproduced with permission from ref 618. Copyright 2025 Springer Nature. Abbreviations: LCT, layer cure time; Vg, gate voltage; Glu, glucose; OECT-CGM, organic electrochemical transistor-continuous glucose monitoring system; Met, metformin; MCBM, microneedle-based continuous biomarker/drug monitoring.

grade devices intended for prolonged dermal contact. Furthermore, the predominance of impermeable polymer substrates in current research poses risks of dermatitis and discomfort during extended wear. Consequently, future investigations must prioritize the development of materials combining high breathability with biocompatibility. Although the inherent porosity, renewability, and low density of paper render it an attractive substrate, its practical utility is historically compromised by hygroscopic susceptibility and chemical degradation. This vulnerability results in signal drift and instability in humid environments. To mitigate these reliability issues, an R2R lamination process was developed for

https://doi.org/10.1021/acs.chemrev.5c00801
Chem. Rev. XXXX, XXX, XXX−XXX

the batch fabrication of waterproof, high-consistency pressure sensors (Figure 12c).[585] The resulting laminated architecture proved suitable for applications ranging from physiological detection to aquatic monitoring. While effectively addressing stability concerns, this packaging strategy introduces a functional trade-off: the lamination process inevitably reduces the intrinsic breathability of the paper, potentially reintroducing the comfort limitations associated with polymeric substrates.

The capacity of R2R technology to efficiently produce high-quality, uniform film electrodes on a massive scale positions it as the preeminent method for the future high-throughput fabrication of wearable electronics. Future advancements must focus on refining R2R printing parameters, overcoming technical impediments, and optimizing module design and interconnections to maximize electrode effective areas and overall device performance. Moreover, integrating rigorous quality control mechanisms within R2R lines presents substantial challenges. The development of inline metrology systems for real-time feedback and immediate adjustment of manufacturing parameters is essential to ensure ink quality stability. In summary, R2R printing offers a promising trajectory for the industrial production of wearable electronics, emphasizing continuous coating, cost efficiency, and performance enhancement. However, the transition from laboratory-scale spin coating to industrial-scale R2R processing encompasses significant translational challenges. Innovations in material selection, process optimization, and holistic module design remain vital for enhancing efficiency, stability, and environmental sustainability.

9. 3D PRINTING

3D printing has established itself as a paradigm-shifting additive manufacturing framework for wearable electronics. By leveraging 3D digital models, this methodology enables the agile fabrication of bespoke sensor architectures and complex electrode geometries (Figure 13a), thereby dramatically accelerating development cycles.[586] The capability to construct intricate, on-demand patterns not only streamlines the rapid prototyping of electrodes but also facilitates extensive product customization,[587] offering a pathway to substantially reduced manufacturing costs for small-batch or geometrically sophisticated wearable systems. While the fabrication of discrete sensor elements is relatively mature, attaining the high spatial resolution necessary for dense, multifunctional sensor arrays remains a critical developmental frontier. Consequently, current research is intensely focused on advancing 3D printing modalities to address the multifaceted requirements of next-generation wearable electronics.

Among the various 3D printing technologies, fused deposition modeling (FDM) is one of the most ubiquitous approaches, favored for its technological maturity and cost-efficiency.[588] FDM operates via the extrusion of a thermoplastic filament, which is heated to a semimolten state and deposited sequentially along a programmed digital toolpath to construct objects layer-by-layer.[589] Upon deposition, the extrudate cools and solidifies to form the final structure. Although FDM offers resolution adequate for applications requiring moderate dimensional fidelity,[588] it is inherently limited when fabricating microarchitectures with fine feature definitions, such as the active layers of miniaturized sensors. In sharp contrast, vat photopolymerization technologies offer distinct advantages regarding spatial resolution and surface topology. Stereolithography (SLA), the pioneer of commercialized 3D printing, utilizes an ultraviolet (UV) laser beam to scan a photopolymer resin point-by-point, selectively cross-linking the irradiated regions.[590] SLA affords superior spatial resolution compared to extrusion-based methods, yielding components with smooth surface finishes and excellent feature definition. This precision renders SLA particularly advantageous for geometrically complex components, including miniaturized cavities[591] and microstructured channels,[592] which are otherwise challenging to realize via FDM.[593] Digital light processing (DLP), another dominant photopolymerization platform, similarly utilizes photocurable resins but distinguishes itself through the deployment of a digital micromirror device (DMD). The DMD acts as a dynamic mask, projecting and curing an entire 2D cross-section in a single exposure.[594] This area-based curing strategy significantly enhances fabrication throughput, with printing speeds reportedly several times faster than SLA under comparable conditions.[594] While photopolymer-based methods involve higher material costs and challenges regarding the mechanical robustness or long-term stability of certain formulations, their high resolution and superior surface finish have driven their adoption in wearable medical electronics.[595,596] For applications demanding biocompatibility and dimensional precision, DLP facilitates the low-volume production of miniature sensing elements.[597] The high patterning fidelity achieved by DLP and SLA is indispensable for reliable fluid handling and stable sensor−environment interfaces.[598] However, the advancement of these technologies in wearable applications hinges on the development of resin systems that are mechanically robust, biocompatible, and functionally integrated. Furthermore, process strategies must be refined to mitigate volumetric shrinkage and residual stress, which currently threaten device accuracy and long-term reliability.

In the realm of flexible and wearable electronics, direct ink writing (DIW) has emerged as a pivotal technique. DIW entails the extrusion of high-viscosity functional inks onto a substrate through a precision nozzle, enabling the construction of 3D architectures without extensive support structures.[599] The defining advantage of DIW is its exceptional material versatility, accommodating a broad spectrum of inks including hydrogels,[599] elastomers,[600] and conductive composites.[601] This compatibility permits the spatially resolved deposition of bioactive, conductive, or stimuli-responsive materials onto soft, flexible substrates, a capability essential for engineering conformal, skin-interfaced, or implantable devices. Consequently, DIW is widely applied in flexible sensors,[68,602] bioelectronics,[603] and soft robotics,[604] where tailored rheology and multimaterial printing enable the engineering of gradient properties and hierarchical architectures. To fully exploit DIW for high-performance electronics, ongoing efforts must focus on refining ink rheology, enhancing microscale printing precision, and improving the mechanical fatigue resistance of printed features under repeated deformation.

9.1. Core Process and Workflow

The 3D printing workflow for wearable electronics translates digital blueprints into functional physical systems through an integrated sequence: digital modeling, computational slicing, layer-by-layer deposition, and postfabrication refinement. The process initiates with a digital model of the target device, which is computationally discretized into a series of 2D cross sections. The layer thickness defines a fundamental trade-off

https://doi.org/10.1021/acs.chemrev.5c00801
Chem. Rev. XXXX, XXX, XXX−XXX

between fabrication throughput and z-axis resolution. During physical construction, hardware interprets this sliced data to deposit functional and structural materials with high fidelity. The precision of the final features is contingent upon deposition resolution and material interactions. Furthermore, achieving robust interlayer adhesion is paramount for ensuring mechanical integrity and operational durability. Finally, postprocessing protocols, including support removal and surface conditioning, are employed to yield the functionalized sensor system.

9.1.1. Material and Ink Design for 3D Printing. The successful translation of 3D printing technologies to wearable electronics is fundamentally contingent upon the rational design of printable materials and functional inks. While 3D printing offers unparalleled design freedom for constructing complex, multimaterial architectures, realizing this potential necessitates that precursor materials satisfy stringent rheological, mechanical, and physicochemical criteria. A primary prerequisite for high-fidelity printing is the precise tailoring of ink rheology. Functional inks must exhibit pronounced shear-thinning behavior, a rapid decrease in viscosity under shear stress during extrusion, followed by swift structural recovery and viscosity increase postdeposition.[605] This thixotropic behavior ensures smooth extrusion while preserving the fidelity of intricate printed features. Ink formulations typically involve the homogeneous dispersion of functional fillers within a compliant matrix to preclude aggregation, which could induce printing defects or compromise electronic performance.[606] Common matrix materials, such as PDMS,[607] thermoplastic polyurethane (TPU),[608] and polycaprolactone (PCL),[609] are selected for the balance of mechanical flexibility, processability, and biocompatibility essential for skin-interfaced applications.

Moreover, the mechanical demands of wearable electronics mandate exceptional durability and fatigue resistance. Beyond electrochemical and mechanical performance, materials must be compatible with curing protocols, demonstrate uniform film-forming capabilities, and maintain stability under operational environmental conditions. The capacity for multimaterial 3D printing is particularly critical, enabling the monolithic integration of functional sensing elements and encapsulation layers. Such consolidated manufacturing strategies streamline fabrication and enhance device integration density, paving the way for highly integrated wearable systems.

9.1.2. Digital Modeling and Design Preparation. The fabrication sequence commences with the generation of a 3D digital model representing the target device, ranging from conformal electrode arrays to integrated microfluidic–electronic hybrid structures. This CAD model must encode complete geometric data, including feature dimensions, internal architectures (e.g., lattice structures), and interface topologies. For wearable applications, critical design considerations include anatomical conformability to complex biological surfaces, designated integration points for rigid components, and precisely defined transition zones between conductive, insulating, and mechanically compliant domains.[604]

9.1.3. Computational Slicing and Toolpath Generation. The continuous 3D model is computationally discretized into 2D layers using specialized slicing algorithms, translating volumetric data into machine-executable code.[593,610,611] These instructions specify optimized toolpath trajectories to minimize discontinuities, programmed deposition sequences for multimaterial systems, and infill patterns that determine mechanical anisotropy. In wearable electronics, such optimization is challenging due to the complex rheological behavior of functional inks and the necessity of mitigating stress concentrations at heterogeneous material interfaces.

9.1.4. Layer-by-Layer Additive Deposition. In multimaterial platforms, parallel delivery channels facilitate in situ material switching while preventing cross-contamination. Central to this architecture is the deposition nozzle assembly; its geometry and actuation mechanisms are key determinants of the minimum achievable feature size and deposition rate. Supporting the process is the substrate platform, which provides mechanical stability and may incorporate active thermal management to modulate interlayer adhesion and residual stress. For flexible electronics, vacuum fixation is often employed to prevent substrate warpage, while platform compliance can be tuned to mitigate delamination risks.

9.1.5. Post-Processing. Following deposition, as-printed structures undergo postprocessing to achieve designated electrical, mechanical, and biological functionalities. Sacrificial support materials are removed mechanically or chemically. Crucially, conductive inks based on metal nanoparticles typically require a sintering step (thermal or photonic) to drive the evaporation of stabilizing ligands and promote particle coalescence.[612] This postdeposition treatment provides the energy necessary to overcome activation barriers for nanoparticle decomposition and surface diffusion-driven coalescence.[613] This process creates a percolated conductive network, thereby minimizing electrical resistivity and ensuring device performance.

9.2. Critical Process Parameters and Physicochemical Significance

The functional performance of 3D-printed wearable electronics is deterministically controlled by a complex interplay of process parameters. These variables define a multidimensional parameter space where synergistic or antagonistic effects often arise. A mechanistic understanding of their individual and collective influence is indispensable for rational process optimization and the reproducible fabrication of high-fidelity devices.

9.2.1. Layer Thickness. Defined as the vertical increment between successive strata, layer thickness is the primary determinant of resolution in the build (z) direction.[614] The selection of this parameter involves a critical trade-off: thinner layers yield superior feature fidelity and smoother surface topographies but increase fabrication time. Furthermore, excessively thin layers may jeopardize interlayer adhesion if consolidation is incomplete before subsequent deposition. Such adhesion deficiencies can lead to delamination under mechanical stress, compromising structural integrity. Future optimization must focus on energy delivery methods that accelerate layer consolidation without sacrificing resolution.

9.2.2. Printing Velocity. Printing velocity, the linear speed of the nozzle relative to the substrate, dictates the deposition rate and modulates the shear environment experienced by the ink. In extrusion-based modalities, velocity must be synchronized with extrusion pressure to control volumetric flux. Deviations from the optimal regime have deleterious consequences: velocities exceeding the material supply rate result in under-extrusion and discontinuous conductive traces, while insufficient speeds lead to overextrusion, feature broadening, and shorting in high-density circuits.[615] Addition-

https://doi.org/10.1021/acs.chemrev.5c00801
Chem. Rev. XXXX, XXX, XXX−XXX

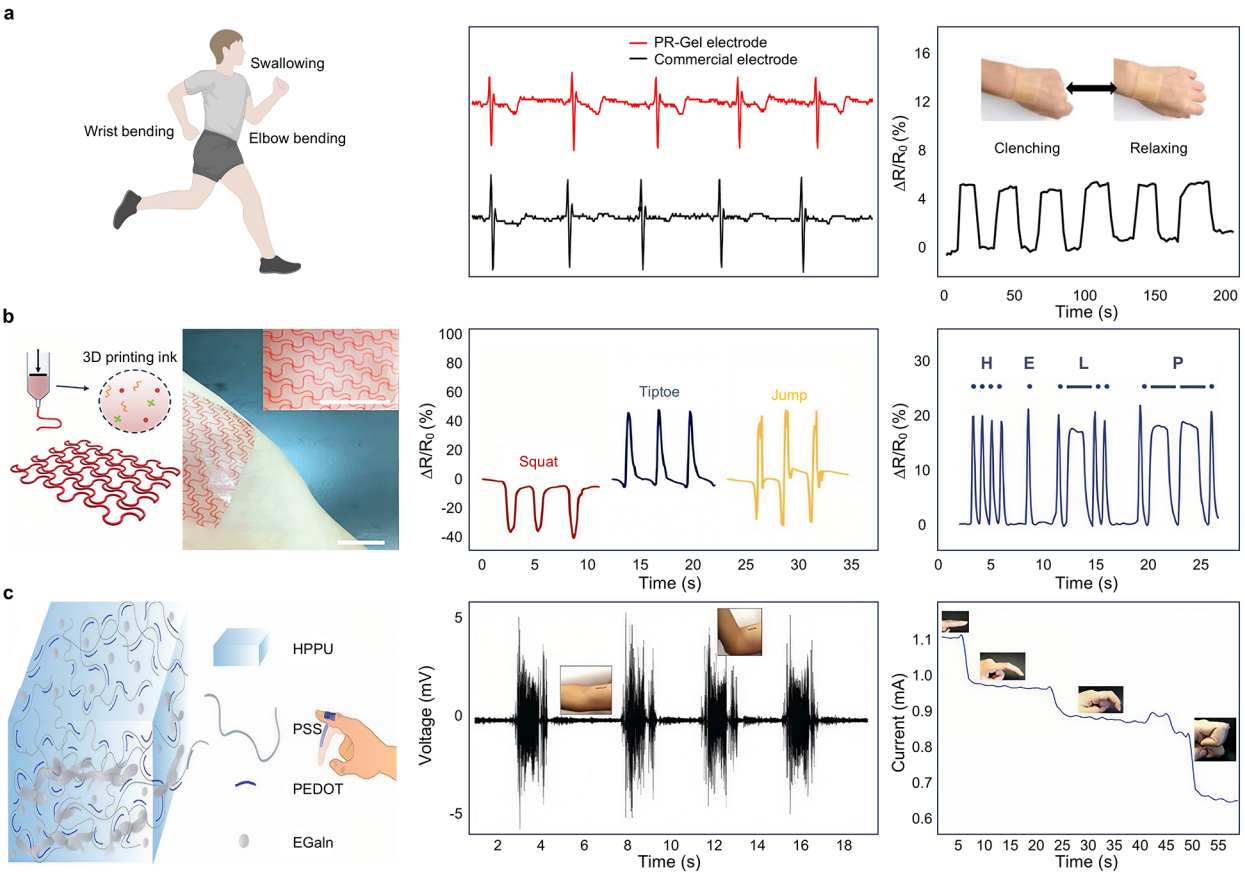

Figure 14. 3D printed wearable biophysical and electrophysiological sensors. (a) Schematic illustration of the PR-Gel-based flexible sensor adhered to anatomical locations including the throat, wrist, and elbow. Depicts the application of a 3D printing PR-Gel-based electrode for real-time monitoring of human ECG signals. Shows the relative resistance changes of the 3D printing PR-Gel-based wearable sensor during cycles of fist clenching and relaxation. Reproduced with permission from ref 619. Copyright 2023 Springer Nature. (b) Illustrates the fabrication process and microstructural features of the 3D skeleton-ionogel composites, alongside photographic images of the composite adhered to the skin surface, scale bars: 1 cm. Present signal monitoring corresponding to squatting, tiptoeing, and jumping movements. Demonstrate transmission of distress signals via Morse code using the sensor system. Reproduced with permission from ref 620. Copyright 2024 John Wiley and Sons. (c) Provides a schematic representation of the aSISC device architecture. Display EMG signals recorded utilizing the aSISC-based wearable apparatus. Illustrates the capability of the aSISC-based wearable strain sensor to discern a broad spectrum of finger bending angles. Reproduced with permission from ref 621. Copyright 2024 John Wiley and Sons. Abbreviations: PR-Gel, polymeric rotaxane hydrogels; HPPU, hydrophilic polyurethane; PSS, polystyrenesulfonate; PEDOT, poly(3,4-ethylenedioxythiophene); EGaIn, eutectic gallium−indium.

ally, printing velocity influences shear-thinning dynamics; elevated shear rates reduce apparent viscosity but may induce elastic instabilities upon extrusion, compromising filament stability.

9.2.3. Nozzle Diameter and Standoff Distance. The nozzle inner diameter fundamentally limits the minimum feature size, while the nozzle-to-substrate standoff distance critically influences feature morphology.[616] Upon exiting the nozzle, the extrudate undergoes radial expansion due to viscoelastic relaxation, followed by compression against the substrate. An insufficient standoff distance risks nozzle clogging and substrate damage, whereas an excessive gap diminishes compressive forces, resulting in widened, poorly defined traces. Lack of precise control over these parameters introduces variability in printed dimensions, directly affecting the impedance of conductive elements. Progress in this area relies on advanced nozzle designs and closed-loop control systems that dynamically adjust the standoff distance.

9.3. Fabrication and Application of 3D Printed Wearable Electronics

9.3.1. 3D Printed Biochemical Sensors. Additive manufacturing has established a robust paradigm for the construction of skin-interfaced biochemical sensors, enabling the seamless integration of microfluidic architectures with transduction elements. This capability is exemplified by "sweatainer" devices tailored for compartmentalized sweat collection and analysis (Figure 13b).[414] Optimization of the layer cure time (LCT) proved critical in this fabrication process, as it dictates print fidelity, dimensional resolution, and optical transparency. The simultaneous deployment of collection and colorimetric sweatainer facilitated the validation of on-body chloride quantification against clinical standards, corroborating physiological phenomena such as the inverse correlation between chloride reabsorption efficiency and perspiration rate during exertion. While these epidermal microfluidic systems represent a significant leap toward noninvasive diagnostics, fundamental limitations regarding universality and data fidelity persist. Specifically, exocrine-based analysis is intrinsically tethered to perspiration kinetics;

https://doi.org/10.1021/acs.chemrev.5c00801
Chem. Rev. XXXX, XXX, XXX−XXX

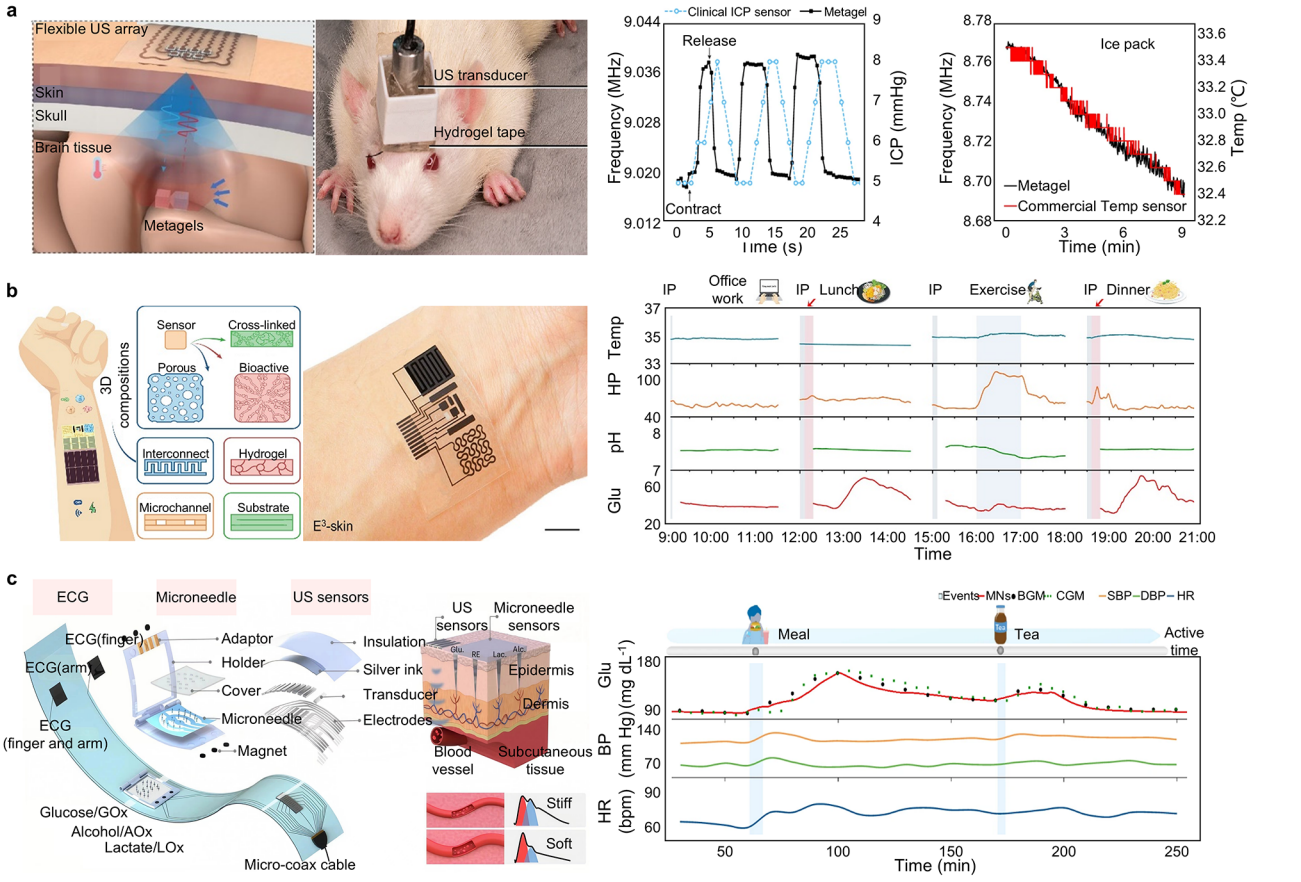

Figure 15. 3D printed wearable multimodal sensors. (a) Schematic representation of a wearable ultrasound helmet integrated with metagels for physiological monitoring applications. Photograph of a freely moving rat implanted with metagels and connected to an ultrasound transducer. Real-time wireless monitoring of ICP fluctuations during cyclic abdominal compression in the rat model. Intracranial temperature profiles obtained via temperature-sensitive metagel following the application of an ice pack. Reproduced with permission from ref 622. Copyright 2024 Springer Nature. (b) Schematic illustration of the approach employed for 3D printing of functional constructs. Optical micrographs of an E^3-skin adhered to a human subject's skin surface; scale bars, 1 cm. Continuous physicochemical monitoring of a human subject over an extended period encompassing various daily activities. Reproduced with permission from ref 100. Copyright 2023 American Association for the Advancement of Science. (c) The hybrid monitoring system integrates a multiplexed microneedle array. Cross-section of the skin with the microneedle array and ultrasound sensor array. Comparison of ISF microneedle glucose monitoring (every 1 s) against glucose measurements with CGM (every 5 min) and BGM (every 10 min), along with simultaneous monitoring of BP and HR. Reproduced with permission from ref 623, Copyright 2025 Springer Nature. Abbreviations: US, ultrasound; ICP, intracranial pressure; Temp, temperature; E^3-skin, epifluidic elastic electronic skin; IP, iontophoresis; Glu, glucose; HR, heart rate; Alc, alcohol; Lac, lactate; MNs, microneedles; BGM, blood glucose monitoring; CGM, continuous glucose monitoring system; SBP, systolic blood pressure; DBP, diastolic blood pressure; ECG, electrocardiography; BP, blood pressure; AOx, alcohol oxidase; GOx, glucose oxidase; LOx, lactate oxidase; RE, reference electrode.

in sedentary or hypothermic states, sample acquisition becomes stochastic, thereby impeding continuous monitoring. Furthermore, the susceptibility of sweat samples to dermal contaminants can compromise colorimetric accuracy. To circumvent these bottlenecks and achieve high-fidelity tracking of metabolites such as glucose, research has pivoted toward minimally invasive ISF sampling. A paramount challenge in continuous glucose monitoring (CGM) for closed-loop diabetes management involves harmonizing signal fidelity with operational robustness and user compliance. In response, a compact, fully integrated wearable CGM was engineered by synergizing biosensing elements with functional hydrogels and minimally invasive mechanics (Figure 13c).[617] The system's sensitivity is tunable, deriving from the linear dependence of the organic electrochemical transistor (OECT) transconductance on the applied gate voltage (V_g). In vivo validation in a hyperglycemic rat model confirmed the efficacy of this approach. However, standard metabolite monitoring lacks the capacity for pharmacokinetic profiling, which is indispensable for precision medicine. Addressing this deficiency, a wearable microneedle-based continuous biomarker/drug monitoring (MCBM) system was developed to facilitate simultaneous pharmacokinetic and pharmacodynamic assessments (Figure 13d).[618] This device integrates a 3D-printed dual-sensor microneedle electrode within a compact housing, employing a layer-by-layer nanoenzyme immobilization strategy to achieve high specificity for the concurrent quantification of glucose and Met in ISF. Clinical accuracy, validated via Clarke error grid analysis, underscores the potential of this technology to advance integrated theranostics, enabling real-time therapeutic modulation based on personalized metabolic profiles.

9.3.2. 3D Printed Biophysical and Electrophysiological Sensors. 3D printing has catalyzed advancements in the fabrication of wearable biophysical and electrophysiological sensors, where the mechanical integrity of functional materials is paramount. A pervasive limitation in conventional hydrogels

https://doi.org/10.1021/acs.chemrev.5c00801
Chem. Rev. XXXX, XXX, XXX−XXX

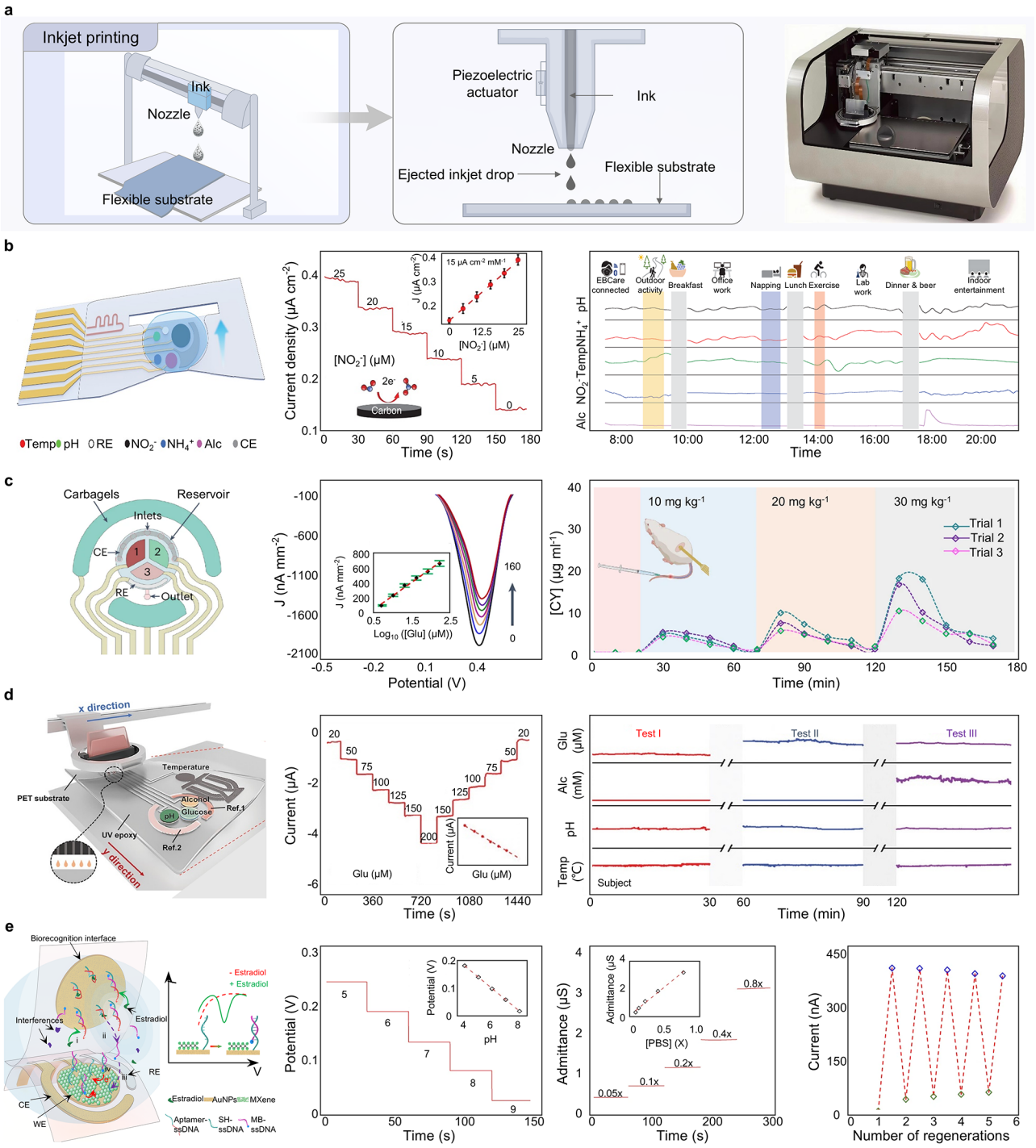

Figure 16. Preparation of wearable electronics via inkjet printed and wearable biochemical sensors. (a) Schematic illustration depicting the fabrication process of inkjet printing wearable electronics. Photographs of printing equipment. (b) Schematic representation of an inkjet printing electrochemical sensing array enabling simultaneous *in situ* multiplexed monitoring of EBC analytes, including NH_4^+, pH, alcohol, NO_2^-, and temperature. Amperometric responses of the NO_2^- sensor in artificial EBC with varying analyte concentrations. Insets: corresponding calibration curves (top right) and schematic diagrams of the NO_2^- sensors (bottom left). Full-day cross-reactivity analysis of EBC samples from a healthy participant monitored by the EBC system *in situ*. Reproduced with permission from ref 436. Copyright 2024 American Association for the Advancement of Science. (c) Schematic design of a wearable sweat sensor patch integrating sweat induction, microfluidic sweat sampling, and multiplexed analyte detection. DPVs of the MIP/NiHCF nanoparticle-based glucose sensor for glucose detection. Inset: calibration curve with linear fitting. CY levels monitored by implantable CY sensors in mice following lateral tail vein injections of varying CY doses. Reproduced with permission from ref 642. Copyright 2025 Springer Nature. (d) Schematic diagrams of a fully printed sensor array for simultaneous multiplexed biosensing, including electrodes for pH, glucose, alcohol, temperature, and reference sensing. Scale bar, 5 mm. Amperometric response of the glucose sensor. Real-time on-body analysis of sweat analytes from a human subject. Reproduced with permission from ref 643. Copyright 2024 John Wiley and Sons. (e) Reagentless *in situ* quantification of oestradiol using an AuNPs−MXene sensor coupled with a target-induced strand-displacement aptamer switch. Potentiometric response and corresponding calibration curve (inset) of pH sensors in artificial sweat. Impedimetric

https://doi.org/10.1021/acs.chemrev.5c00801
Chem. Rev. XXXX, XXX, XXX−XXX

Figure 16. continued

response and corresponding calibration curve (inset) of ionic strength sensors in artificial sweat. Peak current measurements demonstrating regeneration and repeated use of aptamer-based oestradiol sensors with 50 pM oestradiol. Reproduced with permission from ref 343. Copyright 2023 Springer Nature. Abbreviations: Glu, glucose; CY, cyclophosphamide; AuNPs, gold nanoparticles; SH-ssDNA, thiolated single-stranded DNA; MB-ssDNA, methylene blue-tagged single-stranded DNA.

is their susceptibility to fatigue failure under cyclic loading. To mitigate this, a supramolecular toughening strategy was implemented involving the self-assembly of acrylic β-cyclodextrin and bile acid into polymerizable pseudorotaxanes. Subsequent photopolymerization with acrylamide yielded a conductive polymeric rotaxane hydrogel (PR-Gel).[619] This architecture endows the material with the sensitivity required to discriminate between macroscopic somatic movements and subtle neuromuscular fluctuations (Figure 14a). The high resolution afforded by 3D printing allows for the fabrication of structurally intricate sensors capable of stable, real-time ECG monitoring, highlighting the utility of PR-Gel-based electronics. Concurrently, the development of biomimetic artificial skin that replicates the hierarchical mechanics of the human integument offers a pathway toward advanced human−machine interfaces. By coupling finite element analysis with DIW, researchers have engineered ionogel composites featuring a rigid skeletal phase embedded within a soft matrix.[620] This configuration yields mechanical anisotropy and nonlinear pressure−strain responses analogous to native tissue. The resulting biomimetic skin exhibits excellent epidermal conformability, with the skeletal structure visually demarcated (Figure 14b). Its mechanical compliance facilitates the translation of fine motor control into structured data, such as Morse code transmission. While this framework provides a robust method for creating adaptive tissue-like materials, achieving durable, nonirritating adhesion to dynamic surfaces remains a critical engineering hurdle. Furthermore, next-generation epidermal electronics demand conductors that reconcile high electrical conductivity with tissue-level elasticity. To this end, a printable composite comprising LM and a conductive polymer, processed via thermally induced self-assembly, has been reported.[621] The integrated heating phase is essential for solvent elimination, preserving the electromechanical integrity of the asymmetric self-insulated stretchable conductors (aSISC) fabricated via 3D printing (Figure 14c). The versatility of the aSISC platform has been demonstrated in skin-interfaced strain and EMG sensors, suggesting broad applicability in sophisticated biomedical electronics.

9.3.3. 3D Printed Multimodal Sensors. The convergence of physicochemical sensing modalities within wearable and implantable platforms constitutes a pivotal advance toward predictive health analytics. Precise interrogation of intracranial physiology, for instance, is vital for the management of traumatic brain injury. 3D printing has facilitated the creation of an injectable, bioresorbable metagel sensor for the wireless, multimodal monitoring of intracranial ultrasound and thermal signals.[622] Functioning as a standalone implant, this device eliminates the need for percutaneous tethers, a distinct advantage over conventional wired intracranial pressure (ICP) probes (Figure 15a). The temperature-sensitive metagel mirrors the performance of commercial probes, tracking thermal fluctuations with high fidelity. While this bioresorbable paradigm minimizes surgical burden, ensuring long-term material stability and signal integrity during the functional degradation cycle remains a priority for future optimization. Transitioning to noninvasive applications, the scalability of personalized, multimodal devices is often hindered by manufacturing constraints. Addressing this, a versatile semi-solid extrusion technique was employed to fabricate an epifluidic elastic electronic skin (E^3-skin) capable of multiparametric sensing (Figure 15b).[100] This platform amalgamates electrochemical biosensors for sweat analysis with biophysical sensors for temperature and pulse monitoring. In longitudinal studies, the E^3-skin provided a continuous data stream that, when processed via ML algorithms, demonstrated predictive capability regarding behavioral responses. Moreover, comprehensive diabetes management necessitates a holistic metabolic profile that transcends single-analyte monitoring. To this end, a hybrid wristband was developed, integrating a 3D-printed microneedle array for ISF biomarker quantification with an ultrasonic array for hemodynamic monitoring, including blood pressure, arterial stiffness, and heart rate (Figure 15c).[623] This system elucidates the crosstalk between systemic physiological parameters and interstitial biomarkers. By expanding the monitoring scope to include cardiovascular comorbidities, this integrated approach represents a strategic evolution in chronic disease management.

Despite the inherent advantages and promising prospects of 3D printing technology, challenges persist. These encompass the diversity of sensing-active functional materials, sensor performance limits, the need for improved printing speed and precision, and reductions in equipment costs. To surmount these challenges and propel 3D printing technology forward, researchers are focusing on novel material development, optimization of printing processes, and equipment efficiency enhancements. Additionally, substantial improvements in 3D printing precision and speed are anticipated. With optimized algorithms and hardware advancements, future 3D printers are expected to fabricate more refined and intricate structures while significantly augmenting printing speed and production efficiency.

10. INKJET PRINTING

Inkjet printing has established itself as a cornerstone additive manufacturing paradigm for the fabrication of next-generation wearable electronics, characterized by superior material utilization efficiency, precise patterning resolution, and scalability. As a noncontact, digital direct-write technique, it facilitates the directed deposition of functional materials onto flexible substrates via micrometer-scale nozzles, with patterning governed strictly by computational design.[624] The technology's defining attributes render it an exceptionally versatile platform for realizing complex, variable-data device architectures. By selectively ejecting picoliter-scale droplets solely at coordinates dictated by the target design, inkjet systems eliminate the material waste associated with subtractive methods and circumvent the complex charging and deflection hardware required by legacy systems (Figure 16a). These digitally modulated droplets are accurately deposited onto compliant substrates to form nascent sensor arrays, which are

https://doi.org/10.1021/acs.chemrev.5c00801
Chem. Rev. XXXX, XXX, XXX−XXX

subsequently consolidated through specific curing protocols. Consequently, the capacity for rapid prototyping and automated process control positions inkjet printing as an ideal methodology for manufacturing wearable electronics with minimized equipment complexity, resource consumption, and energy footprint.

10.1. Core Process and Workflow

Inkjet printing represents a transformative approach to device fabrication, fundamentally diverging from conventional photolithographic workflows. The technology generally operates via two distinct modalities: continuous inkjet (CIJ) and drop-on-demand (DOD) systems.[625] While CIJ systems rely on a continuous stream of droplets that are selectively charged and deflected, DOD systems eject droplets only when triggered by a digital signal. In the context of wearable electronics, DOD is the predominant modality due to its precise volume control and superior capability for direct-write patterning without the need for fluid recirculation.

10.1.1. Material and Ink Design for Inkjet Printing. The fidelity and functionality of flexible electronics fabricated via inkjet printing are intrinsically linked to the rheological and physicochemical engineering of the ink formulation. This fabrication paradigm relies on the interplay between high-resolution deposition and digital layout control to realize intricate device geometries.[626] Developing a viable ink represents a multivariate optimization challenge involving three primary constituents: the functional active material, the carrier fluid (solvent system), and colloidal stabilizers. The active component dictates intrinsic device metrics, such as sensitivity and LOD, while stabilizing agents are critical for preventing particle agglomeration via steric or electrostatic repulsion. The carrier fluid is selected to tailor the rheology and ensure homogeneous dispersion. Functionally, these inks fall into two broad archetypes. Nanoparticle-based inks consist of colloidal suspensions where the functional layer forms upon solvent evaporation and sintering of the solid load.[627] Conversely, precursor-based inks utilize dissolved molecular species, such as metal salts or organometallics, which undergo in situ thermochemical or photochemical conversion to form the final functional material during postprocessing.[628] Reliable jettability demands that the ink's rheological profile falls within a narrow operational window, typically requiring low viscosity (<20 cP)[629] and optimized surface tension (20−50 mN/m). These parameters govern the acoustics of droplet formation at the nozzle and the spreading dynamics upon substrate impact. To preclude nozzle clogging, the hydrodynamic diameter of suspended particulates must typically be at least 1 order of magnitude smaller than the nozzle orifice. Furthermore, the formulation often necessitates auxiliary agents, including surfactants and humectants, to modulate interfacial tension and inhibit premature solvent evaporation at the nozzle interface.

10.1.2. Process Control and Functional Device. The translation of a digital design into a functional physical device follows a rigorous sequence. Initially, CAD-generated architectures are rasterized into machine-readable deposition maps. Concurrently, the flexible substrate undergoes surface modification. Treatments such as plasma activation[630] or chemical functionalization[631] are employed to tune surface energy, thereby optimizing wettability and enhancing interfacial adhesion with the deposited ink. During printing, piezoelectric or thermal actuators within the printhead generate acoustic pressure waves in response to digital signals, ejecting droplets from the nozzle.[632] These droplets traverse the standoff gap and impinge upon the substrate, where they coalesce to form a continuous pattern. The final phase involves controlled postprocessing to transform the liquid precursor into a robust solid-state layer with the requisite electromechanical properties.[632] The maskless nature of this direct-write approach distinguishes it from screen printing or photolithography, facilitating high-throughput combinatorial screening and rapid design iteration for bespoke electronic applications.

10.1.3. Post-Processing. A critical bottleneck in scaling inkjet technology for mass production lies in the postprocessing phase. The necessity for sintering conductive materials typically conflicts with the low thermal budgets of polymeric flexible substrates.[633] This thermal mismatch often restricts material selection to those processable at lower temperatures, which frequently results in incomplete removal of organic binders and inferior electrical conductivity. This deficiency directly compromises the performance-to-cost ratio of printed devices. Consequently, future research must pivot toward advanced, nonthermal energy transfer techniques, such as photonic sintering (laser/flash)[633] or low-temperature plasma sintering, to decouple the functionalization of the ink from the thermal degradation thresholds of the substrate.[634]

10.2. Critical Process Parameters and Physicochemical Significance

The reliability and resolution of inkjet-printed electronics are governed by the complex coupling of material rheology, process settings, and substrate thermodynamics. Elucidating these critical variables is essential for mitigating defects and enhancing device yield.

10.2.1. Process Control Parameter. In piezoelectric DOD systems,[635] the drive voltage waveform is meticulously shaped (often trapezoidal) to control the acoustic resonance within the fluid chamber. Optimization of rise, dwell, and fall times is required to suppress satellite droplets and ensure velocity uniformity. While jetting frequency determines throughput, droplet velocity dictates impact kinetics; higher velocities enhance spreading but increase the probability of splashing on lyophobic surfaces, necessitating an application-specific balance.[636] Furthermore, thermal management is 2-fold: printhead temperature modulates ink viscosity, while substrate temperature governs drying kinetics. Elevated substrate temperatures can suppress the coffee-ring effect by inducing Marangoni flows; however, excessive evaporation rates relative to coalescence times result in morphological inhomogeneities, underscoring the need for precise thermal regulation.

10.2.2. Substrate−Ink Interaction Parameter. The thermodynamic interaction between the ink and substrate dictates feature resolution and film morphology. To maximize device performance, conductive traces must exhibit high uniformity and minimized line widths.[637] The equilibrium contact angle (θ) is a primary determinant; hydrophilic surfaces facilitate spreading for continuous films, while hydrophobic regimes confine droplets for higher resolution.[638] Additionally, the droplet spacing-to-diameter ratio controls film continuity.[639] Insufficient overlap results in electrically discontinuous islands, whereas excessive overlap induces hydrodynamic instabilities, leading to bulging and scalloped edges.

https://doi.org/10.1021/acs.chemrev.5c00801
Chem. Rev. XXXX, XXX, XXX−XXX

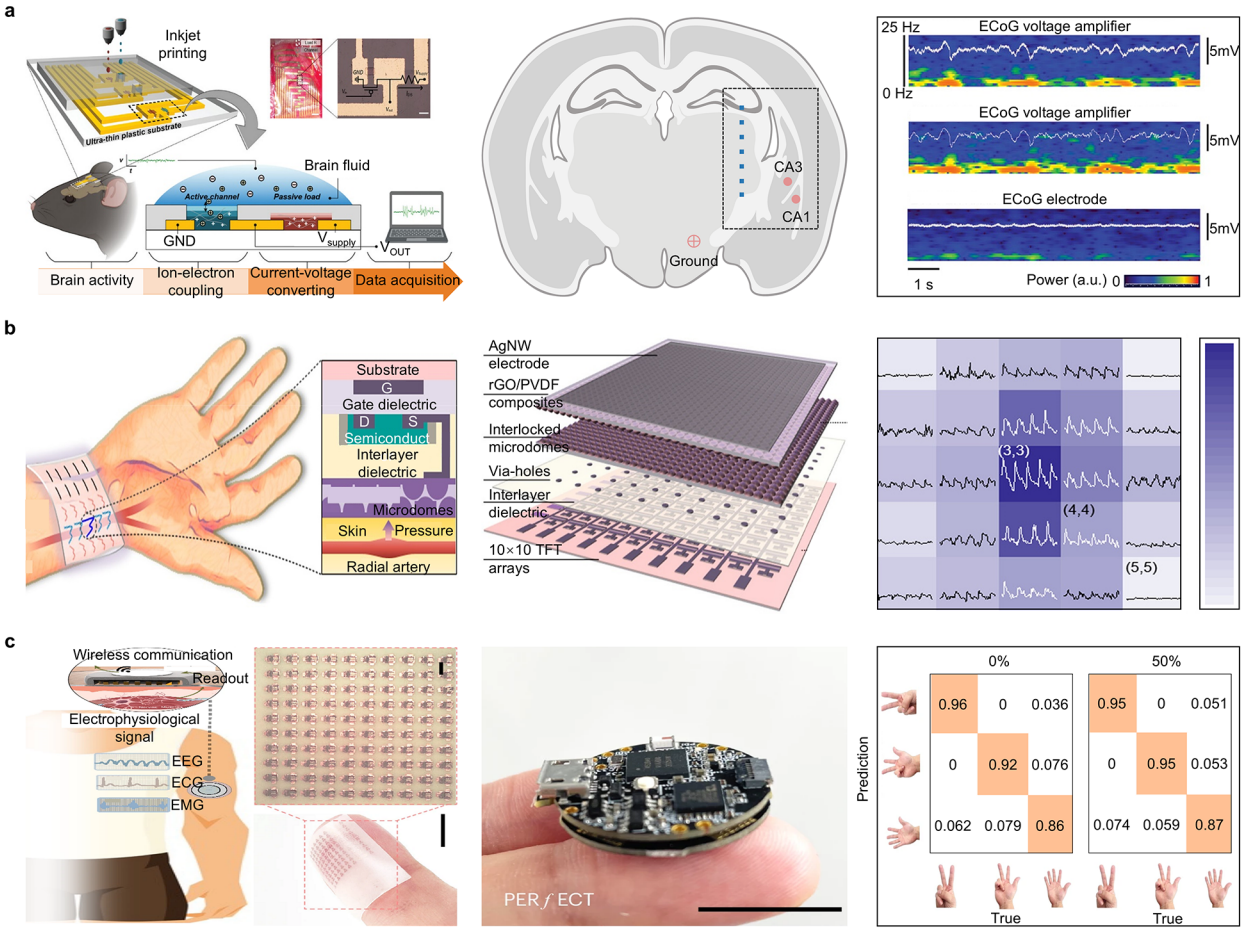

Figure 17. Inkjet printed wearable biophysical and electrophysiological sensors. (a) Configurations of multiple inkjet printing ECoG probes integrating both active OECTs and passive resistors positioned on the cortical surface of rats. Schematic illustration of device placement on a horizontal section of a rat brain. Spectrograms depicting spontaneous oscillatory activity recorded simultaneously via voltage amplifiers with varying channel thicknesses and surface electrodes. Reproduced with permission from ref 644. Copyright 2023 John Wiley and Sons. (b) Schematic representation of pulse wave measurement across the radial artery using Inkjet printing wearable sensor arrays. 3D schematic of wearable active-matrix pressure sensor arrays comprising inkjet printing active-matrix TFT arrays coupled with piezoresistive sensor sheets. Contour map of average pressure amplitudes and real-time arterial pulse signals measured at each pixel. Reproduced with permission from ref 645. Copyright 2022 American Chemical Society. (c) Design strategy for a coin-sized WISE platform, scale bar: 1 cm. Optical images of the personalized electronic reader for the electrochemical transistors control unit; scale bar, 1 cm. Comparison of confusion matrices under 0% and 50% strain. Reproduced with permission from ref 646. Copyright 2024 Springer Nature. Abbreviations: GND, ground, V_{supply}, supply voltage; V_{out}, voltage output; OECT, organic electrochemical transistor; TFT, thin-film transistor.

10.2.3. Nozzle Diameter and Standoff Distance. Nozzle diameter is the principal hardware constraint defining the limit of resolution.[640] While reducing orifice size enables picoliter-volume droplets and finer circuit geometries essential for high-density sensor arrays, it imposes severe constraints on ink formulation. Specifically, the risk of orifice occlusion by particle aggregates necessitates strict colloidal stability and filtration. Moreover, smaller nozzles generally require lower viscosity fluids or higher actuation pressures,[641] exacerbating susceptibility to aerodynamic drift. Therefore, nozzle selection represents a compromise between resolution and process robustness.

The vertical gap between the nozzle and substrate standoff distance is equally critical. Excessive gaps increase the flight time, rendering droplets susceptible to aerodynamic drag and trajectory deviation, which degrades positional accuracy. Furthermore, extended flight times can lead to in-flight solvent loss, altering the viscosity and wetting behavior upon impact. Conversely, insufficient clearance risks mechanical collision and damage to the printhead. Precise optimization of this parameter is therefore requisite to ensure the reproducibility and structural integrity of the fabricated wearable electronics.

10.3. Fabrication and Application of Inkjet Printed Wearable Electronics

10.3.1. Inkjet Printed Biochemical Sensors. In the realm of physiological monitoring, the quantification of biomolecular concentrations provides fundamental insights into metabolic and systemic health. The fabrication of mechanically compliant, noninvasive interfaces for continuous analyte tracking presents a substantial engineering challenge, which has been increasingly addressed through the rheological optimization of functional inks and inkjet printing protocols. To realize high-sensitivity, temporally stable, and wide-dynamic-range multiplexed monitoring, research has focused on advanced ink formulations and droplet-assisted patterning methodologies. These strategies, when integrated with interpenetrating interface architectures, have facilitated reliable sensing within fully integrated multiplexed EBC biosensor

https://doi.org/10.1021/acs.chemrev.5c00801
Chem. Rev. XXXX, XXX, XXX−XXX

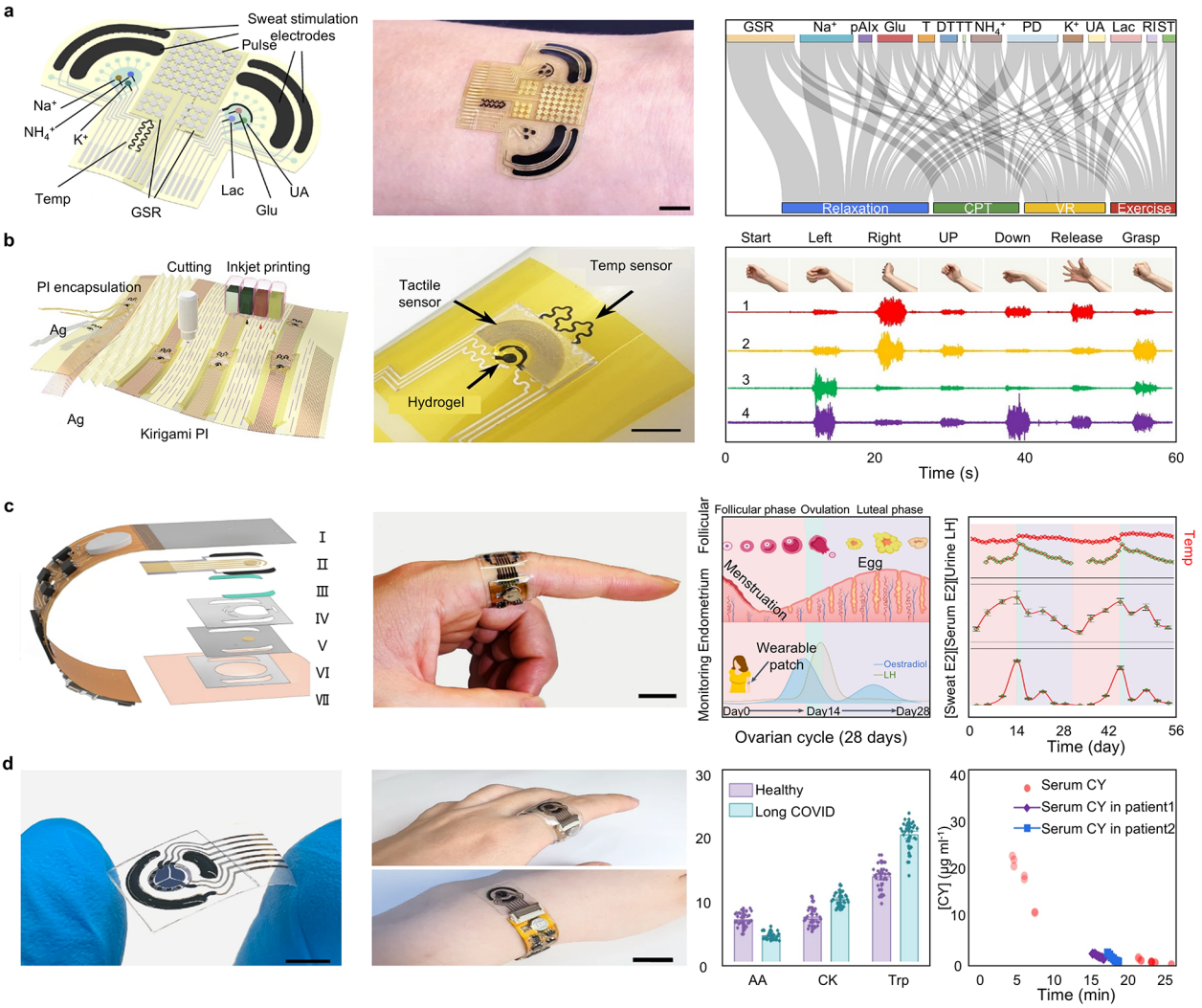

Figure 18. Inkjet printed wearable multimodal sensors. (a) Schematic representation of the flexible CARES sensor patch. Optical images of the CARES patch adhered to human skin; scale bars, 1 cm. Sankey diagram from SHAP analysis illustrating the relative contributions of individual sensors to stressor classification. Reproduced with permission from ref 647. Copyright 2024 Springer Nature. (b) Schematic illustration of the rapid, scalable, and cost-effective fabrication of the kirigami soft E-skin-R via Inkjet printing. Photograph of a multimodal flexible sensor array printed with custom nanomaterial inks; scale bar, 5 mm. sEMG data recorded by the four-channel E-skin-H during six distinct human gestures. Reproduced with permission from ref 116. Copyright 2022 American Association for the Advancement of Science. (c) Layered design of a flexible, wireless microfluidic wearable patch enabling automatic sweat induction via IP, precise sampling through capillary bursting valves (CBVs), and reagentless aptamer-based oestradiol analysis. Photographs of a disposable sensor patch worn on a finger for female hormone monitoring, scale bars: 1 cm. Hormonal fluctuations are tracked over the menstrual cycle. Reproduced with permission from ref 343. Copyright 2023 Springer Nature. (d) Photographs of a wearable patch for noninvasive multiplexed sweat biomarker analysis. Scale bars, 5 mm. Photographs of fully integrated wireless wearable patches worn on the finger and wrist, scale bar: 1 cm. Box plot of sweat AA, CK, and Trp levels from the healthy and long COVID participants. Error bars represent the sd of the mean from 30 measurements on all three participants. CY levels obtained by the wearable sweat sensors from two cancer patients with diagnosed AML after CY infusion. Reproduced with permission from ref 642. Copyright 2025 Springer Nature. Abbreviations: UA, uric acid; Lac, lactate; Glu, glucose; T, temperature; GSR, galvanic skin response; HR, heart rate; IP, iontophoresis; DT, dicrotic peak time; PD, pulse duration; pAIx, peripheral augmentation index; RI, reflection index; ST, systolic time; TT, tidal peak time; CPT, cold pressor test; VR, a virtual reality; PI, polyimide; Exp, experimental result; Sim, simulation result; LH, luteinizing hormone; AA, ascorbic acid; CK, creatinine; Trp, tryptophan; r, Pearson's correlation coefficient; CY, cyclophosphamide; AML, acute myeloid leukaemia.

arrays.[436] Such systems typically incorporate electrochemical arrays for selective biomarker transduction, complemented by pH and temperature modules for in situ signal calibration to mitigate environmental variances (Figure 16b). Empirical validation has demonstrated the utility of these EBC sensors for continuous sampling in ambulatory settings, successfully tracking physiological fluctuations in human subjects during diverse activities including exertion, nutrient intake, and rest. Despite these advances, the broad deployment of electrochemical sensors is frequently hindered by a restricted analyte spectrum, operational drift, and scalability issues. To circumvent these impediments, a distinctive strategy employing printable core−shell nanoparticles has been established for both powered implantable and wearable metabolite biosensors (Figure 16c).[642] These nanostructures feature a MIP shell for customizable molecular recognition and a nickel hexacyanoferrate (NiHCF) core to mediate stable electrochemical transduction. In vivo pharmacokinetic assessments in murine

https://doi.org/10.1021/acs.chemrev.5c00801
Chem. Rev. XXXX, XXX, XXX−XXX

models, involving intravenous drug administration at varying dosages, confirmed the sensor's capacity for real-time therapeutic drug monitoring. This integration of MIP technology with electrochemically active nanomaterials constitutes a pivotal progression in chemical sensing, offering a versatile platform for high-specificity detection. However, while MIPs offer synthetic flexibility, challenges remain regarding cross-reactivity with structural analogs and the incomplete removal of template molecules, which can compromise analytical precision. Future optimization must focus on enhancing template elution protocols and refining cavity specificity to ensure clinical-grade accuracy. Concurrently, electrochemical biosensing via sweat analysis has garnered attention for noninvasive physiological profiling. A persistent bottleneck involves the precise integration of multiplexed arrays on flexible substrates while maintaining reproducibility. Addressing this, a fully inkjet-printed, integrated multiplexed biosensing patch exhibiting superior stability has been reported (Figure 16d).[643] This device advances intelligent healthcare by enabling reliable, wireless dietary and medical monitoring via epidermal analysis. The system demonstrated robust selectivity and sensitivity toward target biomarkers, validating its efficacy for multiplexed sensing on deformable platforms. Building upon these foundations, the field is pivoting toward the detection of ultralow abundance biomarkers, such as female reproductive hormones. A notable development in this domain is a wireless wearable sensor utilizing a target-induced strand-displacement aptamer switch mechanism (Figure 16e).[343] This device enables in situ automatic electrochemical monitoring of oestradiol with subpicomolar sensitivity. The sensor's robust regeneration capabilities are particularly advantageous for longitudinal monitoring, marking a significant stride toward personalized female health management.

10.3.2. Inkjet Printed Biophysical and Electrophysiological Sensors. Inkjet printing has proven to be a versatile lithography-free technique for fabricating sensors targeting biophysical and electrophysiological signals. In advanced neural interfaces, flexible transistor-based active probes offer intrinsic signal amplification and distinct mechanical compliance with biological tissues. However, a primary technical limitation is their inherent current-mode output, which complicates back-end circuit integration and necessitates proximal signal conditioning. To resolve this, organic voltage amplifiers have been engineered via the monolithic integration of OECTs and thin-film polymer resistors on flexible substrates.[644] Functioning as ECoG probes, these devices have successfully recorded local field potentials derived from spontaneous neural activity in rodent models (Figure 17a). Transitioning to noninvasive cardiovascular monitoring, the clinical utility of conventional tonometry is often limited by the need for precise arterial alignment. This constraint has been addressed through the development of inkjet-printed active-matrix pressure sensor arrays for spatiotemporal pulse wave mapping.[645] These arrays combine high-uniformity thin-film transistor (TFT) backplanes with high-sensitivity piezoresistive sheets. By modulating the TFT operating voltage, an optimal balance between sensitivity and power consumption is achieved. The transduction mechanism relies on arterial pulsation deforming interlocked microdomes within the piezoresistive layer, thereby modulating contact resistance to gate the TFT current (Figure 17b). While this architecture resolves positioning sensitivity, reliance on the physical deformation of microstructures introduces potential failure modes related to mechanical fatigue and hysteresis during long-term use. Future iterations must address material viscoelasticity to ensure durable mechanical performance. In the domain of strain sensing, the simultaneous attainment of high sensitivity and extreme stretchability remains a critical objective. A significant advancement is the wearable integrated soft electronics (WISE) platform, constructed from stretchable OECT arrays (Figure 17c).[646] The inclusion of an adhesive supramolecular buffer layer dissipates strain energy, preserving electrical functionality under deformation. Coupled with a personalized electronic reader, the WISE platform leverages the high transconductance of OECTs for high-fidelity EMG acquisition. This intrinsic stretchability mitigates motion artifacts, facilitating the accurate classification of complex gestures and establishing a trajectory for advanced human–machine interfaces.

10.3.3. Inkjet Printed Multimodal Sensors. The complex interplay between the nervous, endocrine, and immune systems necessitates multimodal sensing platforms capable of deconvoluting biological stress responses. Conventional sensors often lack the dimensionality required to evaluate condition-specific stress. Recent work has introduced an electronic skin (E-skin) platform designed for the noninvasive assessment of stress via the simultaneous monitoring of physiological parameters and molecular biomarkers.[647] This consolidated artificial-intelligence-reinforced electronic skin (CARES) continuously tracks three vital signs and six sweat biomarkers (Figure 18a). Shapley additive explanations (SHAP) analysis was employed to quantify the contribution of individual physicochemical sensors to stress classification, thereby elucidating the significance of specific biomarkers. Expanding beyond personal health, ultrasensitive multimodal platforms are increasingly relevant for autonomous robotic perception. While robotic sensing has historically prioritized physical parameters, chemical detection in dry-phase environments remains underdeveloped. To bridge this gap, a mass-producible, fully inkjet-printed soft electronic skin (M-Bot) integrating AI for multimodal sensing has been developed.[116] The fabrication utilized nanomaterial inks with rheological properties tailored for inkjet compatibility (Figure 18b). These arrays are engineered for electrophysiological recording, tactile perception, and hazardous substance detection, including nitroaromatic explosives and pathogens like SARS-CoV-2. While broad-spectrum detection is vital for robotics, clinical scenarios often demand the high-specificity tracking of single key biomarkers. This is exemplified in women's health, where a fully integrated wearable system for autonomous sweat oestradiol sensing has been validated[343] (Figure 18c). Comparative studies involving serum and sweat analysis across menstrual cycles confirmed that sweat oestradiol peaks correlate with preovulation events, establishing its potential as a noninvasive ovulation predictor. Extending these capabilities to pathological monitoring, printed biosensors have been applied to multiplexed sweat analysis for disease management (Figure 18d).[642] Pilot studies have explored sweat biomarkers as indicators for long COVID, while on-body evaluations were conducted on patients with AML and sickle cell disease (SCD) undergoing chemotherapy. These applications underscore the transformative potential of integrating advanced functional materials into wearable formats for comprehensive disease tracking.

Inkjet printing technology is a pivotal method for achieving the cost-effective, large-scale, refined manufacturing of

https://doi.org/10.1021/acs.chemrev.5c00801
Chem. Rev. XXXX, XXX, XXX−XXX

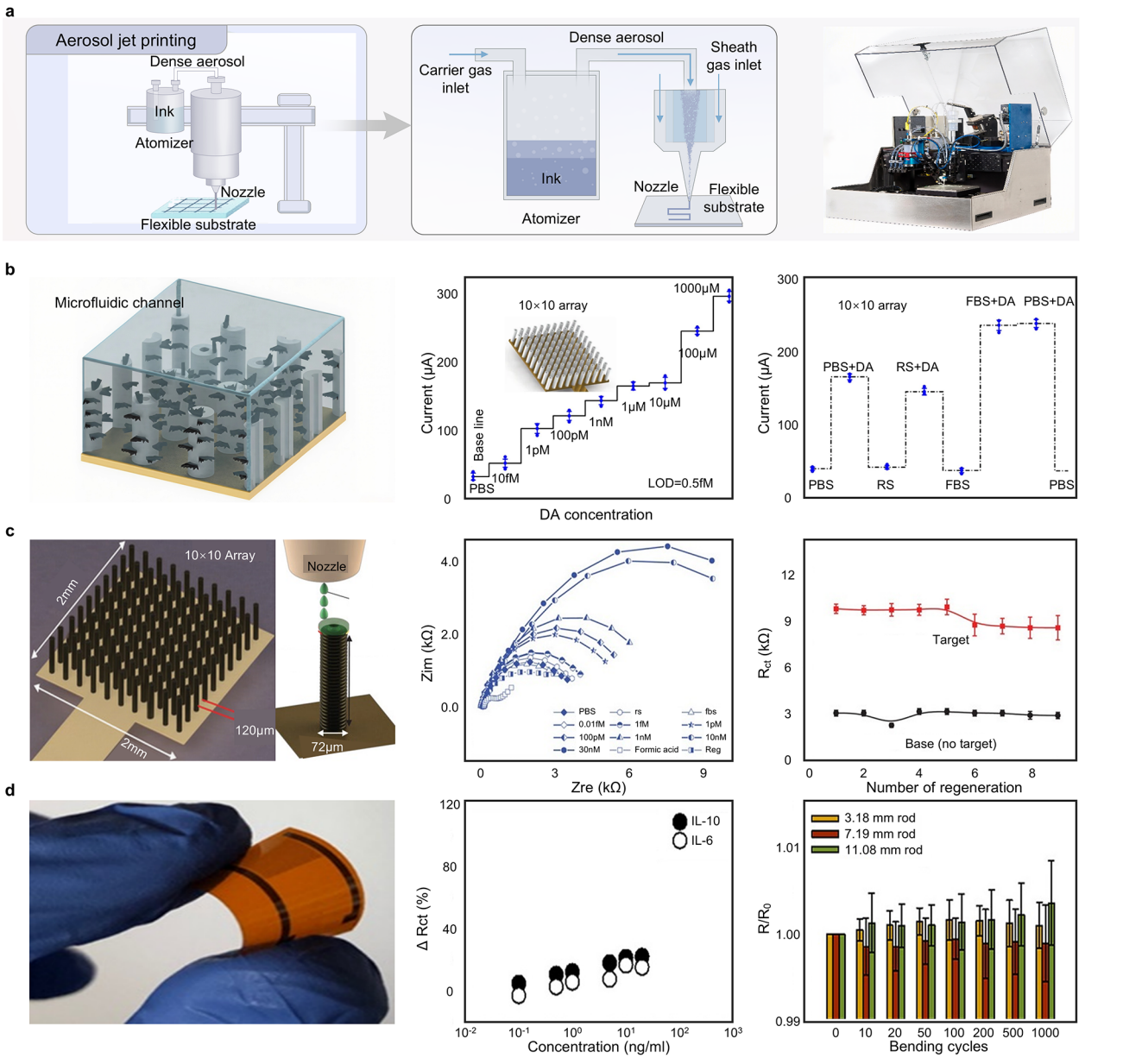

Figure 19. Preparation of wearable electronics via aerosol jet printed and wearable biochemical sensors. (a) Schematic illustration depicting the fabrication process of aerosol jet printed wearable electronics. Photographs of printing equipment. (b) Schematic representations of Brownian motion of target molecules for a 3D electrode within the microfluidic chamber. Current responses with varying DA concentration for multiscale 3D Ag/rGO (10 × 10 array) configurations, respectively. The detection time for all the results in this figure is within 60 s. The chronoamperometric responses of serum with and without DA for the sensor. Reproduced with permission from ref 527. Copyright 2021 Springer Nature. (c) Photograph of a glass substrate patterned with a gold film. Nyquist plots of the sensor obtained via EIS. Regeneration study presenting Nyquist plots alongside charge transfer resistance values during the detection of spike S1 antibodies using the device. Reproduced with permission from ref 662. Copyright 2020 John Wiley and Sons. (d) Photographs of an AJP-fabricated graphene-based immunosensor. Cross-Reaction test. Change in the resistance of AJP graphene IDE vs the number of bending cycles without any biofunctionalization. Reproduced with permission from ref 663. Copyright 2020 American Chemical Society. Abbreviations: US, ultrasound; NP, nanoparticles; WE, working electrode; DA, dopamine.

wearable electronics, with extensive application in constructing electrodes, sensor-active layers, and flexible circuits. While significant improvements have been made in the efficiency and performance of current Inkjet printing ink systems, future advancements necessitate a deeper understanding of the inks' physicochemical properties in practical applications. Developing comprehensive ink performance evaluation systems, including assessing viscosity, particle size distribution of sensing materials, and transmittance, is essential for advancing functional ink development.[624] Moreover, challenges related to the stability, printability, postprocessing, and quality of printed functional inks on wearable flexible substrates remain critical areas of investigation. Lastly, optimizing the balance between sensor sensitivity and monitoring range necessitates further exploration, potentially through the formation of microstructures on electrode surfaces or adjusting the number of inkjet layers to enhance sensor performance.

https://doi.org/10.1021/acs.chemrev.5c00801
Chem. Rev. XXXX, XXX, XXX−XXX

11. AEROSOL JET PRINTING (AJP)

Aerosol jet printing (AJP) has established itself as a pivotal noncontact, direct-write methodology for the additive manufacturing of wearable electronics.[648] This technique functions by generating a refined aerosol from functional inks, which is subsequently transported via an inert carrier gas and aerodynamically focused onto a substrate to define microscale patterns.[649] The fundamental workflow for fabricating wearable sensors via AJP is delineated into distinct operational phases (Figure 19a).

The architectural advantages of AJP for wearable sensor fabrication are manifold. The noncontact deposition mechanism permits conformal patterning onto substrates exhibiting complex three-dimensional topographies or nonplanar geometries, overcoming the planarity constraints of traditional lithography. Furthermore, AJP demonstrates superior resolution capabilities, achieving line widths as narrow as 10 μm,[649] thereby satisfying the integration density required for advanced sensor arrays. A distinguishing characteristic of this technology is its extensive rheological compatibility, accommodating ink viscosities ranging from 1 to 1000 cP. This versatility significantly mitigates nozzle clogging.[650] Material utilization efficiency is notably high, ensuring the conservation of expensive functional precursors. Additionally, the capability for multimaterial deposition enables the monolithic construction of heterogeneous, multilayered sensor architectures. Economically, AJP obviates the need for photomasks and cleanroom environments, offering a digitally driven, high-throughput alternative to photolithography that facilitates rapid prototyping and the agile production of customized, small-batch wearable devices.

11.1. Core Process and Workflow

The fabrication of wearable electronics via AJP involves a synchronized sequence of hydrodynamic and kinematic operations that convert liquid precursors into high-fidelity sensor structures. A thorough comprehension of these stages is prerequisite for process stability and defect minimization.

11.1.1. Material and Ink Design for Aerosol Jet Printing. Deposition kinetics in aerosol-based systems are dictated by a complex matrix of coupled variables, including aerosol and sheath gas flow rates and translation velocity.[651] The intricate interplay among these parameters governs the aerosol density and focusing behavior. Inadequate control over ink rheology or processing conditions can precipitate jetting instabilities, such as varicose breakup or satellite droplet formation, which degrade feature resolution and electrical continuity. To mitigate these deficiencies, ink development must adhere to stringent criteria. First, rheological properties require precise modulation within the 1−1000 cP viscosity window to sustain stable atomization.[652] Second, functional particulates must exhibit narrow, nanoscale size distributions to ensure printing fidelity and prevent orifice occlusion.[653] Future advancements in this domain necessitate the implementation of real-time feedback loops to dynamically adjust process parameters, thereby compensating for rheological fluctuations during extended printing sessions.

11.1.2. Atomization Mechanism. Following formulation, the precursor undergoes atomization, a phase transition generating a dense aerosol mist. Two dominant mechanisms are employed: ultrasonic atomization[654] and pneumatic atomization.[655] Ultrasonic atomization exploits high-frequency acoustic excitation (typically 1−3 MHz) to induce capillary waves at the liquid−gas interface, ejecting droplets via the Rayleigh−Plateau instability. This modality is generally restricted to low-viscosity fluids but yields a narrow droplet size distribution. Conversely, pneumatic atomization utilizes high-velocity gas streams to exert shear forces on the bulk liquid, accommodating significantly higher viscosities. While offering broader material versatility, pneumatic methods typically produce a more polydisperse aerosol, which can necessitate downstream filtration or inertial impaction steps to refine the droplet population.

11.1.3. Aerosol Transport and Focusing. The generated aerosol is propelled from the atomization chamber to the deposition head by a carrier gas (e.g., nitrogen or argon). Within the deposition head, a critical aerodynamic focusing phenomenon occurs: a coaxial sheath gas flow confines the aerosol stream, collimating it into a tight jet with a diameter significantly smaller than the nozzle orifice.[656] The gap between the nozzle exit and the substrate standoff distance is a crucial geometric parameter governing feature definition. Deviations in this distance can lead to beam divergence and loss of resolution; therefore, rigorous control is essential for maintaining consistent morphology.

11.1.4. Pattern Deposition. Pattern definition is realized through the synchronized trajectory of a high-precision, digitally controlled multiaxis stage relative to the substrate. The stage executes programmed vector paths while the aerosol jet deposits material continuously or intermittently. The deposition kinetics are governed by the translation speed: lower velocities facilitate material accumulation, yielding thicker, continuous traces, whereas higher velocities produce thinner, potentially discontinuous features. Multipass strategies allow for the precise tuning of film thickness and conductance. For sophisticated architectures, the process is iterative, enabling the sequential deposition of conductors, dielectrics, and sensing elements to construct functional multilayer devices.[653,657]

11.2. Critical Process Parameters and Physicochemical Significance

The functional integrity of AJP-fabricated devices relies on the rigorous optimization of interdependent variables encompassing ink rheology, aerodynamic conditions, and substrate interactions. Elucidating these process−structure−property relationships is vital for ensuring reproducibility and device performance.

11.2.1. Atomization Parameter. In ultrasonic systems, the excitation frequency dictates the droplet size distribution and generation rate;[658] higher frequencies yield finer droplets but reduce mass throughput. Power input must be balanced to maintain atomization efficiency without inducing excessive Joule heating, which could alter ink viscosity or degrade sensitive precursors. For pneumatic configurations,[659] the gas flow rate and pressure determine the shear magnitude. While higher flow rates enhance atomization fineness, they may induce turbulence within the transport lines, leading to wall losses and inconsistent delivery rates.

11.2.2. Deposition Parameter. The sheath gas flow rate is a critical hydrodynamic parameter,[659] defining the collimation ratio of the aerosol beam. An optimized flow ensures high resolution; however, insufficient sheath flow results in beam divergence, while excessive flow can cause turbulence, deflection, and overspray. This overspray compromises edge definition and can lead to short circuits in high-

https://doi.org/10.1021/acs.chemrev.5c00801
Chem. Rev. XXXX, XXX, XXX−XXX

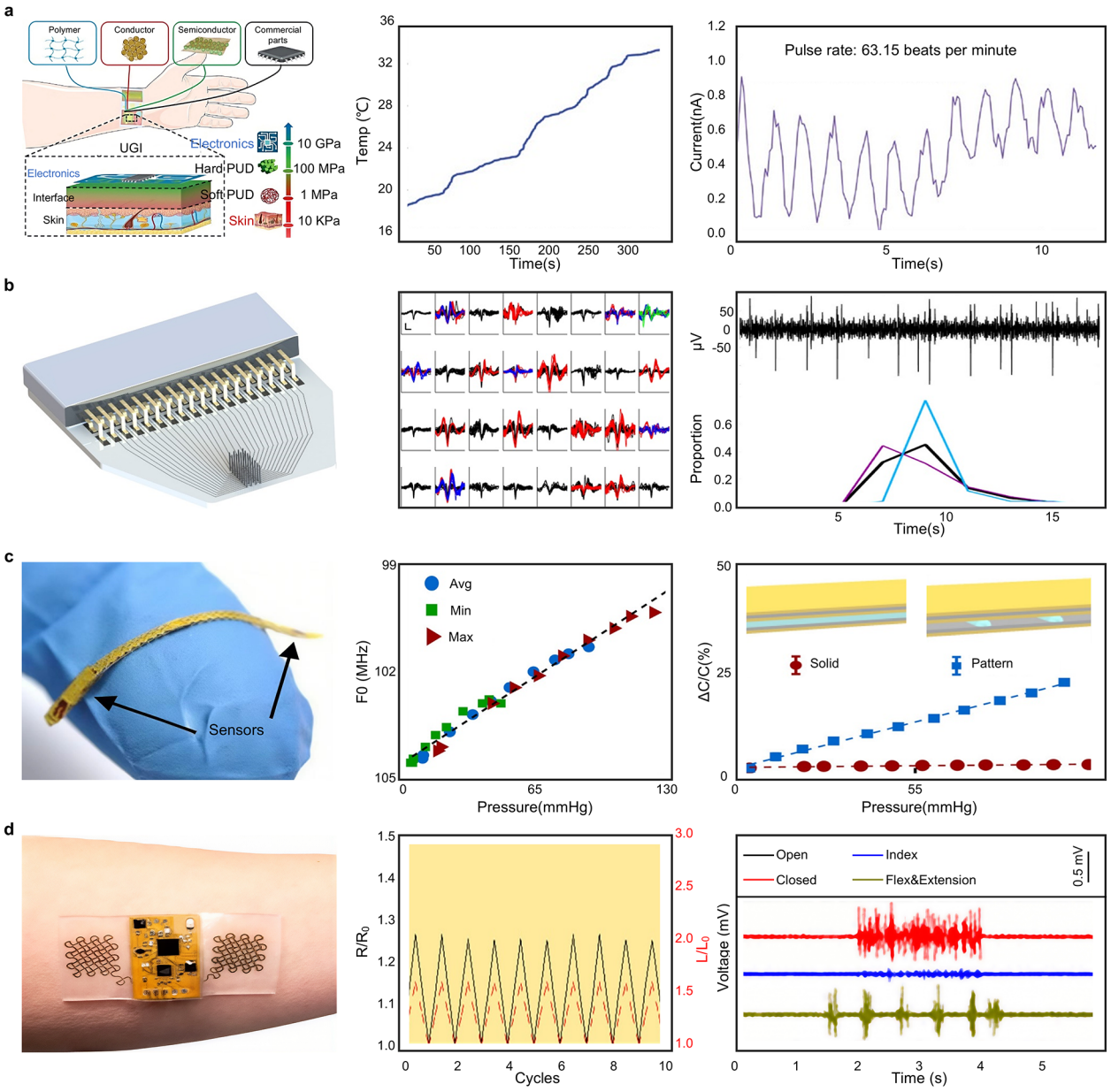

Figure 20. Aerosol jet printed wearable biophysical and electrophysiological sensors. (a) Stretchable devices enabled by universal gradient interface printed using aerosol-based multimaterials printing. AJP-based temperature sensor. AJP-based pulse sensor. Reproduced with permission from ref 112. Copyright 2025 John Wiley and Sons. (b) Schematic of AJ 3D printing of metal nanoparticles rapidly creates structurally robust, fully customizable neural probes, including the circuit board for routing of physiological signals. Spike waveforms extracted from a 32-channel electrode placed in mouse sensorimotor cortex; scale bar, 1 ms × 100 μV. Individual isolated neurons are shown in different colors (black, 1; red, 2; blue, 3; green, 4). Representative trace of neural activity from a single channel. Scale bar, 100 ms. Distribution of average firing rate identified in (A) (magenta), (B) (cyan), and across all eight recording sessions (black). Reproduced with permission from ref 664. Copyright 2022 U.S. National Academy of Sciences. (c) Photo of index finger holding a simultaneous flow and pressure sensor. The top and bottom electrodes are printed separately and laminated together. Summary of wireless pressure sensing of average, maximum, and minimum pressures during pulsatile flow. Pressure sensitivity is enhanced by using a dielectric layer of patterned PDMS lines compared to a solid film with similar thicknesses. Reproduced with permission from ref 665. Copyright 2022 U.S. National Academy of Sciences. (d) Photograph of a fabricated bioelectronic system mounted on the forearm for the recording of EMG. Relative resistance change in an electrode upon cyclic 60% stretching for 10 times. The graph represents relative resistance change (black) according to strain change (red). Representative EMG signals from four different gestures, including open hand (black), closed hand (red), index finger flexion (blue), and wrist flexion (green). Reproduced with permission from ref 666. Copyright 2020 U.S. National Academy of Sciences. Copyright 2020 American Chemical Society. Abbreviations: UGI, universal gradient interface; PUD, polyurethane dispersion; PI, polyimide; PDMS, polydimethylsiloxane; AgNPs, silver nanoparticles; Avg, average; Min, minimum; Max, maximum; US, ultrasound.

density arrays. Improvement strategies involve rigorous computational fluid dynamics modeling to predict optimal flow ratios. Print speed modulates the linear mass density;[660] improper speed selection can result in discontinuous tracks or bulging. Finally, substrate temperature governs solvent evaporation kinetics and contact line dynamics.[661] Thermal

https://doi.org/10.1021/acs.chemrev.5c00801
Chem. Rev. XXXX, XXX, XXX−XXX

modulation is frequently employed to accelerate drying and suppress the "coffee-ring effect" by inducing Marangoni flows that redistribute solutes, thereby enhancing film uniformity and electrical performance.

11.3. Fabrication and Application of Aerosol Jet Printed Wearable Electronics

11.3.1. Aerosol Jet Printed Biochemical Sensors. AJP technology has proven to be a versatile tool for fabricating wearable electronics capable of high-fidelity biochemical signal transduction. The detection of clinically significant biomarkers, particularly neurotransmitters at trace concentrations, is pivotal for early pathology diagnosis; however, reliance solely on surface nanostructuring often fails to achieve the requisite ultralow limits of detection. To address this, a hierarchical sensing platform was engineered by integrating AJP-deposited graphene nanosheets with 3D-printed silver microcolumns, resulting in a multiscale electrode architecture (Figure 19b).[527] In this configuration, dopamine (DA) quantification is achieved via microfluidic injection under static conditions, where the current response correlates linearly with the concentration of DA during its catalytic oxidation to DA-quinone. Under physiological pH, the electrostatic interaction between cationic DA molecules and the negatively charged Ag/reduced graphene oxide (rGO) microcolumn interface facilitates direct electron transfer. The superior electrochemical performance of these 3D-architected electrodes highlights the efficacy of multiscale structural design in sensing applications. Building upon this paradigm, the scope of AJP-based biosensing was expanded from small-molecule neurotransmitters to macromolecular targets, including antibodies. For example, a biosensing platform utilizing 3D-printed electrodes functionalized with AJP-deposited rGO nanoflakes and viral antigens was developed for the rapid serological detection of COVID-19 antibodies.[662] Integrated into a microfluidic system with a standard three-electrode configuration (Figure 19c), the device was characterized via EIS. The sensors demonstrated robust operational stability, maintaining functionality across multiple regeneration cycles for the detection of spike S1 and receptor-binding domain antibodies. Concurrently, an AJP-fabricated graphene immunosensor was established for the simultaneous quantification of interferon-gamma (IFN-γ) and interleukin-10 (IL-10) (Figure 19d).[663] These moieties served as anchor sites for the covalent immobilization of specific antibodies, yielding excellent specificity with negligible cross-reactivity against analogous cytokines. The platform's mechanical resilience further underscores its applicability in flexible, wearable bioanalysis.

11.3.2. Aerosol Jet Printed Biophysical and Electrophysiological Sensors. The advancement of stretchable electronics has facilitated the creation of conformal devices capable of accommodating the dynamic topography of biological surfaces, a prerequisite for high-fidelity epidermal and implantable monitoring. A persistent challenge in this domain is the decoupling of genuine physiological signals from mechanical strain-induced artifacts. To mitigate this, an ultrastretchable, strain-insensitive bioelectronic platform was fabricated using AJP (Figure 20a).[112] Key to this system was a universal gradient interface (UGI) designed to mediate the mechanical impedance mismatch between soft tissues and rigid electronic elements. The multimaterial deposition capability of AJP allowed for submicrometer control over local mechanical properties, resulting in a device with superior motion artifact rejection. This enabled precise monitoring of blood oxygen saturation, temperature, and cardiac rhythms without signal degradation. In the realm of neurological research, microelectrode arrays are indispensable for electrophysiological recording, yet conventional lithographic approaches often lack the flexibility to produce architectures tailored to specific anatomical requirements. A novel manufacturing methodology combining AJP-based high-precision metal deposition with multilayer circuit printing was demonstrated to fabricate customizable 3D nanoparticle-based microelectrode arrays (Figure 20b).[664] This approach yielded high-density arrays with tunable geometries and low channel impedance. In vivo validation within the sensorimotor cortex of anesthetized mice confirmed neural recording capabilities commensurate with traditional rigid platforms, offering a scalable route for next-generation neural interfaces. For cardiovascular management, continuous hemodynamic monitoring via wireless implants offers significant clinical value. A wireless vascular monitoring system, comprising a multimaterial sensing stent integrated with printed soft sensors, was developed to address constraints related to device dimensions and power requirements (Figure 20c).[665] This platform facilitated battery-free real-time telemetry of arterial pressure, pulse rate, and blood flow. While integrating sensing modalities onto vascular stents marks a significant advancement in intelligent implants, a critical impediment to translation involves the hemocompatibility of the printed materials. The interaction between nonbiological surfaces and blood presents a substantial risk of thrombogenesis; therefore, rigorous quantitative assessment of surface bioinertness is essential to prevent embolization and ensure long-term patient safety. Furthermore, the rise of flexible materials has enabled noninvasive biopotential recording. An additive nanomanufacturing strategy utilizing direct AJP of nanomaterials and polymers was employed to fabricate stretchable, dry-contact graphene biosensors (Figure 20d).[666] These sensors, which adhere directly to the skin without conductive gels, exhibited stable resistance and enhanced bioelectric signal quality. When integrated with machine learning (ML) algorithms, the system successfully classified distinct muscle activation patterns for robotic control. While this work presents a comprehensive solution spanning materials to computation, the long-term stability of the skin−sensor interface remains a challenge. Specifically, perspiration and intense physical activity can alter interfacial impedance, potentially compromising signal integrity over prolonged monitoring periods.

The trajectory of AJP technology in wearable sensing is poised for significant evolution, contingent upon addressing several interconnected technical frontiers. A primary imperative is the enhancement of feature definition and registration fidelity, necessitating the engineering of advanced aerodynamic nozzle geometries and high-precision kinematic control architectures. Concurrently, the library of printable feedstocks must be expanded to include functionalized, biocompatible fluids optimized for seamless biointegration. Furthermore, the realization of sophisticated device architectures requires refined protocols for the heterogeneous integration of multimaterial stacks to ensure interfacial mechanical integrity. To transition from prototyping to industrial viability, throughput limitations must be mitigated through increased deposition rates and the implementation of intelligent process control systems, where ML algorithms enable autonomous, in situ parameter optimization. Despite these prospects, barriers

https://doi.org/10.1021/acs.chemrev.5c00801
Chem. Rev. XXXX, XXX, XXX−XXX

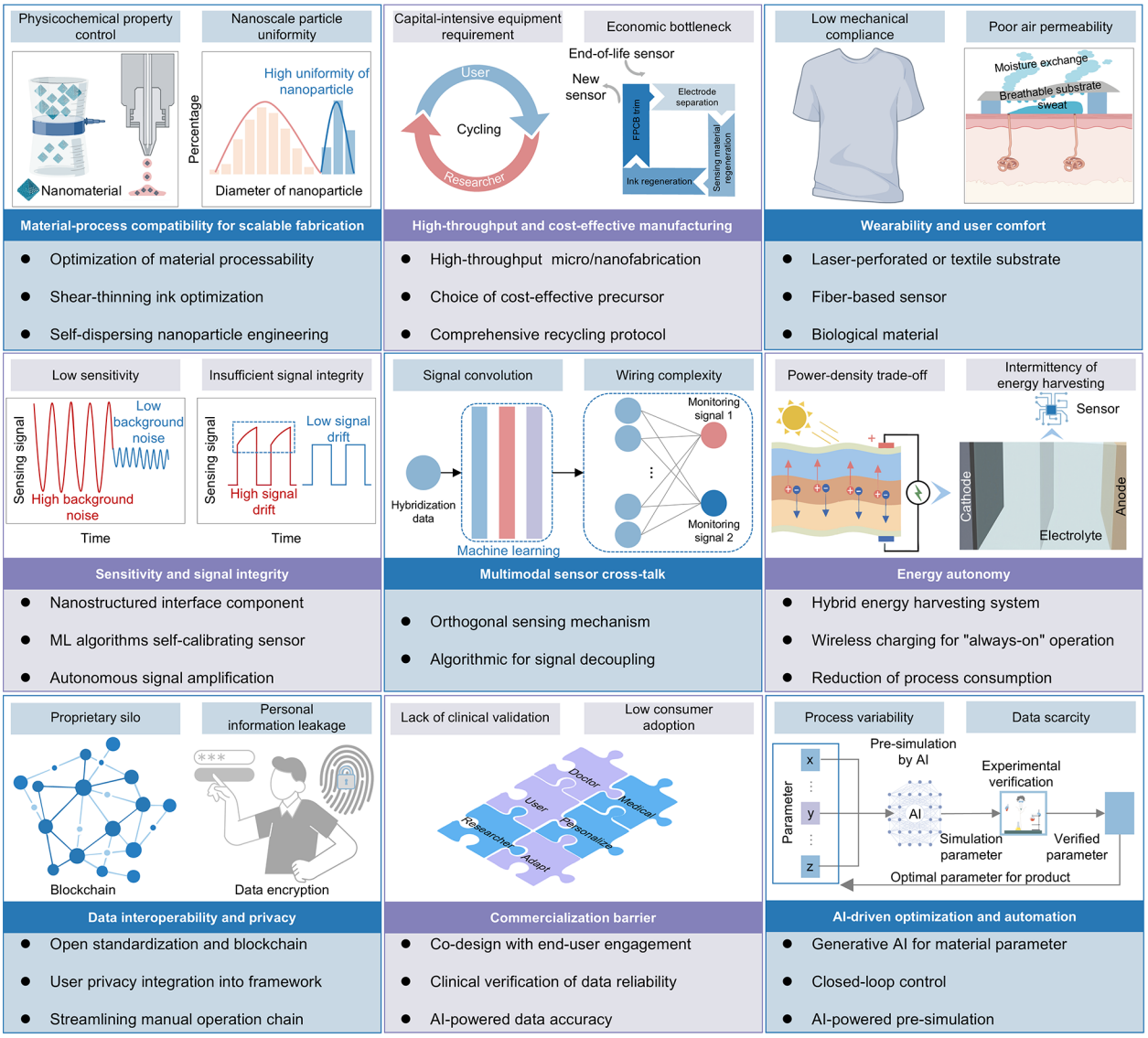

Figure 21. Conclusion and Perspective of wearable electronics. Abbreviations: AI, artificial intelligence; FPCB, flexible printed circuit board; F, force; M, metal; WIFI, wireless fidelity; 5G, fifth-generation mobile communication technology.

to widespread adoption persist. The capital expenditure for AJP systems remains high relative to techniques such as electrospinning. Moreover, the process window is governed by a complex interplay of parameters that demands meticulous optimization. Throughput constraints further limit mass production scalability. Additionally, ink engineering for specialized functional materials requires balancing rheological performance with printability. Future efforts must focus on standardizing processes and investigating environmental stability (e.g., humidity, thermal fluctuations) to unlock the full potential of AJP in high-throughput healthcare applications.

12. CONCLUSION AND PERSPECTIVE

Real-time monitoring of individual clinical parameters is essential for advancing personalized healthcare and telemedicine, a goal increasingly achievable through miniaturized and highly integrated wearable electronics.[667] Recent breakthroughs in wearable electronics, driven by diverse micro/nanofabrication strategies, have dramatically broadened the scope of detectable targets, while significantly improving the analytical performance, functionality, and operational durability of these systems. Among these advancements, alternative micro/nanofabrication techniques stand out as pivotal innovations shaping the future of wearable electronics. Leveraging these fabrication approaches, wearable electronics now span a wide range of applications, unlocking unprecedented opportunities for real-time health monitoring in daily life. Overall, advanced manufacturing technologies such as screen printing, R2R printing, 3D printing, inkjet printing, and AJP have jointly promoted the development of the wearable industry. For example, they must meet the basic requirements of good flexibility, conductivity, biocompatibility, and environmental protection, but they also present their own unique characteristics in terms of viscosity, dispersion, curing mechanism, adaptation to substrate, and industrial adaptability. R&D teams often need to design specialized ink and material formulations for different process routes to optimize process suitability and device performance. For example, screen printing focuses on high viscosity and high load, making it suitable for thick-layer structures and high-volume production.

https://doi.org/10.1021/acs.chemrev.5c00801
Chem. Rev. XXXX, XXX, XXX−XXX

R2R emphasizes high-speed, continuous, and low-temperature curing, which is suitable for large-area coils and multifunctional lamination. 3D printing highlights structural designability and multimaterial integration, while inkjet printing emphasizes high precision, low viscosity, and high pattern resolution. As materials science and processing technology continue to advance, these technologies will further integrate and develop, driving wearable electronics toward higher performance, richer functionality, and larger-scale applications.

This report systematically reviews the current progress of wearable electronics, with a particular focus on their foundation in micro/nanofabrication techniques. It provides a comprehensive examination of alternative micro/nanofabrication strategies that are redefining the landscape of wearable electronics. Specifically, the review begins by evaluating the properties and nature of nanomaterials that underpin the shift toward high-throughput fabrication. Subsequently, by scrutinizing cutting-edge methodologies, including nanomaterial-based printing, the review emphasizes their unique benefits alongside their wide array of applications, such as advanced wearable biochemical, biophysical, electrophysiological, and multimodal sensors. These demonstrated capabilities of these emerging fabrication processes not only enhance device performance but also improve user experience by offering greater comfort, functionality, and seamless integration into everyday life. Looking ahead, the continuous evolution of micro/nanofabrication techniques holds significant promise for the advancement of wearable electronics. By fostering interdisciplinary collaborations and driving innovation, these approaches are poised to further transform the field. The large-scale adoption of micro/nanofabrication technologies is expected to enhance the precision and timeliness of wearable electronics shortly, ushering in new milestones for personalized healthcare and telemedicine. Given the unique conditions inherent to wearable electronic testing environments, additional advancements and optimizations are essential to enhance their applicability in real-world scenarios. The primary challenges and future directions can be summarized as follows (Figure 21):

12.1. Material-Process Compatibility for Scalable Fabrication

The compatibility between high-throughput fabrication approaches and active sensing materials exhibits significant variability across different sensor platforms, presenting universal dimensional constraints. For instance, inkjet printing necessitates nanoscale particle uniformity,[668] requiring costly filtration steps,[669] while 3D printing demands precisely controlled rheological properties (e.g., viscosity), often requiring additives that potentially compromise sensor performance.[670−672] Furthermore, numerous advanced nanomaterials (e.g., graphene, LM) exhibit limited compatibility and narrow processability windows with high-throughput methods, thus constraining scalability.[673]

To overcome these limitations, future efforts should prioritize the development of broadly compatible next-generation sensing materials featuring tunable physicochemical properties, such as shear-thinning inks for 3D printing or self-dispersing nanoparticles for inkjet printing. The strategic combination of top-down (e.g., laser engraved) and bottom-up (e.g., self-assembly) fabrication approaches to broaden material versatility and dimensional tolerance remains essential for enabling large-scale sensor manufacturing.

12.2. High-Throughput and Cost-Effective Manufacturing

The advancement of wearable electronics is fundamentally constrained by challenges in high-throughput manufacturing and economic bottlenecks. Elevated material costs (e.g., graphene, AgNWs) and capital-intensive equipment requirements (e.g., cleanroom tools) impede mass production capabilities. Despite their promising physicochemical properties, the industrial implementation of nanomaterials remains limited due to scalability constraints, stability concerns, and challenges in achieving consistent material specifications.[674−676] Furthermore, throughput-speed trade-offs warrant careful consideration, as high-throughput production necessitates continuous innovation in fabrication methodologies and process optimization.[677] Contemporary micro/nanofabrication strategies, particularly advanced printing techniques, demonstrate significant potential for enhancing production efficiency while facilitating rapid prototyping of highly integrated wearable electronics. However, precision printing techniques (e.g., photolithography) sacrifice processing speed, while rapid methods (e.g., R2R) may compromise resolution and feature definition.

Process integration and streamlined manufacturing workflows can substantially improve production rates through the elimination of intermediate processing steps. Future research directions include implementing AI-driven dynamic parameter adjustment (e.g., real-time viscosity control in 3D printing) to minimize waste and improve yield. Furthermore, developing low-cost alternative materials (e.g., carbonized biowaste for conductive inks) and establishing comprehensive recycling protocols for wearable components represent promising sustainable approaches. For example, selective chemical methods could be employed to extract and recycle sensing materials, while electronic circuits could be systematically disassembled and repurposed into functional components.

12.3. Wearability and User Comfort

The development of wearable electronics necessitates careful consideration of wearability and skin-device interface due to their sustained contact with human skin.[678,679] Despite significant advances, several challenges persist in this domain. Balancing mechanical compliance (stretchability >30%) with durability (>10,000 bending cycles) remains an unresolved challenge in the field. Additionally, there is a notable absence of standardized evaluation metrics for user comfort. Systematic assessment of air permeability characteristics and comprehensive user comfort metrics remains relatively unexplored. Biocompatibility concerns also present significant gaps in current research. Long-term toxicity data for emerging materials (e.g., MXenes, conductive polymers) are lacking, and toxic solvent residues (such as acetone, methanol) are frequently present in fabrication processes, raising potential health concerns.

Permeability represents a crucial parameter that significantly influences user comfort during prolonged wear and warrants further investigation. Future designs should incorporate laser-perforated substrates or textile-integrated sensors to enhance air permeability without compromising adhesion properties. Furthermore, the establishment of a comprehensive wearable comfort evaluation system is imperative, with several critical evaluation criteria to ensure optimal performance and safety of these devices. These criteria should encompass mechanical properties, air permeability, biocompatibility considerations, and subjective user experience assessments. Development of

https://doi.org/10.1021/acs.chemrev.5c00801
Chem. Rev. XXXX, XXX, XXX−XXX

standardized American Society for Testing and Materials/International Organization for Standardization (ASTM/ISO) protocols for long-term wearability evaluation (e.g., sweat-induced degradation, microbial growth) would significantly advance the field. Future developments in wearable electronics should prioritize the advancement of these evaluation protocols to enhance user experience and establish more rigorous safety standards for clinical and consumer applications.

12.4. Sensitivity and Signal Integrity

Contemporary wearable platforms necessitate heightened sensitivity, particularly for signal detection in dynamic and complex physiological environments. Current wearable electronics, such as electrophysiological monitoring devices, face significant challenges. Physiological signals (e.g., cortisol in sweat, microvolt EEG) require SNR exceeding 20 dB, yet issues with signal drift and environmental noise (e.g., motion artifacts) persist throughout extended monitoring periods. For biochemical sensors, the LOD and sensitivity for trace concentrations of biomarkers in biofluids remain insufficient for many clinical applications. Moreover, the complexity of sensor performance in dynamic environments has not been adequately addressed in current research. Fluctuations in skin temperature and hydration states alter sensor baselines, which particularly impacts low-level signal detection by introducing measurement inaccuracies and compromising long-term reliability and stability.

Future research directions should focus on developing nanostructured interface sensor components, such as hierarchical graphene foam or plasmonic nanoparticles, to amplify weak signals. Or develop sensors with intrinsic signal amplification capabilities, such as electrochemical transistors, to facilitate accurate low-level signal detection. Additionally, to address signal drift and baseline instability issues, the development of self-calibrating sensors incorporating on-device ML algorithms could distinguish drift from true signals in real time, significantly enhancing measurement reliability in ambulatory settings.

12.5. Multimodal Sensor Cross-Talk

The development of wearable multimodal electronics encounters significant challenges related to signal convolution and complex wiring, resulting in cross-talk coupling among detection signals from various sensor components. The majority of wearable electronic devices generate readable output signals through the modulation of electrical properties (resistance, current, capacitance) in conductive materials, regardless of the external stimulus type. Contemporary approaches typically employ single electrical parameter analysis for discrete environmental variations, while individual stimuli can be distinguished in isolation, concurrent exposure to multiple environmental factors, such as thermal and mechanical deformation, results in signal convolution.[680] Notably, strain-temperature coupling in resistive sensors can introduce error in dual-parameter detection. Additionally, the high integration density of wearable electronics inevitably leads to interconnect congestion, which reduces flexibility and increases failure rates.

Future investigations should focus on developing orthogonal sensing mechanisms to enhance dual-parameter discrimination accuracy and implementing strategies to decouple stimuli via multiphysics designs (e.g., piezocapacitive strain sensors + thermoelectric temperature sensors). Alternatively, leveraging AI and algorithmic approaches for intelligent signal decoupling presents a promising direction. Edge computing modalities could be advantageous, particularly on-sensor signal separation algorithms (e.g., independent component analysis) to minimize cross-talk before data transmission.

12.6. Energy Autonomy

Wearable electronic systems face significant energy-related challenges, particularly concerning power-density trade-offs and intermittent energy harvesting capabilities. Conventional devices frequently necessitate regular recharging or high power density battery replacement, thereby limiting their usability, portability, and operational longevity. Current power solutions, such as flexible batteries (e.g., Zn-air), often deliver less than 1 mW/cm^2, which is insufficient for continuous wireless operation. Advances in energy supply technologies are directed toward enabling wearable electronics to function autonomously for extended durations without dependence on external power sources, thereby significantly enhancing their functionality and user convenience.[681,682] Traditional self-powered devices that rely on a single energy harvesting mechanism (e.g., human temperature gradient powered devices) are unable to provide a continuous supply of energy, as body motion and thermal gradients typically provide irregular power bursts with less than 10% duty cycle.

Recent innovations have facilitated the development of self-powered wearable electronics capable of harvesting energy from body motion, biofluids, and environmental sources.[2] These self-sustaining systems predominantly consist of two interrelated modules: energy harvesting and energy storage. Future advancements may encompass hybrid energy harvesting systems that integrate triboelectric (motion), photovoltaic (light), and biofuel (sweat) cells with supercapacitors for steady output. Furthermore, progress in wireless charging technologies is anticipated to yield novel solutions, including resonant coupling or RFID harvesting (e.g., 5G-band rectennas) for continuous operation.

12.7. Data Interoperability and Privacy

The advent of advanced data processing methodologies, including cloud computing architectures, AI algorithms, and big data analytics frameworks, has enabled wearable electronics to transmit acquired data to cloud-based systems with high fidelity and minimal latency.[683] Statistical analyses of these data sets subsequently provide users with actionable insights and personalized feedback. However, the current technological ecosystem is constrained by proprietary silos, as evidenced by vendor-locked ecosystems (e.g., Apple Health vs Google Fit), which limit data fusion for holistic health insights. Furthermore, wearable electronics are susceptible to eavesdropping (e.g., ECG data leaks) due to lightweight encryption. User information is uploaded to the cloud through various near-field communication protocols (WIFI, Bluetooth, NFC, etc.), which may lead to personal information leakage.

To address these limitations, future development trajectories for wearable electronics should prioritize open standardization and the adoption of blockchain for secure, decentralized health data sharing with user-controlled permissions. Such standardization would facilitate enhanced information exchange and data interoperability, thereby fostering a more collaborative and open ecosystem. Concurrently, it is essential to train AI models on-device to preserve privacy while improving analytics. User privacy considerations must be systematically

https://doi.org/10.1021/acs.chemrev.5c00801
Chem. Rev. XXXX, XXX, XXX−XXX

integrated into these developmental frameworks to ensure appropriate data protection protocols.

12.8. Commercialization Barrier

The translation of wearable electronics from laboratory prototypes to commercial products constitutes a multifaceted and interdisciplinary endeavor, intersecting domains such as smart healthcare, metaverse applications, and the IoT. Despite these technological advancements, substantial challenges remain in overcoming the commercialization barriers of wearable electronics. A primary challenge is the lack of clinical validation for wearable electronics developed today, with fewer than 5% of lab prototypes meeting Food and Drug Administration (FDA) accuracy standards for medical-grade wearable electronics. Moreover, commercialized wearable electronics are generally expensive and exhibit low consumer adoption. High prices (>$200) and short lifespans (<2 years) deter market penetration.

Future research should prioritize codesign frameworks that involve end-users (patients, athletes) early in the development process to optimize usability. User-centered design methodologies, combined with targeted educational initiatives, are essential to facilitate technological acceptance, which remains a pivotal determinant for sustainable commercialization and market expansion. Consequently, the usage cost can be reduced within a circular economy. Lease−recycle models can be implemented to reduce costs without affecting user experience (e.g., refurbished diabetes monitors).

12.9. AI-Driven Optimization and Automation

Currently, there exists a general problem of process variability in the development of wearable electronics. Most development is conducted through manual experiments, resulting in a lack of automation and scalable equipment. For instance, in micro/nanofabrication, the rheology of nanomaterial inks and printer nozzle dynamics requires real-time monitoring. Additionally, data scarcity poses challenges, particularly in complex biofluids, where there are limited labeled data sets for rare failure modes (e.g., electrochemical delamination).

Future research should prioritize AI-powered technologies for guided material synthesis, utilizing generative AI for materials, such as diffusion models to predict ink formulations for target conductivity and stretchability (e.g., PEDOT:PSS-graphene ratios). Simultaneously, closed-loop control methods should be employed, in-line optical metrology + reinforcement learning to dynamically adjust printing parameters (speed, temperature).

Future research should prioritize emerging micro/nanofabrication technologies to enhance the stability, safety, and rapid responsiveness of novel multimodal sensors, with the ultimate goal of seamless integration into daily medical monitoring and telemedicine systems. In summary, the convergence of these techniques with wearable electronics has driven the development of more comprehensive, detailed, and personalized healthcare solutions. To date, this technology has fueled remarkable progress in wearable electronics. As the field evolves, researchers must remain attuned to emerging trends and challenges to capitalize on these advancements, thereby facilitating the development of smarter, more efficient, user-centric wearable electronics tailored to global needs. Moreover, the nanoscale design capability of these technologies unlocks unprecedented potential in wearable devices, electronics, and other cutting-edge domains.

AUTHOR INFORMATION

Corresponding Author

Minqiang Wang − *Global Institute of Future Technology, Centre for Future Health and Intelligent Exercise, Shanghai Jiao Tong University, Shanghai 200240, China;* orcid.org/0000-0002-7775-8341; Email: minqiangwang@sjtu.edu.cn

Author

Jianxin Zhang − *Global Institute of Future Technology, Centre for Future Health and Intelligent Exercise, Shanghai Jiao Tong University, Shanghai 200240, China;* orcid.org/0000-0003-1429-7071

Complete contact information is available at: https://pubs.acs.org/10.1021/acs.chemrev.5c00801

Author Contributions

CRediT: Jianxin Zhang writing-original draft, writing-review and editing; Minqiang Wang conceptualization, funding acquisition, project administration, resources, supervision, writing-review and editing.

Notes

The authors declare no competing financial interest.

Biographies

Jianxin Zhang received his M.S. degree in Materials and Chemical Engineering from Dalian University of Technology. He joined Prof. Minqiang Wang's research group in 2025 and is currently pursuing his Ph.D. degree in Electronic and Information Engineering at the Shanghai Jiao Tong University. His research interests include analytical chemistry, wearable electronics, and soft energy devices.

Minqiang Wang is currently an Associate Professor in Global Institute of Future Technology at the Shanghai Jiao Tong University. He holds a Ph.D. degree in Clean Energy Science from Southwest University and was a visiting student at the California Institute of Technology during his doctoral studies. He then worked as a senior postdoctoral fellow in Biomedical Engineering at California Institute of Technology, until 2025. His interdisciplinary research focuses on developing versatile materials and bioelectronic wearable systems, which are utilized for both fundamental and applied biomedical studies.

ACKNOWLEDGMENTS

This work was financially supported by the Shanghai Magnolia Talent Plan-Pujiang Project (grant no. 24PJA052). We extend our sincere gratitude to Professor Cui Ye of Shanghai Jiao Tong University School of Medicine for her valuable contributions to the overall framework of this paper. We also thank Shizhe He and Zihan Zhang, undergraduates of Shanghai Jiao Tong University, for their helpful suggestions regarding the presentation of the manuscript.

ABBREVIATIONS

0D = zero-dimensional
1D = one-dimensional
2D = two-dimensional
3D = three-dimensional
5G = fifth-generation mobile communication technology
AA = ascorbic acid
ADC = analog-to-digital conversion
AgNPs = silver nanoparticles

https://doi.org/10.1021/acs.chemrev.5c00801
Chem. Rev. XXXX, XXX, XXX−XXX

AgNWs = silver nanowires
AI = artificial intelligence
AJP = aerosol jet printing
aSISC = asymmetric self-insulated stretchable conductors
ASTM = American Society for Testing and Materials
AuNPs = gold nanoparticles
BB = biceps brachii
BFCs = biofuel cells
BGM = blood glucose monitoring
BLE = bluetooth low energy
BOD = bilirubin oxidase
BP = blood pressure
CAD = computer-aided design
CARES = consolidated artificial-intelligence-reinforced electronic skin
CAST = $Cu_{25}As_{35}Se_6Te_{34}$
CE = counter electrode
CIJ = continuous inkjet
CNTs = carbon nanotubes
CRP = c-reactive protein
CSA = central sleep apnea
CV = cyclic voltammetry
CVD = chemical vapor deposition
CY = cyclophosphamide
DA = dopamine
DAC = digital-to-analog conversion
DIW = direct ink writing
DLP = digital light processing
DMD = digital micromirror device
DMF = dimethylformamide
DNA = DNA
DOD = drop-on-demand
DPV = differential pulse voltammetry
E^3-skin = epifluidic elastic electronic skin
EBC = exhaled breath condensate
ECG = electrocardiography
ECH = electrochemical hydrogel
ECoG = electrocorticography
EEC = equivalent electrical circuit
EEG = electroencephalography
EIS = electrochemical impedance spectroscopy
ELISA = enzyme-linked immunosorbent assay
EMF = epidermal molecular flux
EMG = electromyography
EOG = electrooculography
E-skin = electronic skin
FDA = Food and Drug Administration
FDM = fused deposition modeling
FPCB = flexible printed circuit board
GNPs = graphene nanoplatelets
GOx = glucose oxidase
HR = heart rate
ICP = intracranial pressure
IDE = interdigitated electrode
IFN-γ = interferon-gamma
IL-10 = interleukin-10
IoT = Internet of Things
IP = iontophoresis
ISE = ion-selective electrode
ISF = interstitial fluid
ISM = ion-selective membrane
ISO = International Organization for Standardization
I*sn* = sensing current
LCT = layer cure time
LIBs = lithium-ion batteries
LIG = laser-induced graphene
LIMBs = lithium-ion microbatteries
LM = liquid metal
LOD = limit of detection
LOx = lactate oxidase
MCBM = microneedle-based continuous biomarker/drug monitoring
MCU = microcontroller unit
ME = magnetoelectric
MEAP = metal−polymer electrode array patch
Met = metformin
MIP = molecularly imprinted polymer
ML = machine learning
MMFSA = multimodal and multichannel flexible sensor array
Mo = molybdenum
MOF = metal−organic framework
MoS_2 = molybdenum disulfide
MP = methyl parathion
MSCs = microsupercapacitors
MX-LIMBs = MXene-MSCs and LIMBs
NFC = near-field communication
NiHCF = nickel hexacyanoferrate
NOPPs = nitroaromatic organophosphorus pesticides
NTC = negative temperature coefficient
OECT = organic electrochemical transistor
OSA = obstructive sleep apnea
PANI = polyaniline
PCL = polycaprolactone
PCSA = pressure-constrained sonication activation
PDMS = polydimethylsiloxane
PEDOT:PSS = poly(3,4-ethylenedioxythiophene):polystyrenesulfonate
PENG = piezoelectric nanogenerator
PET = polyethylene terephthalate
PI = polyimide
PPy = polypyrrole
PR-Gel = polymeric rotaxane hydrogels
PTC = positive temperature coefficient
PTFE = polytetrafluoroethylene
PU = polyurethane
PVA = poly(vinyl alcohol)
PVD = physical vapor deposition
QRS = Q-, R-, and S-wave
R^2 = coefficient of determination
R2R = roll-to-roll
RAM = random-access memory
RE = reference electrode
RFID = radio frequency identification
rGO = reduced graphene oxide
RNA = ribonucleic acid
ROM = read-only memory
R*s* = solution resistance
RSD = relative standard deviation
S = sulfur
Se = selenium
SEB = solid epidermal biomarkers
SEBS = styrene-ethylene-butylene-styrene
sEMG = surface electromyography
SHAP = Shapley additive explanations
SkinG = skin conductance

https://doi.org/10.1021/acs.chemrev.5c00801
Chem. Rev. XXXX, XXX, XXX−XXX

SLA = stereolithography
SNR = signal-to-noise ratio
ss-DNA = single-stranded DNA
SWCNT = single-walled carbon nanotube
SWV = square wave voltammetry
TENG = triboelectric nanogenerator
TFT = thin-film transistor
THF = tetrahydrofuran
$Ti_3C_2T_x$ = titanium carbide
TMDs = transition metal dichalcogenides
TPP = tannic acid, poly(vinyl alcohol) (PVA), and poly(3,4-ethylenedioxythiophene): polystyrenesulfonate (PEDOT:PSS)
TPU = thermoplastic polyurethane
Trp = tryptophan
UA = uric acid
UGI = universal gradient interface
UV = ultraviolet
Vg = gate voltage
VOCs = volatile organic compounds
Vst = stimulus voltage
WE = working electrode
WISE = wearable integrated soft electronics
WLAN = wireless local area network
WS_2 = tungsten disulfide
ZIF-8 = zeolitic-imidazolate framework-8

REFERENCES

(1) Luo, Y.; Abidian, M. R.; Ahn, J.-H.; Akinwande, D.; Andrews, A. M.; Antonietti, M.; Bao, Z.; Berggren, M.; Berkey, C. A.; Bettinger, C. J.; Chen, J.; Chen, P.; Cheng, W.; Cheng, X.; Choi, S.-J.; Chortos, A.; Dagdeviren, C.; Dauskardt, R. H.; Di, C.; Dickey, M. D.; Duan, X.; Facchetti, A.; Fan, Z.; Fang, Y.; Feng, J.; Feng, X.; Gao, H.; Gao, W.; Gong, X.; Guo, C. F.; Guo, X.; Hartel, M. C.; He, Z.; Ho, J. S.; Hu, Y.; Huang, Q.; Huang, Y.; Huo, F.; Hussain, M. M.; Javey, A.; Jeong, U.; Jiang, C.; Jiang, X.; Kang, J.; Karnaushenko, D.; Khademhosseini, A.; Kim, D.-H.; Kim, I.-D.; Kireev, D.; Kong, L.; Lee, C.; Lee, N.-E.; Lee, P. S.; Lee, T.-W.; Li, F.; Li, J.; Liang, C.; Lim, C. T.; Lin, Y.; Lipomi, D. J.; Liu, J.; Liu, K.; Liu, N.; Liu, R.; Liu, Y.; Liu, Y.; Liu, Z.; Liu, Z.; Loh, X. J.; Lu, N.; Lv, Z.; Magdassi, S.; Malliaras, G. G.; Matsuhisa, N.; Nathan, A.; Niu, S.; Pan, J.; Pang, C.; Pei, Q.; Peng, H.; Qi, D.; Ren, H.; Rogers, J. A.; Rowe, A.; Schmidt, O. G.; Sekitani, T.; Seo, D.-G.; Shen, G.; Sheng, X.; Shi, Q.; Someya, T.; Song, Y.; Stavrinidou, E.; Su, M.; Sun, X.; Takei, K.; Tao, X.-M.; Tee, B. C. K.; Thean, A. V.-Y.; Trung, T. Q.; Wan, C.; Wang, H.; Wang, J.; Wang, M.; Wang, S.; Wang, T.; Wang, Z. L.; Weiss, P. S.; Wen, H.; Xu, S.; Xu, T.; Yan, H.; Yan, X.; Yang, H.; Yang, L.; Yang, S.; Yin, L.; Yu, C.; Yu, G.; Yu, J.; Yu, S.-H.; Yu, X.; Zamburg, E.; Zhang, H.; Zhang, X.; Zhang, X.; Zhang, X.; Zhang, Y.; Zhang, Y.; Zhao, S.; Zhao, X.; Zheng, Y.; Zheng, Y.-Q.; Zheng, Z.; Zhou, T.; Zhu, B.; Zhu, M.; Zhu, R.; Zhu, Y.; Zhu, Y.; Zou, G.; Chen, X. Technology Roadmap for Flexible Sensors. *ACS Nano* **2023**, *17* (6), 5211−5295.

(2) Tang, W.; Sun, Q.; Wang, Z. L. Self-Powered Sensing in Wearable Electronics−A Paradigm Shift Technology. *Chem. Rev.* **2023**, *123* (21), 12105−12134.

(3) Gao, W.; Emaminejad, S.; Nyein, H. Y. Y.; Challa, S.; Chen, K.; Peck, A.; Fahad, H. M.; Ota, H.; Shiraki, H.; Kiriya, D.; Lien, D.-H.; Brooks, G. A.; Davis, R. W.; Javey, A. Fully Integrated Wearable Sensor Arrays for Multiplexed in Situ Perspiration Analysis. *Nature* **2016**, *529* (7587), 509−514.

(4) Jin, Y.; Alvarez, J. T.; Suitor, E. L.; Swaminathan, K.; Chin, A.; Civici, U. S.; Nuckols, R. W.; Howe, R. D.; Walsh, C. J. Estimation of Joint Torque in Dynamic Activities Using Wearable A-Mode Ultrasound. *Nat. Commun.* **2024**, *15* (1), 5756.

(5) Nguyen, P. Q.; Soenksen, L. R.; Donghia, N. M.; Angenent-Mari, N. M.; De Puig, H.; Huang, A.; Lee, R.; Slomovic, S.; Galbersanini, T.; Lansberry, G.; Sallum, H. M.; Zhao, E. M.; Niemi, J. B.; Collins, J. J. Wearable Materials with Embedded Synthetic Biology Sensors for Biomolecule Detection. *Nat. Biotechnol.* **2021**, *39* (11), 1366−1374.

(6) Yang, Y.; Song, Y.; Bo, X.; Min, J.; Pak, O. S.; Zhu, L.; Wang, M.; Tu, J.; Kogan, A.; Zhang, H.; Hsiai, T. K.; Li, Z.; Gao, W. A Laser-Engraved Wearable Sensor for Sensitive Detection of Uric Acid and Tyrosine in Sweat. *Nat. Biotechnol.* **2020**, *38* (2), 217−224.

(7) Tu, J.; Min, J.; Song, Y.; Xu, C.; Li, J.; Moore, J.; Hanson, J.; Hu, E.; Parimon, T.; Wang, T.-Y.; Davoodi, E.; Chou, T.-F.; Chen, P.; Hsu, J. J.; Rossiter, H. B.; Gao, W. A Wireless Patch for the Monitoring of C-Reactive Protein in Sweat. *Nat. Biomed. Eng.* **2023**, *7* (10), 1293−1306.

(8) Zhao, H.; Chen, W.; Li, Y.; Wang, H.; Li, H.; Li, T.; Han, F.; Sun, J.; Huang, L.; Peng, X.; Chen, J.; Yang, Y.; Qiu, X.; Liu, Y.; Yu, H.; Hou, W.; Li, Q.; Fu, G.; You, C.; Liu, X.; Li, F.; Li, X.; Zhao, G.; Wang, L.; Fang, P.; Li, G.; Zheng, H.; Zhu, M.; Yan, W.; Tian, Q.; Ma, T.; Liu, Z. In Situ Structural-Functional Synchronous Dissection of Dynamic Neuromuscular System via an Integrated Multimodal Wearable Patch. *Sci. Adv.* **2025**, *11* (2), No. eads1486.

(9) Chen, C.; Ding, S.; Wang, J. Digital Health for Aging Populations. *Nat. Med.* **2023**, *29* (7), 1623−1630.

(10) Kaveh, R.; Schwendeman, C.; Pu, L.; Arias, A. C.; Muller, R. Wireless Ear EEG to Monitor Drowsiness. *Nat. Commun.* **2024**, *15* (1), 6520.

(11) Lee, G.; Hossain, O.; Jamalzadegan, S.; Liu, Y.; Wang, H.; Saville, A. C.; Shymanovich, T.; Paul, R.; Rotenberg, D.; Whitfield, A. E.; Ristaino, J. B.; Zhu, Y.; Wei, Q. Abaxial Leaf Surface-Mounted Multimodal Wearable Sensor for Continuous Plant Physiology Monitoring. *Sci. Adv.* **2023**, *9* (15), No. eade2232.

(12) Zhong, Z.; Damacet, P.; Sánchez-González, E.; Eagleton, A. M.; Vereshchuk, N.; Wongratanaphisan, R.; Anderson, J. T.; Goncalves, S.; Peterson, G. W.; Blount, B.; Monti, S.; Barcaro, G.; Ibarra, I. A.; Mirica, K. A. Scalable Templated Fabrication of Cu-Based MOF on Textiles for Simultaneous Sensing, Filtration, and Detoxification of SO2. *Chem.* **2025**, *11*, 102580.

(13) Tanriverdi, U.; Senesi, G.; Asfour, T.; Kurt, H.; Smith, S. L.; Toderita, D.; Shalhoub, J.; Burgess, L.; Bull, A. M. J.; Güder, F. Dynamically Adaptive Soft Metamaterial for Wearable Human-Machine Interfaces. *Nat. Commun.* **2025**, *16* (1), 2621.

(14) Lorach, H.; Galvez, A.; Spagnolo, V.; Martel, F.; Karakas, S.; Intering, N.; Vat, M.; Faivre, O.; Harte, C.; Komi, S.; Ravier, J.; Collin, T.; Coquoz, L.; Sakr, I.; Baaklini, E.; Hernandez-Charpak, S. D.; Dumont, G.; Buschman, R.; Buse, N.; Denison, T.; Van Nes, I.; Asboth, L.; Watrin, A.; Struber, L.; Sauter-Starace, F.; Langar, L.; Auboiroux, V.; Carda, S.; Chabardes, S.; Aksenova, T.; Demesmaeker, R.; Charvet, G.; Bloch, J.; Courtine, G. Walking Naturally after Spinal Cord Injury Using a Brain-Spine Interface. *Nature* **2023**, *618* (7963), 126−133.

(15) Xia, H.; Zhang, Y.; Rajabi, N.; Taleb, F.; Yang, Q.; Kragic, D.; Li, Z. Shaping High-Performance Wearable Robots for Human Motor and Sensory Reconstruction and Enhancement. *Nat. Commun.* **2024**, *15* (1), 1760.

(16) Luo, S.; Jiang, M.; Zhang, S.; Zhu, J.; Yu, S.; Dominguez Silva, I.; Wang, T.; Rouse, E.; Zhou, B.; Yuk, H.; Zhou, X.; Su, H. Experiment-Free Exoskeleton Assistance via Learning in Simulation. *Nature* **2024**, *630* (8016), 353−359.

(17) Niu, Y.; Liu, H.; He, R.; Li, Z.; Ren, H.; Gao, B.; Guo, H.; Genin, G. M.; Xu, F. The New Generation of Soft and Wearable Electronics for Health Monitoring in Varying Environment: From Normal to Extreme Conditions. *Mater. Today* **2020**, *41*, 219−242.

(18) Wang, H.; Li, S.; Lu, H.; Zhu, M.; Liang, H.; Wu, X.; Zhang, Y. Carbon-Based Flexible Devices for Comprehensive Health Monitoring. *Small Methods* **2023**, *7* (2), 2201340.

(19) Liu, S.; Guo, W.; Chen, H.; Yin, Z.; Tang, X.; Sun, Q. Recent Progress on Flexible Self-Powered Tactile Sensing Platforms for Health Monitoring and Robotics. *Small* **2024**, *20* (46), 2405520.

(20) Gao, Y.; Yao, K.; Jia, S.; Huang, Y.; Zhao, G.; Zhang, B.; Liu, Y.; Yu, X. Advances in Materials for Haptic Skin Electronics. *Matter* **2024**, *7* (9), 2826−2845.

https://doi.org/10.1021/acs.chemrev.5c00801
Chem. Rev. XXXX, XXX, XXX−XXX

(21) Tian, H.; Ma, J.; Li, Y.; Xiao, X.; Zhang, M.; Wang, H.; Zhu, N.; Hou, C.; Ulstrup, J. Electrochemical Sensing Fibers for Wearable Health Monitoring Devices. *Biosens. Bioelectron.* **2024**, *246*, 115890.
(22) Tay, R. Y.; Song, Y.; Yao, D. R.; Gao, W. Direct-Ink-Writing 3D-Printed Bioelectronics. *Mater. Today* **2023**, *71*, 135−151.
(23) Li, T.; Zhao, T.; Zhang, H.; Yuan, L.; Cheng, C.; Dai, J.; Xue, L.; Zhou, J.; Liu, H.; Yin, L.; Zhang, J. A Skin-Conformal and Breathable Humidity Sensor for Emotional Mode Recognition and Non-Contact Human-Machine Interface. *Npj Flexible Electron.* **2024**, *8* (1), 3.
(24) Zong, P.; Chen, M.; Wang, X.; Liu, H.; He, Z.; Ou, Y.; Sun, C. Coating Carbon Cloth with Cu3Se2 by Electrodeposition for Pressure Sensing and Enhanced EMI Shielding. *Carbon* **2025**, *232*, 119814.
(25) Liu, Y.; Zhu, H.; Xing, L.; Bu, Q.; Ren, D.; Sun, B. Recent Advances in Inkjet-Printing Technologies for Flexible/Wearable Electronics. *Nanoscale* **2023**, *15* (13), 6025−6051.
(26) Zheng, B.; Xie, Y.; Xu, S.; Meng, A. C.; Wang, S.; Wu, Y.; Yang, S.; Wan, C.; Huang, G.; Tour, J. M.; Lin, J. Programmed Multimaterial Assembly by Synergized 3D Printing and Freeform Laser Induction. *Nat. Commun.* **2024**, *15* (1), 4541.
(27) Zhang, Y.-Z.; Wang, Y.; Cheng, T.; Yao, L.-Q.; Li, X.; Lai, W.-Y.; Huang, W. Printed Supercapacitors: Materials, Printing and Applications. *Chem. Soc. Rev.* **2019**, *48* (12), 3229−3264.
(28) Wang, B.; Yang, D.; Chang, Z.; Zhang, R.; Dai, J.; Fang, Y. Wearable Bioelectronic Masks for Wireless Detection of Respiratory Infectious Diseases by Gaseous Media. *Matter* **2022**, *5* (12), 4347−4362.
(29) Wang, H.; Wang, H.; Wang, Y.; Su, X.; Wang, C.; Zhang, M.; Jian, M.; Xia, K.; Liang, X.; Lu, H.; Li, S.; Zhang, Y. Laser Writing of Janus Graphene/Kevlar Textile for Intelligent Protective Clothing. *ACS Nano* **2020**, *14* (3), 3219−3226.
(30) Sempionatto, J. R.; Lin, M.; Yin, L.; De La Paz, E.; Pei, K.; Sonsa-ard, T.; De Loyola Silva, A. N.; Khorshed, A. A.; Zhang, F.; Tostado, N.; Xu, S.; Wang, J. An Epidermal Patch for the Simultaneous Monitoring of Haemodynamic and Metabolic Biomarkers. *Nat. Biomed. Eng.* **2021**, *5* (7), 737−748.
(31) Ates, H. C.; Nguyen, P. Q.; Gonzalez-Macia, L.; Morales-Narváez, E.; Güder, F.; Collins, J. J.; Dincer, C. End-to-End Design of Wearable Sensors. *Nat. Rev. Mater.* **2022**, *7* (11), 887−907.
(32) Liu, H.; Zhao, G.; Wu, M.; Liu, Z.; Xiang, D.; Wu, C.; Cheng, Y.; Wang, H.; Wang, Z. L.; Li, L. Ionogel Infiltrated Paper as Flexible Electrode for Wearable All-Paper Based Sensors in Active and Passive Modes. *Nano Energy* **2019**, *66*, 104161.
(33) Bang, J.; Ahn, J.; Zhang, J.; Ko, T. H.; Park, B.; Lee, Y. M.; Jung, B. K.; Lee, S. Y.; Ok, J.; Kim, B. H.; Kim, T.; Choi, J.-I.; Lee, C. H.; Oh, S. J. Stretchable and Directly Patternable Double-Layer Structure Electrodes with Complete Coverage. *ACS Nano* **2022**, *16* (8), 12134−12144.
(34) Joh, H.; Lee, S.-W.; Seong, M.; Lee, W. S.; Oh, S. J. Engineering the Charge Transport of Ag Nanocrystals for Highly Accurate, Wearable Temperature Sensors through All-Solution Processes. *Small* **2017**, *13* (24), 1700247.
(35) Truong, T.; Nguyen, T. K.; Huang, X.; Ashok, A.; Yadav, S.; Park, Y.; Thai, M. T.; Nguyen, N.; Fallahi, H.; Peng, S.; Dimitrijev, S.; Toh, Y.; Yamauchi, Y.; Wang, C. H.; Lovell, N. H.; Rogers, J. A.; Do, T. N.; Nguyen, N.; Zhao, H.; Phan, H. Engineering Route for Stretchable, 3D Microarchitectures of Wide Bandgap Semiconductors for Biomedical Applications. *Adv. Funct. Mater.* **2023**, *33* (34), 2211781.
(36) Wang, M.; Yang, Y.; Gao, W. Laser-Engraved Graphene for Flexible and Wearable Electronics. *Trends Chem.* **2021**, *3* (11), 969−981.
(37) Ma, H.; Liang, H.; Zhu, G.; Jin, J.; Song, J.; Chen, A.; Zhang, Y. Laser-Engraved Graphene on Fabrics for Customizable and Scalable Textile Electronics. *Device* **2025**, *3* (2), 100573.
(38) Clark, K. M.; Nekoba, D. T.; Viernes, K. L.; Zhou, J.; Ray, T. R. Fabrication of High-Resolution, Flexible, Laser-Induced Graphene Sensors via Stencil Masking. *Biosens. Bioelectron.* **2024**, *264*, 116649.
(39) Yu, F.; Wang, L.; Yang, X.; Yang, Y.; Li, X.; Gao, Y.; Jiang, Y.; Jiang, K.; Lü, W.; Sun, X.; Li, D. Moisture-Electric Generators Working in Subzero Environments Based on Laser-Engraved Hygroscopic Hydrogel Arrays. *ACS Nano* **2025**, *19* (3), 3807−3817.
(40) Gao, M.; Xu, G.; Zhang, R.; Liu, Z.; Xia, H.; Shao, B.; Xue, C.; Li, J.; Miao, S.; Fu, W.; Zhang, X.; Zhou, J.; Jiang, X.; Liang, K.; Kong, B. Electrospinning Superassembled Mesoporous AIEgen-Organosilica Frameworks Featuring Diversified Forms and Superstability for Wearable and Washable Solid-State Fluorescence Smart Sensors. *Anal. Chem.* **2021**, *93* (4), 2367−2376.
(41) Huang, A.; Zhu, Y.; Peng, S.; Tan, B.; Peng, X. Improved Energy Harvesting Ability of Single-Layer Binary Fiber Nanocomposite Membrane for Multifunctional Wearable Hybrid Piezoelectric and Triboelectric Nanogenerator and Self-Powered Sensors. *ACS Nano* **2024**, *18* (1), 691−702.
(42) Wang, Y.; Chu, L.; Meng, S.; Yang, M.; Yu, Y.; Deng, X.; Qi, C.; Kong, T.; Liu, Z. Scalable and Ultra-sensitive Nanofibers Coaxial Yarn-woven Triboelectric Nanogenerator Textile Sensors for Real-time Gait Analysis. *Adv. Sci.* **2024**, *11* (28), 2401436.
(43) Babu, A.; Aazem, I.; Walden, R.; Bairagi, S.; Mulvihill, D. M.; Pillai, S. C. Electrospun Nanofiber Based TENGs for Wearable Electronics and Self-Powered Sensing. *Chem. Eng. J.* **2023**, *452*, 139060.
(44) Li, Y.; Huang, Y.; Zhao, N. Low-intensity Sensitive and High Stability Flexible Heart Sound Sensor Enabled by Hybrid Near-field/Far-field Electrospinning. *Adv. Funct. Mater.* **2023**, *33* (29), 2300666.
(45) Clevenger, M.; Kim, H.; Song, H. W.; No, K.; Lee, S. Binder-Free Printed PEDOT Wearable Sensors on Everyday Fabrics Using Oxidative Chemical Vapor Deposition. *Sci. Adv.* **2021**, *7* (42), No. eabj8958.
(46) Ren, H.; Zheng, L.; Wang, G.; Gao, X.; Tan, Z.; Shan, J.; Cui, L.; Li, K.; Jian, M.; Zhu, L.; Zhang, Y.; Peng, H.; Wei, D.; Liu, Z. Transfer-Medium-Free Nanofiber-Reinforced Graphene Film and Applications in Wearable Transparent Pressure Sensors. *ACS Nano* **2019**, *13* (5), 5541−5548.
(47) Liang, Q.; Zhang, D.; He, T.; Zhang, Z.; Wang, H.; Chen, S.; Lee, C. Fiber-Based Noncontact Sensor with Stretchability for Underwater Wearable Sensing and VR Applications. *ACS Nano* **2024**, *18* (1), 600−611.
(48) Cai, Y.; Shen, J.; Dai, Z.; Zang, X.; Dong, Q.; Guan, G.; Li, L.; Huang, W.; Dong, X. Extraordinarily Stretchable All-carbon Collaborative Nanoarchitectures for Epidermal Sensors. *Adv. Mater.* **2017**, *29* (31), 1606411.
(49) Hassan, K.; Uddin, A. S. M. I.; Chung, G.-S. Mesh of Ultrasmall Pd/Mg Bimetallic Nanowires as Fast Response Wearable Hydrogen Sensors Formed on Filtration Membrane. *Sens. Actuators B: Chem.* **2017**, *252*, 1035−1044.
(50) Norimasa, O.; Chiba, T.; Hase, M.; Komori, T.; Takashiri, M. Improvement of Thermoelectric Properties of Flexible Bi2Te3 Thin Films in Bent States during Sputtering Deposition and Post-Thermal Annealing. *J. Alloys Compd.* **2022**, *898*, 162889.
(51) Ma, X.; Zhao, J.; Shou, D.; Liu, Y. A Highly-flexible and Breathable Photo-thermo-electric Membrane for Energy Harvesting. *Adv. Energy Mater.* **2024**, *14* (15), 2304032.
(52) Zhang, S.; Xu, J.; Liu, Z.; Huang, Y.; Jiang, S. Facile, Ecofriendly, and Efficient Preparation of Flexible Gold Nanoparticles@bacterial Nanocellulose Surface-Enhanced Raman Scattering Sensors by Magnetron Sputtering for Trace Detection of Hazardous Materials. *ACS Sustainable Chem. Eng.* **2022**, *10* (39), 13059−13069.
(53) Su, G.; Wang, N.; Liu, Y.; Zhang, R.; Li, Z.; Deng, Y.; Tang, B. Z. From Fluorescence-transfer-lightening-printing-assisted Conductive Adhesive Nanocomposite Hydrogels toward Wearable Interactive Optical Information-electronic Strain Sensors. *Adv. Mater.* **2024**, *36* (25), 2400085.
(54) Xu, H.; Liu, J.; Zhang, J.; Zhou, G.; Luo, N.; Zhao, N. Flexible Organic/Inorganic Hybrid Near-infrared Photoplethysmogram Sensor for Cardiovascular Monitoring. *Adv. Mater.* **2017**, *29* (31), 1700975.

https://doi.org/10.1021/acs.chemrev.5c00801
Chem. Rev. XXXX, XXX, XXX−XXX

(55) Choi, M. K.; Park, I.; Kim, D. C.; Joh, E.; Park, O. K.; Kim, J.; Kim, M.; Choi, C.; Yang, J.; Cho, K. W.; Hwang, J.; Nam, J.; Hyeon, T.; Kim, J. H.; Kim, D. Thermally Controlled, Patterned Graphene Transfer Printing for Transparent and Wearable Electronic/Optoelectronic System. *Adv. Funct. Mater.* **2015**, *25* (46), 7109−7118.
(56) Park, J.; Lee, Y.; Lee, H.; Ko, H. Transfer Printing of Electronic Functions on Arbitrary Complex Surfaces. *ACS Nano* **2020**, *14* (1), 12−20.
(57) Zhao, Y.; Sun, Y.; Pei, C.; Yin, X.; Li, X.; Hao, Y.; Zhang, M.; Yuan, M.; Zhou, J.; Chen, Y.; Song, Y. Low-Temperature Fabrication of Stable Black-Phase CsPbI3 Perovskite Flexible Photodetectors toward Wearable Health Monitoring. *Nano Micro Lett.* **2025**, *17* (1), 63.
(58) Peng, M.; Wen, Z.; Sun, X. Recent Progress of Flexible Photodetectors Based on Low-dimensional II-VI Semiconductors and Their Application in Wearable Electronics. *Adv. Funct. Mater.* **2023**, *33* (11), 2211548.
(59) Li, X.; Wang, J.; Min, Y.; Xue, Q.; Du, J.; Fu, N. Conformal Charge Transport Layers for Perovskite Solar Cells and Tandem Devices. *ACS Energy Lett.* **2025**, *10* (7), 3203−3222.
(60) Yan, T.; Zhang, G.; Yu, K.; Chai, H.; Tian, M.; Qu, L.; Dong, H.; Zhang, X. Smartphone Light-Driven Zinc Porphyrinic MOF Nanosheets-Based Enzyme-Free Wearable Photoelectrochemical Sensor for Continuous Sweat Vitamin C Detection. *Chem. Eng. J.* **2023**, *455*, 140779.
(61) Jiang, Y.; Ma, J.; Lv, J.; Ma, H.; Xia, H.; Wang, J.; Yang, C.; Xue, M.; Li, G.; Zhu, N. Facile Wearable Vapor/Liquid Amphibious Methanol Sensor. *ACS Sens.* **2019**, *4* (1), 152−160.
(62) Paschoalin, R. T.; Gomes, N. O.; Almeida, G. F.; Bilatto, S.; Farinas, C. S.; Machado, S. A. S.; Mattoso, L. H. C.; Oliveira, O. N.; Raymundo-Pereira, P. A. Wearable Sensors Made with Solution-Blow Spinning Poly(Lactic Acid) for Non-Enzymatic Pesticide Detection in Agriculture and Food Safety. *Biosens. Bioelectron.* **2022**, *199*, 113875.
(63) Parrilla, M.; Vanhooydonck, A.; Watts, R.; De Wael, K. Wearable Wristband-Based Electrochemical Sensor for the Detection of Phenylalanine in Biofluids. *Biosens. Bioelectron.* **2022**, *197*, 113764.
(64) Fu, Y.; Kang, S.; Xiang, G.; Su, C.; Gao, C.; Tan, L.; Gu, H.; Wang, S.; Zheng, Z.; Dai, S.; Lin, C. Ultraflexible Temperature-Strain Dual-Sensor Based on Chalcogenide Glass-Polymer Film for Human-Machine Interaction. *Adv. Mater.* **2024**, *36* (23), 2313101.
(65) Gao, W.; Ota, H.; Kiriya, D.; Takei, K.; Javey, A. Flexible Electronics toward Wearable Sensing. *Acc. Chem. Res.* **2019**, *52* (3), 523−533.
(66) Yeom, C.; Chen, K.; Kiriya, D.; Yu, Z.; Cho, G.; Javey, A. Large-area Compliant Tactile Sensors Using Printed Carbon Nanotube Active-matrix Backplanes. *Adv. Mater.* **2015**, *27* (9), 1561−1566.
(67) Cao, L.; Wang, Z.; Hu, D.; Dong, H.; Qu, C.; Zheng, Y.; Yang, C.; Zhang, R.; Xing, C.; Li, Z.; Xin, Z.; Chen, D.; Song, Z.; He, Z. Pressure-Constrained Sonication Activation of Flexible Printed Metal Circuit. *Nat. Commun.* **2024**, *15* (1), 8324.
(68) Ma, Z.; Wu, Y.; Lu, S.; Li, J.; Liu, J.; Huang, X.; Zhang, X.; Zhang, Y.; Dong, G.; Qin, L.; Yang, S. Magnetically Assisted 3D Printing of Ultra-antiwear Flexible Sensor. *Adv. Funct. Mater.* **2024**, *34* (42), 2406108.
(69) Chen, S.; Huang, T.; Zuo, H.; Qian, S.; Guo, Y.; Sun, L.; Lei, D.; Wu, Q.; Zhu, B.; He, C.; Mo, X.; Jeffries, E.; Yu, H.; You, Z. A Single Integrated 3D-printing Process Customizes Elastic and Sustainable Triboelectric Nanogenerators for Wearable Electronics. *Adv. Funct. Mater.* **2018**, *28* (46), 1805108.
(70) Zhao, J.; Zhang, Y.; Huang, Y.; Xie, J.; Zhao, X.; Li, C.; Qu, J.; Zhang, Q.; Sun, J.; He, B.; Li, Q.; Lu, C.; Xu, X.; Lu, W.; Li, L.; Yao, Y. 3D Printing Fiber Electrodes for an All-fiber Integrated Electronic Device via Hybridization of an Asymmetric Supercapacitor and a Temperature Sensor. *Adv. Sci.* **2018**, *5* (11), 1801114.
(71) Xia, X.; Xiang, Z.; Gao, Z.; Hu, S.; Zhang, W.; Long, R.; Du, Y.; Liu, Y.; Wu, Y.; Li, W.; Shang, J.; Li, R. Structural Design and DLP 3D Printing Preparation of High Strain Stable Flexible Pressure Sensors. *Adv. Sci.* **2024**, *11* (37), 2304409.
(72) Liu, Y.; Zhang, Q.; Huang, A.; Zhang, K.; Wan, S.; Chen, H.; Fu, Y.; Zuo, W.; Wang, Y.; Cao, X.; Wang, L.; Lemmer, U.; Jiang, W. Fully Inkjet-Printed Ag2Se Flexible Thermoelectric Devices for Sustainable Power Generation. *Nat. Commun.* **2024**, *15* (1), 2141.
(73) Pu, Z.; Zhang, X.; Yu, H.; Tu, J.; Chen, H.; Liu, Y.; Su, X.; Wang, R.; Zhang, L.; Li, D. A Thermal Activated and Differential Self-Calibrated Flexible Epidermal Biomicrofluidic Device for Wearable Accurate Blood Glucose Monitoring. *Sci. Adv.* **2021**, *7* (5), No. eabd0199.
(74) Lin, Y.; Chen, J.; Tavakoli, M. M.; Gao, Y.; Zhu, Y.; Zhang, D.; Kam, M.; He, Z.; Fan, Z. Printable Fabrication of a Fully Integrated and Self-powered Sensor System on Plastic Substrates. *Adv. Mater.* **2019**, *31* (5), 1804285.
(75) Li, S.; Kosek, A.; Jahangir, M. N.; Malhotra, R.; Chang, C. Inkjet Printing of Perovskites for Breaking Performance-Temperature Tradeoffs in Fabric-based Thermistors. *Adv. Funct. Mater.* **2021**, *31* (1), 2006273.
(76) Agarwala, S.; Goh, G. L.; Dinh Le, T.-S.; An, J.; Peh, Z. K.; Yeong, W. Y.; Kim, Y.-J. Wearable Bandage-Based Strain Sensor for Home Healthcare: Combining 3D Aerosol Jet Printing and Laser Sintering. *ACS Sens.* **2019**, *4* (1), 218−226.
(77) Du, Y.; Wang, R.; Zeng, M.; Xu, S.; Saeidi-Javash, M.; Wu, W.; Zhang, Y. Hybrid Printing of Wearable Piezoelectric Sensors. *Nano Energy* **2021**, *90*, 106522.
(78) Mishra, S.; Kim, Y.-S.; Intarasirisawat, J.; Kwon, Y.-T.; Lee, Y.; Mahmood, M.; Lim, H.-R.; Herbert, R.; Yu, K. J.; Ang, C. S.; Yeo, W.-H. Soft, Wireless Periocular Wearable Electronics for Real-Time Detection of Eye Vergence in a Virtual Reality toward Mobile Eye Therapies. *Sci. Adv.* **2020**, *6* (11), No. eaay1729.
(79) Ou, C.; Sangle, A. L.; Datta, A.; Jing, Q.; Busolo, T.; Chalklen, T.; Narayan, V.; Kar-Narayan, S. Fully Printed Organic-Inorganic Nanocomposites for Flexible Thermoelectric Applications. *ACS Appl. Mater. Interfaces* **2018**, *10* (23), 19580−19587.
(80) Liu, T.; Tao, P.; Wang, X.; Wang, H.; He, M.; Wang, Q.; Cui, H.; Wang, J.; Tang, Y.; Tang, J.; Huang, N.; Kuang, C.; Xu, H.; He, X. Ultrahigh-Printing-Speed Photoresists for Additive Manufacturing. *Nat. Nanotechnol.* **2024**, *19* (1), 51−57.
(81) Lian, Y.; Wang, Y.; Yuan, Y.; Ren, Z.; Tang, W.; Liu, Z.; Xing, S.; Ji, K.; Yuan, B.; Yang, Y.; Gao, Y.; Zhang, S.; Zhou, K.; Zhang, G.; Stranks, S. D.; Zhao, B.; Di, D. Downscaling Micro- and Nano-Perovskite LEDs. *Nature* **2025**, *640* (8057), 62−68.
(82) Zhong, D.; Wu, C.; Jiang, Y.; Yuan, Y.; Kim, M.; Nishio, Y.; Shih, C.-C.; Wang, W.; Lai, J.-C.; Ji, X.; Gao, T. Z.; Wang, Y.-X.; Xu, C.; Zheng, Y.; Yu, Z.; Gong, H.; Matsuhisa, N.; Zhao, C.; Lei, Y.; Liu, D.; Zhang, S.; Ochiai, Y.; Liu, S.; Wei, S.; Tok, J. B.-H.; Bao, Z. High-Speed and Large-Scale Intrinsically Stretchable Integrated Circuits. *Nature* **2024**, *627* (8003), 313−320.
(83) Li, L.; Yu, X.; Lin, Z.; Cai, Z.; Cao, Y.; Kong, W.; Xiang, Z.; Gu, Z.; Xing, X.; Duan, X.; Song, Y. Interface Capture Effect Printing Atomic-thick 2D Semiconductor Thin Films. *Adv. Mater.* **2022**, *34* (49), 2207392.
(84) Wu, H.; Ye, F.; Yang, M.; Luo, F.; Tang, X.; Tang, Q.; Qiu, H.; Huang, Z.; Wang, G.; Sun, Z.; Lin, H.; Wei, J.; Li, Y.; Tian, X.; Zhang, J.; Xie, L.; Deng, X.; Yuan, T.; Yu, M.; Liu, Y.; Li, P.; Chen, H.; Zhou, S.; Xu, Q.; Li, P.; Duan, J.; Chen, J.; Li, C.; Yin, S.; Liu, B.; Sun, C.; Su, Q.; Wang, Y.; Deng, H.; Xie, T.; Gao, P.; Kang, Q.; Zhang, Y.; Yan, H.; Yuan, N.; Peng, F.; Yuan, Y.; Ru, X.; He, B.; Chen, L.; Wang, J.; Lu, J.; Qu, M.; Xue, C.; Ding, J.; Fang, L.; Li, Z.; Xu, X. Silicon Heterojunction Back-Contact Solar Cells by Laser Patterning. *Nature* **2024**, *635* (8039), 604−609.
(85) Wang, M.; Yang, Y.; Min, J.; Song, Y.; Tu, J.; Mukasa, D.; Ye, C.; Xu, C.; Heflin, N.; McCune, J. S.; Hsiai, T. K.; Li, Z.; Gao, W. A Wearable Electrochemical Biosensor for the Monitoring of Metabolites and Nutrients. *Nat. Biomed. Eng.* **2022**, *6* (11), 1225−1235.
(86) Yu, W.; Zhao, W.; Zhu, X.; Li, M.; Yi, X.; Liu, X. Laser-printed All-carbon Responsive Material and Soft Robot. *Adv. Mater.* **2024**, *36*, 2401920.
(87) Coles, L.; Ventrella, D.; Carnicer-Lombarte, A.; Elmi, A.; Troughton, J. G.; Mariello, M.; El Hadwe, S.; Woodington, B. J.;

https://doi.org/10.1021/acs.chemrev.5c00801
Chem. Rev. XXXX, XXX, XXX−XXX

Bacci, M. L.; Malliaras, G. G.; Barone, D. G.; Proctor, C. M. Origami-Inspired Soft Fluidic Actuation for Minimally Invasive Large-Area Electrocorticography. *Nat. Commun.* **2024**, *15* (1), 6290.
(88) Yuan, B.; Yang, B.; Xu, P.; Zhang, M. Poly(*p* -Phenylene Benzobisoxazole) Nanofiber: A Promising Nanoscale Building Block toward Extremely Harsh Conditions. *ACS Nano* **2025**, *19* (2), 1981−2012.
(89) Meng, Z.; Zhu, L.; Wang, X.; Zhu, M. Electrospun Nanofibrous Composite Membranes for Separations. *Acc. Mater. Res.* **2023**, *4* (2), 180−192.
(90) Yuan, M.; Feng, J.; Li, H.; Gao, H.; Qiu, Y.; Jiang, L.; Wu, Y. Remote Epitaxial Crystalline Perovskites for Ultrahigh-Resolution Micro-LED Displays. *Nat. Nanotechnol.* **2025**, *20* (3), 381−387.
(91) Shi, Z.; Qin, W.; Hu, Z.; Ma, M.; Liu, H.; Shu, Z.; Jiang, Y.; Xia, H.; Shi, W.; Zhang, C. Y.; Sang, X.; Guo, C.; Li, Y.; Liu, C.; Gong, C.; Wang, H.; Liu, S.; Tapasztó, L.; Gao, C.; Liu, F.; Tang, P.; Liu, Y.; Duan, H.; Xie, E.; Zhang, Z.; Liu, Z.; He, Y. Sub-2-Nm-Droplet-Driven Growth of Amorphous Metal Chalcogenides Approaching the Single-Layer Limit. *Nat. Mater.* **2025**, *24* (8), 1186−1194.
(92) Lobe, S.; Bauer, A.; Uhlenbruck, S.; Fattakhova-Rohlfing, D. Physical Vapor Deposition in Solid-state Battery Development: From Materials to Devices. *Adv. Sci.* **2021**, *8* (11), 2002044.
(93) Zhang, X.; Ericksen, O.; Lee, S.; Akl, M.; Song, M.-K.; Lan, H.; Pal, P.; Suh, J. M.; Lindemann, S.; Ryu, J.-E.; Shao, Y.; Zheng, X.; Han, N. M.; Bhatia, B.; Kim, H.; Kum, H. S.; Chang, C. S.; Shi, Y.; Eom, C.-B.; Kim, J. Atomic Lift-off of Epitaxial Membranes for Cooling-Free Infrared Detection. *Nature* **2025**, *641* (8061), 98−105.
(94) Rabehi, I. N.; Mariotti, S.; Fukuda, K.; Lee, S. Y.; Zhao, D.; Ji, P.; Yuan, S.; Zhang, J.; Ding, C.; Mitrofanov, K.; Madea, D.; Kabe, R.; Yokota, T.; Ono, L. K.; Someya, T.; Qi, Y. Dual Hole Transport Layer for Ultra-Flexible Perovskite Solar Cells with Unprecedented Stability. *Joule* **2025**, *9*, 102209.
(95) Tang, H.; Shen, Z.; Shen, Y.; Yan, G.; Wang, Y.; Han, Q.; Han, L. Reinforcing Self-Assembly of Hole Transport Molecules for Stable Inverted Perovskite Solar Cells. *Science* **2024**, *383* (6688), 1236−1240.
(96) Liu, L.; Cai, Z.; Xue, S.; Huang, H.; Chen, S.; Gou, S.; Zhang, Z.; Guo, Y.; Yao, Y.; Bao, W.; Zhou, P. A Mass Transfer Technology for High-Density Two-Dimensional Device Integration. *Nat. Electron.* **2025**.
(97) Gao, Y.; Ota, H.; Schaler, E. W.; Chen, K.; Zhao, A.; Gao, W.; Fahad, H. M.; Leng, Y.; Zheng, A.; Xiong, F.; Zhang, C.; Tai, L.; Zhao, P.; Fearing, R. S.; Javey, A. Wearable Microfluidic Diaphragm Pressure Sensor for Health and Tactile Touch Monitoring. *Adv. Mater.* **2017**, *29* (39), 1701985.
(98) Kelso, M. V.; Mahenderkar, N. K.; Chen, Q.; Tubbesing, J. Z.; Switzer, J. A. Spin Coating Epitaxial Films. *Science* **2019**, *364* (6436), 166−169.
(99) Wang, X.-Y.; Ding, Y.-F.; Zhang, X.-Y.; Zhou, Y.-Y.; Pan, C.-K.; Li, Y.-H.; Liu, N.-F.; Yao, Z.-F.; Chen, Y.-S.; Xie, Z.-H.; Huang, Y.-F.; Xu, Y.-C.; Wu, H.-T.; Huang, C.-X.; Xiong, M.; Ding, L.; Yu, Z.-D.; Li, Q.-Y.; Zheng, Y.-Q.; Wang, J.-Y.; Pei, J. Light-Triggered Regionally Controlled n-Doping of Organic Semiconductors. *Nature* **2025**, *642* (8068), 599−604.
(100) Song, Y.; Tay, R. Y.; Li, J.; Xu, C.; Min, J.; Shirzaei Sani, E.; Kim, G.; Heng, W.; Kim, I.; Gao, W. 3D-Printed Epifluidic Electronic Skin for Machine Learning-Powered Multimodal Health Surveillance. *Sci. Adv.* **2023**, *9* (37), No. eadi6492.
(101) Tierney, M. J.; Tamada, J. A.; Potts, R. O.; Jovanovic, L.; Garg, S. Clinical Evaluation of the GlucoWatch® Biographer: A Continual, Non-Invasive Glucose Monitor for Patients with Diabetes. *Biosens. Bioelectron.* **2001**, *16* (9−12), 621−629.
(102) Melzer, M.; Mönch, J. I.; Makarov, D.; Zabila, Y.; Cañón Bermúdez, G. S.; Karnaushenko, D.; Baunack, S.; Bahr, F.; Yan, C.; Kaltenbrunner, M.; Schmidt, O. G. Wearable Magnetic Field Sensors for Flexible Electronics. *Adv. Mater.* **2015**, *27* (7), 1274−1280.
(103) Bariya, M.; Shahpar, Z.; Park, H.; Sun, J.; Jung, Y.; Gao, W.; Nyein, H. Y. Y.; Liaw, T. S.; Tai, L.-C.; Ngo, Q. P.; Chao, M.; Zhao, Y.; Hettick, M.; Cho, G.; Javey, A. Roll-to-Roll Gravure Printed Electrochemical Sensors for Wearable and Medical Devices. *ACS Nano* **2018**, *12* (7), 6978−6987.
(104) Kwon, Y.-T.; Kim, Y.-S.; Kwon, S.; Mahmood, M.; Lim, H.-R.; Park, S.-W.; Kang, S.-O.; Choi, J. J.; Herbert, R.; Jang, Y. C.; Choa, Y.-H.; Yeo, W.-H. All-Printed Nanomembrane Wireless Bioelectronics Using a Biocompatible Solderable Graphene for Multimodal Human-Machine Interfaces. *Nat. Commun.* **2020**, *11* (1), 3450.
(105) Kireev, D.; Sel, K.; Ibrahim, B.; Kumar, N.; Akbari, A.; Jafari, R.; Akinwande, D. Continuous Cuffless Monitoring of Arterial Blood Pressure via Graphene Bioimpedance Tattoos. *Nat. Nanotechnol.* **2022**, *17* (8), 864−870.
(106) Zhuang, Q.; Yao, K.; Zhang, C.; Song, X.; Zhou, J.; Zhang, Y.; Huang, Q.; Zhou, Y.; Yu, X.; Zheng, Z. Permeable, Three-Dimensional Integrated Electronic Skins with Stretchable Hybrid Liquid Metal Solders. *Nat. Electron.* **2024**, *7* (7), 598−609.
(107) Wang, M.; Ye, C.; Yang, Y.; Mukasa, D.; Wang, C.; Xu, C.; Min, J.; Solomon, S. A.; Tu, J.; Shen, G.; Tang, S.; Hsiai, T. K.; Li, Z.; McCune, J. S.; Gao, W. Printable Molecule-Selective Core-Shell Nanoparticles for Wearable and Implantable Sensing. *Nat. Mater.* **2025**, *24* (4), 589−598.
(108) Guo, X.; Lu, X.; Jiang, P.; Bao, X. Touchless Thermosensation Enabled by Flexible Infrared Photothermoelectric Detector for Temperature Prewarning Function of Electronic Skin. *Adv. Mater.* **2024**, *36* (23), 2313911.
(109) Liu, G.; Tian, Z.; Yang, Z.; Xue, Z.; Zhang, M.; Hu, X.; Wang, Y.; Yang, Y.; Chu, P. K.; Mei, Y.; Liao, L.; Hu, W.; Di, Z. Graphene-Assisted Metal Transfer Printing for Wafer-Scale Integration of Metal Electrodes and Two-Dimensional Materials. *Nat. Electron.* **2022**, *5* (5), 275−280.
(110) Tian, X.; Li, F.; Tang, Z.; Wang, S.; Weng, K.; Liu, D.; Lu, S.; Liu, W.; Fu, Z.; Li, W.; Qiu, H.; Tu, M.; Zhang, H.; Li, J. Crosslinking-Induced Patterning of MOFs by Direct Photo- and Electron-Beam Lithography. *Nat. Commun.* **2024**, *15* (1), 2920.
(111) Nyein, H. Y. Y.; Bariya, M.; Kivimäki, L.; Uusitalo, S.; Liaw, T. S.; Jansson, E.; Ahn, C. H.; Hangasky, J. A.; Zhao, J.; Lin, Y.; Happonen, T.; Chao, M.; Liedert, C.; Zhao, Y.; Tai, L.-C.; Hiltunen, J.; Javey, A. Regional and Correlative Sweat Analysis Using High-Throughput Microfluidic Sensing Patches toward Decoding Sweat. *Sci. Adv.* **2019**, *5* (8), No. eaaw9906.
(112) Song, K.; Zhou, J.; Wei, C.; Ponnuchamy, A.; Bappy, M. O.; Liao, Y.; Jiang, Q.; Du, Y.; Evans, C. J.; Wyatt, B. C.; O'Sullivan, T.; Roeder, R. K.; Anasori, B.; Hoffman, A. J.; Jin, L.; Duan, X.; Zhang, Y. A Printed Microscopic Universal Gradient Interface for Super Stretchable Strain-insensitive Bioelectronics. *Adv. Mater.* **2025**, *37* (11), 2414203.
(113) Moin, A.; Zhou, A.; Rahimi, A.; Menon, A.; Benatti, S.; Alexandrov, G.; Tamakloe, S.; Ting, J.; Yamamoto, N.; Khan, Y.; Burghardt, F.; Benini, L.; Arias, A. C.; Rabaey, J. M. A Wearable Biosensing System with In-Sensor Adaptive Machine Learning for Hand Gesture Recognition. *Nat. Electron.* **2021**, *4* (1), 54−63.
(114) Kang, K.; Xie, S.; Huang, L.; Han, Y.; Huang, P. Y.; Mak, K. F.; Kim, C.-J.; Muller, D.; Park, J. High-Mobility Three-Atom-Thick Semiconducting Films with Wafer-Scale Homogeneity. *Nature* **2015**, *520* (7549), 656−660.
(115) Wang, Y.; Chen, F.; Chen, Q.; Liu, W.; Huang, Q.; Hou, X.; Li, S.; Cheng, C.; Xie, X.; Meng, N.; Liao, Y. Bioinspired Photothermal Zwitterionic Fibrous Membrane for High-Efficiency Solar Desalination and Electricity Generation. *Nat. Commun.* **2025**, *16* (1), 6373.
(116) Yu, Y.; Li, J.; Solomon, S. A.; Min, J.; Tu, J.; Guo, W.; Xu, C.; Song, Y.; Gao, W. All-Printed Soft Human-Machine Interface for Robotic Physicochemical Sensing. *Sci. Rob.* **2022**, *7* (67), No. eabn0495.
(117) Zhang, Y.; Yang, Z.; Qiao, C.; Liu, Y.; Wang, C.; Zeng, X.; Hou, J.; Huo, D.; Hou, C. Synergistic Enhancement of Wearable Biosensor through Pt Single-Atom Catalyst for Sweat Analysis. *Biosens. Bioelectron.* **2024**, *258*, 116354.
(118) Kim, T. Y.; Hong, S. H.; Jeong, S. H.; Bae, H.; Cheong, S.; Choi, H.; Hahn, S. K. Multifunctional Intelligent Wearable Devices

https://doi.org/10.1021/acs.chemrev.5c00801
Chem. Rev. XXXX, XXX, XXX−XXX

Using Logical Circuits of Monolithic Gold Nanowires. *Adv. Mater.* **2023**, *35* (45), 2303401.
(119) Lee, S.; Ho, D. H.; Jekal, J.; Cho, S. Y.; Choi, Y. J.; Oh, S.; Choi, Y. Y.; Lee, T.; Jang, K.-I.; Cho, J. H. Fabric-Based Lamina Emergent MXene-Based Electrode for Electrophysiological Monitoring. *Nat. Commun.* **2024**, *15* (1), 5974.
(120) Zhang, J.; Chai, F.; Li, J.; Wang, S.; Zhang, S.; Li, F.; Liang, A.; Luo, A.; Wang, D.; Jiang, X. Weakly Ionized Gold Nanoparticles Amplify Immunoassays for Ultrasensitive Point-of-Care Sensors. *Sci. Adv.* **2024**, *10* (28), No. eadn5698.
(121) Ko, Y.-J.; Lim, C.; Jin, J.; Kim, M. G.; Lee, J. Y.; Seong, T.-Y.; Lee, K.-Y.; Min, B. K.; Choi, J.-Y.; Noh, T.; Hwang, G. W.; Lee, W. H.; Oh, H.-S. Extrinsic Hydrophobicity-Controlled Silver Nanoparticles as Efficient and Stable Catalysts for CO2 Electrolysis. *Nat. Commun.* **2024**, *15* (1), 3356.
(122) Edwards, E. H.; Jelušić, J.; Kosko, R. M.; McClelland, K. P.; Ngarnim, S. S.; Chiang, W.; Lampa-Pastirk, S.; Krauss, T. D.; Bren, K. L. *Shewanella Oneidensis* MR-1 Respires CdSe Quantum Dots for Photocatalytic Hydrogen Evolution. *Proc. Natl. Acad. Sci. U. S. A.* **2023**, *120* (17), No. e2206975120.
(123) Lin, X.; Yang, Y.; Li, X.; Lv, Y.; Wang, Z.; Du, J.; Luo, X.; Zhou, D.; Xiao, C.; Wu, K. Blue Lasers Using Low-Toxicity Colloidal Quantum Dots. *Nat. Nanotechnol.* **2025**, *20* (2), 229−236.
(124) Wei, J.; Zhang, X.; Mugo, S. M.; Zhang, Q. A Portable Sweat Sensor Based on Carbon Quantum Dots for Multiplex Detection of Cardiovascular Health Biomarkers. *Anal. Chem.* **2022**, *94* (37), 12772−12780.
(125) Wang, J.; Fan, X.; Han, X.; Lv, K.; Zhao, Y.; Zhao, Z.; Zhao, D. Ultrasmall Inorganic Mesoporous Nanoparticles: Preparation, Functionalization, and Application. *Adv. Mater.* **2024**, *36* (28), 2312374.
(126) Wang, Y.; Yao, J.; Wu, S.; Zhi, C.; Yin, L.; Song, Z.; Wang, J.; Ling, L.; Ma, Y.; Zhang, D.; Li, J.; Li, L.; Chen, B. Encapsulation of Metal Nanoclusters into Hydrogen-Bonded Organic Frameworks for Double-Response-Reverse Ammonia Fluorescence Sensing. *Chem.* **2025**, *11* (7), 102457.
(127) Nisa, F. U.; Tahir, M.; Khalid, S.; Amin, N.; Yin, H.; Long, Y.; Tang, H.; Iiaz, K.; Khan, A. U.; Naseem, M.; Peng, Z.; Ma, Z.; Wu, L.; Uddin, M. F.; Khan, A. J.; Qu, L.; Ahmad, W.; He, L. Revolutionizing Micro-Scale Energy Storage by 0D Carbon Nanostructures: Synthesis, Integration, Performance Optimization Mechanisms and Sustainable Applications. *Adv. Funct. Mater.* **2025**, *35* (13), 2418053.
(128) Li, S.; Meng, X.; Zhu, C.; Xu, W.; Sun, Y.; Lu, X.; Dai, Y. Revolutionizing Inorganic Nanofibers: Bridging Functional Elements to a Future System. *ACS Nano* **2025**, *19* (15), 14579−14604.
(129) Kimura, Y.; Cui, Y.; Suzuki, T.; Tanaka, Y.; Tanaka, T.; Toku, Y.; Ju, Y. Growth of Metal Nanowire Forests Controlled through Stress Fields Induced by Grain Gradients. *Science* **2024**, *385* (6709), 641−646.
(130) Zhang, Z.; Chen, Y.; Shen, P.; Chen, J.; Wang, S.; Wang, B.; Ma, S.; Lyu, B.; Zhou, X.; Lou, S.; Wu, Z.; Xie, Y.; Zhang, C.; Wang, L.; Xu, K.; Li, H.; Wang, G.; Watanabe, K.; Taniguchi, T.; Qian, D.; Jia, J.; Liang, Q.; Wang, X.; Yang, W.; Zhang, G.; Jin, C.; Ouyang, W.; Shi, Z. Homochiral Carbon Nanotube van Der Waals Crystals. *Science* **2025**, *387* (6740), 1310−1316.
(131) Wu, X.; Li, J.; Jiang, Q.; Zhang, W.; Wang, B.; Li, R.; Zhao, S.; Wang, F.; Huang, Y.; Lyu, P.; Zhao, Y.; Zhu, J.; Zhang, R. An All-Weather Radiative Human Body Cooling Textile. *Nat. Sustainability* **2023**, *6* (11), 1446−1454.
(132) Klaassen, D. J.; Eek, L.; Rudenko, A. N.; Van 'T Westende, E. D.; Castenmiller, C.; Zhang, Z.; De Boeij, P. L.; Van Houselt, A.; Ezawa, M.; Zandvliet, H. J. W.; Morais Smith, C.; Bampoulis, P. Realization of a One-Dimensional Topological Insulator in Ultrathin Germanene Nanoribbons. *Nat. Commun.* **2025**, *16* (1), 2059.
(133) Huang, Y.; Gao, M.; Fu, Y.; Li, J.; Wang, F.; Yang, S.; Wang, M.; Qian, Z.; Lu, X.; Zhang, P.; Wang, R. Hierarchical Porous Carbon Nanofibers Embedded with One-Dimensional Conjugated Metal-organic Framework Anodes for Ammonium-Ion Hybrid Supercapacitors. *Energy Storage Mater.* **2024**, *70*, 103522.
(134) Yang, W.; Pan, D.; Liu, S.; Jia, G.; Wang, Y.; Liu, H.; Liu, C.; Shen, C. Multifunctional Wearable Conductive Nanofiber Membrane with Antibacterial and Breathable Ability for Superior Sensing, Electromagnetic Interference Shielding, and Thermal Management. *Adv. Funct. Mater.* **2025**, *35* (6), 2414811.
(135) Peng, L.; Peng, H.; Wang, S.; Li, X.; Mo, J.; Wang, X.; Tang, Y.; Che, R.; Wang, Z.; Li, W.; Zhao, D. One-Dimensionally Oriented Self-Assembly of Ordered Mesoporous Nanofibers Featuring Tailorable Mesophases via Kinetic Control. *Nat. Commun.* **2023**, *14* (1), 8148.
(136) Manchi, P.; Paranjape, M. V.; Kurakula, A.; Graham, S. A.; Kavarthapu, V. S.; Yu, J. S. PDA-ag/TiO_2 Nanoparticles-loaded Electrospun Nylon Composite Nanofibrous Film-based Triboelectric Nanogenerators for Wearable Biomechanical Energy Harvesting and Multifunctional Sensors. *Adv. Funct. Mater.* **2025**, *35* (9), 2416018.
(137) Xiao, S.; Liu, B.; Zhou, R.; Liu, Z.; Li, Q.; Wang, T. Room-Temperature H2 Sensing Interfered by CO Based on Interfacial Effects in Palladium-Tungsten Oxide Nanoparticles. *Sens. Actuators B: Chem.* **2018**, *254*, 966−972.
(138) Tan, C.; Cao, X.; Wu, X.-J.; He, Q.; Yang, J.; Zhang, X.; Chen, J.; Zhao, W.; Han, S.; Nam, G.-H.; Sindoro, M.; Zhang, H. Recent Advances in Ultrathin Two-Dimensional Nanomaterials. *Chem. Rev.* **2017**, *117* (9), 6225−6331.
(139) Zheng, Y.; Wang, Y.; Liu, D.; Zhao, J.; Li, Y. Unlocking Self-antioxidant Capability and Processability of Additive-free MXene Ink towards High-performance Customizable Supercapacitors. *Angew. Chem., Int. Ed.* **2025**, *64* (3), No. e202415742.
(140) Katiyar, A. K.; Hoang, A. T.; Xu, D.; Hong, J.; Kim, B. J.; Ji, S.; Ahn, J.-H. 2D Materials in Flexible Electronics: Recent Advances and Future Prospectives. *Chem. Rev.* **2024**, *124* (2), 318−419.
(141) Thakur, A.; Highland, W. J.; Wyatt, B. C.; Xu, J.; Chandran B S, N.; Zhang, B.; Hood, Z. D.; Adhikari, S. P.; Oveisi, E.; Pacakova, B.; Vega, F.; Simon, J.; Fruhling, C.; Reigle, B.; Asadi, M.; Michałowski, P. P.; Shalaev, V. M.; Boltasseva, A.; Beechem, T. E.; Liu, C.; Anasori, B. Synthesis of a 2D Tungsten MXene for Electrocatalysis. *Nat. Synth.* **2025**, *4* (7), 888−900.
(142) Lyu, B.; Chen, J.; Wang, S.; Lou, S.; Shen, P.; Xie, J.; Qiu, L.; Mitchell, I.; Li, C.; Hu, C.; Zhou, X.; Watanabe, K.; Taniguchi, T.; Wang, X.; Jia, J.; Liang, Q.; Chen, G.; Li, T.; Wang, S.; Ouyang, W.; Hod, O.; Ding, F.; Urbakh, M.; Shi, Z. Graphene Nanoribbons Grown in hBN Stacks for High-Performance Electronics. *Nature* **2024**, *628* (8009), 758−764.
(143) Peng, Y.; Cui, C.; Li, L.; Wang, Y.; Wang, Q.; Tian, J.; Huang, Z.; Huang, B.; Zhang, Y.; Li, X.; Tang, J.; Chu, Y.; Yang, W.; Shi, D.; Du, L.; Li, N.; Zhang, G. Medium-Scale Flexible Integrated Circuits Based on 2D Semiconductors. *Nat. Commun.* **2024**, *15* (1), 10833.
(144) Mei, L.; Gao, Z.; Yang, R.; Zhang, Z.; Sun, M.; Liang, X.; Zhang, Y.; Ying, T.; Hu, H.; Li, D.; Zhang, Q.; Gu, M. D.; Gu, L.; Zhou, J.; Huang, B.; Voiry, D.; Zeng, X. C.; Chai, Y.; Li, J.; Yu, X.; Zeng, Z. Phase-Switchable Preparation of Solution-Processable WS2Mono- or Bilayers. *Nat. Synth.* **2025**, *4* (3), 303−313.
(145) Rahman, M. S.; Shon, A.; Joseph, R.; Pavlov, A.; Stefanov, A.; Namkoong, M.; Guo, H.; Bui, D.; Master, R.; Sharma, A.; Lee, J.; Rivas, M.; Elati, A.; Jones-Hall, Y.; Zhao, F.; Park, H.; Hook, M. A.; Tian, L. Soft, Stretchable Conductive Hydrogels for High-Performance Electronic Implants. *Sci. Adv.* **2025**, *11* (12), No. eads4415.
(146) Xi, Z.; Hu, H.; Chen, Q.; Ning, M.; Wang, S.; Yu, H.; Sun, Y.; Wang, D.; Jin, H.; Cheng, H. 2D Catalysts for Electrocatalytic Nitrate Reduction and C-N Coupling Reactions. *Adv. Funct. Mater.* **2025**, *35*, 2425611.
(147) Zhang, J.; Ma, J.; Zhang, W.; Ma, H.; Geng, X.; Zhang, H.; Liu, Q.; Zhu, J.; Li, C.; Su, Y.; Zhu, N. Wearable Sensors Deriving from Cationic-Induced 2D-2D Co-Assembled Films for Nutrient Monitoring. *Electrochim. Acta* **2024**, *477*, 143787.
(148) Pishvar, M.; Harne, R. L. Foundations for Soft, Smart Matter by Active Mechanical Metamaterials. *Adv. Sci.* **2020**, *7* (18), 2001384.
(149) Lu, H.; Zhang, L.; Jiang, J.; Song, J.; Zhou, Z.; Wu, W.; Cheng, Z.; Yan, T.; Hu, H.; Zhao, T.; Xu, Z.; Luo, S.; Li, H.; Zhang, J.; Lawrie, C. H. Pressure Induced Molecular-Arrangement and Charge-

https://doi.org/10.1021/acs.chemrev.5c00801
Chem. Rev. XXXX, XXX, XXX−XXX

Density Perturbance in Doped Polymer for Intelligent Motion and Vocal Recognitions. *Adv. Mater.* **2025**, *37* (27), 2500077.
(150) Wang, M.; Wang, G.; Zheng, M.; Liu, W.; Lv, W.; Ma, Y.; Guo, J.; Ebo, B. High-Performance Flexible Pressure Sensor Based on Synergistic Enhancement of Magnetic Field Oriented Carbon Nanotube/Graphene and Microdome Array Structure. *Chem. Eng. J.* **2025**, *511*, 162053.
(151) Liu, Y.; Zhou, Y.; Qin, H.; Yang, T.; Chen, X.; Li, L.; Han, Z.; Wang, K.; Zhang, B.; Lu, W.; Chen, L.-Q.; Bernholc, J.; Wang, Q. Electro-Thermal Actuation in Percolative Ferroelectric Polymer Nanocomposites. *Nat. Mater.* **2023**, *22* (7), 873−879.
(152) Song, L.; Wang, Z.; Chen, S.; Shen, Y.; Yin, J.; Wang, R. Phytic Acid-induced Gradient Hydrogels for Highly Sensitive and Broad Range Pressure Sensing. *Adv. Mater.* **2025**, *37* (9), 2417978.
(153) Jung, D.; Kim, Y.; Lee, H.; Jung, S.; Park, C.; Hyeon, T.; Kim, D. Metal-Like Stretchable Nanocomposite Using Locally-Bundled Nanowires for Skin-Mountable Devices. *Adv. Mater.* **2023**, *35* (44), 2303458.
(154) Wang, H.; Lu, R.; Yan, J.; Peng, J.; Tomsia, A. P.; Liang, R.; Sun, G.; Liu, M.; Jiang, L.; Cheng, Q. Tough and Conductive Nacre-inspired MXene/Epoxy Layered Bulk Nanocomposites. *Angew. Chem., Int. Ed.* **2023**, *62* (9), No. e202216874.
(155) Xu, J.; Li, Y.; Liu, T.; Wang, D.; Sun, F.; Hu, P.; Wang, L.; Chen, J.; Wang, X.; Yao, B.; Fu, J. Room-Temperature Self-Healing Soft Composite Network with Unprecedented Crack Propagation Resistance Enabled by a Supramolecular Assembled Lamellar Structure. *Adv. Mater.* **2023**, *35* (26), 2300937.
(156) Liu, W.; Zhang, Y.; Li, B.; Dai, T.; Huang, Y.; Chen, X.; Chen, Z. CuO_2 -ICG Nanocomposite: A Multifunctional Solution for Diabetic Wound Management with Antibacterial and Anti-inflammatory Effects. *Adv. Funct. Mater.* **2025**, *35*, 2501858.
(157) Yun, G.; Cole, T.; Zhang, Y.; Zheng, J.; Sun, S.; Ou-yang, Y.; Shu, J.; Lu, H.; Zhang, Q.; Wang, Y.; Pham, D.; Hasan, T.; Li, W.; Zhang, S.; Tang, S.-Y. Electro-Mechano Responsive Elastomers with Self-Tunable Conductivity and Stiffness. *Sci. Adv.* **2023**, *9* (4), No. eadf1141.
(158) Chen, M.; An, X.; Zhao, F.; Chen, P.; Wang, J.; Zhang, M.; Lu, A. Boosting Sensitivity of Cellulose Pressure Sensor via Hierarchically Porous Structure. *Nano Micro Lett.* **2025**, *17* (1), 205.
(159) Chen, R.; Luo, T.; Wang, J.; Wang, R.; Zhang, C.; Xie, Y.; Qin, L.; Yao, H.; Zhou, W. Nonlinearity Synergy: An Elegant Strategy for Realizing High-Sensitivity and Wide-Linear-Range Pressure Sensing. *Nat. Commun.* **2023**, *14* (1), 6641.
(160) Idrus-Saidi, S. A.; Tang, J.; Lambie, S.; Han, J.; Mayyas, M.; Ghasemian, M. B.; Allioux, F.-M.; Cai, S.; Koshy, P.; Mostaghimi, P.; Steenbergen, K. G.; Barnard, A. S.; Daeneke, T.; Gaston, N.; Kalantar-Zadeh, K. Liquid Metal Synthesis Solvents for Metallic Crystals. *Science* **2022**, *378* (6624), 1118−1124.
(161) Sun, K.; Liang, X.; Wang, X.; Wu, Y. A.; Jana, S.; Zou, Y.; Zhao, X.; Chen, H.; Zou, X. Highly Efficient and Durable Anode Catalyst Layer Constructed with Deformable Hollow IrO_x Nanospheres in Low-Iridium PEM Water Electrolyzer. *Angew. Chem., Int. Ed.* **2025**, *64* (21), No. e202504531.
(162) Geng, X.; Li, S.; Mawella-Vithanage, L.; Ma, T.; Kilani, M.; Wang, B.; Ma, L.; Hewa-Rahinduwage, C. C.; Shafikova, A.; Nikolla, E.; Mao, G.; Brock, S. L.; Zhang, L.; Luo, L. Atomically Dispersed Pb Ionic Sites in PbCdSe Quantum Dot Gels Enhance Room-Temperature NO2 Sensing. *Nat. Commun.* **2021**, *12* (1), 4895.
(163) He, W.; Wang, M.; Mei, G.; Liu, S.; Khan, A. Q.; Li, C.; Feng, D.; Su, Z.; Bao, L.; Wang, G.; Liu, E.; Zhu, Y.; Bai, J.; Zhu, M.; Zhou, X.; Liu, Z. Establishing Superfine Nanofibrils for Robust Polyelectrolyte Artificial Spider Silk and Powerful Artificial Muscles. *Nat. Commun.* **2024**, *15* (1), 3485.
(164) Guo, P.; Tian, B.; Liang, J.; Yang, X.; Tang, G.; Li, Q.; Liu, Q.; Zheng, K.; Chen, X.; Wu, W. An All-Printed, Fast-Response Flexible Humidity Sensor Based on Hexagonal-WO_3 Nanowires for Multifunctional Applications. *Adv. Mater.* **2023**, *35* (41), 2304420.
(165) Qaiser, N.; Al-Modaf, F.; Khan, S. M.; Shaikh, S. F.; El-Atab, N.; Hussain, M. M. A Robust Wearable Point-of-Care CNT-Based Strain Sensor for Wirelessly Monitoring Throat-Related Illnesses. *Adv. Funct. Mater.* **2021**, *31* (29), 2103375.
(166) Su, Z.; Chen, X.; Sun, M.; Yang, X.; Kang, J.; Cai, Z.; Guo, L. Amorphous Nanobelts for Efficient Electrocatalytic Ammonia Production. *Angew. Chem., Int. Ed.* **2025**, *64* (4), No. e202416878.
(167) Xia, Y.; Mathis, T. S.; Zhao, M.-Q.; Anasori, B.; Dang, A.; Zhou, Z.; Cho, H.; Gogotsi, Y.; Yang, S. Thickness-Independent Capacitance of Vertically Aligned Liquid-Crystalline MXenes. *Nature* **2018**, *557* (7705), 409−412.
(168) Guo, S.; Wu, K.; Li, C.; Wang, H.; Sun, Z.; Xi, D.; Zhang, S.; Ding, W.; Zaghloul, M. E.; Wang, C.; Castro, F. A.; Yang, D.; Zhao, Y. Integrated Contact Lens Sensor System Based on Multifunctional Ultrathin MoS2 Transistors. *Matter* **2021**, *4* (3), 969−985.
(169) Liang, J.; Wang, Y.; Ma, X.; Song, X.; Wang, H.; Shen, T.; Sun, J.; Hu, Y.; Liu, Y.; Wu, Z.; Yu, T.; Tie, Z.; Jin, Z. Directional Oxygen Defect Engineering in Black Phosphorus Aerogel for Flexible and Stable Moisture-electric Generators. *Adv. Funct. Mater.* **2025**, *35* (15), 2418834.
(170) Liu, Y.; Xu, Z.; Ji, X.; Xu, X.; Chen, F.; Pan, X.; Fu, Z.; Chen, Y.; Zhang, Z.; Liu, H.; Cheng, B.; Liang, J. Ag-Thiolate Interactions to Enable an Ultrasensitive and Stretchable MXene Strain Sensor with High Temporospatial Resolution. *Nat. Commun.* **2024**, *15* (1), 5354.
(171) Wang, W.; Zhou, H.; Xu, Z.; Li, Z.; Zhang, L.; Wan, P. Flexible Conformally Bioadhesive MXene Hydrogel Electronics for Machine Learning-Facilitated Human-Interactive Sensing. *Adv. Mater.* **2024**, *36* (31), 2401035.
(172) Fan, Y.; Yan, Y.; Nwokonkwo, O.; Rivera, D. J.; Pan, W.; Chen, E.; Kim, J.-Y.; Simon, J.; Saffer-Meng, M.; Wang, X.; Muhich, C.; Winter, L. R. Tuning Nitrate Reduction Reaction Selectivity via Selective Adsorption in Electrified Membranes. *Nat. Chem. Eng.* **2025**, *2* (6), 379−390.
(173) Yang, J.; Li, M.; Fang, S.; Wang, Y.; He, H.; Wang, C.; Zhang, Z.; Yuan, B.; Jiang, L.; Baughman, R. H.; Cheng, Q. Water-Induced Strong Isotropic MXene-Bridged Graphene Sheets for Electrochemical Energy Storage. *Science* **2024**, *383* (6684), 771−777.
(174) Yao, S.; Zhang, C.; Bai, L.; Wang, S.; Liu, Y.; Li, L.; Li, X.; He, J.; Wang, L.; Li, D. Tailoring Stretchable, Biocompatible, and 3D Printable Properties of Carbon-Based Conductive Hydrogel for Bioelectronic Interface Applications. *Adv. Funct. Mater.* **2025**, *35* (12), 2418554.
(175) Xie, R.; Cao, Y.; Sun, R.; Wang, R.; Morgan, A.; Kim, J.; Callens, S. J. P.; Xie, K.; Zou, J.; Lin, J.; Zhou, K.; Lu, X.; Stevens, M. M. Magnetically Driven Formation of 3D Freestanding Soft Bioscaffolds. *Sci. Adv.* **2024**, *10* (5), No. eadl1549.
(176) Doddapaneni, V. V. K.; Song, C.; Dhas, J. A.; Cheng, N.; Camp, I.; Chang, A.; Pan, C.; Paul, B. K.; Pasebani, S.; Feng, Z.; Sierros, K. A.; Chang, C. Beyond Solution-Based Printing: Unveiling Innovations and Advancements in Solvent-Free Printing Technologies. *Adv. Funct. Mater.* **2025**, *35* (3-), 2423498.
(177) Cho, K. W.; Sunwoo, S.-H.; Hong, Y. J.; Koo, J. H.; Kim, J. H.; Baik, S.; Hyeon, T.; Kim, D.-H. Soft Bioelectronics Based on Nanomaterials. *Chem. Rev.* **2022**, *122* (5), 5068−5143.
(178) Yao, S.; Ren, P.; Song, R.; Liu, Y.; Huang, Q.; Dong, J.; O'Connor, B. T.; Zhu, Y. Nanomaterial-Enabled Flexible and Stretchable Sensing Systems: Processing, Integration, and Applications. *Adv. Mater.* **2020**, *32* (15), 1902343.
(179) Zhang, Z.; Cui, J.; Wang, B.; Wang, Z.; Kang, R.; Guo, D. A Novel Approach of Mechanical Chemical Grinding. *J. Alloys Compd.* **2017**, *726*, 514−524.
(180) Wang, G.; Geng, Y.; Zhao, Z.; Zhang, Q.; Li, X.; Wu, Z.; Bi, S.; Zhan, H.; Liu, W. Exploring the in Situ Formation Mechanism of Polymeric Aluminum Chloride-Silica Gel Composites under Mechanical Grinding Conditions: As a High-Performance Nanocatalyst for the Synthesis of Xanthene and Pyrimidinone Compounds. *ACS Omega* **2022**, *7* (36), 32577−32587.
(181) Katiyar, N. K.; Biswas, K.; Tiwary, C. S. Cryomilling as Environmentally Friendly Synthesis Route to Prepare Nanomaterials. *Int. Mater. Rev.* **2021**, *66* (7), 493−532.

https://doi.org/10.1021/acs.chemrev.5c00801
Chem. Rev. XXXX, XXX, XXX−XXX

(182) Wei, X.; Xu, K.; Wang, Y.; Zhang, Z.; Chen, Z. 3D Printing of Flexible $BaTiO_3$ /Polydimethylsiloxane Piezocomposite with Aligned Particles for Enhanced Energy Harvesting. *ACS Appl. Mater. Interfaces* **2024**, *16* (9), 11740−11748.
(183) Rani, G. M.; Kim, H.; Pammi, S. V. N.; Umapathi, R.; Huh, Y. S. Next-generation Flexible and Wearable Triboelectric Nanogenerator Based on PVDF-HFP@GCN Composite for Mechanical Energy Scavenging and Sleep Pattern Detection. *Adv. Funct. Mater.* **2025**, No. e19594.
(184) Gu, Z.; Ma, R.; Chen, X.; Lin, Z.; Yang, Y.; Tan, B.; Sun, J.; Chen, T. Polyvinyl Alcohol Modified Plant Fiber Hydrogel Pressure and Strain Dual-Model Sensors for Biomedical Signal Detection. *Adv. Compos. Hybrid Mater.* **2025**, *8* (2), 214.
(185) Wang, L.; Huang, F.; Yao, X.; Yuan, S.; Yu, X.; Tu, S.-T.; Chen, S. Collaborative Enhancement of Humidity Sensing Performance by KCl-Doped CuO/SnO_2 p-n Heterostructures for Monitoring Human Activities. *ACS Omega* **2023**, *8* (5), 4878−4888.
(186) Huang, F.; Wang, H.; Chen, J.; Yang, B. Dry Ball Milling and Wet Ball Milling for Fabricating Copper-Yttria Composites. *Rare Met.* **2018**, *37* (10), 859−867.
(187) Lee, D.; Lee, B.; Park, K. H.; Ryu, H. J.; Jeon, S.; Hong, S. H. Scalable Exfoliation Process for Highly Soluble Boron Nitride Nanoplatelets by Hydroxide-Assisted Ball Milling. *Nano Lett.* **2015**, *15* (2), 1238−1244.
(188) Novoselov, K. S.; Geim, A. K.; Morozov, S. V.; Jiang, D.; Zhang, Y.; Dubonos, S. V.; Grigorieva, I. V.; Firsov, A. A. Electric Field Effect in Atomically Thin Carbon Films. *Science* **2004**, *306* (5696), 666−669.
(189) Niu, L.; Coleman, J. N.; Zhang, H.; Shin, H.; Chhowalla, M.; Zheng, Z. Production of Two-dimensional Nanomaterials via Liquid-based Direct Exfoliation. *Small* **2016**, *12* (3), 272−293.
(190) Chen, L.; Mao, Z.; Wang, Y.; Kang, Y.; Wang, Y.; Mei, L.; Ji, X. Edge Modification Facilitated Heterogenization and Exfoliation of Two-Dimensional Nanomaterials for Cancer Catalytic Therapy. *Sci. Adv.* **2022**, *8* (39), No. eabo7372.
(191) Liu, H.; Ding, Y.; Xu, Y.; Kuai, Y.; Chen, J.; Zhang, H.; Lan, Y.; Wei, Z. Interfacial Π-electron Cloud Extension and Charge Transfer between Preferable Single-crystalline Conjugated MOFs and Graphene for Ultrafast Pulse Generation. *Adv. Mater.* **2025**, *37* (13), 2420043.
(192) Diwathe, M. C.; Gogate, P. R. Ultrasound Assisted Intensified Synthesis of 1-Benzyloxy-4-Nitrobenzene in the Presence of Phase Transfer Catalyst. *Chem. Eng. J.* **2018**, *346*, 438−446.
(193) Lunkov, A.; Shagdarova, B.; Lyalina, T.; Dubinnyi, M. A.; Karpova, N.; Lopatin, S.; Il'ina, A.; Varlamov, V. Simple Method for Ultrasound Assisted ≪click≫ Modification of Azido-Chitosan Derivatives by CuAAC. *Carbohydr. Polym.* **2022**, *282*, 119109.
(194) Tahara, K.; Kubo, Y.; Hashimoto, S.; Ishikawa, T.; Kaneko, H.; Brown, A.; Hirsch, B. E.; Feyter, S. D.; Tobe, Y. Porous Self-Assembled Molecular Networks as Templates for Chiral-Position-Controlled Chemical Functionalization of Graphitic Surfaces. *J. Am. Chem. Soc.* **2020**, *142* (16), 7699−7708.
(195) Chen, Y.; Szkopek, T.; Cerruti, M. Functional Porous Graphene Materials by Pickering Emulsion Templating: From Emulsion Stabilization to Structural Design and Fabrication. *Adv. Colloid Interface Sci.* **2025**, *342*, 103536.
(196) He, N.; Zou, Y.; Chen, C.; Tan, M.; Zhang, Y.; Li, X.; Jia, Z.; Zhang, J.; Long, H.; Peng, H.; Yu, K.; Jiang, B.; Han, Z.; Liu, N.; Li, Y.; Ma, L. Constructing Ordered and Tunable Extrinsic Porosity in Covalent Organic Frameworks via Water-Mediated Soft-Template Strategy. *Nat. Commun.* **2024**, *15* (1), 3896.
(197) Diab, M.; Mokari, T. Bioinspired Hierarchical Porous Structures for Engineering Advanced Functional Inorganic Materials. *Adv. Mater.* **2018**, *30* (41), 1706349.
(198) Yount, J.; Piercey, D. G. Electrochemical Synthesis of High-Nitrogen Materials and Energetic Materials. *Chem. Rev.* **2022**, *122* (9), 8809−8840.
(199) Kim, T.; Park, C.; Samuel, E. P.; Kim, Y.-I.; An, S.; Yoon, S. S. Wearable Sensors and Supercapacitors Using Electroplated-Ni/ZnO Antibacterial Fabric. *J. Mater. Sci. Technol.* **2022**, *100*, 254−264.
(200) Zhao, J.; Cong, Z.; Hu, J.; Lu, H.; Wang, L.; Wang, H.; Malyi, O. I.; Pu, X.; Zhang, Y.; Shao, H.; Tang, Y.; Wang, Z. L. Regulating Zinc Electroplating Chemistry to Achieve High Energy Coaxial Fiber Zn Ion Supercapacitor for Self-Powered Textile-Based Monitoring System. *Nano Energy* **2022**, *93*, 106893.
(201) Zhang, T.; Zhai, M.; Zhao, M.; Ma, X.; Wang, Z.; Wang, L.; Liu, Y.; Chen, D. Microwave-Assisted Scalable CNTs/TPU Yarns for Highly Durable and Sensitive Wearable Sensors. *Mater. Today Chem.* **2025**, *47*, 102811.
(202) Kim, C.-E.; Ha, T.-J. Capacitive-Type Wearable Temperature Sensors Based on Yttria-Stabilized Zirconia Films Fabricated via Microwave-Assisted All-Solution-Process and Their Application for Detection of Touch Stimuli. *J. Alloys Compd.* **2025**, *1011*, 178334.
(203) Morais, M.; Carlos, E.; Rovisco, A.; Calmeiro, T.; Gamboa, H.; Fortunato, E.; Martins, R.; Barquinha, P. Flexographic Printed Microwave-Assisted Grown Zinc Oxide Nanostructures for Sensing Applications. *Mater. Horiz.* **2024**, *11* (24), 6463−6475.
(204) Liu, J.; He, G.; Shan, W.; Yu, Y.; Huo, Y.; Zhang, Y.; Wang, M.; Yu, R.; Liu, S.; He, H. Introducing Tin to Develop Ternary Metal Oxides with Excellent Hydrothermal Stability for NH3 Selective Catalytic Reduction of NO. *Appl. Catal., B* **2021**, *291*, 120125.
(205) Zhou, F.; Zhao, H.; Chen, K.; Cao, S.; Shi, Z.; Lan, M. Flexible Electrochemical Sensor with Fe/Co Bimetallic Oxides for Sensitive Analysis of Glucose in Human Tears. *Anal. Chim. Acta* **2023**, *1243*, 340781.
(206) Chen, R.; Cai, X.; He, X.; Hong, X.; Liu, Y.; So, J.-K.; Wang, B.; Zhou, Y.; Cheng, L.; Shen, Z. X. High Mass-Loading CoO@NiCo-LDH//FeNiS Flexible Supercapacitor with High Energy Density and Fast Kinetics. *Chem. Eng. J.* **2024**, *484*, 149736.
(207) Zhang, W.; Ma, J.; Zhang, J.; Mo, H.; Yang, K.; Zhu, N. Wearable Self-powered Smart Sensors Enabled by 2D Flower-like Ni-Co Layered Double Hydroxides for Copper Monitoring in Sweat. *Adv. Mater. Technol.* **2024**, *9* (21), 2400163.
(208) Zhang, H.; Shen, L.; Geng, X.; Zhang, J.; Jiang, Y.; Ma, H.; Liu, Q.; Yang, K.; Ma, J.; Zhu, N. MXene-rGO Aerogel Assisted Na3.5MnTi(PO4)3 Cathode for High-Performance Sodium-Ion Batteries. *Chem. Eng. J.* **2023**, *466*, 143132.
(209) Mackenzie, J. D.; Bescher, E. P. Chemical Routes in the Synthesis of Nanomaterials Using the Sol-Gel Process. *Acc. Chem. Res.* **2007**, *40* (9), 810−818.
(210) Miyata, H.; Suzuki, H.; Sugahara, Y.; Zhang, K.; Asahi, T.; Yamauchi, Y. Full-multiscale Spontaneous Organization for Optically Anisotropic Titania Films. *Small* **2025**, *21* (14), 2501782.
(211) Qi, S.; Lei, Z.; Huo, Q.; Zhao, J.; Huang, T.; Meng, N.; Liao, J.; Yi, J.; Shang, C.; Zhang, X.; Yang, H.; Hu, Q.; He, C. Ultrathin High-entropy Fe-based Spinel Oxide Nanosheets with Metalloid Band Structures for Efficient Nitrate Reduction toward Ammonia. *Adv. Mater.* **2024**, *36* (27), 2403958.
(212) Choy, K. Chemical Vapour Deposition of Coatings. *Prog. Mater. Sci.* **2003**, *48* (2), 57−170.
(213) Xia, K.; Wang, C.; Jian, M.; Wang, Q.; Zhang, Y. CVD Growth of Fingerprint-like Patterned 3D Graphene Film for an Ultrasensitive Pressure Sensor. *Nano Res.* **2018**, *11* (2), 1124−1134.
(214) Mukherjee, A.; Dianatdar, A.; Gładysz, M. Z.; Hemmatpour, H.; Hendriksen, M.; Rudolf, P.; Włodarczyk-Biegun, M. K.; Kamperman, M.; Prakash Kottapalli, A. G.; Bose, R. K. Electrically Conductive and Highly Stretchable Piezoresistive Polymer Nanocomposites via Oxidative Chemical Vapor Deposition. *ACS Appl. Mater. Interfaces* **2023**, *15* (26), 31899−31916.
(215) Sun, L.; Yuan, G.; Gao, L.; Yang, J.; Chhowalla, M.; Gharahcheshmeh, M. H.; Gleason, K. K.; Choi, Y. S.; Hong, B. H.; Liu, Z. Chemical Vapour Deposition. *Nat. Rev. Methods Primers* **2021**, *1* (1), 5.
(216) Das, P. S.; Chhetry, A.; Maharjan, P.; Rasel, M. S.; Park, J. Y. A Laser Ablated Graphene-Based Flexible Self-Powered Pressure Sensor

https://doi.org/10.1021/acs.chemrev.5c00801
Chem. Rev. XXXX, XXX, XXX−XXX

for Human Gestures and Finger Pulse Monitoring. *Nano Res.* **2019**, *12* (8), 1789−1795.
(217) Cheng, L.; Yeung, C. S.; Huang, L.; Ye, G.; Yan, J.; Li, W.; Yiu, C.; Chen, F.-R.; Shen, H.; Tang, B. Z.; Ren, Y.; Yu, X.; Ye, R. Flash Healing of Laser-Induced Graphene. *Nat. Commun.* **2024**, *15* (1), 2925.
(218) Lim, H.; Kwon, H.; Kang, H.; Jang, J. E.; Kwon, H.-J. Semiconducting MOFs on Ultraviolet Laser-Induced Graphene with a Hierarchical Pore Architecture for NO2Monitoring. *Nat. Commun.* **2023**, *14* (1), 3114.
(219) Yang, X.; Yang, X.; Hou, Z.; Li, M.; Luo, S.; Zhao, J.; Wang, K.; Guo, Y.; Sun, P.; Tan, F.; Yan, Y.; Liu, L.; Wang, L.; Han, Y.; Zeng, F.; Zimmerman, A. R.; Gao, B. Efficient Removal of Aqueous Ciprofloxacin Antibiotic by ZnO/CuO-Bentonite Composites Synthesized via Carbon-Bed Pyrolysis of Bentonite and Metal Co-Precipitation. *Sci. Total Environ.* **2024**, *955*, 176955.
(220) Zhang, J.; Ma, J.; Zhang, W.; Zhang, H.; Geng, X.; Yang, K.; Zhang, J.; Mo, H.; Li, W.; Lu, B.; Liu, X.; Zhu, N. Breathable Wearable Smartsensors Deriving from Interface Self-Assembled Film for Tracking < span Style = ″font-Variant:Small-Caps;″>l -Cysteine. *Anal. Chem.* **2024**, *96* (32), 13070−13077.
(221) Ma, J.; Jiang, Y.; Shen, L.; Ma, H.; Sun, T.; Lv, F.; Kiran, A.; Zhu, N. Wearable Biomolecule Smartsensors Based on One-Step Fabricated Berlin Green Printed Arrays. *Biosens. Bioelectron.* **2019**, *144*, 111637.
(222) Abid, N.; Abid, N.; Khan, A. M.; Shujait, S.; Chaudhary, K.; Ikram, M.; Imran, M.; Haider, J.; Khan, M.; Khan, Q.; Maqbool, M. Synthesis of Nanomaterials Using Various Top-down and Bottom-up Approaches, Influencing Factors, Advantages, and Disadvantages: A Review. *Adv. Colloid Interface Sci.* **2022**, *300*, 102597.
(223) Cui, L.; Zhang, S.; Ju, J.; Liu, T.; Zheng, Y.; Xu, J.; Wang, Y.; Li, J.; Zhao, J.; Ma, J.; Wang, J.; Xu, G.; Chan, T.-S.; Huang, Y.-C.; Haw, S.-C.; Chen, J.-M.; Hu, Z.; Cui, G. A Cathode Homogenization Strategy for Enabling Long-Cycle-Life All-Solid-State Lithium Batteries. *Nat. Energy* **2024**.
(224) Hornbuckle, B. C.; Smeltzer, J. A.; Sharma, S.; Nagar, S.; Marvel, C. J.; Cantwell, P. R.; Harmer, M. P.; Solanki, K.; Darling, K. A. A High-Temperature Nanostructured Cu-Ta-Li Alloy with Complexion-Stabilized Precipitates. *Science* **2025**, *387* (6741), 1413−1417.
(225) Liu, Y.; Liu, Y.; Tang, Q.; Xu, M.; Ren, J.; Guo, C.; Chen, C.; Geng, W.; Lei, W.; Zhao, X.; Liu, D. Efficient Mechanical Exfoliation of MXene Nanosheets. *Chem. Eng. J.* **2023**, *468*, 143439.
(226) Zhang, H.; Xiang, Q.; Liu, Z.; Zhang, X.; Zhao, Y.; Tan, H. Supercritical Mechano-Exfoliation Process. *Nat. Commun.* **2024**, *15* (1), 9329.
(227) Chan, H.-K.; Chan, H.-K.; Kwok, P. C. L. Production Methods for Nanodrug Particles Using the Bottom-up Approach. *Adv. Drug Delivery Rev.* **2011**, *63* (6), 406−416.
(228) Wen, X.; Fu, J.; Zhang, X.; Meng, X.; Tian, Y.; Li, J.; Yu, G.; Hao, Y.; Zhu, Y. Achieving Immune Activation by Suppressing the IDO1 Checkpoint with Sono-Targeted Biobromination for Antitumor Combination Immunotherapy. *J. Am. Chem. Soc.* **2024**, *146* (35), 24580−24590.
(229) Liu, Y.; Goebl, J.; Yin, Y. Templated Synthesis of Nanostructured Materials. *Chem. Soc. Rev.* **2013**, *42* (7), 2610−2653.
(230) Kaur, A.; Bajaj, B.; Kaushik, A.; Saini, A.; Sud, D. A Review on Template Assisted Synthesis of Multi-Functional Metal Oxide Nanostructures: Status and Prospects. *Mater. Sci. Eng., B* **2022**, *286*, 116005.
(231) Zhang, Z.; Fang, Q.; Yang, X.; Zuo, S.; Cheng, T.; Yamauchi, Y.; Tang, J. Additives-modified Electrodeposition for Synthesis of Hydrophobic Cu/Cu_2 O with Ag Single Atoms to Drive CO_2 Electroreduction. *Adv. Mater.* **2025**, *37* (8), 2411498.
(232) Yu, X.; Hou, Y.; Ren, X.; Sun, C.; Wang, M. Research Progress on the Removal, Recovery and Direct High-Value Materialization of Valuable Metal Elements in Electroplating/Electroless Plating Waste Solution. *J. Water Process Eng.* **2022**, *46*, 102577.
(233) Zhao, W.; Wang, X.; Bahri, M.; Zhu, Q.; Li, B.; Wu, K.; Wang, Z.; Li, H.; Shi, X.; Shi, D.; Ji, C.; Browning, N. D.; Sun, J.; Wang, J.; Zhao, D. Water-Assisted Microwave Synthesis of Imide-Linked Covalent Organic Frameworks in Minutes. *J. Am. Chem. Soc.* **2025**, *147*, 16319.
(234) Yang, Y.; Miao, C.; Wang, R.; Zhang, R.; Li, X.; Wang, J.; Wang, X.; Yao, J. Advances in Morphology-Controlled Alumina and Its Supported Pd Catalysts: Synthesis and Applications. *Chem. Soc. Rev.* **2024**, *53* (10), 5014−5053.
(235) Yang, Y.; Hu, T.; Zhao, K.; Wang, Y.; Zhu, Y.; Wang, S.; Zhou, Z.; Gu, L.; Tan, C.; Liang, R. Metal Doping Enabling Defective CoMo-layered Double Hydroxide Nanosheets as Highly Efficient Photosensitizers for NIR-II Photodynamic Cancer Therapy. *Adv. Mater.* **2025**, *37* (4), 2405847.
(236) Wang, K.; Qiao, X.; Ren, H.; Chen, Y.; Zhang, Z. Industrialization of Covalent Organic Frameworks. *J. Am. Chem. Soc.* **2025**, *147* (10), 8063−8082.
(237) Cai, Z.; Liu, B.; Zou, X.; Cheng, H.-M. Chemical Vapor Deposition Growth and Applications of Two-Dimensional Materials and Their Heterostructures. *Chem. Rev.* **2018**, *118* (13), 6091−6133.
(238) Ye, F.; Ayub, A.; Karimi, R.; Wettig, S.; Sanderson, J.; Musselman, K. P. Defect-rich $MoSe_2$ 2H/1T Hybrid Nanoparticles Prepared from Femtosecond Laser Ablation in Liquid and Their Enhanced Photothermal Conversion Efficiencies. *Adv. Mater.* **2023**, *35* (30), 2301129.
(239) Luo, Y.; Shen, J.; Yao, Y.; Dai, J.; Ling, F.; Li, L.; Jiang, Y.; Wu, X.; Rui, X.; Yu, Y. Inhibiting the Jahn-Teller Effect of Manganese Hexacyanoferrate via Ni and Cu Codoping for Advanced Sodium-ion Batteries. *Adv. Mater.* **2024**, *36* (32), 2405458.
(240) Gao, Y.; Zhang, X.; Zhang, H.; Peng, J.; Hua, W.; Xiao, Y.; Liu, X.; Li, L.; Qiao, Y.; Wang, J.; Zhang, C.; Chou, S. Zero-waste Polyanion and Prussian Blue Composites toward Practical Sodium-ion Batteries. *Adv. Mater.* **2025**, *37* (8), 2409782.
(241) Park, Y.; Shim, J.; Jeong, S.; Yi, G.; Chae, H.; Bae, J. W.; Kim, S. O.; Pang, C. Microtopography-guided Conductive Patterns of Liquid-driven Graphene Nanoplatelet Networks for Stretchable and Skin-conformal Sensor Array. *Adv. Mater.* **2017**, *29* (21), 1606453.
(242) Zheng, Q.; Lee, J.; Shen, X.; Chen, X.; Kim, J.-K. Graphene-Based Wearable Piezoresistive Physical Sensors. *Mater. Today* **2020**, *36*, 158−179.
(243) Cheng, W.; Sun, L.; Dong, J.; Han, Z.; Wei, L.; Lu, L.; Sun, R. Application Progress and Challenges of 1D Fiber Electrodes in Wearable Devices. *Energy Storage Mater.* **2025**, *75*, 104059.
(244) Sun, M.; Wang, S.; Liang, Y.; Wang, C.; Zhang, Y.; Liu, H.; Zhang, Y.; Han, L. Flexible Graphene Field-Effect Transistors and Their Application in Flexible Biomedical Sensing. *Nano Micro Lett.* **2025**, *17* (1), 34.
(245) Gao, L.; Yang, J.; Zhao, Y.; Zhao, X.; Zhou, K.; Zhai, W.; Zheng, G.; Dai, K.; Liu, C.; Shen, C. Multilayer Bionic Tunable Strain Sensor with Mutually Non-interfering Conductive Networks for Machine Learning-assisted Gesture Recognition. *Adv. Funct. Mater.* **2025**, *35* (11), 2416911.
(246) Cui, L.; Wang, G.; Zhao, S.; Dang, M.; Wang, W.; Yin, J.; Zhu, J. Robust Photonically Sintered Self-Assembled Metallic Nanofilms with Substrate-Dependent Electromechanical Properties for Hypersensitive Strain Sensors. *Sci. China Mater.* **2025**, *68* (7), 2471−2479.
(247) Chen, X.; Zhang, Y.; Ma, C.; Liu, H. Large-Area, Stretchable, Ordered Silver Nanowires Electrode by Superwetting-Induced Transfer of Ionic Liquid@silver Nanowires Complex. *Chem. Eng. J.* **2023**, *476*, 146505.
(248) Xu, C.; Wang, Y.; Zhang, J.; Wan, J.; Xiang, Z.; Nie, Z.; Xu, J.; Lin, X.; Zhao, P.; Wang, Y.; Zhang, S.; Zhang, J.; Liu, C.; Xue, N.; Zhao, W.; Han, M. Three-Dimensional Micro Strain Gauges as Flexible, Modular Tactile Sensors for Versatile Integration with Micro- and Macroelectronics. *Sci. Adv.* **2024**, *10* (34), No. eadp6094.
(249) Lim, C.; Park, C.; Sunwoo, S.-H.; Kim, Y. G.; Lee, S.; Han, S. I.; Kim, D.; Kim, J. H.; Kim, D.-H.; Hyeon, T. Facile and Scalable Synthesis of Whiskered Gold Nanosheets for Stretchable, Conductive,

https://doi.org/10.1021/acs.chemrev.5c00801
Chem. Rev. XXXX, XXX, XXX−XXX

and Biocompatible Nanocomposites. *ACS Nano* **2022**, *16* (7), 10431−10442.
(250) Taheri, M.; Deen, I. A.; Packirisamy, M.; Deen, M. J. Metal Oxide -Based Electrical/Electrochemical Sensors for Health Monitoring Systems. *Trends Anal. Chem.* **2024**, *171*, 117509.
(251) Fischer, K.; Mayr, S. G. In-plane Mechanical Response of TiO_2 Nanotube Arrays - Intrinsic Properties and Impact of Adsorbates for Sensor Applications. *Adv. Mater.* **2011**, *23* (33), 3838−3841.
(252) Baro, B.; Khimhun, S.; Das, U.; Bayan, S. ZnO Based Triboelectric Nanogenerator on Textile Platform for Wearable Sweat Sensing Application. *Nano Energy* **2023**, *108*, 108212.
(253) Akhtar, I.; Chang, S. Stretchable Sensor Made of MWCNT/ZnO Nanohybrid Particles in PDMS. *Adv. Mater. Technol.* **2020**, *5* (9), 2000229.
(254) Mondal, S.; Kim, S. J.; Choi, C.-G. Honeycomb-like MoS_2 Nanotube Array-Based Wearable Sensors for Noninvasive Detection of Human Skin Moisture. *ACS Appl. Mater. Interfaces* **2020**, *12* (14), 17029−17038.
(255) Jin, L.; Yang, K.; Chen, L.; Yan, R.; He, L.; Ye, M.; Qiao, H.; Chu, X.; Gao, H.; Zhang, K. Flexible Synergistic MoS_2 Quantum Dots/PEDOT: PSS Film Sensor for Acetaldehyde Sensing at Room Temperature. *Anal. Chem.* **2023**, *95* (23), 8859−8868.
(256) Cho, B.; Kim, A. R.; Kim, D. J.; Chung, H.-S.; Choi, S. Y.; Kwon, J.-D.; Park, S. W.; Kim, Y.; Lee, B. H.; Lee, K. H.; Kim, D.-H.; Nam, J.; Hahm, M. G. Two-Dimensional Atomic-Layered Alloy Junctions for High-Performance Wearable Chemical Sensor. *ACS Appl. Mater. Interfaces* **2016**, *8* (30), 19635−19642.
(257) Ko, K. Y.; Lee, S.; Park, K.; Kim, Y.; Woo, W. J.; Kim, D.; Song, J.-G.; Park, J.; Kim, J. H.; Lee, Z.; Kim, H. High-Performance Gas Sensor Using a Large-Area $WS_{2x}Se_{2-2x}$ Alloy for Low-Power Operation Wearable Applications. *ACS Appl. Mater. Interfaces* **2018**, *10* (40), 34163−34171.
(258) Zeng, H.; Gao, C.; Yu, Y.; Jiang, M.; Deng, T.; Zhu, J. Wet Spinning Enabled Advanced PEDOT:PSS Composite Fibers for Smart Devices. *Acc. Mater. Res.* **2025**, *6*, 952.
(259) Li, Y.; Pang, Y.; Wang, L.; Li, Q.; Liu, B.; Li, J.; Liu, S.; Zhao, Q. Boosting the Performance of PEDOT:PSS Based Electronics via Ionic Liquids. *Adv. Mater.* **2024**, *36* (13), 2310973.
(260) Gao, M.; Zhang, X.; Li, S.; Gao, H.; Li, X.; Xu, D.; Xu, L. Boric Acid-Functionalized PANI-ABA/PA Hydrogel-Based Flexible pH Sensor for Real-Time Sweat Monitoring. *Anal. Chim. Acta* **2025**, *1362*, 344188.
(261) Ren, X.; Yang, M.; Yang, T.; Xu, C.; Ye, Y.; Wu, X.; Zheng, X.; Wang, B.; Wan, Y.; Luo, Z. Highly Conductive PPy-PEDOT:PSS Hybrid Hydrogel with Superior Biocompatibility for Bioelectronics Application. *ACS Appl. Mater. Interfaces* **2021**, *13* (21), 25374−25382.
(262) Ma, C.; Ma, M.; Si, C.; Ji, X.; Wan, P. Flexible MXene-based Composites for Wearable Devices. *Adv. Funct. Mater.* **2021**, *31* (22), 2009524.
(263) Feng, Y.; Liu, H.; Zhu, W.; Guan, L.; Yang, X.; Zvyagin, A. V.; Zhao, Y.; Shen, C.; Yang, B.; Lin, Q. Muscle-inspired MXene Conductive Hydrogels with Anisotropy and Low-temperature Tolerance for Wearable Flexible Sensors and Arrays. *Adv. Funct. Mater.* **2021**, *31* (46), 2105264.
(264) Qin, R.; Nong, J.; Wang, K.; Liu, Y.; Zhou, S.; Hu, M.; Zhao, H.; Shan, G. Recent Advances in Flexible Pressure Sensors Based on MXene Materials. *Adv. Mater.* **2024**, *36* (24), 2312761.
(265) Sreenilayam, S. P.; Ul Ahad, I.; Nicolosi, V.; Brabazon, D. MXene Materials Based Printed Flexible Devices for Healthcare, Biomedical and Energy Storage Applications. *Mater. Today* **2021**, *43*, 99−131.
(266) Gao, F.-L.; Liu, J.; Li, X.-P.; Ma, Q.; Zhang, T.; Yu, Z.-Z.; Shang, J.; Li, R.-W.; Li, X. $Ti_3C_2T_x$ MXene-Based Multifunctional Tactile Sensors for Precisely Detecting and Distinguishing Temperature and Pressure Stimuli. *ACS Nano* **2023**, *17* (16), 16036−16047.
(267) Mohanty, B.; Kumari, S.; Yadav, P.; Kanoo, P.; Chakraborty, A. Metal-Organic Frameworks (MOFs) and MOF Composites Based Biosensors. *Coord. Chem. Rev.* **2024**, *519*, 216102.
(268) Ling, W.; Liew, G.; Li, Y.; Hao, Y.; Pan, H.; Wang, H.; Ning, B.; Xu, H.; Huang, X. Materials and Techniques for Implantable Nutrient Sensing Using Flexible Sensors Integrated with Metal-Organic Frameworks. *Adv. Mater.* **2018**, *30* (23), 1800917.
(269) Zhou, K.; Zhang, C.; Xiong, Z.; Chen, H.; Li, T.; Ding, G.; Yang, B.; Liao, Q.; Zhou, Y.; Han, S. Template-directed Growth of Hierarchical MOF Hybrid Arrays for Tactile Sensor. *Adv. Funct. Mater.* **2020**, *30* (38), 2001296.
(270) Kim, J.-O.; Koo, W.-T.; Kim, H.; Park, C.; Lee, T.; Hutomo, C. A.; Choi, S. Q.; Kim, D. S.; Kim, I.-D.; Park, S. Large-Area Synthesis of Nanoscopic Catalyst-Decorated Conductive MOF Film Using Microfluidic-Based Solution Shearing. *Nat. Commun.* **2021**, *12* (1), 4294.
(271) Rabiee, N. Wearable MOF Biosensors: A New Frontier in Real-Time Health Monitoring. *Trends Anal. Chem.* **2025**, *184*, 118156.
(272) Gao, L.; Zhu, C.; Li, L.; Zhang, C.; Liu, J.; Yu, H.-D.; Huang, W. All Paper-Based Flexible and Wearable Piezoresistive Pressure Sensor. *ACS Appl. Mater. Interfaces* **2019**, *11* (28), 25034−25042.
(273) Zhan, Z.; Lin, R.; Tran, V.-T.; An, J.; Wei, Y.; Du, H.; Tran, T.; Lu, W. Paper/Carbon Nanotube-Based Wearable Pressure Sensor for Physiological Signal Acquisition and Soft Robotic Skin. *ACS Appl. Mater. Interfaces* **2017**, *9* (43), 37921−37928.
(274) Liu, H.; Jiang, H.; Du, F.; Zhang, D.; Li, Z.; Zhou, H. Flexible and Degradable Paper-Based Strain Sensor with Low Cost. *ACS Sustainable Chem. Eng.* **2017**, *5* (11), 10538−10543.
(275) Fan, W.; He, Q.; Meng, K.; Tan, X.; Zhou, Z.; Zhang, G.; Yang, J.; Wang, Z. L. Machine-Knitted Washable Sensor Array Textile for Precise Epidermal Physiological Signal Monitoring. *Sci. Adv.* **2020**, *6* (11), No. eaay2840.
(276) Wicaksono, I.; Tucker, C. I.; Sun, T.; Guerrero, C. A.; Liu, C.; Woo, W. M.; Pence, E. J.; Dagdeviren, C. A Tailored, Electronic Textile Conformable Suit for Large-Scale Spatiotemporal Physiological Sensing in Vivo. *Npj Flexible Electron.* **2020**, *4* (1), 5.
(277) Zhan, Y.; Poisson, J.; Meng, X.; Wang, Z.; Chen, L.; Wu, T.; Koehler, R.; Zhang, K. Electrospun Lignin/ZnO Nanofibrous Membranes for Self-powered Ultrasensitive Flexible Airflow Sensor and Wearable Device. *Adv. Mater.* **2025**, *37*, 2502211.
(278) Li, Z.; Zhang, S.; Chen, Y.; Ling, H.; Zhao, L.; Luo, G.; Wang, X.; Hartel, M. C.; Liu, H.; Xue, Y.; Haghniaz, R.; Lee, K.; Sun, W.; Kim, H.; Lee, J.; Zhao, Y.; Zhao, Y.; Emaminejad, S.; Ahadian, S.; Ashammakhi, N.; Dokmeci, M. R.; Jiang, Z.; Khademhosseini, A. Gelatin Methacryloyl-based Tactile Sensors for Medical Wearables. *Adv. Funct. Mater.* **2020**, *30* (49), 2003601.
(279) He, Q.; Cheng, Y.; Deng, Y.; Wen, F.; Lai, Y.; Li, H. Conductive Hydrogel for Flexible Bioelectronic Device: Current Progress and Future Perspective. *Adv. Funct. Mater.* **2024**, *34* (1), 2308974.
(280) Shin, Y.; Lee, H. S.; Hong, Y. J.; Sunwoo, S.-H.; Park, O. K.; Choi, S. H.; Kim, D.-H.; Lee, S. Low-Impedance Tissue-Device Interface Using Homogeneously Conductive Hydrogels Chemically Bonded to Stretchable Bioelectronics. *Sci. Adv.* **2024**, *10* (12), No. eadi7724.
(281) Ma, J.; Zhong, J.; Sun, F.; Liu, B.; Peng, Z.; Lian, J.; Wu, X.; Li, L.; Hao, M.; Zhang, T. Hydrogel Sensors for Biomedical Electronics. *Chem. Eng. J.* **2024**, *481*, 148317.
(282) Mamun, M. A. A.; Yuce, M. R. Recent Progress in Nanomaterial Enabled Chemical Sensors for Wearable Environmental Monitoring Applications. *Adv. Funct. Mater.* **2020**, *30* (51), 2005703.
(283) Gavgani, J. N.; Hasani, A.; Nouri, M.; Mahyari, M.; Salehi, A. Highly Sensitive and Flexible Ammonia Sensor Based on S and N Co-Doped Graphene Quantum Dots/Polyaniline Hybrid at Room Temperature. *Sens. Actuators B: Chem.* **2016**, *229*, 239−248.
(284) Wang, R.; Liu, C.; Li, Z.; Li, Y.; Yu, X. Ultra-Stretchable, Adhesive, Conductive, and Antifreezing Multinetwork Borate Ester-Based Hydrogel for Wearable Strain Sensor and VOC Absorption. *ACS Sens.* **2024**, *9* (10), 5322−5332.
(285) Lv, W.; Yang, J.; Xu, Q.; Mehrez, J. A.-A.; Shi, J.; Quan, W.; Luo, H.; Zeng, M.; Hu, N.; Wang, T.; Wei, H.; Yang, Z. Wide-Range

https://doi.org/10.1021/acs.chemrev.5c00801
Chem. Rev. XXXX, XXX, XXX−XXX

and High-Accuracy Wireless Sensor with Self-Humidity Compensation for Real-Time Ammonia Monitoring. *Nat. Commun.* **2024**, *15* (1), 6936.
(286) Zhang, T.; Chen, S.; Petkov, P. St.; Zhang, P.; Qi, H.; Nguyen, N. N.; Zhang, W.; Yoon, J.; Li, P.; Brumme, T.; Alfonsov, A.; Liao, Z.; Hambsch, M.; Xu, S.; Mester, L.; Kataev, V.; Büchner, B.; Mannsfeld, S. C. B.; Zschech, E.; Parkin, S. S. P.; Kaiser, U.; Heine, T.; Dong, R.; Hillenbrand, R.; Feng, X. Two-Dimensional Polyaniline Crystal with Metallic out-of-Plane Conductivity. *Nature* **2025**, *638* (8050), 411−417.
(287) Li, T.; Qi, H.; Zhao, C.; Li, Z.; Zhou, W.; Li, G.; Zhuo, H.; Zhai, W. Robust Skin-Integrated Conductive Biogel for High-Fidelity Detection under Mechanical Stress. *Nat. Commun.* **2025**, *16* (1), 88.
(288) Youn, H.; Choi, T.; Shim, J.; Park, S. Y.; Kwon, M.; Kim, S.; Kim, H. Soft Sputtering of Large-area 2D MoS_2 Layers Using Isolated Plasma Soft Deposition for Humidity Sensors. *Adv. Mater.* **2025**, *37* (8), 2414800.
(289) Radisavljevic, B.; Radenovic, A.; Brivio, J.; Giacometti, V.; Kis, A. Single-Layer MoS2 Transistors. *Nat. Nanotechnol.* **2011**, *6* (3), 147−150.
(290) Lim, J.; Lee, J.-I.; Wang, Y.; Gauriot, N.; Sebastian, E.; Chhowalla, M.; Schnedermann, C.; Rao, A. Photoredox Phase Engineering of Transition Metal Dichalcogenides. *Nature* **2024**, *633* (8028), 83−89.
(291) Abudousu, A.; Tang, Y.; Wang, Z.; Lin, F.; Cui, W. Biomaterial Design for Proactive Modulation of the Complement System. *Nat. Rev. Bioeng.* **2025**, *3* (5), 355−356.
(292) Huang, X.; Zhang, Q.; Yang, Y.; Chow, L.; Ma, J.; Xu, G.; Guo, F.; He, X.; Li, Z.; Zhao, G.; Su, J.; Guo, G.; Wang, J.; Jiao, Y.; Gao, Z.; Li, J.; Zhou, J.; Yiu, C. K.; Li, J.; Chen, Y.; Wu, P.; Yao, K.; Liu, Y.; Li, D.; Zhang, B.; Chu, H.; Hu, Y.; Huang, Y.; Chen, Z.; Ren, K.; Fang, B.; Yang, R.; Li, H.; Tao, X.; Ma, X.; Yu, X. A Skin-Interfaced Three-Dimensional Closed-Loop Sensing and Therapeutic Electronic Wound Bandage. *Nat. Commun.* **2025**, *16* (1), 5782.
(293) Liu, W.; Du, Z.; Duan, Z.; Li, L.; Shen, G. Neuroprosthetic Contact Lens Enabled Sensorimotor System for Point-of-Care Monitoring and Feedback of Intraocular Pressure. *Nat. Commun.* **2024**, *15* (1), 5635.
(294) Ding, C.; Wang, J.; Yuan, W.; Zhou, X.; Lin, Y.; Zhu, G.; Li, J.; Zhong, T.; Su, W.; Cui, Z. Durability Study of Thermal Transfer Printed Textile Electrodes for Wearable Electronic Applications. *ACS Appl. Mater. Interfaces* **2022**, *14* (25), 29144−29155.
(295) Li, M.; Wang, C.; Yu, Q.; Chen, H.; Ma, Y.; Wei, L.; Wu, M. X.; Yao, M.; Lu, M. A Wearable and Stretchable Dual-Wavelength LED Device for Home Care of Chronic Infected Wounds. *Nat. Commun.* **2024**, *15* (1), 9380.
(296) Xu, Y.; De La Paz, E.; Paul, A.; Mahato, K.; Sempionatto, J. R.; Tostado, N.; Lee, M.; Hota, G.; Lin, M.; Uppal, A.; Chen, W.; Dua, S.; Yin, L.; Wuerstle, B. L.; Deiss, S.; Mercier, P.; Xu, S.; Wang, J.; Cauwenberghs, G. In-Ear Integrated Sensor Array for the Continuous Monitoring of Brain Activity and of Lactate in Sweat. *Nat. Biomed. Eng.* **2023**, *7* (10), 1307−1320.
(297) Gao, C.; Liu, Y.; Gu, Z.; Li, J.; Sun, Y.; Li, W.; Liu, K.; Xu, D.; Yu, B.; Xu, W. Hierarchical Structured Fabrics with Enhanced Pressure Sensing Performance Based on Orientated Growth of Functional Bacterial Cellulose. *Adv. Fiber Mater.* **2024**, *6* (5), 1554−1568.
(298) Choi, Y.; Jin, P.; Lee, S.; Song, Y.; Tay, R. Y.; Kim, G.; Yoo, J.; Han, H.; Yeom, J.; Cho, J. H.; Kim, D.-H.; Gao, W. All-Printed Chip-Less Wearable Neuromorphic System for Multimodal Physicochemical Health Monitoring. *Nat. Commun.* **2025**, *16* (1), 5689.
(299) Wang, P.; Wu, J.; Xiao, X.; Fan, Y.; Han, X.; Sun, Y. Engineering Injectable Coassembled Hydrogel by Photothermal Driven Chitosan-Stabilized MoS_2 Nanosheets for Infected Wound Healing. *ACS Nano* **2024**, *18* (39), 26961−26974.
(300) De Marzo, G.; Mastronardi, V. M.; Todaro, M. T.; Blasi, L.; Antonaci, V.; Algieri, L.; Scaraggi, M.; De Vittorio, M. Sustainable Electronic Biomaterials for Body-Compliant Devices: Challenges and Perspectives for Wearable Bio-Mechanical Sensors and Body Energy Harvesters. *Nano Energy* **2024**, *123*, 109336.
(301) Shi, J.; Kim, S.; Li, P.; Dong, F.; Yang, C.; Nam, B.; Han, C.; Eig, E.; Shi, L. L.; Niu, S.; Yue, J.; Tian, B. Active Biointegrated Living Electronics for Managing Inflammation. *Science* **2024**, *384* (6699), 1023−1030.
(302) Huang, W.; Ying, R.; Wang, W.; Guo, Y.; He, Y.; Mo, X.; Xue, C.; Mao, X. A Macroporous Hydrogel Dressing with Enhanced Antibacterial and Anti-inflammatory Capabilities for Accelerated Wound Healing. *Adv. Funct. Mater.* **2020**, *30* (21), 2000644.
(303) Liu, N.; Li, Q.; Wan, H.; Chang, L.; Wang, H.; Fang, J.; Ding, T.; Wen, Q.; Zhou, L.; Xiao, X. High-Temperature Stability in Air of Ti3C2Tx MXene-Based Composite with Extracted Bentonite. *Nat. Commun.* **2022**, *13* (1), 5551.
(304) Kim, J.; Yoon, Y.; Kim, S. K.; Park, S.; Song, W.; Myung, S.; Jung, H.; Lee, S. S.; Yoon, D. H.; An, K. Chemically Stabilized and Functionalized 2D-MXene with Deep Eutectic Solvents as Versatile Dispersion Medium. *Adv. Funct. Mater.* **2021**, *31* (13), 2008722.
(305) Wan, S.; Chen, Y.; Huang, C.; Huang, Z.; Liang, C.; Deng, X.; Cheng, Q. Scalable Ultrastrong MXene Films with Superior Osteogenesis. *Nature* **2024**, *634* (8036), 1103−1110.
(306) Zhou, W.; Fei, Y.; Zhang, Y.-S.; Miao, X.; Jiang, S.-D.; Liu, J. Triplet-Ground-State Nonalternant Nanographene with High Stability and Long Spin Lifetimes. *Nat. Commun.* **2025**, *16* (1), 1006.
(307) Wang, L.; Wang, L.; Meng, X.; Xiao, F. New Strategies for the Preparation of Sinter-resistant Metal-nanoparticle-based Catalysts. *Adv. Mater.* **2019**, *31* (50), 1901905.
(308) Yu, K.; Li, C.; Gu, W.; Wang, M.; Li, J.; Wen, K.; Xiao, Y.; Liu, S.; Liang, Y.; Guo, W.; Zhao, W.; Bai, J.; Ye, D.; Zhu, Y.; Zhu, M.; Zhou, X.; Liu, Z. High-Strength Cellulose Fibres Enabled by Molecular Packing. *Nat. Sustainability* **2025**, *8* (4), 411−421.
(309) Peng, B.; Li, Q.; Yu, B.; Zhang, J.; Yang, S.; Lu, R.; Sun, X.; Li, X.; Ning, Y. Dual Nanofillers Reinforced Polymer-inorganic Nanocomposite Film with Enhanced Mechanical Properties. *Small* **2024**, *20* (48), 2406160.
(310) Roy, A.; Zenker, S.; Jain, S.; Afshari, R.; Oz, Y.; Zheng, Y.; Annabi, N. A Highly Stretchable, Conductive, and Transparent Bioadhesive Hydrogel as a Flexible Sensor for Enhanced Real-time Human Health Monitoring. *Adv. Mater.* **2024**, *36* (35), 2404225.
(311) Wu, Y.; Li, X.; He, P.; Zou, J.; Zhuang, C.; Li, X.; Jin, Q.; Peng, T.; Zhang, X.; Zheng, D.; Peng, F.; He, S.; Zhong, L.; Tang, K.; Wang, X. Sweat-permeable, Microbiota-preserving, Mechanically Antibacterial Patch for Long-term Interfacing with Perspiring Skin. *Adv. Funct. Mater.* **2025**, *35* (9), 2416129.
(312) Zhu, C.; Chen, G.; Li, S.; Yang, H.; Zheng, J.; Wang, D.; Yang, H.; Wong, L. W. Y.; Fu, J. Breathable Ultrathin Film Sensors Based on Nanomesh Reinforced Anti-dehydrating Organohydrogels for Motion Monitoring. *Adv. Funct. Mater.* **2024**, *34* (52), 2411725.
(313) Wan, J.; Nie, Z.; Xu, J.; Zhang, Z.; Yao, S.; Xiang, Z.; Lin, X.; Lu, Y.; Xu, C.; Zhao, P.; Wang, Y.; Zhang, J.; Wang, Y.; Zhang, S.; Wang, J.; Man, W.; Zhang, M.; Han, M. Millimeter-Scale Magnetic Implants Paired with a Fully Integrated Wearable Device for Wireless Biophysical and Biochemical Sensing. *Sci. Adv.* **2024**, *10* (12), No. eadm9314.
(314) Wang, X.; Wu, G.; Zhang, X.; Lv, F.; Yang, Z.; Nan, X.; Zhang, Z.; Xue, C.; Cheng, H.; Gao, L. Traditional Chinese Medicine (TCM)-inspired Fully Printed Soft Pressure Sensor Array with Self-adaptive Pressurization for Highly Reliable Individualized Long-term Pulse Diagnostics. *Adv. Mater.* **2025**, *37* (1), 2410312.
(315) Mahato, K.; Saha, T.; Ding, S.; Sandhu, S. S.; Chang, A.-Y.; Wang, J. Hybrid Multimodal Wearable Sensors for Comprehensive Health Monitoring. *Nat. Electron.* **2024**, *7* (9), 735−750.
(316) Chen, Y.; Fu, K. X.; Cotton, R.; Ou, Z.; Kwak, J. W.; Chien, J.-C.; Kesler, V.; Nyein, H. Y. Y.; Eisenstein, M.; Tom Soh, H. A Biochemical Sensor with Continuous Extended Stability in Vivo. *Nat. Biomed. Eng.* **2025**, *9*, 1517.
(317) Li, Y.; Zhao, H.; Han, G.; Li, Z.; Mugo, S. M.; Wang, H.; Zhang, Q. Portable Saliva Sensor Based on Dual Recognition

https://doi.org/10.1021/acs.chemrev.5c00801
Chem. Rev. XXXX, XXX, XXX−XXX

Elements for Detection of Caries Pathogenic Bacteria. *Anal. Chem.* **2024**, *96* (24), 9780−9789.
(318) Wu, J.; Liu, H.; Chen, W.; Ma, B.; Ju, H. Device Integration of Electrochemical Biosensors. *Nat. Rev. Bioeng.* **2023**, *1* (5), 346−360.
(319) Ye, C.; Lukas, H.; Wang, M.; Lee, Y.; Gao, W. Nucleic Acid-Based Wearable and Implantable Electrochemical Sensors. *Chem. Soc. Rev.* **2024**, *53* (15), 7960−7982.
(320) Liu, H.; Yang, A.; Song, J.; Wang, N.; Lam, P.; Li, Y.; Law, H. K.; Yan, F. Ultrafast, Sensitive, and Portable Detection of COVID-19 IgG Using Flexible Organic Electrochemical Transistors. *Sci. Adv.* **2021**, *7* (38), No. eabg8387.
(321) Tyagi, S.; Kramer, F. R. Molecular Beacons: Probes That Fluoresce upon Hybridization. *Nat. Biotechnol.* **1996**, *14* (3), 303−308.
(322) Xu, M.; Xin, W.; Xu, J.; Wang, A.; Ma, S.; Dai, D.; Wang, Y.; Yang, D.; Zhao, L.; Li, H. Biosilicification-Mimicking Chiral Nanostructures for Targeted Treatment of Inflammatory Bowel Disease. *Nat. Commun.* **2025**, *16* (1), 2551.
(323) Wang, R.; Song, S.; Qin, J.; Yoshimura, K.; Peng, F.; Chu, Y.; Li, Y.; Fan, Y.; Jin, J.; Dang, M.; Dai, E.; Pei, G.; Han, G.; Hao, D.; Li, Y.; Chatterjee, D.; Harada, K.; Pizzi, M. P.; Scott, A. W.; Tatlonghari, G.; Yan, X.; Xu, Z.; Hu, C.; Mo, S.; Shanbhag, N.; Lu, Y.; Sewastjanow-Silva, M.; Fouad Abdelhakeem, A. A.; Peng, G.; Hanash, S. M.; Calin, G. A.; Yee, C.; Mazur, P.; Marsden, A. N.; Futreal, A.; Wang, Z.; Cheng, X.; Ajani, J. A.; Wang, L. Evolution of Immune and Stromal Cell States and Ecotypes during Gastric Adenocarcinoma Progression. *Cancer Cell* **2023**, *41* (8), 1407−1426.
(324) Li, N.; Kang, S.; Liu, Z.; Wai, S.; Cheng, Z.; Dai, Y.; Solanki, A.; Li, S.; Li, Y.; Strzalka, J.; White, M. J. V.; Kim, Y.-H.; Tian, B.; Hubbell, J. A.; Wang, S. Immune-Compatible Designs of Semiconducting Polymers for Bioelectronics with Suppressed Foreign-Body Response. *Nat. Mater.* **2026**, *25*, 124.
(325) Uberoi, A.; McCready-Vangi, A.; Grice, E. A. The Wound Microbiota: Microbial Mechanisms of Impaired Wound Healing and Infection. *Nat. Rev. Microbiol.* **2024**, *22* (8), 507−521.
(326) Zheng, X. T.; Yang, Z.; Sutarlie, L.; Thangaveloo, M.; Yu, Y.; Salleh, N. A. B. M.; Chin, J. S.; Xiong, Z.; Becker, D. L.; Loh, X. J.; Tee, B. C. K.; Su, X. Battery-Free and AI-Enabled Multiplexed Sensor Patches for Wound Monitoring. *Sci. Adv.* **2023**, *9* (24), No. eadg6670.
(327) Kunpatee, K.; Khantasup, K.; Komolpis, K.; Yakoh, A.; Nuanualsuwan, S.; Sain, M. M.; Chaiyo, S. Ratiometric Electrochemical Lateral Flow Immunoassay for the Detection of Streptococcus Suis Serotype 2. *Biosens. Bioelectron.* **2023**, *242*, 115742.
(328) Tian, S.; Qin, Y.; Wu, Y.; Dong, M. Design, Performance, Processing, and Validation of a Pooled CRISPR Perturbation Screen for Bacterial Toxins. *Nat. Protoc.* **2025**, *20* (5), 1158−1195.
(329) Gao, Y.; Cai, C.; Adamo, S.; Biteus, E.; Kamal, H.; Dager, L.; Miners, K. L.; Llewellyn-Lacey, S.; Ladell, K.; Amratia, P. S.; Bentley, K.; Kollnberger, S.; Wu, J.; Akhirunnesa, M.; Jones, S. A.; Julin, P.; Lidman, C.; Stanton, R. J.; Goepfert, P. A.; Peluso, M. J.; Deeks, S. G.; Davies, H. E.; Aleman, S.; Buggert, M.; Price, D. A. Identification of Soluble Biomarkers That Associate with Distinct Manifestations of Long COVID. *Nat. Immunol.* **2025**, *26* (5), 692−705.
(330) Luebbert, L.; Sullivan, D. K.; Carilli, M.; Eldjárn Hjörleifsson, K.; Viloria Winnett, A.; Chari, T.; Pachter, L. Detection of Viral Sequences at Single-Cell Resolution Identifies Novel Viruses Associated with Host Gene Expression Changes. *Nat. Biotechnol.* **2025**, DOI: 10.1038/s41587-025-02614-y.
(331) Sun, X.; Liu, C.; Lu, X.; Ling, Z.; Yi, C.; Zhang, Z.; Li, Z.; Jin, M.; Wang, W.; Tang, S.; Wang, F.; Wang, F.; Wangmo, S.; Chen, S.; Li, L.; Ma, L.; Zhang, Y.; Yang, Z.; Dong, X.; Qian, Z.; Ding, J.; Wang, D.; Cong, Y.; Sun, B. Unique Binding Pattern for a Lineage of Human Antibodies with Broad Reactivity against Influenza a Virus. *Nat. Commun.* **2022**, *13* (1), 2378.
(332) Malmström, E.; Malmström, L.; Hauri, S.; Mohanty, T.; Scott, A.; Karlsson, C.; Gueto-Tettay, C.; Åhrman, E.; Nozohoor, S.; Tingstedt, B.; Regner, S.; Elfving, P.; Bjermer, L.; Forsvall, A.; Doyle, A.; Magnusson, M.; Hedenfalk, I.; Kannisto, P.; Brandt, C.; Nilsson, E.; Dahlin, L. B.; Malm, J.; Linder, A.; Niméus, E.; Malmström, J. Human Proteome Distribution Atlas for Tissue-Specific Plasma Proteome Dynamics. *Cell* **2025**, *188*, 2810.
(333) The Lung Cancer Cohort Consortium (LC3) Albanes, D.; Alcala, K.; Alcala, N.; Amos, C. I.; Arslan, A. A.; Bassett, J. K.; Brennan, P.; Cai, Q.; Chen, C.; Feng, X.; Freedman, N. D.; Guida, F.; Hung, R. J.; Hveem, K.; Johansson, M.; Johansson, M.; Koh, W.-P.; Langhammer, A.; Milne, R. L.; Muller, D.; Onwuka, J.; Sørgjerd, E. P.; Robbins, H. A.; Sesso, H. D.; Severi, G.; Shu, X.-O.; Sieri, S.; Smith-Byrne, K.; Stevens, V.; Tinker, L.; Tjønneland, A.; Visvanathan, K.; Wang, Y.; Wang, R.; Weinstein, S.; Yuan, J.-M.; Zahed, H.; Zhang, X.; Zheng, W. The Blood Proteome of Imminent Lung Cancer Diagnosis. *Nat. Commun.* **2023**, *14* (1), 3042.
(334) Guo, T.; Steen, J. A.; Mann, M. Mass-Spectrometry-Based Proteomics: From Single Cells to Clinical Applications. *Nature* **2025**, *638* (8052), 901−911.
(335) Yi, Y.; Song, P.; Li, Z.; Ju, J.; Sun, G.; Ren, Q.; Zhou, K.; Liu, L.; Wu, H.-C. Nanopore-Based Enzyme-Linked Immunosorbent Assay for Cancer Biomarker Detection. *Nat. Nanotechnol.* **2025**, *20*, 1079.
(336) Lee, H.; Xie, T.; Kang, B.; Yu, X.; Schaffter, S. W.; Schulman, R. Plug-and-Play Protein Biosensors Using Aptamer-Regulated in Vitro Transcription. *Nat. Commun.* **2024**, *15* (1), 7973.
(337) Lv, J.; Pan, C.; Cai, Y.; Han, X.; Wang, C.; Ma, J.; Pang, J.; Xu, F.; Wu, S.; Kou, T.; Ren, F.; Zhu, Z.-J.; Zhang, T.; Wang, J.; Chen, Y. Plasma Metabolomics Reveals the Shared and Distinct Metabolic Disturbances Associated with Cardiovascular Events in Coronary Artery Disease. *Nat. Commun.* **2024**, *15* (1), 5729.
(338) Wei, X.; Lin, Y.; Wu, Z.; Qiu, Y.; Tang, Y.; Eguchi, M.; Asahi, T.; Yamauchi, Y.; Zhu, C. Bridged pt-OH-mn Mediator in N-coordinated Mn Single Atoms and Pt Nanoparticles for Electrochemical Biomolecule Oxidation and Discrimination. *Angew. Chem., Int. Ed.* **2024**, *63* (31), No. e202405571.
(339) Nishitani, S.; Tran, T.; Puglise, A.; Yang, S.; Landry, M. P. Engineered Glucose Oxidase-carbon Nanotube Conjugates for Tissue-translatable Glucose Nanosensors. *Angew. Chem., Int. Ed.* **2024**, *63* (8), No. e202311476.
(340) Wu, Z.-Q.; Cao, X.-Q.; Hua, Y.; Yu, C.-M. A Bifunctional Wearable Sensor Based on a Nanoporous Membrane for Simultaneous Detection of Sweat Lactate and Temperature. *Anal. Chem.* **2024**, *96*, 3087.
(341) Wang, M.; Yang, Y.; Min, J.; Song, Y.; Tu, J.; Mukasa, D.; Ye, C.; Xu, C.; Heflin, N.; McCune, J. S.; Hsiai, T. K.; Li, Z.; Gao, W. A Wearable Electrochemical Biosensor for the Monitoring of Metabolites and Nutrients. *Nat. Biomed. Eng.* **2022**, *6* (11), 1225−1235.
(342) Lu, H.; Xu, S.; Guo, Z.; Zhao, M.; Liu, Z. Redox-Responsive Molecularly Imprinted Nanoparticles for Targeted Intracellular Delivery of Protein toward Cancer Therapy. *ACS Nano* **2021**, *15* (11), 18214−18225.
(343) Ye, C.; Wang; Min, J.; Tay, R. Y.; Lukas, H.; Sempionatto, J. R.; Li, J.; Xu, C.; Gao, W. A Wearable Aptamer Nanobiosensor for Non-Invasive Female Hormone Monitoring. *Nat. Nanotechnol.* **2024**, *19* (3), 330−337.
(344) Zhou, L.; Yang, R.; Li, X.; Dong, N.; Zhu, B.; Wang, J.; Lin, X.; Su, B. COF-Coated Microelectrode for Space-Confined Electrochemical Sensing of Dopamine in Parkinson's Disease Model Mouse Brain. *J. Am. Chem. Soc.* **2023**, *145* (43), 23727−23738.
(345) Zhai, Q.; Yap, L. W.; Wang, R.; Gong, S.; Guo, Z.; Liu, Y.; Lyu, Q.; Wang, J.; Simon, G. P.; Cheng, W. Vertically Aligned Gold Nanowires as Stretchable and Wearable Epidermal Ion-Selective Electrode for Noninvasive Multiplexed Sweat Analysis. *Anal. Chem.* **2020**, *92* (6), 4647−4655.
(346) Maganzini, N.; Reschke, A.; Cartwright, A. P.; Gidi, Y.; Thompson, I. A. P.; Yee, S.; Hariri, A.; Dory, C.; Rosenberg-Hasson, Y.; Pan, J.; Eisenstein, M.; Vučković, J.; Cornell, T. T.; Soh, H. T. Rapid, Sensitive Detection of Protein Biomarkers in Minimally-processed Blood Products with a Monolithic Sandwich Immunoassay Reagent. *Adv. Mater.* **2025**, *37* (11), 2412613.
(347) Li, X.; Sun, R.; Pan, J.; Shi, Z.; An, Z.; Dai, C.; Lv, J.; Liu, G.; Liang, H.; Liu, J.; Lu, Y.; Zhang, F.; Liu, Q. Rapid and On-Site

Wireless Immunoassay of Respiratory Virus Aerosols via Hydrogel-Modulated Resonators. *Nat. Commun.* **2024**, *15* (1), 4035.
(348) Ebo, J. S.; Saunders, J. C.; Devine, P. W. A.; Gordon, A. M.; Warwick, A. S.; Schiffrin, B.; Chin, S. E.; England, E.; Button, J. D.; Lloyd, C.; Bond, N. J.; Ashcroft, A. E.; Radford, S. E.; Lowe, D. C.; Brockwell, D. J. An in Vivo Platform to Select and Evolve Aggregation-Resistant Proteins. *Nat. Commun.* **2020**, *11* (1), 1816.
(349) Kuru, E.; Rittichier, J.; De Puig, H.; Flores, A.; Rout, S.; Han, I.; Reese, A. E.; Bartlett, T. M.; De Moliner, F.; Bernier, S. G.; Galpin, J. D.; Marchand, J.; Bedell, W.; Robinson-McCarthy, L.; Ahern, C. A.; Bernhardt, T. G.; Rudner, D. Z.; Collins, J. J.; Vendrell, M.; Church, G. M. Rapid Discovery and Evolution of Nanosensors Containing Fluorogenic Amino Acids. *Nat. Commun.* **2024**, *15* (1), 7531.
(350) Hao, L.; Wang, H.; Liu, C.; Wu, Z.; Yi, J.; Bian, K.; Zhang, Y.; Liu, D.; Yang, W.; Zhang, B. Spatiotemporal Proximity-Enhanced Biocatalytic Cascades Within Metal-Organic Frameworks for Wearable and Theranostic Applications. *Adv. Mater.* **2024**, *36* (52), 2414050.
(351) Cho, S.; Shaban, S. M.; Song, R.; Zhang, H.; Yang, D.; Kim, M.-J.; Xiong, Y.; Li, X.; Madsen, K.; Wapnick, S.; Zhang, S.; Chen, Z.; Kim, J.; Guinto, G.; Li, M.; Lee, M.; Nuxoll, R. F.; Shajari, S.; Wang, J.; Son, S.; Shin, J.; Aranyosi, A. J.; Wright, D. E.; Kim, T.; Ghaffari, R.; Huang, Y.; Kim, D.-H.; Rogers, J. A. A Skin-Interfaced Microfluidic Platform Supports Dynamic Sweat Biochemical Analysis during Human Exercise. *Sci. Transl. Med.* **2024**, *16* (763), No. eado5366.
(352) Arwani, R. T.; Tan, S. C. L.; Sundarapandi, A.; Goh, W. P.; Liu, Y.; Leong, F. Y.; Yang, W.; Zheng, X. T.; Yu, Y.; Jiang, C.; Ang, Y. C.; Kong, L.; Teo, S. L.; Chen, P.; Su, X.; Li, H.; Liu, Z.; Chen, X.; Yang, L.; Liu, Y. Stretchable Ionic-Electronic Bilayer Hydrogel Electronics Enable in Situ Detection of Solid-State Epidermal Biomarkers. *Nat. Mater.* **2024**, *23* (8), 1115−1122.
(353) Lopes, V.; Abreu, T.; Abrantes, M.; Nemala, S. S.; De Boni, F.; Prato, M.; Alpuim, P.; Capasso, A. Graphene-Based Glucose Sensors with an Attomolar Limit of Detection. *J. Am. Chem. Soc.* **2025**, *147* (15), 13059−13070.
(354) Das, J.; Gomis, S.; Chen, J. B.; Yousefi, H.; Ahmed, S.; Mahmud, A.; Zhou, W.; Sargent, E. H.; Kelley, S. O. Reagentless Biomolecular Analysis Using a Molecular Pendulum. *Nat. Chem.* **2021**, *13* (5), 428−434.
(355) Mahmud, A.; Chang, D.; Das, J.; Gomis, S.; Foroutan, F.; Chen, J. B.; Pandey, L.; Flynn, C. D.; Yousefi, H.; Geraili, A.; Ross, H. J.; Sargent, E. H.; Kelley, S. O. Monitoring Cardiac Biomarkers with Aptamer-based Molecular Pendulum Sensors. *Angew. Chem., Int. Ed.* **2023**, *62* (20), No. e202213567.
(356) Kokkiligadda, S.; Mondal, A.; Um, S. H.; Park, S. H.; Biswas, C. Observation of Ultrahigh Photoconductivity in DNA-MoS_2 Nano-Biocomposite. *Adv. Mater.* **2024**, *36* (29), 2400124.
(357) Lin, S.; Cheng, X.; Zhu, J.; Wang, B.; Jelinek, D.; Zhao, Y.; Wu, T.-Y.; Horrillo, A.; Tan, J.; Yeung, J.; Yan, W.; Forman, S.; Coller, H. A.; Milla, C.; Emaminejad, S. Wearable Microneedle-Based Electrochemical Aptamer Biosensing for Precision Dosing of Drugs with Narrow Therapeutic Windows. *Sci. Adv.* **2022**, *8* (38), No. eabq4539.
(358) Wang, B.; Zhao, C.; Wang, Z.; Yang, K.-A.; Cheng, X.; Liu, W.; Yu, W.; Lin, S.; Zhao, Y.; Cheung, K. M.; Lin, H.; Hojaiji, H.; Weiss, P. S.; Stojanović, M. N.; Tomiyama, A. J.; Andrews, A. M.; Emaminejad, S. Wearable Aptamer-Field-Effect Transistor Sensing System for Noninvasive Cortisol Monitoring. *Sci. Adv.* **2022**, *8* (1), No. eabk0967.
(359) Zheng, L.; Yang, G.; Muhammad, I.; Qu, F. Aptamer-Based Biosensing Detection for Exosomes: From Selection to Aptasensors. *Trends Anal. Chem.* **2024**, *170*, 117422.
(360) Xu, S.; Wang, L.; Liu, Z. Molecularly Imprinted Polymer Nanoparticles: An Emerging Versatile Platform for Cancer Therapy. *Angew. Chem., Int. Ed.* **2021**, *60* (8), 3858−3869.
(361) Liu, Y.; Su, X.; Fan, P.; Liu, X.; Pan, Y.; Ping, J. Computationally-Assisted Wearable System for Continuous Cortisol Monitoring. *Sci. Bull.* **2025**, *70*, 2004.
(362) Mukasa, D.; Wang, M.; Min, J.; Yang, Y.; Solomon, S. A.; Han, H.; Ye, C.; Gao, W. A Computationally Assisted Approach for Designing Wearable Biosensors toward Non-Invasive Personalized Molecular Analysis. *Adv. Mater.* **2023**, *35* (35), 2212161.
(363) Jiang, Y.; Yang, Y.; Shen, L.; Ma, J.; Ma, H.; Zhu, N. Recent Advances of Prussian Blue-Based Wearable Biosensors for Healthcare. *Anal. Chem.* **2022**, *94* (1), 297−311.
(364) Chen, G.; Kou, X.; Huang, S.; Tong, L.; Shen, Y.; Zhu, W.; Zhu, F.; Ouyang, G. Modulating the Biofunctionality of Metal-Organic-framework-encapsulated Enzymes through Controllable Embedding Patterns. *Angew. Chem., Int. Ed.* **2020**, *59* (7), 2867−2874.
(365) Chinnappan, R.; Ramadan, Q.; Zourob, M. An Integrated Lab-on-a-Chip Platform for Pre-Concentration and Detection of Colorectal Cancer Exosomes Using Anti-CD63 Aptamer as a Recognition Element. *Biosens. Bioelectron.* **2023**, *220*, 114856.
(366) Yang, Y.; Sheng, C.; Dong, F.; Liu, S. An Integrated Wearable Differential Microneedle Array for Continuous Glucose Monitoring in Interstitial Fluids. *Biosens. Bioelectron.* **2024**, *256*, 116280.
(367) Di, K.; Wei, J.; Ding, L.; Shao, Z.; Sha, J.; Zhou, X.; Heng, H.; Feng, X.; Wang, K. A Wearable Sensor Device Based on Screen-Printed Chip with Biofuel Cell-Driven Electrochromic Display for Noninvasive Monitoring of Glucose Concentration. *Chin. Chem. Lett.* **2025**, *36* (2), 109911.
(368) Ma, J.; Jiang, Y.; Shen, L.; Ma, H.; Sun, T.; Lv, F.; Liu, Y.; Liu, J.; Zhu, N. Oil-Water Self-Assembly Engineering of Prussian Blue/Quantum Dots Decorated Graphene Film for Wearable Textile Biosensors and Photoelectronic Unit. *Chem. Eng. J.* **2022**, *427*, 131824.
(369) Park, W.; Seo, H.; Kim, J.; Hong, Y.-M.; Song, H.; Joo, B. J.; Kim, S.; Kim, E.; Yae, C.-G.; Kim, J.; Jin, J.; Kim, J.; Lee, Y.; Kim, J.; Kim, H. K.; Park, J.-U. In-Depth Correlation Analysis between Tear Glucose and Blood Glucose Using a Wireless Smart Contact Lens. *Nat. Commun.* **2024**, *15* (1), 2828.
(370) Min, J.; Ahn, H.; Lukas, H.; Ma, X.; Bhansali, R.; Sunwoo, S.-H.; Wang, C.; Xu, Y.; Yao, D. R.; Kim, G.; Li, Z.; Hsiai, T. K.; Emami, A.; Jung, H.-T.; Gao, W. Continuous Biochemical Profiling of the Gastrointestinal Tract Using an Integrated Smart Capsule. *Nat. Electron.* **2025**, *8*, 844.
(371) Li, J.; Baird, M. A.; Davis, M. A.; Tai, W.; Zweifel, L. S.; Waldorf, K. M. A.; Gale, M., Jr; Rajagopal, L.; Pierce, R. H.; Gao, X. Dramatic Enhancement of the Detection Limits of Bioassays via Ultrafast Deposition of Polydopamine. *Nat. Biomed. Eng.* **2017**, *1* (6), 82.
(372) Ye, C.; Shi, D.; Zhu, Y.; Shi, P.; Zhao, N.; Sun, Z.; Zhang, Z.; Zhang, D.; Lv, Y.; Wu, W.; Yu, J.; Karimi-Maleh, H.; Li, H.; Fu, L.; Jiang, N.; Liu, J.; Lin, C.-T. Graphene Electrochemical Biosensors Combining Effervescent Solid-Phase Extraction (ESPE) for Rapid, Ultrasensitive, and Simultaneous Determination of DA, AA, and UA. *Biosens. Bioelectron.* **2025**, *268*, 116899.
(373) Huang, H.; Yue, Y.; Chen, Z.; Chen, Y.; Wu, S.; Liao, J.; Liu, S.; Wen, H. Electrochemical Sensor Based on a Nanocomposite Prepared from TmPO4 and Graphene Oxide for Simultaneous Voltammetric Detection of Ascorbic Acid, Dopamine and Uric Acid. *Microchim. Acta* **2019**, *186* (3), 189.
(374) Zhou, M.; Urrutia Gomez, J. E.; Mandsberg, N. K.; Liu, S.; Schmidt, S.; Meier, M.; Levkin, P. A.; Jahnke, H.; Popova, A. Electrode Droplet Microarray (eDMA): An Impedance Platform for Label-free Parallel Monitoring of Cellular Drug Response in Nanoliter Droplets. *Adv. Healthcare Mater.* **2025**, *14* (3), 2402046.
(375) Chen, S.; Qi, H.; Kuang, Y.; Li, Q.; Chen, X.; Wang, Y. Monitoring the Mechanical Responses of Tumor Metastasis Based on a Microfluidic Chip Integrated with an Electrochemical Detection System. *Lab Chip* **2025**, *25* (15), 3858−3867.
(376) Ouedraogo, L. J. G.; Kling, M.; Hashemi, N. N. Graphene Microelectrodes for Real-Time Impedance Spectroscopy of Neural Cells in Organ-on-a-Chip. *APL Mater.* **2025**, *13* (2), 21113.

https://doi.org/10.1021/acs.chemrev.5c00801
Chem. Rev. XXXX, XXX, XXX−XXX

(377) Singh, M.; Kathuroju, P. K.; Jampana, N. Polypyrrole Based Amperometric Glucose Biosensors. *Sens. Actuators B: Chem.* **2009**, *143* (1), 430−443.
(378) Liu, S.; Zhong, L.; Tang, Y.; Lai, M.; Wang, H.; Bao, Y.; Ma, Y.; Wang, W.; Niu, L.; Gan, S. Graphene Oxide-Poly(Vinyl Alcohol) Hydrogel-Coated Solid-Contact Ion-Selective Electrodes for Wearable Sweat Potassium Ion Sensing. *Anal. Chem.* **2024**, *96* (21), 8594−8603.
(379) Ishii, M.; Yamashita, Y.; Watanabe, S.; Ariga, K.; Takeya, J. Doping of Molecular Semiconductors through Proton-Coupled Electron Transfer. *Nature* **2023**, *622* (7982), 285−291.
(380) Guo, Y.; Huang, N.; Yang, B.; Wang, C.; Zhuang, H.; Tian, Q.; Zhai, Z.; Liu, L.; Jiang, X. Hybrid Diamond/Graphite Films as Electrodes for Anodic Stripping Voltammetry of Trace Ag + and Cu 2+. *Sens. Actuators B: Chem.* **2016**, *231*, 194−202.
(381) Wu, Y.; Li, X.; Madsen, K. E.; Zhang, H.; Cho, S.; Song, R.; Nuxoll, R. F.; Xiong, Y.; Liu, J.; Feng, J.; Yang, T.; Zhang, K.; Aranyosi, A. J.; Wright, D. E.; Ghaffari, R.; Huang, Y.; Nuzzo, R. G.; Rogers, J. A. Skin-Interfaced Microfluidic Biosensors for Colorimetric Measurements of the Concentrations of Ketones in Sweat. *Lab Chip* **2024**, *24* (18), 4288−4295.
(382) Gao, Y.; Nguyen, D. T.; Yeo, T.; Lim, S. B.; Tan, W. X.; Madden, L. E.; Jin, L.; Long, J. Y. K.; Aloweni, F. A. B.; Liew, Y. J. A.; Tan, M. L. L.; Ang, S. Y.; Maniya, S. D.; Abdelwahab, I.; Loh, K. P.; Chen, C.-H.; Becker, D. L.; Leavesley, D.; Ho, J. S.; Lim, C. T. A Flexible Multiplexed Immunosensor for Point-of-Care in Situ Wound Monitoring. *Sci. Adv.* **2021**, *7* (21), No. eabg9614.
(383) Shan, B.; Broza, Y. Y.; Li, W.; Wang, Y.; Wu, S.; Liu, Z.; Wang, J.; Gui, S.; Wang, L.; Zhang, Z.; Liu, W.; Zhou, S.; Jin, W.; Zhang, Q.; Hu, D.; Lin, L.; Zhang, Q.; Li, W.; Wang, J.; Liu, H.; Pan, Y.; Haick, H. Multiplexed Nanomaterial-Based Sensor Array for Detection of COVID-19 in Exhaled Breath. *ACS Nano* **2020**, *14* (9), 12125−12132.
(384) Shin, J.; Song, J. W.; Flavin, M. T.; Cho, S.; Li, S.; Tan, A.; Pyun, K. R.; Huang, A. G.; Wang, H.; Jeong, S.; Madsen, K. E.; Trueb, J.; Kim, M.; Nguyen, K.; Yang, A.; Hsu, Y.; Sung, W.; Lee, J.; Phyo, S.; Kim, J.-H.; Banks, A.; Chang, J.-K.; Paller, A. S.; Huang, Y.; Ameer, G. A.; Rogers, J. A. A Non-Contact Wearable Device for Monitoring Epidermal Molecular Flux. *Nature* **2025**, *640* (8058), 375−383.
(385) You, S. S.; Gierlach, A.; Schmidt, P.; Selsing, G.; Moon, I.; Ishida, K.; Jenkins, J.; Madani, W. A. M.; Yang, S.-Y.; Huang, H.-W.; Owyang, S.; Hayward, A.; Chandrakasan, A. P.; Traverso, G. An Ingestible Device for Gastric Electrophysiology. *Nat. Electron.* **2024**, *7* (6), 497−508.
(386) Choi, J.; Ghaffari, R.; Baker, L. B.; Rogers, J. A. Skin-Interfaced Systems for Sweat Collection and Analytics. *Sci. Adv.* **2018**, *4* (2), No. eaar3921.
(387) Nyein, H. Y. Y.; Bariya, M.; Tran, B.; Ahn, C. H.; Brown, B. J.; Ji, W.; Davis, N.; Javey, A. A Wearable Patch for Continuous Analysis of Thermoregulatory Sweat at Rest. *Nat. Commun.* **2021**, *12* (1), 1823.
(388) Brothers, M. C.; DeBrosse, M.; Grigsby, C. C.; Naik, R. R.; Hussain, S. M.; Heikenfeld, J.; Kim, S. S. Achievements and Challenges for Real-Time Sensing of Analytes in Sweat within Wearable Platforms. *Acc. Chem. Res.* **2019**, *52* (2), 297−306.
(389) Friedel, M.; Thompson, I. A. P.; Kasting, G.; Polsky, R.; Cunningham, D.; Soh, H. T.; Heikenfeld, J. Opportunities and Challenges in the Diagnostic Utility of Dermal Interstitial Fluid. *Nat. Biomed. Eng.* **2023**, *7* (12), 1541−1555.
(390) Zhao, S.; Lu, Z.; Cai, R.; Wang, H.; Gao, S.; Yang, C.; Zhang, Y.; Luo, B.; Zhang, W.; Yang, Y.; Wang, S.; Sheng, T.; Wang, S.; You, J.; Zhou, R.; Ji, H.; Gong, H.; Ye, X.; Yu, J.; Zhu, H.-H.; Zhang, Y.; Gu, Z. A Wearable Osmotic Microneedle Patch Provides High-Capacity Sustained Drug Delivery in Animal Models. *Sci. Transl. Med.* **2024**, *16* (775), No. eadp3611.
(391) Kusama, S.; Sato, K.; Matsui, Y.; Kimura, N.; Abe, H.; Yoshida, S.; Nishizawa, M. Transdermal Electroosmotic Flow Generated by a Porous Microneedle Array Patch. *Nat. Commun.* **2021**, *12* (1), 658.
(392) Behnam, V.; McManamen, A. M.; Ballard, H. G.; Aldana, B.; Tamimi, M.; Milosavić, N.; Stojanovic, M. N.; Rubin, M. R.; Sia, S. K. mPatch: A Wearable Hydrogel Microneedle Patch for *in Vivo* Optical Sensing of Calcium. *Angew. Chem., Int. Ed.* **2025**, *64* (2), No. e202414871.
(393) Zheng, X.; Zhang, F.; Wang, K.; Zhang, W.; Li, Y.; Sun, Y.; Sun, X.; Li, C.; Dong, B.; Wang, L.; Xu, L. Smart Biosensors and Intelligent Devices for Salivary Biomarker Detection. *Trends Anal. Chem.* **2021**, *140*, 116281.
(394) Arakawa, T.; Tomoto, K.; Nitta, H.; Toma, K.; Takeuchi, S.; Sekita, T.; Minakuchi, S.; Mitsubayashi, K. A Wearable Cellulose Acetate-Coated Mouthguard Biosensor for in Vivo Salivary Glucose Measurement. *Anal. Chem.* **2020**, *92* (18), 12201−12207.
(395) Jang, J.; Kim, J.; Shin, H.; Park, Y.-G.; Joo, B. J.; Seo, H.; Won, J.; Kim, D. W.; Lee, C. Y.; Kim, H. K.; Park, J.-U. Smart Contact Lens and Transparent Heat Patch for Remote Monitoring and Therapy of Chronic Ocular Surface Inflammation Using Mobiles. *Sci. Adv.* **2021**, *7* (14), No. eabf7194.
(396) Huang, M.; Ma, X.; Wu, Z.; Li, J.; Shi, Y.; Yang, T.; Xu, J.; Wang, S.; Lv, K.; Lin, Y. Ammonium Sensing Patch with Ultrawide Linear Range and Eliminated Interference for Universal Body Fluids Analysis. *Nano Micro Lett.* **2025**, *17* (1), 92.
(397) Yin, S.; Chen, X.; Li, R.; Sun, L.; Yao, C.; Li, Z. Wearable, Biocompatible, and Dual-Emission Ocular Multisensor Patch for Continuous Profiling of Fluoroquinolone Antibiotics in Tears. *ACS Nano* **2024**, *18* (28), 18522−18533.
(398) Cheng, P.; Zeng, Z.; Liu, J.; Liew, S. S.; Hu, Y.; Xu, M.; Pu, K. Urinary Bioorthogonal Reporters for the Monitoring of the Efficacy of Chemotherapy for Lung Cancer and of Associated Kidney Injury. *Nat. Biomed. Eng.* **2025**, *9* (5), 686−699.
(399) Zhou, Q.; Xu, W.; Wang, L.; Wang, S.; Pan, J.; Fang, Y.; Liang, H.; Pan, C.; Xia, F. Triboelectric Nanogenerator-Based Self-Powered Urinary Protein Detection Utilizing Triboelectric Material with Colorimetric Function. *ACS Nano* **2025**, *19* (1), 1566−1576.
(400) Huang, H.; Chen, Y.; Xu, W.; Cao, L.; Qian, K.; Bischof, E.; Kennedy, B. K.; Pu, J. Decoding Aging Clocks: New Insights from Metabolomics. *Cell Metab.* **2025**, *37* (1), 34−58.
(401) Vorperian, S. K.; DeFelice, B. C.; Buonomo, J. A.; Chinchinian, H. J.; Gray, I. J.; Yan, J.; Mach, K. E.; La, V.; Lee, T. J.; Liao, J. C.; Lafayette, R.; Loeb, G. B.; Bertozzi, C. R.; Quake, S. R. Deconvolution of Human Urine across the Transcriptome and Metabolome. *Clin. Chem.* **2024**, *70* (11), 1344−1354.
(402) Liu, Z.; Song, H.; Lin, G.; Zhong, W.; Zhang, Y.; Yang, A.; Liu, Y.; Duan, J.; Zhou, Y.; Jiao, K.; Ding, D.; Feng, Y.; Yue, J.; Zhao, W.; Lin, X. Wireless Intelligent Patch for Closed-loop in Situ Wound Management. *Adv. Sci.* **2024**, *11* (29), 2400451.
(403) Jiang, Y.; Trotsyuk, A. A.; Niu, S.; Henn, D.; Chen, K.; Shih, C.-C.; Larson, M. R.; Mermin-Bunnell, A. M.; Mittal, S.; Lai, J.-C.; Saberi, A.; Beard, E.; Jing, S.; Zhong, D.; Steele, S. R.; Sun, K.; Jain, T.; Zhao, E.; Neimeth, C. R.; Viana, W. G.; Tang, J.; Sivaraj, D.; Padmanabhan, J.; Rodrigues, M.; Perrault, D. P.; Chattopadhyay, A.; Maan, Z. N.; Leeolou, M. C.; Bonham, C. A.; Kwon, S. H.; Kussie, H. C.; Fischer, K. S.; Gurusankar, G.; Liang, K.; Zhang, K.; Nag, R.; Snyder, M. P.; Januszyk, M.; Gurtner, G. C.; Bao, Z. Wireless, Closed-Loop, Smart Bandage with Integrated Sensors and Stimulators for Advanced Wound Care and Accelerated Healing. *Nat. Biotechnol.* **2023**, *41* (5), 652−662.
(404) Wang, R.; Du, Y.; Wan, X.; Xu, J.; Chen, J. On-Mask Magnetoelastic Sensor Network for Self-Powered Respiratory Monitoring. *ACS Nano* **2025**, *19* (29), 26862−26870.
(405) Bruderer, T.; Gaisl, T.; Gaugg, M. T.; Nowak, N.; Streckenbach, B.; Müller, S.; Moeller, A.; Kohler, M.; Zenobi, R. On-Line Analysis of Exhaled Breath: *Focus Review*. *Chem. Rev.* **2019**, *119* (19), 10803−10828.
(406) Özçam, M.; Lynch, S. V. The Gut-Airway Microbiome Axis in Health and Respiratory Diseases. *Nat. Rev. Microbiol.* **2024**, *22* (8), 492−506.
(407) Zhang, T.; Sun, B.; Qian, J.; Wang, T.; Zhang, Y.; Xie, H.; Hua, C.; Qiang, Z.; Ren, J. Ultrabroad Pressure Sensing, Ultra-

https://doi.org/10.1021/acs.chemrev.5c00801
Chem. Rev. XXXX, XXX, XXX−XXX

sensitive, Multi-signal Ionogel-based Microneedles for Wearable Respiratory Health Monitoring. *Adv. Funct. Mater.* **2025**, No. e10723.
(408) Uberoi, A.; Murga-Garrido, S. M.; Bhanap, P.; Campbell, A. E.; Knight, S. A. B.; Wei, M.; Chan, A.; Senay, T.; Tegegne, S.; White, E. K.; Sutter, C. H.; Mesaros, C.; Sutter, T. R.; Grice, E. A. Commensal-Derived Tryptophan Metabolites Fortify the Skin Barrier: Insights from a 50-Species Gnotobiotic Model of Human Skin Microbiome. *Cell Chem. Biol.* **2025**, *32* (1), 111−125.
(409) Yuan, Y.; Zhong, B.; Qin, X.; Xu, H.; Li, Z.; Li, L.; Wang, X.; Zhang, W.; Lou, Z.; Fan, Y.; Wang, L. An Epidermal Serine Sensing System for Skin Healthcare. *Nat. Commun.* **2025**, *16* (1), 2681.
(410) Saha, T.; Del Caño, R.; De La Paz, E.; Sandhu, S. S.; Wang, J. Access and Management of Sweat for Non-invasive Biomarker Monitoring: A Comprehensive Review. *Small* **2023**, *19* (51), 2206064.
(411) Wang, X.; He, A.; Yu, B.; Zhang, L.; Pang, W.; Zhang, H.; Niu, P. Uncovering the Sweat Biofouling Components and Distributions in Electrochemical Sensors. *Anal. Chem.* **2022**, *94* (41), 14402−14409.
(412) Saha, T.; Khan, M. I.; Sandhu, S. S.; Yin, L.; Earney, S.; Zhang, C.; Djassemi, O.; Wang, Z.; Han, J.; Abdal, A.; Srivatsa, S.; Ding, S.; Wang, J. A Passive Perspiration Inspired Wearable Platform for Continuous Glucose Monitoring. *Adv. Sci.* **2024**, *11* (41), 2405518.
(413) Shin, S.; Liu, R.; Yang, Y.; Lasalde-Ramírez, J. A.; Kim, G.; Won, C.; Min, J.; Wang, C.; Fan, K.; Han, H.; Uwakwe, C.; Heng, W.; Hsiai, T. K.; Li, Z.; FitzGerald, J. D.; Gao, W. A Bioinspired Microfluidic Wearable Sensor for Multiday Sweat Sampling, Transport, and Metabolic Analysis. *Sci. Adv.* **2025**, *11* (33), No. eadw9024.
(414) Wu, C.-H.; Ma, H. J. H.; Baessler, P.; Balanay, R. K.; Ray, T. R. Skin-Interfaced Microfluidic Systems with Spatially Engineered 3D Fluidics for Sweat Capture and Analysis. *Sci. Adv.* **2023**, *9* (18), No. eadg4272.
(415) Jeon, J.; Lee, S.; Chae, S.; Lee, J. H.; Kim, H.; Yu, E.-S.; Na, H.; Kang, T.; Park, H.-S.; Lee, D.; Jeong, K.-H. All-Flexible Chronoepifluidic Nanoplasmonic Patch for Label-Free Metabolite Profiling in Sweat. *Nat. Commun.* **2025**, *16* (1), 8017.
(416) Ursem, R. F. R.; Steijlen, A.; Parrilla, M.; Bastemeijer, J.; Bossche, A.; De Wael, K. Worth Your Sweat: Wearable Microfluidic Flow Rate Sensors for Meaningful Sweat Analytics. *Lab Chip* **2025**, *25* (5), 1296−1315.
(417) Zhong, B.; Qin, X.; Xu, H.; Liu, L.; Li, L.; Li, Z.; Cao, L.; Lou, Z.; Jackman, J. A.; Cho, N.-J.; Wang, L. Interindividual- and Blood-Correlated Sweat Phenylalanine Multimodal Analytical Biochips for Tracking Exercise Metabolism. *Nat. Commun.* **2024**, *15* (1), 624.
(418) Hu, Y.; Converse, C.; Lyons, M. C.; Hsu, W. H. Neural Control of Sweat Secretion: A Review. *Br. J. Dermatol.* **2018**, *178* (6), No. e448.
(419) Heikenfeld, J.; Jajack, A.; Feldman, B.; Granger, S. W.; Gaitonde, S.; Begtrup, G.; Katchman, B. A. Accessing Analytes in Biofluids for Peripheral Biochemical Monitoring. *Nat. Biotechnol.* **2019**, *37* (4), 407−419.
(420) Arwani, R. T.; Tan, S. C. L.; Sundarapandi, A.; Goh, W. P.; Liu, Y.; Leong, F. Y.; Yang, W.; Zheng, X. T.; Yu, Y.; Jiang, C.; Ang, Y. C.; Kong, L.; Teo, S. L.; Chen, P.; Su, X.; Li, H.; Liu, Z.; Chen, X.; Yang, L.; Liu, Y. Stretchable Ionic-Electronic Bilayer Hydrogel Electronics Enable in Situ Detection of Solid-State Epidermal Biomarkers. *Nat. Mater.* **2024**, *23* (8), 1115−1122.
(421) Futane, A.; Senthil, M.; S, J.; Srinivasan, A.; R, K.; Narayanamurthy, V. Sweat Analysis for Urea Sensing: Trends and Challenges. *Anal. Methods* **2023**, *15* (35), 4405−4426.
(422) Yang, Z.-R.; Suo, H.; Fan, J.-W.; Lv, N.; Du, K.; Ma, T.; Qin, H.; Li, Y.; Yang, L.; Zhou, N.; Jiang, H.; Tao, J.; Zhu, J. Endogenous Stimuli-Responsive Separating Microneedles to Inhibit Hypertrophic Scar through Remodeling the Pathological Microenvironment. *Nat. Commun.* **2024**, *15* (1), 2038.
(423) Chen, S.; Guo, Z.; Lu, B.; Sun, M.; Wang, S.; Li, S.; Jiang, Y.; Wei, Q.; Wang, D.; Jiang, X. A Wearable Device for Continuous Immunoassay-Based Monitoring of C-Peptide in Interstitial Fluid. *Sci. Adv.* **2025**, *11* (29), No. eadw2182.
(424) Wan, S.; Wang, Y.; Li, X.; Qiu, J.; Liu, J.; Gao, B. Challenges and Advances of Interstitial Skin Fluid Wearable Smart Sensors on Emerging Microneedle Platforms. *Anal. Chem.* **2025**, *97* (24), 12467−12479.
(425) Zhu, Y.; Haghniaz, R.; Hartel, M. C.; Guan, S.; Bahari, J.; Li, Z.; Baidya, A.; Cao, K.; Gao, X.; Li, J.; Wu, Z.; Cheng, X.; Li, B.; Emaminejad, S.; Weiss, P. S.; Khademhosseini, A. A Breathable, Passive-Cooling, Non-Inflammatory, and Biodegradable Aerogel Electronic Skin for Wearable Physical-Electrophysiological-Chemical Analysis. *Adv. Mater.* **2023**, *35* (10), 2209300.
(426) Zheng, H.; Pu, Z.; Wu, H.; Li, C.; Zhang, X.; Li, D. Reverse Iontophoresis with the Development of Flexible Electronics: A Review. *Biosens. Bioelectron.* **2023**, *223*, 115036.
(427) Wang, Z.; Luan, J.; Seth, A.; Liu, L.; You, M.; Gupta, P.; Rathi, P.; Wang, Y.; Cao, S.; Jiang, Q.; Zhang, X.; Gupta, R.; Zhou, Q.; Morrissey, J. J.; Scheller, E. L.; Rudra, J. S.; Singamaneni, S. Microneedle Patch for the Ultrasensitive Quantification of Protein Biomarkers in Interstitial Fluid. *Nat. Biomed. Eng.* **2021**, *5* (1), 64−76.
(428) Liao, C.; Chen, X.; Fu, Y. Salivary Analysis: An Emerging Paradigm for Non-invasive Healthcare Diagnosis and Monitoring. *Interdiscip. Med.* **2023**, *1* (3), No. e20230009.
(429) Shi, Z.; Lu, Y.; Shen, S.; Xu, Y.; Shu, C.; Wu, Y.; Lv, J.; Li, X.; Yan, Z.; An, Z.; Dai, C.; Su, L.; Zhang, F.; Liu, Q. Wearable Battery-Free Theranostic Dental Patch for Wireless Intraoral Sensing and Drug Delivery. *Npj Flexible Electron.* **2022**, *6* (1), 49.
(430) Kim, K. R.; Kang, T. W.; Kim, H.; Lee, Y. J.; Lee, S. H.; Yi, H.; Kim, H. S.; Kim, H.; Min, J.; Ready, J.; Millard-Stafford, M.; Yeo, W. All-in-one, Wireless, Multi-sensor Integrated Athlete Health Monitor for Real-time Continuous Detection of Dehydration and Physiological Stress. *Adv. Sci.* **2024**, *11* (33), 2403238.
(431) Lu, D.; Li, H.; Xiao, N.; Jiang, M.; Zuna, Y.; Feng, S.; Li, Z.; Long, J.; Marty, J. L.; Zhu, Z. Salivary Glucose Detection Based on Platinum Metal Hydrogel Prepared Mouthguard Electrochemical Sensor. *Talanta* **2025**, *283*, 127197.
(432) Giaretta, J.; Zulli, R.; Prabhakar, T.; Rath, R. J.; Naficy, S.; Spilimbergo, S.; Weiss, P. S.; Farajikhah, S.; Dehghani, F. Glucose Sensing in Saliva. *Adv. Sens. Res.* **2024**, *3* (11), 2400065.
(433) Brasier, N.; Wang, J.; Gao, W.; Sempionatto, J. R.; Dincer, C.; Ates, H. C.; Güder, F.; Olenik, S.; Schauwecker, I.; Schaffarczyk, D.; Vayena, E.; Ritz, N.; Weisser, M.; Mtenga, S.; Ghaffari, R.; Rogers, J. A.; Goldhahn, J. Applied Body-Fluid Analysis by Wearable Devices. *Nature* **2024**, *636* (8041), 57−68.
(434) Dong, Y.; An, W.; Zhang, Y.; Kang, Z.; Gao, B.; Lv, J.; Jiang, Y.; Niu, C.; Mao, Y.; Zhang, D. An Artificial Intelligence-Assisted, Kilometer-Scale Wireless and Wearable Biochemical Sensing Platform for Monitoring of Key Biomarkers in Urine. *Biosens. Bioelectron.* **2025**, *288*, 117844.
(435) Liu, J.; Li, Z.; Sun, M.; Zhou, L.; Wu, X.; Lu, Y.; Shao, Y.; Liu, C.; Huang, N.; Hu, B.; Wu, Z.; You, C.; Li, L.; Wang, M.; Tao, L.; Di, Z.; Sheng, X.; Mei, Y.; Song, E. Flexible Bioelectronic Systems with Large-Scale Temperature Sensor Arrays for Monitoring and Treatments of Localized Wound Inflammation. *Proc. Natl. Acad. Sci. U. S. A.* **2024**, *121* (49), No. e2412423121.
(436) Heng, W.; Yin, S.; Min, J.; Wang, C.; Han, H.; Shirzaei Sani, E.; Li, J.; Song, Y.; Rossiter, H. B.; Gao, W. A Smart Mask for Exhaled Breath Condensate Harvesting and Analysis. *Science* **2024**, *385* (6712), 954−961.
(437) Li, X.; Zeng, W.; Zhuo, S.; Qian, B.; Chen, Q.; Luo, Q.; Qian, R. Highly Sensitive Room-temperature Detection of Ammonia in the Breath of Kidney Disease Patients Using Fe_2 Mo_3 O_8 /MoO_2 @MoS_2 Nanocomposite Gas Sensor. *Adv. Sci.* **2024**, *11* (32), 2405942.
(438) Sun, Y.; Tian, G.; Deng, W.; Yang, W. Ionic Hydrogel Sensors toward Next-gen Personalized Healthcare. *Adv. Mater.* **2025**, No. e09122.
(439) Li, D.; Cui, T.-R.; Liu, J.-H.; Shao, W.-C.; Liu, X.; Chen, Z.-K.; Xu, Z.-G.; Li, X.; Xu, S.-Y.; Xie, Z.-Y.; Jian, J.-M.; Wang, X.; Tao, L.-Q.; Wu, X.-M.; Cheng, Z.-W.; Dong, Z.-R.; Liu, H.-F.; Yang, Y.; Zhou, J.; Ren, T.-L. Motion-Unrestricted Dynamic Electrocardiogram

https://doi.org/10.1021/acs.chemrev.5c00801
Chem. Rev. XXXX, XXX, XXX−XXX

System Utilizing Imperceptible Electronics. *Nat. Commun.* **2025**, *16* (1), 3259.
(440) Yang, S.; Cheng, J.; Shang, J.; Hang, C.; Qi, J.; Zhong, L.; Rao, Q.; He, L.; Liu, C.; Ding, L.; Zhang, M.; Chakrabarty, S.; Jiang, X. Stretchable Surface Electromyography Electrode Array Patch for Tendon Location and Muscle Injury Prevention. *Nat. Commun.* **2023**, *14* (1), 6494.
(441) Yang, A.; Song, J.; Liu, H.; Zhao, Z.; Li, L.; Yan, F. Wearable Organic Electrochemical Transistor Array for Skin-surface Electrocardiogram Mapping above a Human Heart. *Adv. Funct. Mater.* **2023**, *33* (17), 2215037.
(442) Grinnell, A. D. Dynamics of Nerve-Muscle Interaction in Developing and Mature Neuromuscular Junctions. *Physiol. Rev.* **1995**, *75* (4), 789−834.
(443) Wang, H.; Du, X.; Liu, N. An Electron-Ion Dual-Conductive Electrode Enables Wearable Monitoring of Electromyography Signals. *Device* **2025**, *3* (1), 100563.
(444) Mushtaq, F.; Welke, D.; Gallagher, A.; Pavlov, Y. G.; Kouara, L.; Bosch-Bayard, J.; Van Den Bosch, J. J. F.; Arvaneh, M.; Bland, A. R.; Chaumon, M.; Borck, C.; He, X.; Luck, S. J.; Machizawa, M. G.; Pernet, C.; Puce, A.; Segalowitz, S. J.; Rogers, C.; Awais, M.; Babiloni, C.; Bailey, N. W.; Baillet, S.; Bendall, R. C. A.; Brady, D.; Bringas-Vega, M. L.; Busch, N. A.; Calzada-Reyes, A.; Chatard, A.; Clayson, P. E.; Cohen, M. X.; Cole, J.; Constant, M.; Corneyllie, A.; Coyle, D.; Cruse, D.; Delis, I.; Delorme, A.; Fair, D.; Falk, T. H.; Gamer, M.; Ganis, G.; Gloy, K.; Gregory, S.; Hassall, C. D.; Hiley, K. E.; Ivry, R. B.; Jerbi, K.; Jenkins, M.; Kaiser, J.; Keil, A.; Knight, R. T.; Kochen, S.; Kotchoubey, B.; Krigolson, O. E.; Langer, N.; Liesefeld, H. R.; Lippé, S.; London, R. E.; MacNamara, A.; Makeig, S.; Marinovic, W.; Martínez-Montes, E.; Marzuki, A. A.; Mathew, R. K.; Michel, C.; Millán, J. D. R.; Mon-Williams, M.; Morales-Chacón, L.; Naar, R.; Nilsonne, G.; Niso, G.; Nyhus, E.; Oostenveld, R.; Paul, K.; Paulus, W.; Pfabigan, D. M.; Pourtois, G.; Rampp, S.; Rausch, M.; Robbins, K.; Rossini, P. M.; Ruzzoli, M.; Schmidt, B.; Senderecka, M.; Srinivasan, N.; Stegmann, Y.; Thompson, P. M.; Valdes-Sosa, M.; Van Der Molen, M. J. W.; Veniero, D.; Verona, E.; Voytek, B.; Yao, D.; Evans, A. C.; Valdes-Sosa, P. One Hundred Years of EEG for Brain and Behaviour Research. *Nat. Hum. Behav.* **2024**, *8* (8), 1437−1443.
(445) Song, D.; Li, X.; Jang, M.; Lee, Y.; Zhai, Y.; Hu, W.; Yan, H.; Zhang, S.; Chen, L.; Lu, C.; Kim, K.; Liu, N. An Ultra-thin MXene Film for Multimodal Sensing of Neuroelectrical Signals with Artifacts Removal. *Adv. Mater.* **2023**, *35* (48), 2304956.
(446) Deng, Q.; Wu, C.; Parker, E.; Zhu, J.; Liu, T. C.-Y.; Duan, R.; Yang, L. Mystery of Gamma Wave Stimulation in Brain Disorders. *Mol. Neurodegener.* **2024**, *19* (1), 96.
(447) Liu, H.; Zhang, S.; Li, Z.; Lu, T. J.; Lin, H.; Zhu, Y.; Ahadian, S.; Emaminejad, S.; Dokmeci, M. R.; Xu, F.; Khademhosseini, A. Harnessing the Wide-Range Strain Sensitivity of Bilayered PEDOT:PSS Films for Wearable Health Monitoring. *Matter* **2021**, *4* (9), 2886−2901.
(448) Lu, Y.; Zhang, H.; Zhao, Y.; Liu, H.; Nie, Z.; Xu, F.; Zhu, J.; Huang, W. Robust Fiber-Shaped Flexible Temperature Sensors for Safety Monitoring with Ultrahigh Sensitivity. *Adv. Mater.* **2024**, *36* (18), 2310613.
(449) Yang, H.; Li, J.; Xiao, X.; Wang, J.; Li, Y.; Li, K.; Li, Z.; Yang, H.; Wang, Q.; Yang, J.; Ho, J. S.; Yeh, P.-L.; Mouthaan, K.; Wang, X.; Shah, S.; Chen, P.-Y. Topographic Design in Wearable MXene Sensors with In-Sensor Machine Learning for Full-Body Avatar Reconstruction. *Nat. Commun.* **2022**, *13* (1), 5311.
(450) Zhao, X.; Zhou, Y.; Li, A.; Xu, J.; Karjagi, S.; Hahm, E.; Rulloda, L.; Li, J.; Hollister, J.; Kavehpour, P.; Chen, J. A Self-Filtering Liquid Acoustic Sensor for Voice Recognition. *Nat. Electron.* **2024**, *7* (10), 924−932.
(451) Hu, H.; Huang, H.; Li, M.; Gao, X.; Yin, L.; Qi, R.; Wu, R. S.; Chen, X.; Ma, Y.; Shi, K.; Li, C.; Maus, T. M.; Huang, B.; Lu, C.; Lin, M.; Zhou, S.; Lou, Z.; Gu, Y.; Chen, Y.; Lei, Y.; Wang, X.; Wang, R.; Yue, W.; Yang, X.; Bian, Y.; Mu, J.; Park, G.; Xiang, S.; Cai, S.; Corey, P. W.; Wang, J.; Xu, S. A Wearable Cardiac Ultrasound Imager. *Nature* **2023**, *613* (7945), 667−675.
(452) Jin, Y.; Xue, S.; He, Y. Flexible Pressure Sensors Enhanced by 3D-printed Microstructures. *Adv. Mater.* **2025**, *37*, 2500076.
(453) Min, S.; Kim, D. H.; Joe, D. J.; Kim, B. W.; Jung, Y. H.; Lee, J. H.; Lee, B.; Doh, I.; An, J.; Youn, Y.; Joung, B.; Yoo, C. D.; Ahn, H.; Lee, K. J. Clinical Validation of a Wearable Piezoelectric Blood-Pressure Sensor for Continuous Health Monitoring. *Adv. Mater.* **2023**, *35* (26), 2301627.
(454) Fan, W.; Lei, R.; Dou, H.; Wu, Z.; Lu, L.; Wang, S.; Liu, X.; Chen, W.; Rezakazemi, M.; Aminabhavi, T. M.; Li, Y.; Ge, S. Sweat Permeable and Ultrahigh Strength 3D PVDF Piezoelectric Nanoyarn Fabric Strain Sensor. *Nat. Commun.* **2024**, *15* (1), 3509.
(455) Yang, T.; Hu, J.; Yan, Z.; Edeleva, M.; Cardon, L.; Zhang, J. Facilely Fabricated Ultrasensitive, High-Tensile Dual Bionic-Inspired Strain Sensor Based on AgNWs@CNTs/TPU Composites. *Chem. Eng. J.* **2025**, *513*, 162964.
(456) Nie, Z.; Kwak, J. W.; Han, M.; Rogers, J. A. Mechanically Active Materials and Devices for Bio-interfaced Pressure Sensors—a Review. *Adv. Mater.* **2024**, *36* (43), 2205609.
(457) Xiang, Q.; Zhao, G.; Tang, T.; Zhang, H.; Liu, Z.; Zhang, X.; Zhao, Y.; Tan, H. All-carbon Piezoresistive Sensor: Enhanced Sensitivity and Wide Linear Range via Multiscale Design for Wearable Applications. *Adv. Funct. Mater.* **2025**, *35* (15), 2418706.
(458) Yang, D.; Zhao, K.; Yang, R.; Zhou, S.; Chen, M.; Tian, H.; Qu, D. A Rational Design of Bio-Derived Disulfide CANs for Wearable Capacitive Pressure Sensor. *Adv. Mater.* **2024**, *36* (30), 2403880.
(459) Pai, Y.; Xu, C.; Zhu, R.; Ding, X.; Bai, S.; Liang, Z.; Chen, L. Piezoelectric-augmented Thermoelectric Ionogels for Self-powered Multimodal Medical Sensors. *Adv. Mater.* **2025**, *37* (6), 2414663.
(460) Lu, D.; Liu, T.; Meng, X.; Luo, B.; Yuan, J.; Liu, Y.; Zhang, S.; Cai, C.; Gao, C.; Wang, J.; Wang, S.; Nie, S. Wearable Triboelectric Visual Sensors for Tactile Perception. *Adv. Mater.* **2023**, *35* (7), 2209117.
(461) Liu, Y.; Wang, J.; Liu, T.; Wei, Z.; Luo, B.; Chi, M.; Zhang, S.; Cai, C.; Gao, C.; Zhao, T.; Wang, S.; Nie, S. Triboelectric Tactile Sensor for Pressure and Temperature Sensing in High-Temperature Applications. *Nat. Commun.* **2025**, *16* (1), 383.
(462) Wei, Q.; Rojas, D.; Wang, Q.; Zapata-Pérez, R.; Xuan, X.; Molinero-Fernández, Á.; Crespo, G. A.; Cuartero, M. Wearable 3D-Printed Microneedle Sensor for Intradermal Temperature Monitoring. *ACS Sens.* **2025**, *10* (6), 4027−4037.
(463) Zhang, Z.; Zhao, W.; Ma, Y.; Yao, Y.; Yu, T.; Zhang, W.; Guo, H.; Duan, X.; Yan, R.; Xu, D.; Chen, M. A Flexible Integrated Temperature-Pressure Sensor for Wearable Detection of Thermal Runaway in Lithium Batteries. *Appl. Energy* **2025**, *381*, 125191.
(464) Deng, Y.; Arafa, H. M.; Yang, T.; Albadawi, H.; Fowl, R. J.; Zhang, Z.; Kandula, V.; Ramesh, A.; Correia, C.; Huang, Y.; Oklu, R.; Rogers, J. A.; Carlini, A. S. A Soft Thermal Sensor for the Continuous Assessment of Flow in Vascular Access. *Nat. Commun.* **2025**, *16* (1), 38.
(465) Jiang, J.; Zhang, L.; Ming, C.; Zhou, H.; Bose, P.; Guo, Y.; Hu, Y.; Wang, B.; Chen, Z.; Jia, R.; Pendse, S.; Xiang, Y.; Xia, Y.; Lu, Z.; Wen, X.; Cai, Y.; Sun, C.; Wang, G.-C.; Lu, T.-M.; Gall, D.; Sun, Y.-Y.; Koratkar, N.; Fohtung, E.; Shi, Y.; Shi, J. Giant Pyroelectricity in Nanomembranes. *Nature* **2022**, *607* (7919), 480−485.
(466) Xing, R.; Zhang, X.; Fan, X.; Xie, R.; Wu, L.; Fang, X. Coupling Strategies of Multi-physical Fields in 2D Materials-based Photodetectors. *Adv. Mater.* **2025**, *37* (16), 2501833.
(467) Li, S.; Wang, Y.; Liu, Z.; Chen, B.; Liu, M.; He, X.; Yang, S. Flexible Pyroelectric Energy Harvesters from Nanocomposites of Liquid Crystal Elastomers/Lead Zirconate Titanate Nanoparticles. *Sci. Adv.* **2025**, *11* (7), No. eadt6136.
(468) Tan, H.; Zhao, Y.; Jin, P.; Xu, X.; Zhou, X.; Marchesoni, F.; Huang, J. Bioinspired Energy-Free Temperature Gradient Regulator for Significant Enhancement of Thermoelectric Conversion Efficiency. *Proc. Natl. Acad. Sci. U. S. A.* **2025**, *122* (7), No. e2424421122.
(469) Du, M.; Wen, Y.; Chen, Z.; Xu, Y.; Qin, J.; Cheng, H.; Du, Y.; Zhang, K.; Shin, S.; Ouyang, J. A Polymer Film with Very High Seebeck Coefficient and Overall Thermoelectric Properties by

https://doi.org/10.1021/acs.chemrev.5c00801
Chem. Rev. XXXX, XXX, XXX−XXX

Secondary Doping, Dedoping Engineering and Ionic Energy Filtering. *Adv. Funct. Mater.* **2025**, *35* (1), 2411815.
(470) Liu, L.; Dou, Y.; Wang, J.; Zhao, Y.; Kong, W.; Ma, C.; He, D.; Wang, H.; Zhang, H.; Chang, A.; Zhao, P. Recent Advances in Flexible Temperature Sensors: Materials, Mechanism, Fabrication, and Applications. *Adv. Sci.* **2024**, *11*, 2405003.
(471) Li, J.; He, X.; Wang, J.; Zhu, S.; Zhang, M.; Wu, C.; Dong, G.; Liu, R.; Wang, L.; Chen, L.; Cai, K. Nanoarchitectonics of High-Performance and Flexible n-Type Organic-Inorganic Composite Thermoelectric Fibers for Wearable Electronics. *ACS Nano* **2025**, *19* (11), 11440−11449.
(472) Hassan, M.; Abbas, G.; Li, N.; Afzal, A.; Haider, Z.; Ahmed, S.; Xu, X.; Pan, C.; Peng, Z. Significance of Flexible Substrates for Wearable and Implantable Devices: Recent Advances and Perspectives. *Adv. Mater. Technol.* **2022**, *7* (3), 2100773.
(473) Yu, S.; Ye, Q.; Yang, B.; Liu, X.; Zhou, H.; Hu, L.; Lu, C. Ultrasensitive, Highly Stretchable and Multifunctional Strain Sensors Based on Scorpion-Leg-Inspired Gradient Crack Arrays. *Chem. Eng. J.* **2024**, *497*, 154952.
(474) Shao, Y.; Yan, J.; Zhi, Y.; Li, C.; Li, Q.; Wang, K.; Xia, R.; Xiang, X.; Liu, L.; Chen, G.; Zhang, H.; Cai, D.; Wang, H.; Cheng, X.; Yang, C.; Ren, F.; Yu, Y. A Universal Packaging Substrate for Mechanically Stable Assembly of Stretchable Electronics. *Nat. Commun.* **2024**, *15* (1), 6106.
(475) Xiang, S.; Chen, G.; Wen, Q.; Li, H.; Luo, X.; Zhong, J.; Shen, S.; Di Carlo, A.; Fan, X.; Chen, J. Fully Addressable Textile Sensor Array for Self-Powered Haptic Interfacing. *Matter* **2024**, *7* (1), 82−94.
(476) Xia, Y.; Li, J.; Ji, Z.; Zhou, K.; Zhang, Y.; Liu, Y.; Tsang, S. W.; Wong, K. W.; Wang, Q.; Wang, W.; Cabot, A.; Yang, X.; Lim, K. H. Surface-engineering Cellulose Nanofibers via in Situ PEDOT Polymerization for Superior Thermoelectric Properties. *Adv. Mater.* **2025**, *37*, 2506338.
(477) Du, Y.; Zhou, C.; Feng, Y.; Qiu, L. Flexible, Multimodal Device for Measurement of Body Temperature, Core Temperature, Thermal Conductivity and Water Content. *Npj Flexible Electron.* **2024**, *8* (1), 85.
(478) Wang, Z.; Song, Y.; Zhang, G.; Luo, Q.; Xu, K.; Gao, D.; Yu, B.; Loke, D.; Zhong, S.; Zhang, Y. Advances of Embedded Resistive Random Access Memory in Industrial Manufacturing and Its Potential Applications. *Int. J. Extreme Manuf.* **2024**, *6* (3), 032006.
(479) Chen, S.; Fan, S.; Qiao, Z.; Wu, Z.; Lin, B.; Li, Z.; Riegler, M. A.; Wong, M. Y. H.; Opheim, A.; Korostynska, O.; Nielsen, K. M.; Glott, T.; Martinsen, A. C. T.; Telle-Hansen, V. H.; Lim, C. T. Transforming Healthcare: Intelligent Wearable Sensors Empowered by Smart Materials and Artificial Intelligence. *Adv. Mater.* **2025**, *37*, 2500412.
(480) Kong, L.; Li, W.; Zhang, T.; Ma, H.; Cao, Y.; Wang, K.; Zhou, Y.; Shamim, A.; Zheng, L.; Wang, X.; Huang, W. Wireless Technologies in Flexible and Wearable Sensing: From Materials Design, System Integration to Applications. *Adv. Mater.* **2024**, *36* (27), 2400333.
(481) Tian, X.; Zeng, Q.; Kurt, S. A.; Li, R. R.; Nguyen, D. T.; Xiong, Z.; Li, Z.; Yang, X.; Xiao, X.; Wu, C.; Tee, B. C. K.; Nikolayev, D.; Charles, C. J.; Ho, J. S. Implant-to-Implant Wireless Networking with Metamaterial Textiles. *Nat. Commun.* **2023**, *14* (1), 4335.
(482) He, X.; Shi, X.-L.; Wu, X.; Li, C.; Liu, W.-D.; Zhang, H.; Yu, X.; Wang, L.; Qin, X.; Chen, Z.-G. Three-Dimensional Flexible Thermoelectric Fabrics for Smart Wearables. *Nat. Commun.* **2025**, *16* (1), 2523.
(483) Xu, L.; Chen, W.; Li, Q.; Gupta, R.; Bagchi, B.; Lovat, L. B.; Tiwari, M. K. Printing Nacre-mimetic MXene-based E-textile Devices for Sensing and Breathing-pattern Recognition Using Machine Learning. *Adv. Funct. Mater.* **2025**, *35*, No. e08370.
(484) Min, J.; Demchyshyn, S.; Sempionatto, J. R.; Song, Y.; Hailegnaw, B.; Xu, C.; Yang, Y.; Solomon, S.; Putz, C.; Lehner, L. E.; Schwarz, J. F.; Schwarzinger, C.; Scharber, M. C.; Shirzaei Sani, E.; Kaltenbrunner, M.; Gao, W. An Autonomous Wearable Biosensor Powered by a Perovskite Solar Cell. *Nat. Electron.* **2023**, *6* (8), 630−641.
(485) Guan, S.; Yang, Y.; Wang, Y.; Zhu, X.; Ye, D.; Chen, R.; Liao, Q. A Dual-functional MXene-based Bioanode for Wearable Self-charging Biosupercapacitors. *Adv. Mater.* **2024**, *36* (1), 2305854.
(486) Wang, Q.; Hu, D.; Huang, X.; Yuan, Z.; Zhong, L.; Sun, Q.; Wang, F.; Xu, S.; Chen, S. Achieving High Performance of Triboelectric Nanogenerators via Voltage Boosting Strategy. *Adv. Funct. Mater.* **2024**, *34* (49), 2409088.
(487) Chen, X.; Yin, L.; Lv, J.; Gross, A. J.; Le, M.; Gutierrez, N. G.; Li, Y.; Jeerapan, I.; Giroud, F.; Berezovska, A.; O'Reilly, R. K.; Xu, S.; Cosnier, S.; Wang, J. Stretchable and Flexible Buckypaper-based Lactate Biofuel Cell for Wearable Electronics. *Adv. Funct. Mater.* **2019**, *29* (46), 1905785.
(488) Yu, Y.; Nassar, J.; Xu, C.; Min, J.; Yang, Y.; Dai, A.; Doshi, R.; Huang, A.; Song, Y.; Gehlhar, R.; Ames, A. D.; Gao, W. Biofuel-Powered Soft Electronic Skin with Multiplexed and Wireless Sensing for Human-Machine Interfaces. *Sci. Rob.* **2020**, *5* (41), No. eaaz7946.
(489) Su, Y.; Lu, L.; Zhou, M. Wearable Microbial Fuel Cells for Sustainable Self-Powered Electronic Skins. *ACS Appl. Mater. Interfaces* **2022**, *14* (7), 8664−8668.
(490) Xiang, H.; Peng, L.; Yang, Q.; Wang, Z. L.; Cao, X. Triboelectric Nanogenerator for High-Entropy Energy, Self-Powered Sensors, and Popular Education. *Sci. Adv.* **2024**, *10* (48), No. eads2291.
(491) Das, T.; Tripathy, S.; Kumar, A.; Kar, M. Flexible Piezoelectric Nanogenerator as a Self-Charging Piezo-Supercapacitor for Energy Harvesting and Storage Application. *Nano Energy* **2025**, *136*, 110752.
(492) Fan, F.-R.; Tian, Z.-Q.; Lin Wang, Z. Flexible Triboelectric Generator. *Nano Energy* **2012**, *1* (2), 328−334.
(493) Song, Y.; Min, J.; Yu, Y.; Wang, H.; Yang, Y.; Zhang, H.; Gao, W. Wireless Battery-Free Wearable Sweat Sensor Powered by Human Motion. *Sci. Adv.* **2020**, *6* (40), No. eaay9842.
(494) Park, M.; Park, T.; Park, S.; Yoon, S. J.; Koo, S. H.; Park, Y.-L. Stretchable Glove for Accurate and Robust Hand Pose Reconstruction Based on Comprehensive Motion Data. *Nat. Commun.* **2024**, *15* (1), 5821.
(495) Zhang, L.; Shi, X.-L.; Shang, H.; Gu, H.; Chen, W.; Li, M.; Huang, D.; Dong, H.; Wang, X.; Ding, F.; Chen, Z.-G. High-Performance Ag2Se-Based Thermoelectrics for Wearable Electronics. *Nat. Commun.* **2025**, *16* (1), 5002.
(496) Garmroudi, F.; Serhiienko, I.; Parzer, M.; Ghosh, S.; Ziolkowski, P.; Oppitz, G.; Nguyen, H. D.; Bourgès, C.; Hattori, Y.; Riss, A.; Steyrer, S.; Rogl, G.; Rogl, P.; Schafler, E.; Kawamoto, N.; Müller, E.; Bauer, E.; De Boor, J.; Mori, T. Decoupled Charge and Heat Transport in Fe2VAl Composite Thermoelectrics with Topological-Insulating Grain Boundary Networks. *Nat. Commun.* **2025**, *16* (1), 2976.
(497) Kim, C. S.; Yang, H. M.; Lee, J.; Lee, G. S.; Choi, H.; Kim, Y. J.; Lim, S. H.; Cho, S. H.; Cho, B. J. Self-Powered Wearable Electrocardiography Using a Wearable Thermoelectric Power Generator. *ACS Energy Lett.* **2018**, *3* (3), 501−507.
(498) Li, Y.; Ru, X.; Yang, M.; Zheng, Y.; Yin, S.; Hong, C.; Peng, F.; Qu, M.; Xue, C.; Lu, J.; Fang, L.; Su, C.; Chen, D.; Xu, J.; Yan, C.; Li, Z.; Xu, X.; Shao, Z. Flexible Silicon Solar Cells with High Power-to-Weight Ratios. *Nature* **2024**, *626* (7997), 105−110.
(499) Kojima, A.; Teshima, K.; Shirai, Y.; Miyasaka, T. Organometal Halide Perovskites as Visible-Light Sensitizers for Photovoltaic Cells. *J. Am. Chem. Soc.* **2009**, *131* (17), 6050−6051.
(500) Wang, Z.; Zhang, D.; Yang, L.; Allam, O.; Gao, Y.; Su, Y.; Xu, M.; Mo, S.; Wu, Q.; Wang, Z.; Liu, J.; He, J.; Li, R.; Jia, X.; Li, Z.; Yang, L.; Weber, M. D.; Yu, Y.; Zhang, X.; Marks, T. J.; Stingelin, N.; Kacher, J.; Jang, S. S.; Facchetti, A.; Shao, M. Mechanically Robust and Stretchable Organic Solar Cells Plasticized by Small-Molecule Acceptors. *Science* **2025**, *387* (6732), 381−387.
(501) Hajiaghajani, A.; Afandizadeh Zargari, A. H.; Dautta, M.; Jimenez, A.; Kurdahi, F.; Tseng, P. Textile-Integrated Metamaterials for near-Field Multibody Area Networks. *Nat. Electron.* **2021**, *4* (11), 808−817.
(502) Wang, S.; Cui, Q.; Abiri, P.; Roustaei, M.; Zhu, E.; Li, Y.-R.; Wang, K.; Duarte, S.; Yang, L.; Ebrahimi, R.; Bersohn, M.; Chen, J.;

https://doi.org/10.1021/acs.chemrev.5c00801
Chem. Rev. XXXX, XXX, XXX−XXX

Hsiai, T. K. A Self-Assembled Implantable Microtubular Pacemaker for Wireless Cardiac Electrotherapy. *Sci. Adv.* **2023**, *9* (42), No. eadj0540.
(503) Woods, J. E.; Alrashdan, F.; Chen, E. C.; Tan, W.; John, M.; Jaworski, L.; Bernard, D.; Post, A.; Moctezuma-Ramirez, A.; Elgalad, A.; Steele, A. G.; Barber, S. M.; Horner, P. J.; Faraji, A. H.; Sayenko, D. G.; Razavi, M.; Robinson, J. T. Distributed Battery-Free Bioelectronic Implants with Improved Network Power Transfer Efficiency via Magnetoelectrics. *Nat. Biomed. Eng.* **2025**, DOI: 10.1038/s41551-025-01489-3.
(504) Gao, Z.; Zhou, Y.; Zhang, J.; Foroughi, J.; Peng, S.; Baughman, R. H.; Wang, Z. L.; Wang, C. H. Advanced Energy Harvesters and Energy Storage for Powering Wearable and Implantable Medical Devices. *Adv. Mater.* **2024**, *36* (42), 2404492.
(505) Huang, J.; Ren, Z.; Zhang, Y.; Fong, P. W.; Chandran, H. T.; Liang, Q.; Yao, K.; Tang, H.; Xia, H.; Zhang, H.; Yu, X.; Zheng, Z.; Li, G. Tandem Self-powered Flexible Electrochromic Energy Supplier for Sustainable All-day Operations. *Adv. Energy Mater.* **2022**, *12* (30), 2201042.
(506) Shui, T.; Liang, Y.; Wejrzanowski, T.; Liu, J.; Kure-Chu, S.-Z.; Hihara, T.; Zhang, T.; Liang, F.; Sun, C.; She, W.; Zhang, W.; Sun, Z. M. Electrolyte Evolution for Flexible Energy Storage Systems: From Liquid to Solid, from Rigid to Soft, and from Organic to Aqueous. *Chem. Rev.* **2025**, *125*, 7167.
(507) Xie, Z.; Huang, Z.; Li, H.; Xu, T.; Zhao, H.; Wang, Y.; Pang, X.; Cao, Z.; Altoé, V.; Klivansky, L. M.; Wang, Z.; Shelton, S. W.; Lai, S.; Liu, P.; Zhu, C.; Connolly, M. D.; Ralston, C. Y.; Gu, X.; Peng, Z.; Zhang, J.; Liu, Y. Advancing High-Temperature Electrostatic Energy Storage *via* Linker Engineering of Metal-Organic Frameworks in Polymer Nanocomposites. *Energy Environ. Sci.* **2025**, *18* (2), 620−630.
(508) Lu, C.; Jiang, H.; Cheng, X.; He, J.; Long, Y.; Chang, Y.; Gong, X.; Zhang, K.; Li, J.; Zhu, Z.; Wu, J.; Wang, J.; Zheng, Y.; Shi, X.; Ye, L.; Liao, M.; Sun, X.; Wang, B.; Chen, P.; Wang, Y.; Peng, H. High-Performance Fibre Battery with Polymer Gel Electrolyte. *Nature* **2024**, *629* (8010), 86−91.
(509) Zhang, B.; Cai, X.; Li, J.; Zhang, H.; Li, D.; Ge, H.; Liang, S.; Lu, B.; Zhao, J.; Zhou, J. Biocompatible and Stable Quasi-Solid-State Zinc-Ion Batteries for Real-Time Responsive Wireless Wearable Electronics. *Energy Environ. Sci.* **2024**, *17* (11), 3878−3887.
(510) Song, I. T.; Kang, J.; Koh, J.; Choi, H.; Yang, H.; Park, E.; Lee, J.; Cho, W.; Lee, Y.; Lee, S.; Kim, N.; Lee, M.; Kim, K. Thermal Runaway Prevention through Scalable Fabrication of Safety Reinforced Layer in Practical Li-Ion Batteries. *Nat. Commun.* **2024**, *15* (1), 8294.
(511) Xia, H.; Xu, G.; Cao, X.; Miao, C.; Zhang, H.; Chen, P.; Zhou, Y.; Zhang, W.; Sun, Z. Single-ion-conducting Hydrogel Electrolytes Based on Slide-ring Pseudo-polyrotaxane for Ultralong-cycling Flexible Zinc-ion Batteries. *Adv. Mater.* **2023**, *35* (36), 2301996.
(512) Chu, N.; Wang, T.; Guo, Z.; Li, X.; Wang, H.; Xu, T.; Zang, J.; Wang, Y.; Li, X.; Luo, Y.; Yang, H. Y.; Kong, D. 3D-Printed Hierarchically Porous MOF-Derived Cathodes for Realizing High-Performance Flexible Quasi-Solid-State Aqueous Zinc-Cobalt Batteries. *ACS Nano* **2025**, *19*, 29327.
(513) Wang, W.; Li, C.; Liu, S.; Zhang, J.; Zhang, D.; Du, J.; Zhang, Q.; Yao, Y. Flexible Quasi-solid-state Aqueous Zinc-ion Batteries: Design Principles, Functionalization Strategies, and Applications. *Adv. Energy Mater.* **2023**, *13* (18), 2300250.
(514) Chen, Q.; Liang, W.; Tang, Z.; Jin, J.; Zhang, J.; Hou, G.; Mai, L.; Tang, Y. Aqueous Ammonium Ion Storage Materials: A Structure Perspective. *Mater. Today* **2024**, *72*, 359−376.
(515) Li, X.; Han, D.; Zhang, Y.; Zhou, H.; Zhang, T.; Wang, L.; Zhang, Y. Direct Laser Scribing of All-solid-state In-plane Proton Microsupercapacitors on Ionic Covalent Organic Framework Films. *Adv. Funct. Mater.* **2025**, *35* (31), 2423854.
(516) Pameté, E.; Köps, L.; Kreth, F. A.; Pohlmann, S.; Varzi, A.; Brousse, T.; Balducci, A.; Presser, V. The Many Deaths of Supercapacitors: Degradation, Aging, and Performance Fading. *Adv. Energy Mater.* **2023**, *13* (29), 2301008.
(517) Gao, C.; Liu, J.; Han, Y.; Chen, R.; Huang, J.; Gu, Y.; Zhao, Y.; Qu, L. An Energy-adjustable, Deformable, and Packable Wireless Charging Fiber Supercapacitor. *Adv. Mater.* **2024**, *36* (49), 2413292.
(518) Liu, C.-W.; Chang-Chien, L.-R. Area Efficient High-Performance Digitally Controlled Power Management Unit. *IEEE Trans. Ind. Electron.* **2021**, *68* (3), 2437−2446.
(519) Han, W. B.; Ko, G.-J.; Yang, S. M.; Kang, H.; Lee, J. H.; Shin, J.-W.; Jang, T.-M.; Han, S.; Kim, D.-J.; Lim, J. H.; Rajaram, K.; Bandodkar, A. J.; Hwang, S.-W. Micropatterned Elastomeric Composites for Encapsulation of Transient Electronics. *ACS Nano* **2023**, *17* (15), 14822−14830.
(520) Wei, J.; Xiao, P.; Chen, T. Water-resistant Conductive Gels toward Underwater Wearable Sensing. *Adv. Mater.* **2023**, *35* (42), 2211758.
(521) Wang, Z.; Li, S.-B.; Yang, X.; Wang, H.; Xie, L.-J.; Tao, Z.-C.; Kong, Q.-Q.; Zhang, S.-C.; Jia, H.; Jiang, D.; Chen, C.-M. Towards Wearable Multifunctional Cellulose Nanofiber/Silver Nanowire/Graphene Oxide Film: Electromagnetic Protection, Antibacterial, and Motion Monitoring. *Chem. Eng. J.* **2024**, *502*, 157751.
(522) Li, H.; Zhang, H.; Liu, X.; Jie, J.; Yin, M.; Du, J. Chinese Nian Gao Inspired Textured Janus Hydrogel for Body Signal Sensing and Human Machine Interaction. *Adv. Sci.* **2025**, *12*, No. e09573.
(523) Chen, Z.; Lai, K.; Wang, A.; Ji, H.; Yu, S.; Fang, Z.; Liu, D.; Peng, J.; Lai, W. Electron Transfer-Driven Nanozymes Boost Biosensor Sensitivity via a Synergistic Signal Amplification Strategy. *ACS Nano* **2025**, *19* (9), 9282−9291.
(524) Ni, Y.; Zang, X.; Yang, Y.; Gong, Z.; Li, H.; Chen, J.; Wu, C.; Huang, J.; Lai, Y. Environmental Stability Stretchable Organic Hydrogel Humidity Sensor for Respiratory Monitoring with Ultrahigh Sensitivity. *Adv. Funct. Mater.* **2024**, *34* (38), 2402853.
(525) Li, Y.; Zhang, W.; Zhao, C.; Li, W.; Dong, E.; Xu, M.; Huang, H.; Yang, Y.; Li, L.; Zheng, L.; Mao, M.; Yao, S.; Wang, L.; Ma, J.; Wang, X.; Huang, W. Breaking the Saturation of Sensitivity for Ultrawide Range Flexible Pressure Sensors by Soft-strain Effect. *Adv. Mater.* **2024**, *36*, 2405405.
(526) Duan, Y.; Sun, Z.; Zhang, Q.; Dong, Y.; Lin, Y.; Ji, D.; Qin, X. Constructing Electrospun 3D Liquid Metal Adhesion Channel on Stretchable Yarns for Broad-Range Strain-Insensitivity Smart Textiles. *Nat. Commun.* **2025**, *16* (1), 6362.
(527) Ali, Md. A.; Hu, C.; Yuan, B.; Jahan, S.; Saleh, M. S.; Guo, Z.; Gellman, A. J.; Panat, R. Breaking the Barrier to Biomolecule Limit-of-Detection via 3D Printed Multi-Length-Scale Graphene-Coated Electrodes. *Nat. Commun.* **2021**, *12* (1), 7077.
(528) Pan, B.; Su, P.; Jin, M.; Huang, X.; Wang, Z.; Zhang, R.; Xu, H.; Liu, W.; Ye, Y. Ultrathin Hierarchical Hydrogel-Carbon Nanocomposite for Highly Stretchable Fast-Response Water-Proof Wearable Humidity Sensors. *Mater. Horiz.* **2023**, *10* (11), 5263−5276.
(529) Chang, K.; Guo, M.; Pu, L.; Dong, J.; Li, L.; Ma, P.; Huang, Y.; Liu, T. Wearable Nanofibrous Tactile Sensors with Fast Response and Wireless Communication. *Chem. Eng. J.* **2023**, *451*, 138578.
(530) Wu, L.; Li, X.; Choi, J.; Zhao, Z.; Qian, L.; Yu, B.; Park, I. Beetle-Inspired Gradient Slant Structures for Capacitive Pressure Sensor with a Broad Linear Response Range. *Adv. Funct. Mater.* **2024**, *34* (26), 2312370.
(531) Hu, F. X.; Hu, T.; Chen, S.; Wang, D.; Rao, Q.; Liu, Y.; Dai, F.; Guo, C.; Yang, H. B.; Li, C. M. Single-Atom Cobalt-Based Electrochemical Biomimetic Uric Acid Sensor with Wide Linear Range and Ultralow Detection Limit. *Nano Micro Lett.* **2021**, *13* (1), 7.
(532) Yang, R.; Dutta, A.; Li, B.; Tiwari, N.; Zhang, W.; Niu, Z.; Gao, Y.; Erdely, D.; Xin, X.; Li, T.; Cheng, H. Iontronic Pressure Sensor with High Sensitivity over Ultra-Broad Linear Range Enabled by Laser-Induced Gradient Micro-Pyramids. *Nat. Commun.* **2023**, *14* (1), 2907.
(533) Yoon, H.; Jeong, S.; Lee, B.; Hong, Y. A Site-Selective Integration Strategy for Microdevices on Conformable Substrates. *Nat. Electron.* **2024**, *7* (5), 383−395.

(534) Bai, J.; Gu, W.; Bai, Y.; Li, Y.; Yang, L.; Fu, L.; Li, S.; Li, T.; Zhang, T. Multifunctional Flexible Sensor Based on PU-TA@MXene Janus Architecture for Selective Direction Recognition. *Adv. Mater.* **2023**, *35* (35), 2302847.
(535) Ding, Q.; Luo, Y.; Shi, W.; Wang, H.; Li, J.; Zhou, Y.; Zhu, X.; Yao, D.; Wu, Z.; Tao, K.; Liu, F.; Xu, P.; Long, H.; Wan, P.; Huo, F.; Wu, J. Hydrogel-based Self-powered, Oxygen-resistant, and Flexible Sensors for Ultrasensitive and Selective NO_2 Detection. *Adv. Funct. Mater.* **2026**, *36*, No. e12817.
(536) Zhu, B.; Guo, J.; Li, W.; Luo, T.; Lei, F.; Li, G.; Yang, J. Integrated Electromechanical Structure for Iontronic Pressure Sensors with Linear High-Sensitivity Response and Robust Sensing Stability. *Adv. Funct. Mater.* **2024**, *34* (42), 2406762.
(537) Choi, J.; Oh, M. S.; Cho, A.; Ryu, J.; Kim, Y.-J.; Kang, H.; Cho, S.-Y.; Im, S. G.; Kim, S. J.; Jung, H.-T. Simple Approach to Enhance Long-Term Environmental Stability of MXene Using Initiated Chemical Vapor Deposition Surface Coating. *ACS Nano* **2023**, *17* (11), 10898−10905.
(538) Wu, Y.; Zeng, Y.; Chen, Y.; Li, C.; Qiu, R.; Liu, W. Photocurable 3D Printing of High Toughness and Self-healing Hydrogels for Customized Wearable Flexible Sensors. *Adv. Funct. Mater.* **2021**, *31* (52), 2107202.
(539) Chen, S.; Ouyang, Q.; Meng, X.; Yang, Y.; Li, C.; Miao, X.; Chen, Z.; Zhao, G.; Lei, Y.; Ghanem, B.; Gautam, S.; Cheng, J.; Yan, Z. Starfish-Inspired Wearable Bioelectronic Systems for Physiological Signal Monitoring during Motion and Real-Time Heart Disease Diagnosis. *Sci. Adv.* **2025**, *11* (14), No. eadv2406.
(540) Choi, G.; Kim, J.; Kim, H.; Bae, H.; Kim, B.; Lee, H. J.; Jang, H.; Seong, M.; Tawfik, S. M.; Kim, J. J.; Jeong, H. E. Motion-adaptive Tessellated Skin Patches with Switchable Adhesion for Wearable Electronics. *Adv. Mater.* **2025**, *37* (4), 2412271.
(541) Ye, Z.; Zhao, G.; Yang, M.; Xu, Y.; Ren, Y.; Chen, Z.; Andrabi, S. M.; Xie, J.; Gao, W.; Yan, Z.; Chen, P.-Y. A Highly Sensitive and Multiplexed Wireless Sensing System with Skin-like Compliance and Stretchability for Wearable Applications. *Sci. Adv.* **2025**, *11* (44), No. eadt4923.
(542) Ding, S.; Saha, T.; Yin, L.; Liu, R.; Khan, M. I.; Chang, A.-Y.; Lee, H.; Zhao, H.; Liu, Y.; Nazemi, A. S.; Zhou, J.; Chen, C.; Li, Z.; Zhang, C.; Earney, S.; Tang, S.; Djassemi, O.; Chen, X.; Lin, M.; Sandhu, S. S.; Moon, J.-M.; Moonla, C.; Nandhakumar, P.; Park, Y.; Mahato, K.; Xu, S.; Wang, J. A Fingertip-Wearable Microgrid System for Autonomous Energy Management and Metabolic Monitoring. *Nat. Electron.* **2024**, *7* (9), 788−799.
(543) Xia, X.; Chen, X.; Shi, J.; Li, Z.; Jiang, B.; Huang, K.; Guo, M.; Yang, Z.; Liao, Z.; Song, C.; Guo, C. F. Micropillar-Enabled Tough Adhesion and Enhanced Sensing. *Matter* **2025**, *8* (10), 102221.
(544) Huang, W.; Xu, Y.; Yang, Y.; Sun, J.; Hu, M.; Hao, F.; Xiao, F. Wearable Sensor for Continuous Monitoring Multiple Biofluids: Improved Performances by Conductive Metal-organic Framework with Dual-redox Sites on Flexible Graphene Fiber Microelectrode. *Adv. Funct. Mater.* **2025**, *35* (31), 2424018.
(545) Tabatabaee, R. S.; Naghdi, T.; Peyravian, M.; Kiani, M. A.; Golmohammadi, H. An Invisible Dermal Nanotattoo-Based Smart Wearable Sensor for eDiagnostics of Jaundice. *ACS Nano* **2024**, *18* (41), 28012−28025.
(546) Park, K.; Jeong, H.; Jung, Y.; Suh, J.-H.; Je, M.; Kim, J. Using Biopotential and Bio-Impedance for Intuitive Human-Robot Interaction. *Nat. Rev. Electr. Eng.* **2025**, *2* (8), 555−571.
(547) Yang, B.; Wang, H.; Kong, J.; Fang, X. Long-Term Monitoring of Ultratrace Nucleic Acids Using Tetrahedral Nanostructure-Based NgAgo on Wearable Microneedles. *Nat. Commun.* **2024**, *15* (1), 1936.
(548) Wu, M.; Li, L.; Yu, R.; Zhang, Z.; Zhu, B.; Lin, J.; Zhou, L.; Su, B. Tailored Diffusion Limiting Membrane for Microneedle Glucose Sensors with Wide Linear Range. *Talanta* **2024**, *273*, 125933.
(549) He, J.; Xiao, P.; Lu, W.; Shi, J.; Zhang, L.; Liang, Y.; Pan, C.; Kuo, S.-W.; Chen, T. A Universal High Accuracy Wearable Pulse Monitoring System via High Sensitivity and Large Linearity Graphene Pressure Sensor. *Nano Energy* **2019**, *59*, 422−433.
(550) Min, S.; An, J.; Lee, J. H.; Kim, J. H.; Joe, D. J.; Eom, S. H.; Yoo, C. D.; Ahn, H.-S.; Hwang, J.-Y.; Xu, S.; Rogers, J. A.; Lee, K. J. Wearable Blood Pressure Sensors for Cardiovascular Monitoring and Machine Learning Algorithms for Blood Pressure Estimation. *Nat. Rev. Cardiol.* **2025**, *22* (9), 629−648.
(551) Lee, J.-C.; Kim, S. Y.; Song, J.; Jang, H.; Kim, M.; Kim, H.; Choi, S. Q.; Kim, S.; Jolly, P.; Kang, T.; Park, S.; Ingber, D. E. Micrometer-Thick and Porous Nanocomposite Coating for Electrochemical Sensors with Exceptional Antifouling and Electroconducting Properties. *Nat. Commun.* **2024**, *15* (1), 711.
(552) Pan, L.; Cai, P.; Mei, L.; Cheng, Y.; Zeng, Y.; Wang, M.; Wang, T.; Jiang, Y.; Ji, B.; Li, D.; Chen, X. A Compliant Ionic Adhesive Electrode with Ultralow Bioelectronic Impedance. *Adv. Mater.* **2020**, *32* (38), 2003723.
(553) Chen, W.; Shi, X.-L.; Li, M.; Liu, T.; Mao, Y.; Liu, Q.; Dargusch, M.; Zou, J.; Lu, G. Q. M.; Chen, Z.-G. Nanobinders Advance Screen-Printed Flexible Thermoelectrics. *Science* **2024**, *386* (6727), 1265−1271.
(554) Kim, K. Y.; Kang, J.; Song, S.; Lee, K.; Hwang, S.-W.; Ko, S. H.; Jeon, H.; Han, J.-H.; Lee, W. An Ultrathin Organic-Inorganic Integrated Device for Optical Biomarker Monitoring. *Nat. Electron.* **2024**, *7* (10), 914−923.
(555) Chen, C.; Chen, J.; Han, H.; Chao, L.; Hu, J.; Niu, T.; Dong, H.; Yang, S.; Xia, Y.; Chen, Y.; Huang, W. Perovskite Solar Cells Based on Screen-Printed Thin Films. *Nature* **2022**, *612* (7939), 266−271.
(556) Han, X.; Lin, X.; Sun, Y.; Huang, L.; Huo, F.; Xie, R. Advancements in Flexible Electronics Fabrication: Film Formation, Patterning, and Interface Optimization for Cutting-Edge Healthcare Monitoring Devices. *ACS Appl. Mater. Interfaces* **2024**, *16*, 54976.
(557) Wang, Y.; He, J.; Cao, D.; Cakmak, E.; Zhao, X.; Wu, Q.; Zhao, Y.; Ren, H.; Sun, X.; Li, Y.; Zhu, H. Opening Twisted Polymer Chains for Simultaneously High Printability and Battery Fast-Charge. *Energy Storage Mater.* **2023**, *55*, 42−54.
(558) Yan, B.; Liu, S.; Yuan, Y.; Hou, X.; Zhou, M.; Yu, Y.; Wang, Q.; He, C.; Wang, P. Polymer-regulating MXene@dopamine Electroactive Gel-inks for Textile-based Multi-protective Wearables. *Adv. Funct. Mater.* **2024**, *34* (36), 2401097.
(559) Kumar, P.; Singh, S.; Gupta, B. K. Future Prospects of Luminescent Nanomaterial Based Security Inks: From Synthesis to Anti-Counterfeiting Applications. *Nanoscale* **2016**, *8* (30), 14297−14340.
(560) Ji, W.; Liu, H.; Liu, Y.; Zhang, W.; Zhou, T.; Liu, X.; Tao, C.; Dai, J.; Zha, B.; Xie, R.; Wu, J.; Wu, Q.; Zhang, W.; Li, L.; Huo, F. Large-Scale Fully Printed "Lego Bricks" Type Wearable Sweat Sensor for Physical Activity Monitoring. *Npj Flexible Electron.* **2023**, *7* (1), 53.
(561) Dou, X.; Wang, H.; Liu, Z.; Zheng, B.; Zheng, Z.; Liu, X.; Guo, R. Epoxy Resin-Assisted Cu Catalytic Printing for Flexible Cu Conductors on Smooth and Rough Substrates. *ACS Appl. Mater. Interfaces* **2023**, *15* (44), 51915−51925.
(562) Tzianni, E. I.; Sakkas, V. A.; Prodromidis, M. I. Wax Screen-Printable Ink for Massive Fabrication of Negligible-to-Nil Cost Fabric-Based Microfluidic (Bio)Sensing Devices for Colorimetric Analysis of Sweat. *Talanta* **2024**, *269*, 125475.
(563) Liang, J.; Tong, K.; Pei, Q. A Water-Based Silver-Nanowire Screen-Print Ink for the Fabrication of Stretchable Conductors and Wearable Thin-Film Transistors. *Adv. Mater.* **2016**, *28* (28), 5986−5996.
(564) Wu, H.; Xie, Y.; Ma, Y.; Zhang, B.; Xia, B.; Zhang, P.; Qian, W.; He, D.; Zhang, X.; Li, B.; Nan, C. Aqueous MXene/Xanthan Gum Hybrid Inks for Screen-printing Electromagnetic Shielding, Joule Heater, and Piezoresistive Sensor. *Small* **2022**, *18* (16), 2107087.
(565) Liu, H.; Zhang, Y.; Huang, Y.; Liu, Y.; Zhang, Y.; Deng, W.; Zou, G.; Yang, Y.; Hou, H.; Ji, X. Exploiting Interfacial Ionic Confinement to Suppress PVDF Phase Separation for High-Performance Solid-State Li Battery. *Energy Storage Mater.* **2025**, *83*, 104716.

https://doi.org/10.1021/acs.chemrev.5c00801
Chem. Rev. XXXX, XXX, XXX−XXX

(566) Kang, G.; Zhong, Y.; Du, X.; Shao, Z.; Jiang, J.; Wang, X.; Li, W.; Guo, S.; Gao, L.; Fang, Z.; Zheng, G. Low-Temperature Sintering of Silver-Ammonia Complex Organic Composite Ink Shows High Conductivity for Humidity Sensors. *Mater. Des.* **2023**, *234*, 112374.
(567) Ma, J.; Fei, Y.; Zhang, J.; Wu, H. Wearable Multiple Sensing Platform for Enhanced Biomolecules Monitoring in Food. *Food Chem.* **2025**, *469*, 142540.
(568) Phillips, C.; Beynon, D.; Hamblyn, S.; Davies, G.; Gethin, D.; Claypole, T. A Study of the Abrasion of Squeegees Used in Screen Printing and Its Effect on Performance with Application in Printed Electronics. *Coatings* **2014**, *4* (2), 356−379.
(569) Zhu, L.; Zhou, X.; Zhang, J.; Xia, Y.; Wu, M.; Zhang, Y.; Lu, Z.; Li, W.; Liu, L.; Liu, H.; Yu, J.; Xiong, J. Self-Adhesive Elastic Conductive Ink with High Permeability and Low Diffusivity for Direct Printing of Universal Textile Electronics. *ACS Nano* **2024**, *18* (51), 34750−34762.
(570) Yin, L.; Cao, M.; Kim, K. N.; Lin, M.; Moon, J.-M.; Sempionatto, J. R.; Yu, J.; Liu, R.; Wicker, C.; Trifonov, A.; Zhang, F.; Hu, H.; Moreto, J. R.; Go, J.; Xu, S.; Wang, J. A Stretchable Epidermal Sweat Sensing Platform with an Integrated Printed Battery and Electrochromic Display. *Nat. Electron.* **2022**, *5* (10), 694−705.
(571) Tang, C.; Yi, W.; Xu, M.; Jin, Y.; Zhang, Z.; Chen, X.; Liao, C.; Kang, M.; Gao, S.; Smielewski, P.; Occhipinti, L. G. A Deep Learning-Enabled Smart Garment for Accurate and Versatile Monitoring of Sleep Conditions in Daily Life. *Proc. Natl. Acad. Sci. U. S. A.* **2025**, *122* (7), No. e2420498122.
(572) Zheng, S.; Wang, H.; Das, P.; Zhang, Y.; Cao, Y.; Ma, J.; Liu, S. F.; Wu, Z. Multitasking MXene Inks Enable High-performance Printable Microelectrochemical Energy Storage Devices for All-flexible Self-powered Integrated Systems. *Adv. Mater.* **2021**, *33* (10), 2005449.
(573) Zhang, Y.; Li, Z.; Fan, X.; Liu, Y.; Li, Z.; Zheng, Z.; Lin, Z.; Zhang, W.; Mu, Q.; Mo, G.; Xia, Y.; Mou, L. A Fully Integrated, Non-Invasive, and Multimodal Wearable Device for Sweat Stimulation, Collection and Multiple Physiological Signals Analysis. *Chem. Eng. J.* **2025**, *505*, 159209.
(574) Kim, Y. Y.; Yang, T.-Y.; Suhonen, R.; Kemppainen, A.; Hwang, K.; Jeon, N. J.; Seo, J. Roll-to-Roll Gravure-Printed Flexible Perovskite Solar Cells Using Eco-Friendly Antisolvent Bathing with Wide Processing Window. *Nat. Commun.* **2020**, *11* (1), 5146.
(575) Sutherland, L. J.; Vak, D.; Gao, M.; Peiris, T. A. N.; Jasieniak, J.; Simon, G. P.; Weerasinghe, H. Vacuum-Free and Solvent-Free Deposition of Electrodes for Roll-to-Roll Fabricated Perovskite Solar Cells. *Adv. Energy Mater.* **2022**, *12* (40), 2202142.
(576) Park, J.; Shin, K.; Lee, C. Roll-to-Roll Coating Technology and Its Applications: A Review. *Int. J. Precis. Eng. Manuf.* **2016**, *17* (4), 537−550.
(577) Li, A.; Zhang, P.; Kan, E.; Gong, J. Wettability Adjustment to Enhance Mass Transfer for Heterogeneous Electrocatalysis and Photocatalysis. *Escience* **2024**, *4* (1), 100157.
(578) Lee, S. H.; Lee, S. Fabrication of Comb-Structured Acceleration Sensors by Roll-to-Roll Gravure Printing. *Int. J. Precis. Eng. Manuf. green Technol.* **2022**, *9* (2), 409−420.
(579) Wang, Y.; Cao, D.; Sun, X.; Ren, H.; Ji, T.; Jin, X.; Morse, J.; Stewart, B.; Zhu, H. Large-Scale Manufacturing of Pattern-Integrated Paper Li-Ion Microbatteries through Roll-to-Roll Flexographic Printing. *Adv. Mater. Technol.* **2022**, *7* (11), 2200303.
(580) Cagnani, G. R.; Ibáñez-Redín, G.; Tirich, B.; Gonçalves, D.; Balogh, D. T.; Oliveira, O. N. Fully-Printed Electrochemical Sensors Made with Flexible Screen-Printed Electrodes Modified by Roll-to-Roll Slot-Die Coating. *Biosens. Bioelectron.* **2020**, *165*, 112428.
(581) Liu, Y.; Wang, Z.; Pan, Y.; Liu, T.; Zhang, Y.; Zhang, Q.; Mo, L.; Luo, Q.; Ma, C. The Influence Mechanism of Ink Viscosity on Ink Transfer Rates and Film Defects of the Roll-to-Roll Printed Organic Photoactive Layers. *Sci. China Mater.* **2024**, *67* (8), 2600−2610.
(582) Mahajan, A.; Hyun, W. J.; Walker, S. B.; Rojas, G. A.; Choi, J.; Lewis, J. A.; Francis, L. F.; Frisbie, C. D. A Self-aligned Strategy for Printed Electronics: Exploiting Capillary Flow on Microstructured Plastic Surfaces. *Adv. Electron. Mater.* **2015**, *1* (9), 1500137.
(583) Wong, H. C.; Grenci, G.; Wu, J.; Viasnoff, V.; Low, H. Y. Roll-to-Roll Fabrication of Residual-Layer-Free Micro/Nanoscale Membranes with Precise Pore Architectures and Tunable Surface Textures. *Ind. Eng. Chem. Res.* **2018**, *57* (41), 13759−13768.
(584) Ulloa, A. M.; Glassmaker, N.; Oduncu, M. R.; Xu, P.; Wei, A.; Cakmak, M.; Stanciu, L. Roll-to-Roll Manufactured Sensors for Nitroaromatic Organophosphorus Pesticides Detection. *ACS Appl. Mater. Interfaces* **2021**, *13* (30), 35961−35971.
(585) Zhang, C.; Chen, R.; Luo, W.; Wang, J.; Chen, D.; Chen, P.; Liu, S.; Xie, Y.; Zhou, W.; Luo, T. Batch Fabrication of Paper-Based Waterproof Flexible Pressure Sensors Enabled by Roll-to-Roll Lamination. *ACS Appl. Mater. Interfaces* **2023**, *15* (35), 41950−41960.
(586) Yin, Z.; Clark, K. M.; Ray, T. R. Emerging Additive Manufacturing Methods for Wearable Sensors: Opportunities to Expand Access to Personalized Health Monitoring. *Adv. Sens. Res.* **2024**, *3* (3), 2300137.
(587) Wu, J.; Li, S.; Lan, Y.; Chen, S.; Li, Z.; Li, Z. Research Progress on 3D Printed Flexible Supercapacitors Based on Nanomaterial Inks. *J. Energy Storage* **2025**, *118*, 116140.
(588) Vaishnav, K. N.; Verma, R. P.; Saha, B. Advancements in 3D-Printed Wearable Sensors: A Modern Healthcare. *Mater. Today* **2025**, *89*, 502−535.
(589) Ma, T.; Zhang, Y.; Ruan, K.; Guo, H.; He, M.; Shi, X.; Guo, Y.; Kong, J.; Gu, J. Advances in < span Style = ″font-Variant:Small-Caps;″>3D Printing for Polymer Composites: A Review. *Infomat* **2024**, *6* (6), No. e12568.
(590) Song, W.; Li, H.; Li, F. The Integration of Environmental Governance and 3D Printing Technology: Current Situation and Prospects. *Chem. Eng. J.* **2025**, *505*, 159498.
(591) Wei, Y.-H.; Guo, Z.-F.; Wang, Y.-F.; Lin, T.; Hou, W.-W.; Duan, S.-W.; Tao, L.-Q.; Tian, H.; Yang, Y.; Ren, T.-L. Frequency-Tunable Sound Amplification in a Conch-like Cavity with Graphene Thermoacoustic Resonance. *Sci. Adv.* **2025**, *11* (23), No. eadv2801.
(592) Galliani, M.; Ismailova, E.; Azizian, P.; Makhinia, A.; Cabot, J. M. Vertical Textile Microfluidics: Advancing on-Garment Sweat Sampling for Real-Time Biosensing. *Npj Flexible Electron.* **2025**, *9* (1), 38.
(593) Khan, K.; Hussain, M. I.; Tareen, A. K.; Asghar, A.; Hamza, M.; Chen, Z. Advances in Vat Photopolymerization 3D Printing: Multifunctional Materials, Process Innovations, and Emerging Applications. *Mater. Sci. Eng.: R: Rep.* **2026**, *167*, 101120.
(594) Yi, J.; Yang, S.; Yue, L.; Lei, I. M. Digital Light Processing 3D Printing of Flexible Devices: Actuators, Sensors and Energy Devices. *Microsyst. Nanoeng.* **2025**, *11* (1), 51.
(595) Vidler, C.; Halwes, M.; Kolesnik, K.; Segeritz, P.; Mail, M.; Barlow, A. J.; Koehl, E. M.; Ramakrishnan, A.; Caballero Aguilar, L. M.; Nisbet, D. R.; Scott, D. J.; Heath, D. E.; Crozier, K. B.; Collins, D. J. Dynamic Interface Printing. *Nature* **2024**, *634* (8036), 1096−1102.
(596) Fan, P.; Liu, Y.; Pan, Y.; Ying, Y.; Ping, J. Three-Dimensional Micro- and Nanomanufacturing Techniques for High-Fidelity Wearable Bioelectronics. *Nat. Rev. Electr. Eng.* **2025**, *2* (6), 390−406.
(597) Zhao, Y. C.; Wang, Z.; Nasser, A.; Sun, A.; Wang, Z.; Zhang, Y.; Ren, J.; Zhao, H.; Yap, N. A.; Wang, Y.; Li, Z.; Butcher, K. S.; Passam, F.; Ang, T.; Ju, L. A. Rapid Glass-substrate Digital Light 3D Printing Enables Anatomically Accurate Stroke Patient-specific Carotid Artery-on-chips for Personalized Thrombosis Investigation. *Adv. Mater.* **2025**, No. e08890.
(598) Kim, W. Y.; Yoon, S. M.; Park, S. R.; Kim, M. S.; Lee, S. H.; Choi, S. H.; Shin, S.; Kwon, S.; Kim, C. J.; Lee, K. M.; Nam, S.-H.; Bae, S.; Kang, P. M.; Fang, N. X.; Kim, S.; Cho, Y. T. Digitally Fabricated 3D Slippery Architectures for Multifunctional Liquid Manipulation. *Nat. Commun.* **2025**, *16* (1), 9026.
(599) Ho, M.; Ramirez, A. B.; Akbarnia, N.; Croiset, E.; Prince, E.; Fuller, G. G.; Kamkar, M. Direct Ink Writing of Conductive Hydrogels. *Adv. Funct. Mater.* **2025**, *35* (22), 2415507.
(600) Ng, A.; Telles, R.; Riley, K. S.; Lewis, J. A.; Cook, C. C.; Lee, E.; Yang, S. Coaxial Direct Ink Writing of Cholesteric Liquid Crystal Elastomers in 3D Architectures. *Adv. Mater.* **2025**, *37* (10), 2416621.

https://doi.org/10.1021/acs.chemrev.5c00801
Chem. Rev. XXXX, XXX, XXX−XXX

(601) Reis Carneiro, M.; Lopes, T.; Silva, A. F.; Majidi, C.; Tavakoli, M. Micropatterned Biphasic Printed Electrodes for High-fidelity On-skin Bioelectronics. *Adv. Funct. Mater.* **2025**, No. e05419.
(602) Liu, L.; Mo, L.; Han, S.; Liu, X.; Sun, J.; Han, Z.; Sun, Z.; Geng, M.; Hu, H.; Zhang, J.; Zhang, H.; Xin, Z.; Hu, K.; Li, H. Enhancing Flexible Capacitive Sensor Performance through the Synergy of Thermally Expandable Microspheres and Carbon Nanotubes via 3D Direct Ink Writing. *Adv. Funct. Mater.* **2025**, No. e14093.
(603) Shan, L.; Xue, Y.; Chen, X.; Wang, Y.; Feng, Y.; Dong, L.; Wang, C.; Zhang, P.; Wang, F.; Guo, L.; Liu, J. Mechanically Compliant and Impedance Matching Hydrogel Bioelectronics for Low-voltage Peripheral Neuromodulation. *Adv. Mater.* **2025**, No. e11014.
(604) Chen, H.; Chen, Z.; Liu, Z.; Xiong, J.; Yan, Q.; Fei, T.; Zhao, X.; Xue, F.; Zheng, H.; Lian, H.; Chen, Y.; Xu, L.; Peng, Q.; He, X. From Coils to Crawls: A Snake-Inspired Soft Robot for Multimodal Locomotion and Grasping. *Nano Micro Lett.* **2025**, *17* (1), 243.
(605) Brown, N. C.; Ames, D. C.; Mueller, J. Multimaterial Extrusion 3D Printing Printheads. *Nat. Rev. Mater.* **2025**, *10*, 807.
(606) Lee, B.; Cho, H.; Moon, S.; Ko, Y.; Ryu, Y.-S.; Kim, H.; Jeong, J.; Chung, S. Omnidirectional Printing of Elastic Conductors for Three-Dimensional Stretchable Electronics. *Nat. Electron.* **2023**, *6* (4), 307−318.
(607) Zhou, S.; Lin, F.; Guan, Q.; Ding, L.; Saiz, E.; Li, M. Fluorescent Hydrogel Platform for 3D Information Storage and Encryption Anti-Counterfeiting. *Device* **2025**, *3* (6), 100722.
(608) Zhang, B.; Meng, Z.; Wang, Y. Thermally Responsive Multistable Metanet with Enhanced Energy Absorption Capacity. *Adv. Funct. Mater.* **2026**, *36*, No. e10749.
(609) Jones, L. S.; Rodriguez Cetina Biefer, H.; Mekkattu, M.; Thijssen, Q.; Amicone, A.; Bock, A.; Weisskopf, M.; Zorndt, D.; Meier, D.; Zheng, L.; Generali, M.; Katzschmann, R. K.; Dzemali, O. Volumetric 3D Printing and Melt-electrowriting to Fabricate Implantable Reinforced Cardiac Tissue Patches. *Adv. Mater.* **2025**, *37*, 2504765.
(610) Chen, X.; Fang, G.; Liao, W.-H.; Wang, C. C. L. Field-Based Toolpath Generation for 3D Printing Continuous Fibre Reinforced Thermoplastic Composites. *Addit. Manuf.* **2022**, *49*, 102470.
(611) Truby, R. L.; Lewis, J. A. Printing Soft Matter in Three Dimensions. *Nature* **2016**, *540* (7633), 371−378.
(612) Zhu, Y.; Qin, J.; Shi, G.; Sun, C.; Ingram, M.; Qian, S.; Lu, J.; Zhang, S.; Zhong, Y. L. A Focus Review on 3D Printing of Wearable Energy Storage Devices. *Carbon Energy* **2022**, *4* (6), 1242−1261.
(613) Han, L.; Li, K.; Wang, Z.; Men, W.; Wu, X.; Sun, X.; Zhang, J.; Cheng, J. 3D Printing Flexible Wearable Electronics with Diversified Environmentally Adaptive for Biomechanical Energy Harvesting and Personal Electromagnetic Safety. *Adv. Funct. Mater.* **2025**, *35* (37), 2424743.
(614) Shi, G.; Tian, M.; Chen, Y.; Zhong, L.; Zhang, W.; Chen, Z.; Sun, S.; Xia, R.; Iwuoha, E. I.; Peng, X. Nanocellulose-Based Ink for Vertically 3D Printing Micro-Architectures with High-Resolution. *Adv. Funct. Mater.* **2024**, *34* (17), 2311060.
(615) Qu, H.; Liu, K.; Liu, J.; Gao, C.; Ruan, C. A Heterogeneous Pore Design Algorithm for Material Extrusion Additive Manufacturing. *Addit. Manuf.* **2024**, *94*, 104449.
(616) Kang, S. W.; Mueller, J. Multiscale 3D Printing via Active Nozzle Size and Shape Control. *Sci. Adv.* **2024**, *10* (23), No. eadn7772.
(617) Bai, J.; Liu, D.; Tian, X.; Wang, Y.; Cui, B.; Yang, Y.; Dai, S.; Lin, W.; Zhu, J.; Wang, J.; Xu, A.; Gu, Z.; Zhang, S. Coin-Sized, Fully Integrated, and Minimally Invasive Continuous Glucose Monitoring System Based on Organic Electrochemical Transistors. *Sci. Adv.* **2024**, *10* (16), No. eadl1856.
(618) Yang, J.; Gong, X.; Zheng, Y.; Duan, H.; Chen, S.; Wu, T.; Yi, C.; Jiang, L.; Haick, H. Microneedle-Based Integrated Pharmacokinetic and Pharmacodynamic Evaluation Platform for Personalized Medicine. *Nat. Commun.* **2025**, *16* (1), 6260.
(619) Xiong, X.; Chen, Y.; Wang, Z.; Liu, H.; Le, M.; Lin, C.; Wu, G.; Wang, L.; Shi, X.; Jia, Y.-G.; Zhao, Y. Polymerizable Rotaxane Hydrogels for Three-Dimensional Printing Fabrication of Wearable Sensors. *Nat. Commun.* **2023**, *14* (1), 1331.
(620) Zhang, M.; Zhao, L.; Tian, F.; Zhao, X.; Zhang, Y.; Yang, X.; Huang, W.; Yu, R. Bionic Artificial Skin Based on Self-Healable Ionogel Composites with Tailored Mechanics and Robust Interfaces. *Adv. Mater.* **2024**, *36* (35), 2405776.
(621) Ahmed, S.; Momin, M.; Ren, J.; Lee, H.; Zhou, T. Self-Assembly Enabled Printable Asymmetric Self-Insulated Stretchable Conductor for Human Interface. *Adv. Mater.* **2024**, *36* (25), 2400082.
(622) Tang, H.; Yang, Y.; Liu, Z.; Li, W.; Zhang, Y.; Huang, Y.; Kang, T.; Yu, Y.; Li, N.; Tian, Y.; Liu, X.; Cheng, Y.; Yin, Z.; Jiang, X.; Chen, X.; Zang, J. Injectable Ultrasonic Sensor for Wireless Monitoring of Intracranial Signals. *Nature* **2024**, *630* (8015), 84−90.
(623) Chang, A.-Y.; Lin, M.; Yin, L.; Reynoso, M.; Ding, S.; Liu, R.; Dugas, Y.; Casanova, A.; Park, G.; Li, Z.; Luan, H.; Askarinam, N.; Zhang, F.; Xu, S.; Wang, J. Integration of Chemical and Physical Inputs for Monitoring Metabolites and Cardiac Signals in Diabetes. *Nat. Biomed. Eng.* **2025**, DOI: 10.1038/s41551-025-01439-z.
(624) Abdolmaleki, H.; Kidmose, P.; Agarwala, S. Droplet-Based Techniques for Printing of Functional Inks for Flexible Physical Sensors. *Adv. Mater.* **2021**, *33* (20), 2006792.
(625) Zhang, C.; Zhang, L.; Pu, Z.; Bao, B.; Ouyang, W.; Li, D. Fabricating 1D Stretchable Fiber-Shaped Electronics Based on Inkjet Printing Technology for Wearable Applications. *Nano Energy* **2023**, *113*, 108574.
(626) Ren, X.; Qiu, F.; Deng, W.; Fang, X.; Wu, Y.; Yu, S.; Liu, X.; Grigorian, S.; Shi, J.; Jie, J.; Zhang, X.; Zhang, X. Topology-Mediated Molecule Nucleation Anchoring Enables Inkjet Printing of Organic Semiconducting Single Crystals for High-Performance Printed Electronics. *ACS Nano* **2023**, *17* (24), 25175−25184.
(627) Hu, G.; Yang, L.; Yang, Z.; Wang, Y.; Jin, X.; Dai, J.; Wu, Q.; Liu, S.; Zhu, X.; Wang, X.; Wu, T.-C.; Howe, R. C. T.; Albrow-Owen, T.; Ng, L. W. T.; Yang, Q.; Occhipinti, L. G.; Woodward, R. I.; Kelleher, E. J. R.; Sun, Z.; Huang, X.; Zhang, M.; Bain, C. D.; Hasan, T. A General Ink Formulation of 2D Crystals for Wafer-Scale Inkjet Printing. *Sci. Adv.* **2020**, *6* (33), No. eaba5029.
(628) Ni, M.; Zhuo, Z.; Liu, B.; Han, X.; Yang, J.; Sun, L.; Yang, Y.; Cai, J.; An, X.; Bai, L.; Xu, M.; Lin, J.; Feng, Q.; Xie, G.; Wu, Y.; Huang, W. Intrinsically Stretchable Fully π-Conjugated Polymers with Inter-Aggregate Capillary Interaction for Deep-Blue Flexible Inkjet-Printed Light-Emitting Diodes. *Nat. Commun.* **2025**, *16* (1), 330.
(629) McKerricher, G.; Vaseem, M.; Shamim, A. Fully Inkjet-Printed Microwave Passive Electronics. *Microsyst. Nanoeng.* **2017**, *3* (1), 16075.
(630) Wang, Y.; Zhang, Y.-Z.; Dubbink, D.; Ten Elshof, J. E. Inkjet Printing of δ-MnO2 Nanosheets for Flexible Solid-State Micro-Supercapacitor. *Nano Energy* **2018**, *49*, 481−488.
(631) Bae, K.; Heo, B.; Hwang, K.; Jo, E.; Kang, Y.; Pyo, S.; Kim, J. Washable Heat-Resistant and Inkjet-Printed Devices on Cotton Fabric for Wearable Applications. *Nat. Commun.* **2025**, *16* (1), 8615.
(632) Gupta, D.; Derman, I. D.; Xu, C.; Huang, Y.; Ozbolat, I. T. Droplet-Based Bioprinting. *Nat. Rev. Methods Primers* **2025**, *5* (1), 25.
(633) Mohan, N.; Ahuir-Torres, J. I.; Kotadia, H. R.; Elger, G. Laser Sintering of Cu Particle-Free Inks for High-Performance Printed Electronics. *Npj Flexible Electron.* **2025**, *9* (1), 18.
(634) Gunasekaran, N. K.; Jalajamony, H. M.; Adhinarayanan, S.; De, S.; Adu, R.; Strobel, S.; Ramesh, G. T.; Fernandez, R. E. Direct Printing of Metal Oxide Nanostructures for Wearable Electrochemical Sensing. *Sci. Rep.* **2025**, *15* (1), 22380.
(635) Zhao, D.; Zhou, H.; Wang, Y.; Yin, J.; Huang, Y. Drop-on-Demand (DOD) Inkjet Dynamics of Printing Viscoelastic Conductive Ink. *Addit. Manuf.* **2021**, *48*, 102451.
(636) Shah, R.; Mohan, R. V. Computational Modeling of Droplet-Based Printing Using Multiphase Volume of Fluid (VOF) Method: Prediction of Flow, Spread Behavior, and Printability. *Fluids* **2025**, *10* (5), 123.

(637) Hamad, A.; Archacki, A.; Mian, A. Characteristics of Nanosilver Ink (UTDAg) Microdroplets and Lines on Polyimide during Inkjet Printing at High Stage Velocity. *Mater. Adv.* **2020**, *1* (1), 99−107.
(638) You, K.; Wang, Z.; Lin, J.; Guo, X.; Lin, L.; Liu, Y.; Li, F.; Huang, W. On-demand Picoliter-level-droplet Inkjet Printing for Micro Fabrication and Functional Applications. *Small* **2024**, *20* (46), 2402638.
(639) Steinhaus, B.; Spicer, P. T.; Shen, A. Q. Droplet Size Effects on Film Drainage between Droplet and Substrate. *Langmuir* **2006**, *22* (12), 5308−5313.
(640) Wu, Y.; Yang, X.; Gupta, D.; Alioglu, M. A.; Qin, M.; Ozbolat, V.; Li, Y.; Ozbolat, I. T. Dissecting the Interplay Mechanism among Process Parameters toward the Biofabrication of High-quality Shapes in Embedded Bioprinting. *Adv. Funct. Mater.* **2024**, *34* (21), 2313088.
(641) Ahmadi, M.; Ehrmann, K.; Koch, T.; Liska, R.; Stampfl, J. From Unregulated Networks to Designed Microstructures: Introducing Heterogeneity at Different Length Scales in Photopolymers for Additive Manufacturing. *Chem. Rev.* **2024**, *124* (7), 3978−4020.
(642) Wang, M.; Ye, C.; Yang, Y.; Mukasa, D.; Wang, C.; Xu, C.; Min, J.; Solomon, S. A.; Tu, J.; Shen, G.; Tang, S.; Hsiai, T. K.; Li, Z.; McCune, J. S.; Gao, W. Printable Molecule-Selective Core-Shell Nanoparticles for Wearable and Implantable Sensing. *Nat. Mater.* **2025**, *24* (4), 589−598.
(643) Ma, S.; Wan, Z.; Wang, C.; Song, Z.; Ding, Y.; Zhang, D.; Chan, C. L. J.; Shu, L.; Huang, L.; Yang, Z.; Wang, F.; Bai, J.; Fan, Z.; Lin, Y. Ultra-Sensitive and Stable Multiplexed Biosensors Array in Fully Printed and Integrated Platforms for Reliable Perspiration Analysis. *Adv. Mater.* **2024**, *36* (24), 2311106.
(644) Lee, Y.; Carnicer-Lombarte, A.; Han, S.; Woodington, B. J.; Chai, S.; Polyravas, A. G.; Velasco-Bosom, S.; Kim, E.; Malliaras, G. G.; Jung, S. Tunable Organic Active Neural Probe Enabling Near-Sensor Signal Processing. *Adv. Mater.* **2023**, *35* (38), 2301782.
(645) Baek, S.; Lee, Y.; Baek, J.; Kwon, J.; Kim, S.; Lee, S.; Strunk, K.-P.; Stehlin, S.; Melzer, C.; Park, S.-M.; Ko, H.; Jung, S. Spatiotemporal Measurement of Arterial Pulse Waves Enabled by Wearable Active-Matrix Pressure Sensor Arrays. *ACS Nano* **2022**, *16* (1), 368−377.
(646) Liu, D.; Tian, X.; Bai, J.; Wang, S.; Dai, S.; Wang, Y.; Wang, Z.; Zhang, S. A Wearable In-Sensor Computing Platform Based on Stretchable Organic Electrochemical Transistors. *Nat. Electron.* **2024**, *7* (12), 1176−1185.
(647) Xu, C.; Song, Y.; Sempionatto, J. R.; Solomon, S. A.; Yu, Y.; Nyein, H. Y. Y.; Tay, R. Y.; Li, J.; Heng, W.; Min, J.; Lao, A.; Hsiai, T. K.; Sumner, J. A.; Gao, W. A Physicochemical-Sensing Electronic Skin for Stress Response Monitoring. *Nat. Electron.* **2024**, *7* (2), 168−179.
(648) Huang, B.; Wu, S.; Liu, J.; Liu, J.; Peng, B.; Zhou, Z. Aerosol Jet Printing of Polyelectrolyte-Modified MXene Ink for a Multifunctional Humidity and Temperature Flexible Sensor. *Chem. Eng. J.* **2025**, *519*, 165403.
(649) Ritchie, S. M.; Hu, C.; Panat, R. Realizing Arbitrary 3D Microarchitectures with Curved and Near-Sharp Segments via Toolpath Strategies in Aerosol Jet Printing. *Addit. Manuf.* **2024**, *95*, 104549.
(650) Mosa, Md. A.; Jo, J. Y.; Park, S.; Kwon, K. Aerosol Printing of 3D Conductive Microstructures via Precision Dot Modulation. *Small* **2025**, *21* (31), 2504037.
(651) Fassler, A. L.; Kohlmeyer, R. R.; Rajput, S.; Horrocks, G. A.; Deneault, J. R.; Durstock, M. F. Study on the Feasibility of Combined 3D Printing for Integrated and Conformal Batteries. *J. Power Sources* **2024**, *600*, 234241.
(652) Mazzotta, A.; Taccola, S.; Cesini, I.; Sanchez Sifuentes, M.; Harris, R. A.; Mattoli, V. Low-Voltage Wearable Tactile Display with Thermo-Pneumatic Actuation. *Npj Flexible Electron.* **2025**, *9* (1), 70.
(653) Niu, Y.; Wang, Z.; Li, Y.; Huang, B.; Ma, T.; Jiang, X.; Cheng, H.; Zhang, K.; Yi, C. Ultrathin MXene/Ag-Ag Nanocomposite Films for 3D-Conformal Electromagnetic Shielding via Aerosol Jet Printing. *Chem. Eng. J.* **2025**, *506*, 160122.
(654) Priyadarshi, A.; Bin Shahrani, S.; Choma, T.; Zrodowski, L.; Qin, L.; Leung, C. L. A.; Clark, S. J.; Fezzaa, K.; Mi, J.; Lee, P. D.; Eskin, D.; Tzanakis, I. New Insights into the Mechanism of Ultrasonic Atomization for the Production of Metal Powders in Additive Manufacturing. *Addit. Manuf.* **2024**, *83*, 104033.
(655) Ćatić, N.; Wells, L.; Al Nahas, K.; Smith, M.; Jing, Q.; Keyser, U. F.; Cama, J.; Kar-Narayan, S. Aerosol-Jet Printing Facilitates the Rapid Prototyping of Microfluidic Devices with Versatile Geometries and Precise Channel Functionalization. *Appl. Mater. Today* **2020**, *19*, 100618.
(656) McKibben, N.; Ryel, B.; Manzi, J.; Muramutsa, F.; Daw, J.; Subbaraman, H.; Estrada, D.; Deng, Z. Aerosol Jet Printing of Piezoelectric Surface Acoustic Wave Thermometer. *Microsyst. Nanoeng.* **2023**, *9* (1), 51.
(657) Kouchi, F. R.; Varghese, T. V.; Burgoyne, H.; Mansoor, N. E.; Seol, M.; McKibben, N.; Nirantar, S.; Chinnathambi, K.; Eixenberger, J.; Maryon, O.; Shuck, C. E.; Gogotsi, Y.; Koehne, J. E.; Estrada, D. StableTi$_3$ C$_2$ T $_x$ MXene Ink Formulation and High-resolution Aerosol Jet Printing for High-performance MXene Supercapacitors. *Small Methods* **2025**, *9*, 2500499.
(658) Xu, B.; Yang, M.; Cheng, W.; Li, X.; Xu, X.; Li, W.; Zhang, H.; Zhou, M. Precision Aerosol-Jet Micropatterning of Liquid Metal for High-Performance Flexible Strain Sensors. *Nat. Commun.* **2025**, *16* (1), 7920.
(659) Jeong, H.; Lee, J. H.; Kim, S.; Han, S.; Moon, H.; Song, J.-Y.; Park, A.-Y. Optimization of Process Parameters in Micro-Scale Pneumatic Aerosol Jet Printing for High-Yield Precise Electrodes. *Sci. Rep.* **2023**, *13* (1), 21297.
(660) Wang, Q.; Ma, M.; Duongthipthewa, A.; Zhang, W.; Lang, Y.; Luo, G.; Su, Y.; Liu, M.; Zhou, L.; Su, Z. "Totally-Additive-Manufacturing"-Functionalized Carbon Fiber-Reinforced Polymer Composites with an Ultrasensitive Self-Sensing Network. *Composites, Part A* **2025**, *189*, 108596.
(661) Zhou, X.; Zhang, L.; Zhang, S.; Liang, J.; Zhang, K.; Zhao, Z.; Zhao, S.; Wang, Y.; Guo, Y.; Zhang, D.; Jiang, L.; Chen, H. Self-Assembly of 3D-Printed Multiscale Micropillar-Based Organic Electrochemical Transistors for Ultrasensitive Dopamine Sensing. *ACS Nano* **2025**, *19*, 39615.
(662) Ali, Md. A.; Hu, C.; Jahan, S.; Yuan, B.; Saleh, M. S.; Ju, E.; Gao, S.; Panat, R. Sensing of COVID-19 Antibodies in Seconds via Aerosol Jet Nanoprinted Reduced-graphene-oxide-coated 3D Electrodes. *Adv. Mater.* **2021**, *33* (7), 2006647.
(663) Parate, K.; Rangnekar, S. V.; Jing, D.; Mendivelso-Perez, D. L.; Ding, S.; Secor, E. B.; Smith, E. A.; Hostetter, J. M.; Hersam, M. C.; Claussen, J. C. Aerosol-Jet-Printed Graphene Immunosensor for Label-Free Cytokine Monitoring in Serum. *ACS Appl. Mater. Interfaces* **2020**, *12* (7), 8592−8603.
(664) Saleh, M. S.; Ritchie, S. M.; Nicholas, M. A.; Gordon, H. L.; Hu, C.; Jahan, S.; Yuan, B.; Bezbaruah, R.; Reddy, J. W.; Ahmed, Z.; Chamanzar, M.; Yttri, E. A.; Panat, R. P. CMU Array: A 3D Nanoprinted, Fully Customizable High-Density Microelectrode Array Platform. *Sci. Adv.* **2022**, *8* (40), No. eabj4853.
(665) Herbert, R.; Lim, H.-R.; Rigo, B.; Yeo, W.-H. Fully Implantable Wireless Batteryless Vascular Electronics with Printed Soft Sensors for Multiplex Sensing of Hemodynamics. *Sci. Adv.* **2022**, *8* (19), No. eabm1175.
(666) Kwon, Y.-T.; Kim, H.; Mahmood, M.; Kim, Y.-S.; Demolder, C.; Yeo, W.-H. Printed, Wireless, Soft Bioelectronics and Deep Learning Algorithm for Smart Human-Machine Interfaces. *ACS Appl. Mater. Interfaces* **2020**, *12* (44), 49398−49406.
(667) Kalasin, S.; Surareungchai, W. Challenges of Emerging Wearable Sensors for Remote Monitoring toward Telemedicine Healthcare. *Anal. Chem.* **2023**, *95* (3), 1773−1784.
(668) Zub, K.; Hoeppener, S.; Schubert, U. S. Inkjet Printing and 3D Printing Strategies for Biosensing, Analytical, and Diagnostic Applications. *Adv. Mater.* **2022**, *34* (31), 2105015.
(669) Wang, M.; Cui, J.; Wang, Y.; Yang, L.; Jia, Z.; Gao, C.; Zhang, H. Microfluidic Paper-Based Analytical Devices for the Determination

https://doi.org/10.1021/acs.chemrev.5c00801
Chem. Rev. XXXX, XXX, XXX−XXX

of Food Contaminants: Developments and Applications. *J. Agric. Food Chem.* **2022**, *70* (27), 8188−8206.
(670) Wang, Y.; Yue, H.; Liu, A.; Cui, Y.; Hou, Y.; Ni, X.; Pereira, R. F.; Huang, B.; Vyas, C.; Bartolo, P. Dual Crosslinkable Bioink for Direct and Embedded 3D Bioprinting at Physiological Temperature. *Mater. Today* **2025**, *85*, 1−16.
(671) Webber, D.; Orth, A.; Vidyapin, V.; Zhang, Y.; Picard, M.; Liu, D.; Sampson, K. L.; Lacelle, T.; Paquet, C.; Boisvert, J. Printing of Low-Viscosity Materials Using Tomographic Additive Manufacturing. *Addit. Manuf.* **2024**, *94*, 104480.
(672) Jiang, J.; Yuan, C.; Zhang, X.; Gu, L.; Yao, Y.; Wang, X.; He, Y.; Shao, L. 3D Bioprinting of Liquid High-cell-proportion Bioinks in Liquid Granular Bath. *Adv. Mater.* **2024**, *36* (49), 2412127.
(673) Park, T.; Leem, J. W.; Kim, Y. L.; Lee, C. H. Photonic Nanomaterials for Wearable Health Solutions. *Adv. Mater.* **2025**, *37*, 2418705.
(674) Chen, K.; Shi, L.; Zhang, Y.; Liu, Z. Scalable Chemical-Vapour-Deposition Growth of Three-Dimensional Graphene Materials towards Energy-Related Applications. *Chem. Soc. Rev.* **2018**, *47* (9), 3018−3036.
(675) Zhong, Y. L.; Tian, Z.; Simon, G. P.; Li, D. Scalable Production of Graphene via Wet Chemistry: Progress and Challenges. *Mater. Today* **2015**, *18* (2), 73−78.
(676) Huang, H.; Shi, H.; Das, P.; Qin, J.; Li, Y.; Wang, X.; Su, F.; Wen, P.; Li, S.; Lu, P.; Liu, F.; Li, Y.; Zhang, Y.; Wang, Y.; Wu, Z.; Cheng, H. The Chemistry and Promising Applications of Graphene and Porous Graphene Materials. *Adv. Funct. Mater.* **2020**, *30* (41), 1909035.
(677) Luo, Y.; Wang, M.; Wan, C.; Cai, P.; Loh, X. J.; Chen, X. Devising Materials Manufacturing toward Lab-to-fab Translation of Flexible Electronics. *Adv. Mater.* **2020**, *32* (37), 2001903.
(678) Zhang, Z.; Yang, J.; Wang, H.; Wang, C.; Gu, Y.; Xu, Y.; Lee, S.; Yokota, T.; Haick, H.; Someya, T.; Wang, Y. A 10-Micrometer-Thick Nanomesh-Reinforced Gas-Permeable Hydrogel Skin Sensor for Long-Term Electrophysiological Monitoring. *Sci. Adv.* **2024**, *10* (2), No. eadj5389.
(679) Zhou, S.; Park, G.; Longardner, K.; Lin, M.; Qi, B.; Yang, X.; Gao, X.; Huang, H.; Chen, X.; Bian, Y.; Hu, H.; Wu, R. S.; Yue, W.; Li, M.; Lu, C.; Wang, R.; Qin, S.; Tasali, E.; Karrison, T.; Thomas, I.; Smarr, B.; Kistler, E. B.; Khiami, B. A.; Litvan, I.; Xu, S. Clinical Validation of a Wearable Ultrasound Sensor of Blood Pressure. *Nat. Biomed. Eng.* **2025**, *9*, 865.
(680) Wang, P.; Yu, W.; Li, G.; Meng, C.; Guo, S. Printable, Flexible, Breathable and Sweatproof Bifunctional Sensors Based on an All-Nanofiber Platform for Fully Decoupled Pressure-Temperature Sensing Application. *Chem. Eng. J.* **2023**, *452*, 139174.
(681) Ding, Q.; Wang, H.; Zhou, Y.; Zhang, Z.; Luo, Y.; Wu, Z.; Yang, L.; Xie, R.; Yang, B.; Tao, K.; Pan, S.; Liu, F.; Fu, J.; Huo, F.; Wu, J. Self-powered Switchable Gas-humidity Difunctional Flexible Chemosensors Based on Smart Adaptable Hydrogel. *Adv. Mater.* **2025**, *37*, 2502369.
(682) Xu, L.; Chen, Q.; Pichchamuttu, S. V.; Wu, L.; Pate, E.; Wu, C.; Li, T.; Zheng, X.; Yang, C.; Jin, K.; Liu, P.; Li, T.; Hu, L. Stretchable, Breathable, Wearable Batteries Using a Holey Design. *Matter* **2025**, *8* (3), 101959.
(683) Xu, C.; Solomon, S. A.; Gao, W. Artificial Intelligence-Powered Electronic Skin. *Nat. Mach. Intell.* **2023**, *5* (12), 1344−1355.

https://doi.org/10.1021/acs.chemrev.5c00801
Chem. Rev. XXXX, XXX, XXX−XXX